GEOMAGNETICALLY INDUCED CURRENTS (GIC) IN LARGE POWER SYSTEMS INCLUDING TRANSFORMER TIME RESPONSE

THESIS BY:
DAVID TEMITOPE OLUWASEHUN OYEDOKUN
DEPARTMENT OF ELECTRICAL ENGINEERING
UNIVERSITY OF CAPE TOWN

This thesis was submitted to the University of Cape Town in fulfilment of the academic requirements for the Doctor of Philosophy degree in Electrical Engineering

Acknowledgements

I am glad that I accepted the challenge to do my PhD research in the field of geomagnetically induced currents (GIC). During my research, I was privileged to participate in several meetings, workshops and conferences. These events provided me with the opportunity to share ideas with various people, from senior researchers and professors to my colleagues in the Department of Electrical Engineering at UCT. Despite the difficulties faced, I enjoyed all aspects of my research in this emerging field. More often than not, these engagements challenged me to think deeper and ensured that my research was thorough. I am not able to mention all those who contributed significantly to my research. However, I would like to thank:

- my colleagues in the power engineering group of the Department of Electrical Engineering at UCT. Their dedication and active participation in our weekly seminar helped refine my ideas for my thesis.

- my supervisors, Prof. C.T. Gaunt and Prof. K.A. Folly, who assisted me academically. I benefited from their wealth of experience and knowledge.

- Prof. C.T. Gaunt for providing me with the much needed financial assistance throughout my research.

- Chris Wozniak for his contribution to the development of the laboratory test procedure.

- Hilary Chisepo whose MSc laboratory work formed the basis upon which I was able to conduct laboratory experiments.

- Dr. P.J. Cilliers and Dr. S. Lotz of the South African National Space Agency (SANSA) for constructive comments on the algorithms that addressed my hypothesis.

- my family who gave me the encouragement I needed and provided the support structure for my perseverance.
- my wife, Dr Anthonia Oyedokun for her love, care and support throughout my research.

I would like to quote from Prof. C.T. Gaunt's PhD thesis: *"For all this help there is no debt to repay, except to help others in their turn."* ☺

Declaration

Although much literature was consulted during the preparation of this thesis, caution was exercised to properly reference all work. The rest is my own work and it has not been submitted (prior to this submission) to any academic institution for examination.

The number of words in the main text of the thesis do not exceed 80,000.

…….
DTO Oyedokun
25 November 2015.

Abstract

Geomagnetically induced currents (GIC) are the result of changing geomagnetic fields which are a consequence of a geomagnetic disturbance (GMD). The flow of GIC through transmission lines and transformers across the power network could have severe consequences, if the magnitudes of the GIC are high enough. Problems that could arise from the flow of GIC in transmission networks include an increase in the amount of reactive power demand by GIC-laden transformers, half-wave saturation, excessive heating in transformers, incorrect operation of transmission line protection schemes and voltage collapse in affected sections of the network.

In the past, GIC were calculated without taking the transformer's response time into account. The limitation of this approach is that the size and core type of the transformer is neglected. This may affect the assessment of GIC in the power network as the flux pattern and winding inductance distribution are not uniform across all transformer core structures. This thesis postulates that these characteristics could have far-reaching effects on the GIC that flows through a transformer as a function of time.

Based on this assumption, a novel way of calculating GIC is introduced in this thesis. This method combines the uniform plane wave model and the network Nodal Admittance Matrix (NAM) method and incorporated for the first time, the transformer time response, which does not appear to have been considered in previous calculation methods.

A general formula, which describes the transformer's time response to GIC was derived, followed by the derivation of the electric field induced in each transmission line.

A key input to the prospective GIC with transformer time response calculation, is a set of piecewise linear equations derived from a laboratory test and PSCAD simulations. These suitably characterise the response of three transformer core structures, namely: bank of single phase (3(1P-3L)), three-phase three-limb (3P-3L) and three-phase five-limb transformers (3P-5L). Each of these core types were considered as a Generator Step-up Unit (GSU) and a Transmission Transformer (TT).

The results of the laboratory experiment and simulations in PSCAD led to the conclusion that the transformer time response to GIC is irregular across the transformer cores that were tested. The 300 VA transformer core structure with the shortest response time is the 3P-3L, followed by the 3P-5L and the 3(1P-3L). For the 500 MVA transformers, the order was: 3P-3L; 3(1P-3L); and 3P-5L. The 3P-3L transformers permit the flow of GIC through the windings of the transformer over a shorter length of time. Therefore based on the order in response time, during GMDs leading to higher GIC, the prospective GIC with or without transformer time response flowing through 3P-3L transformers will be similar.

Furthermore, the response time to GIC in 3P-3L, 3P-5L and 3(1P-3L) transformer core types are load-dependant. The 3(1P-3L) and 3P-5L transformers operating as TT's (modelled as transformers at 40 % load) have the longest response time to GIC, while 3P-3L transformers operating as a GSU (modelled as transformers at full load) have the longest response time to DC. The shortest response time to DC was with a GSU at light load (modelled as transformers at 80 % load), which was consistent across the three transformer core types. This correlates well with the notion that power networks could stand a better chance of surviving a high GMD when all generating units and loads are online.

Three different core structures were modelled with a variation of DC current levels and load conditions, both in PSCAD and in the laboratory. These results are unique to the transformer models used, but are representative of major types of core configurations used on power networks. These results provide an indication that it is incorrect to lump the responses of all transformers and transformer time response should be taken into consideration, especially when sampling at intervals as low as 2 seconds.

List of abbreviations

CME	coronal mass ejection
DC	direct current
FFT	Fast Fourier Transform
GIC	geomagnetically induced currents
GMD	geomagnetic disturbance
GSU	generator step up unit (transformer)
NGC	National Grid Company
NI	National Instruments
SECS	spherical elementary current systems
TT	transmission transformer
SSC	sudden storm commencement
UT	universal time
3P-3L	three-phase three-limb
3P-5L	three-phase five-limb
3(1P-3L)	three single-phase three-limb

Table of Contents

List of Figures

List of Tables

CHAPTER 1

INTRODUCTION

Geomagnetically induced currents (GIC) are the result of changing geomagnetic fields which are a consequence of a geomagnetic disturbance. During solar storms, enormous explosions of plasma are ejected from the sun's surface into interplanetary space. These ejections are called Coronal Mass Ejections (CME) [1-3]. CMEs disrupt the solar wind [4] through interplanetary space and the resulting interaction with the Earth's magnetic field is known as a geomagnetic storm [5, 6].

During geomagnetic storms, solar wind pressure and wind speed can suddenly increase on average from 2 nPa to 30 nPa and from 400 km/s to 2000 km/s, respectively, if the CME is directed towards the Earth [7]. Geo-effective CMEs lead to large fluctuations of the Earth's magnetic fields, which induce an electric field according to Faraday's law of induction [8]. This gives rise to quasi-DC currents in electric power systems through the grounded neutrals of power transformers. These geomagnetically induced currents have frequencies less than 1 Hz [9, 10].

The flow of GIC through transmission lines and transformers across a power network could have negative consequences. These include an increase in the reactive power demanded by GIC-laden transformers [11, 12], transformers operating within the region of non-linearity due to half-wave saturation [13, 14], excessive heating [15] in transformers leading to thermal damage, incorrect operation of transmission line protection schemes [16, 17] and voltage problems in affected sections of the network [18, 19]. To mitigate the flow of GIC, DC current blocking devices have been designed and some have been developed [20, 21]. In Finland, neutral-point reactors have been used decrease the GIC magnitudes in its high-voltage system [22]. In England, series capacitors have been used to block GIC [23, 24] in transmission lines. However, studies by Erinmez *et al* [24] showed that it would be

advantageous to strategically place the devices to prevent the risk of adversely increasing the flow of GIC in other parts of the network.

In the past, GIC were calculated using either a uniform or non-uniform electric field model in the geophysical solution. A number of methods for the network calculation have been used which include the Lehtinen-Pirjola method [25, 26] and the Nodal Admittance Matrix (NAM) method [27]. Details of these are discussed in chapter 2. Over the years, software has been developed to carry out these calculations [28-35]. The general assumption in the network calculation is that GIC, which are quasi-DC currents, should be treated as DC currents. In some cases, measured GIC have been compared with calculated GIC with a variation in correlation. The literature review shows that researchers have taken into account the transmission line resistance, transformer resistance, grounding resistance and ground conductivity, but have hardly paid attention to the transformer's time response to GIC [27], [29], [30-34], [36]. This thesis suggests that the transformer time response to GIC, which may be core dependent, contributes to the differences between the measured and calculated GIC flowing through a transformer.

Therefore, this thesis investigates the GIC calculation approach, which includes the transformer time response to changing GIC, with the objective of determining whether the time response is significant in modelling GIC. The method proposed in this thesis combines the uniform plane wave model, network NAM method [36] and incorporates the transformer time response.

To this end a software programme was written in Matlab. This contribution extends the capabilities of existing GIC calculators, such as the GIC calculator in the PowerWorld Simulator, Version 17 by Overbye [35]. PowerWorld Simulator takes into account the core structure to determine the reactive power demand by transformers due to GIC.

1.1 BACKGROUND TO THESIS

Power networks comprise components like transformers, transmission lines, reactors, capacitor banks, protection instruments, etc., [37]. This research deals mainly with GIC in

power transformers and transmission lines. Bolduc [38] indicated that the other components of power networks are also affected by GIC which may lead to the disruption of the entire power network. The Hydro-Quebec blackout in 1989 [38], which occurred due to a geomagnetic disturbance, and led to millions of people being in the dark for hours towards the end of winter, is an example of what can happen [38, 39]. The flow of GIC in the Swedish power grid during the Halloween storm on 30 October 2003 led to a large-scale blackout which affected about 50,000 customers for about one hour [40].

The calculation of GIC involves calculating the electric field induced in the transmission lines as a result of the changing Earth's magnetic field, the resulting currents in the transmission line and the currents flowing through the grounded neutrals of transformers [16], [41]. Several methods have been used to determine the electric field induced in the Earth and consequently, calculate the GIC flowing in transmission lines and transformers. In 1940, McNish [42] derived a mathematical expression for the Earth's electric field, but entirely omitted the conductivity of the Earth. In 1966, the Earth's electric field was calculated by Kellogg [43] using Maxwell's equation. In this method, a plane downward propagating wave (towards the Earth) was used to represent the magnetic field. This model took the conductivity of the ground into consideration. However, Kellogg assumed that the conductivity of the ground was uniform which later was found not to be the case generally.

In 1970, Albertson and Van Baelen [44] derived a mathematical relation between changes in the Earth's magnetic field and the induced electric field which leads to the flow of GIC. Their method considered the conductivity distribution of the Earth and used a recording of the measured Earth's magnetic field.

In 1985, Lehtinen & Pirjola [25] developed a method for calculating GIC. This method which is further discussed in chapter 2, is appropriate for a network that is exposed to a uniform or non-uniform electric field. This method was subsequently used in 2000 and 2002 by Koen and Gaunt [31], [45] for the calculation of GIC in the Southern Africa electricity transmission network. Koen's study led to three conclusions: (i) the Lehtinen-Pirjola method is suitable for calculating GIC in the Southern Africa electricity transmission network, (ii) a significant amount of GIC are present during strong geomagnetic disturbances and (iii) a strong

correlation between transformer failures and past geomagnetic disturbances exists in South Africa. Recently, this method was also used for the analysis of GIC in Brazil [34].

In 1998, Boteler and Pirjola [46] demonstrated that the GIC produced by a uniform electric field when modelled in series with the transmission line or between the transformer and ground are the same. However, for a non-uniform electric field, only the line approach can be used. This is because according to Boteler and Pirjola [46], realistic electric fields have a non-conservative vector function component which cannot be represented by a conservative electric field.

The mesh impedance method and the NAM method can be used for solving the network calculation by modelling the electric field in series with the transmission line [28]. The advantage of the NAM method over the mesh impedance method is that the need to derive voltage equations for all the loops in the network is avoided. For very large power networks such as the South African electricity transmission network, this is a significant advantage since the complexity of the calculation and computational time is reduced. In 2007, the NAM method was used to calculate the low of GIC in a real-time GIC simulator [36].

The electric field can easily be calculated, as mentioned earlier, if the magnetic source field is assumed to be uniform. Other methods that have been adopted to calculate electric fields for non-uniform source fields include spherical elementary current systems (SECS) [47-49] and the complex image method (CIM) [33]. Bernhardi *et al* [7] in 2008 improved GIC calculation in Southern Africa by using SECS to calculate the electric field and the Lehtinen-Pirjola method for the network. In contrast to the uniform plane wave model, SECS assumes that the electric field distribution is non-uniform for the entire network, whilst segments of the network experience uniform plane wave electric field distribution. That is, transmission line segments experience a uniform electric field. Their results indicated that SECS is a more accurate method when compared to the uniform plane wave approach for electric field calculation, especially in a large network.

Not all reports of GIC measurements in the power grid is accompanied by the calculated GIC for the same time frame. An example of this is the publication on the GIC measurements in

Japan [50]. Having both GIC measurements and calculated values for a substation enables the validation of the calculation, which can be used to calculate GIC at other stations with no GIC measurement setups.

In some cases of GIC calculation, the calculated GIC values were compared with measured GIC [30]. For instance, Koen and Gaunt [30] used the uniform plane wave model and the Lehtinen-Pirjola method to calculate GIC flowing through a 400/132/15 kV 240 MVA autotransformer at the Grassridge substation in South Africa on 31 March 2001. The calculated GIC profile was compared with the measured GIC during the same time frame. Although the profiles were very similar, the measured GIC were higher than the calculated GIC for most of the time. Koen and Gaunt suggested that a proportionating constant be introduced to reduce the variance between measured and calculated GIC. This suggestion is similar to that made by Viljanen in 1998 [51], where he compared the measured GIC flowing in the Nurmijärvi - Loviisa transmission line in Finland with the calculated GIC in the same line, using the uniform plane wave electric field model and the Lehtinen-Pirjola method.

In his comparison, he used a multiplier *c* to fit the measured GIC and calculated GIC as closely as possible. A possible source of discrepancy between measured and calculated GIC is the Earth's conductivity structure. Therefore, the multiplier c was deduced from local geomagnetic readings in order to "calibrate" the calculated GIC. In line with the impact of ground conductivity models on the correlation between measured and calculated GIC, Trichtchenko and Boteler [52] found that, depending on the site where the transformers are located, the ground conductivity structure may act like a high pass filter or a low pass filter, thereby allowing corresponding frequencies which determine the measured GIC profile.

A uniform ground conductivity profile was used to calculate the electric field in this work.

Discrepancies between measured and calculated GIC was also observed in the research conducted by Marti *et al* [18] when they compared the absolute values of the measured GIC and the absolute values of the calculated GIC through a 500/230 kV 750 MVA autotransformer. With the assumption that GIC in the transformer will flow through the common winding to ground, differences of up to 100 % between the two were found.

Another case where measured and calculated GIC differed was at the Vykhodnoy substation in Russia during the storm on 15 March 2012 [53].

Overbye *et al* [35] suggested the introduction of a factor *k* for different transformer core types for the integration of geomagnetic disturbances into power flow calculations, with specific focus on the additional reactive power linked to GIC. This was based on the notion that different transformer core types respond to GIC differently [54]. Similarly, several research papers have graded the response of different transformer core types to GIC [55], [56]. Viljanen, Pirjola and Makinen in their discusses on Boteler's research publication [57], which stated that the time constant of large transformers is an aspect that may correlate their response to GIC according to core types, felt that this aspect had not been adequately investigated. Thus it became important to find a way of incorporating the time response of different transformer core types to GIC into GIC calculation.

1.2 OBJECTIVES OF THE THESIS

Calculation of GIC is crucial to the understanding of the impact of GIC on transformers and the entire power network. As mentioned earlier, several comparisons between calculated GIC and measured GIC in transformers have been made in the past. In almost all cases, there are discrepancies of various magnitudes between the two.

The objectives of this thesis are to summarise the above discrepancies between calculated and measured GIC, investigate the contribution of the transformer core type and transformer time response. Furthermore, this thesis will propose a calculation method to improve GIC modelling by reducing the difference between measured and calculated GIC. This will be accomplished by taking into account the transformer's time response to GIC.

The use of a non-uniform electric field has been reported [7] to reduce the error between measured and calculated GIC to an extent. In a previous study by Boteler [46], it was stated that GIC calculations are correct based on their input electric field. The validity of the calculated GIC is determined by how well the calculated GIC matches the measured GIC in instances where the measured GIC is available. This research was focused on the

transformer time response as a potential source or discrepancy between measured and calculated GIC.

1.3 HYPOTHESIS

This thesis tests the following hypothesis:

> ***The integration of transformer core characteristics and time response to GIC into GIC calculations improves the modelling of GIC as indicated by reduced differences between measured GIC and calculated GIC, and helps to improve the understanding of the transformer response to GIC.***

The validity of this hypothesis is tested by investigating the following guiding questions:

1. How is the network part of GIC calculation affected by transformer response to changing geo-electric fields?
2. What is the time response of transformers to a changing geo-electric field imposed at low frequencies and how does it vary with transformer core type?
3. Why was the time response of transformers neglected in the past? Are the reasons valid?
4. To what extent can the modelled and tested transformers represent all transformers?
5. How does the sampling time interval of the magnetic field and measured GIC affect GIC calculations?

1.4 RESEARCH METHODOLOGY

An extensive review of relevant literature was conducted at the beginning of this research. This review included calculation techniques based on various models and cases where measured GIC were compared with calculated GIC.

Thereafter, a new GIC calculation technique was developed by combining the best of the GIC calculation approaches reviewed in literature with transformer time response

modelling. The new GIC calculation technique was tested with and without the transformer time response.

PSCAD/EMTDC simulations were used to test for the effect of transformer time response to GIC-like currents. This was followed by a similar test in the laboratory.

The existing PSCAD/EMTDC transformer models includes saturation and is apparently suitable for the simulations related to the transformer time response. Therefore, no new PSCAD models were developed.

The effect of the transformer time response on the flow of GIC through transformers was analysed to determine the significance of the transformer time response.

1.5 OUTLINE OF THIS THESIS

This outline of this thesis is presented below.

In chapter 2, the uniform plane wave model, spherical elementary current systems and complex image method for calculating electric fields are reviewed. This is followed by a review of the Lehtinen-Pirjola method and NAM method.

In the third chapter, the mathematical derivation for calculating the prospective GIC with transformer time response is shown. Thereafter, the magnitude of electric field induced on a transmission line is derived using the uniform plane wave model. The last section of chapter 3 presents the derivation of the prospective GIC without the transformer time response using the NAM method.

The protocol for the laboratory experiments and PSCAD simulations is presented in chapter 4. The laboratory experimental setup and PSCAD simulation setup are also explained in this chapter.

Chapter 5 describes the transformer time response to GIC tests in the laboratory and the results for the three 300 VA transformer core types namely; bank of three single-phase

three-limb transformers referred to as 3(1P-3L), three-phase three-limb transformer referred to as 3P-3L and the three-phase five-limb transformer referred to as 3P-5L.

Chapter 6 describes the time response to GIC simulation results of the 300 VA, 3(1P-3L), 3P-3L and 3P-5L transformer core type in PSCAD. This is followed by a comparison of the laboratory test result and the PSCAD simulation result. The next section in this chapter describes the tests conducted on the same transformer core types but rated at 500 MVA to represent large power transformers. Finally, the chapter offers the analysis of the average transformer response time to GIC.

In chapter 7, the prospective GIC without the transformer time response calculation method is validated. Following this, four case studies are presented with step-by-step calculation of the prospective GIC with transformer time response with a variety of transformer core structures. Using the measured GIC at Grassridge substation in South Africa, the effect of using different time intervals of the magnetic field on GIC calculation is investigated.

Chapter 8 discusses the findings of this research and in chapter 9, conclusions are drawn from the findings of the research.

1.6 NOVEL CONTRIBUTIONS

The research:

1. Presented new knowledge on GIC flow through transformers and their responses, including the difference between Generator Step-up Units (GSU) and Transmission Transformers (TT);
2. Showed that the profile of GIC flow through different transformer core structures of the same capacity are not the same.
3. Proved that a sampling interval between 2 seconds and 10 seconds is sufficient to adequately measure GIC and the geomagnetic field used for GIC calculations.

CHAPTER 2

REVIEW OF GIC CALCULATION METHODS

Calculating GIC involves two major parts [58]. The first part is the geophysical response of the geo-electric field to a given geomagnetic disturbance arising from ionospheric and magnetospheric currents, which is discussed in section 2.1. The second part is the derivation of GIC in the network from the geo-electric fields, which is discussed in section 2.2. In section 2.3, GIC calculation software is discussed. All the software and techniques discussed in this chapter were developed between 1940 and 2013. Some software calculates GIC, while other software calculates the reactive power demand due to GIC.

2.1 ELECTRIC FIELD CALCULATION

In 1940, McNish derived a mathematical expression for the Earth's electric field using the formula in equation 2.1 [42]:

$$E = -\frac{\partial A}{\partial t} \tag{2.1}$$

where *E* is the induced electric field, *A* is the magnetic vector potential of the auroral line current flowing in the atmosphere and *t* is time.

In this model, the conductivity of the Earth was neglected which made it incomplete. The Earth conductivity model is an important factor to be considered, because the Earth conductivity affects the size of the electric field. In some applications, a uniform Earth conductivity structure is sufficient, while the non-uniform Earth conductivity structure can be considered for more accurate results.

In 1966, the Earth's electric field was calculated by Kellogg [43] from Maxwell's equation as:

$$curl\ E = -\frac{\partial B}{\partial t} \tag{2.2}$$

where *E* is the induced electric field and *B* is the magnetic field.

In this method, a plane downward propagating wave is used to represent the magnetic field and the conductivity of the ground is assumed to be uniform [43, 44].

Albertson and Van Baelen [44] derived a mathematical relationship between changes in the Earth's magnetic field and the induced electric field. These changes lead to the flow of GIC. This method takes into consideration the conductivity distribution of the Earth and uses a log of the measured Earth's magnetic field [25], [59-61].

The electric field E_o was calculated as:

$$E_0 = Re\ (E_y) \tag{2.3a}$$

where R_e is the real part, and

$$E_y = \int_0^\infty E_y(v)dv \tag{2.3b}$$

But

$E_y(v)$ is defined in equation 2.4 as:

$$E_y(v) = \frac{Je^{jwt}}{\pi} e^{-vh} \frac{jw\mu_0 Z_s(v)}{jw\mu_0 + vZ_s(v)} \cos vx \tag{2.4}$$

The variable v describes partly the induced electric field [44].

In 2004, Viljanen *et al* [60] stated that to solve the geophysical problem, a model of the magnetospheric-ionospheric current system as a function of time and the Earth's conductivity structure is needed. Then, in theory, Maxwell's equations and boundary conditions for the Earth's electric and magnetic fields can be solved. However in practice, inputs to these equations are partially unknown. Even if the inputs are known, the solution is time-consuming, which is a significant drawback [62]. Other methods include the uniform plane wave model, the spherical elementary current systems (SECS) method (introduced and validated in 1997 by Amm [49]) and the complex image method (CIM) [62], [33].

2.1.1. Uniform plane wave model

The uniform plane wave model application to the calculation of induced electric field in transmission lines was introduced by Viljanen and Pirjola [61]. It is based on Faraday's law of induction. This law states that a time-varying magnetic field in a conductive medium induces an electric field, the magnitude of which depends on the rate of change of the magnetic field. In this model, the Earth is described as a half space where the geomagnetic field propagates vertically, but the wave front is horizontal in the Earth with a constant conductivity. The horizontal electric field E_y can be written in terms of the horizontal magnetic field B_y due to the orthogonal relationship between the two as shown in equation 2.5a.

$$E_y = -\sqrt{\frac{\omega}{\mu_0 \sigma}}\, e^{i\frac{\pi}{4}} B_x \qquad (2.5a)$$

where ω is the angular frequency, σ is the Earth conductivity, μ_o is the permeability of the Earth and B_x is the horizontal geomagnetic field component.

Taking the inverse Fourier transform of equation 2.5a to give the time domain convolution integral, equation 2.5b is derived. The derived equation shows the relationship between the magnetic and the electric field.

$$\mathrm{E(t)} = -\frac{1}{\sqrt{\sigma \pi \mu_o}} \int_0^{\infty} \frac{\mathrm{g(t-u)}}{\sqrt{\mathrm{u}}}\, \mathrm{du} \qquad (2.5b)$$

where *g(t)* is the time derivative of the perpendicular magnetic field, σ is the Earth's conductivity, μ_o is the Earth permeability, *t* is time and *u* is time delay.

In planar geometry, where the x–axis corresponds to geographic north, y-axis to the geographic east and z downwards, the electric field $E(T_N)$ in the network can be calculated using equation 2.6 as:

$$\mathrm{E(T_N)} = \frac{2}{\sqrt{\pi \sigma \mu_0 \Delta}} (\mathrm{R_{N-1}} - \mathrm{R_N} - \sqrt{\mathrm{M}}\mathrm{b_{N-M}}) \qquad (2.6)$$

Where Δ is the sampling interval, N is the sample number, and b is the magnetic component.

M is the number of past samples of the B-field considered. M is calculated by dividing the integral duration, which is normally 20 minutes, by the sampling time interval of the magnetic field data [63]. Therefore, for two-minute sampling time interval magnetic field data, M= 10.

Equation 2.6 which is the time series expansion of the E-field for a homogeneous Earth model, is an approximation of the inverse Fourier transform.

Calculated GIC values are sensitive to the choice of M, especially during rapid changes in the Earth's magnetic field. This is because the electric field calculation formula has M as one of its inputs. Therefore, this number can be increased or decreased based on specific application needs, especially when measured GIC values are compared with calculated GIC values.

$\mathrm{E}(\mathrm{T_N})$ = Electric field sample at sampling instant, $\mathrm{T_N}$.

$$\mathrm{R_N} = \sum_{\mathrm{n=N-M+1}}^{\mathrm{N}} \mathrm{b_n}\sqrt{\mathrm{N-n+1}} \qquad (2.7)$$

where:

$$\mathrm{b_n} = \mathrm{B_n} - \mathrm{B_{n-1}} \qquad (2.8a)$$

N and n are integer numbers.

Due to the orthogonal relationship between magnetic and electric fields, E_x is calculated from B_y and E_y is the calculated from B_x.

Alternatively, in practice a more appropriate method can be used to calculate the geo-electric field from ground-based geo-magnetic field data and local surface impedance. In the frequency domain, the geo-electric field is the ratio of the surface impedance and the geomagnetic field [60]. This is shown in equations 2.8b and 2.8c.

$$E_x(\omega) = \frac{B_y(\omega)}{Z(\omega)\mu_0} \qquad (2.8b)$$

$$E_y(\omega) = \frac{-B_y(\omega)}{Z(\omega)\mu_0} \quad (2.8c)$$

where $Z(\omega)$ is the local surface impedance, namely the transfer function that relates the geo-electric and geomagnetic fields. The frequency ω characterises the surface impedance [33].

The inverse Fourier transform of $E_x(\omega)$ and $E_y(\omega)$ gives the north and east component of the geo-electric field, respectively.

2.1.2 Spherical elementary current systems (SECS) method

Elementary currents are derived by fitting the modelled field to the measured field in a spherical coordinate system. A planar model is used to simplify the computations without much effect on the modelled fields. According to research conducted by Tjimbandi in 2007 [64], this holds because the Earth's curvature can be neglected for regional computations. Two types of SECS were identified by Amm [49], one being divergence-free ($\vec{J}_{\mathrm{df,el}}$):

$$\vec{J}_{\mathrm{df,el}}(\overrightarrow{r'}) = \frac{I_{o,df}}{4\pi R_I}\cot\left(\frac{\vartheta'}{2}\right)e_{\vartheta'} \quad (2.9)$$

and the other curl-free ($\vec{J}_{\mathrm{cf,el}}$):

$$\vec{J}_{\mathrm{cf,el}}(\overrightarrow{r'}) = \frac{I_{o,cf}}{4\pi R_I}\cot\left(\frac{\vartheta'}{2}\right)e_{\vartheta'} \quad (2.10)$$

where R_I is the radius of the ionosphere and $I_{O_{\begin{cases}df\\cf\end{cases}}}$ are the divergence-free and curl-free scaling factors of the elementary systems.

Both are written in the spherical coordinate system $(r', \vartheta', \varphi')$ with unit vectors $(e_{r^i}, e_{\vartheta'}, e_{\varphi'})$ of which the North Pole is in the centre of the elementary system. The application of SECS to the computation of GIC [65] is based on the fact that the horizontal geomagnetic variations of the Earth's surface can be explained by a horizontal divergence-free curl system at the ionospheric level. The actual 3-D ionospheric current system cannot

be determined by using only ground collected magnetic data. However, a horizontal equivalent current system exists for every 3-D ionospheric current system [60], [49].

The surface current density $J(r)$ of an elementary system in cylindrical coordinates is:

$$\mathrm{J(r)} = \frac{\mathrm{I}}{(2\pi \mathrm{r})}\mathrm{e}_{\varphi} \qquad (2.11)$$

where: *I* is the amplitude of the current density, $\mathrm{r} = \sqrt{\mathrm{x}^2 + \mathrm{y}^2}$ and the *x*, *y* plane is the Earth's surface. e_{φ} is the unit vector in the direction of φ.

Therefore, the electric field at the Earth's surface due to one element is derived as:

$$\mathrm{E} = -\frac{\mathrm{i}\omega\mu_0 \mathrm{I}}{4\pi}\frac{\sqrt{\mathrm{r}^2+\mathrm{h}^2}-\mathrm{h}}{\mathrm{r}}\mathrm{e}_{\varphi} \qquad (2.12)$$

where μ_o is the Earth permeability, ω is the angular frequency and *I* is the amplitude of any surface current density at height *h* in cylindrical coordinates.

The magnetic field is derived by:

$$\mathrm{B} = \frac{\mu_0 \mathrm{I}}{4\pi \mathrm{r}}\left(\left(1 - \frac{\mathrm{h}}{\sqrt{\mathrm{r}^2+\mathrm{h}^2}}\right)\mathrm{e}_{\mathrm{r}} + \frac{\mathrm{r}}{\sqrt{\mathrm{r}^2+\mathrm{h}^2}}\mathrm{e}_{\mathrm{z}}\right) \qquad (2.13)$$

where *z* is the z-axis pointing vertically downwards.

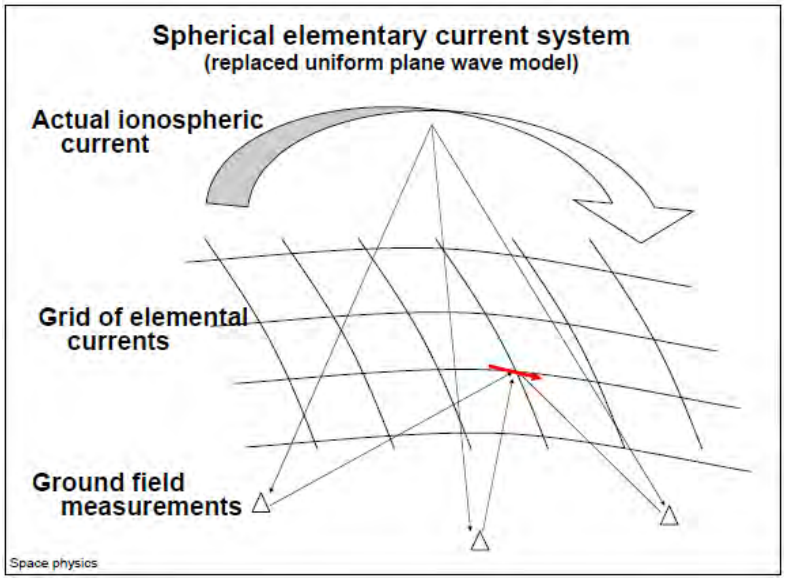

Figure 2.1 The SECS showing the ground field measurements and the grid of elementary currents [7]

The elementary ionospheric currents are placed in an equally spaced grid pattern over the area of interest, as seen in Figure 2.1 [49, 60].

This method was used by Bernhardi *et al* [7] in 2008 to improve the accuracy of GIC calculations for Southern Africa. They concluded that SECS allows for the interpolation of geomagnetic fields as accurately as possible, with the existing configuration of magnetic observatories in the region. Their results with SECS were closer to the measured GIC when compared to GIC calculated using the uniform plane wave method.

2.1.3 The Complex Image method (CIM)

The complex image method (CIM) has also been used to calculate electric fields produced by a line current (electrojet) source. This method adopts a layered conductivity model of the Earth [62, 66] and is considered to be very accurate and fast [66, 67]. In 2003, Pulkkinen *et al* [47] introduced a combination of SECS and CIM.

2.2 NETWORK CALCULATION

2.2.1 Lehtinen-Pirjola method

One of the most common methods that has been used for network calculation is the Lehtinen - Pirjola method [25, 26].

To illustrate this method, a small three-bus network is shown in Figure 2.2 with the induced electric field shown on the lines as E_{ij} and E_{jk}. The nodal resistances R_{ij}, R_j and R_{jk} represent the resistances at each substation per phase.

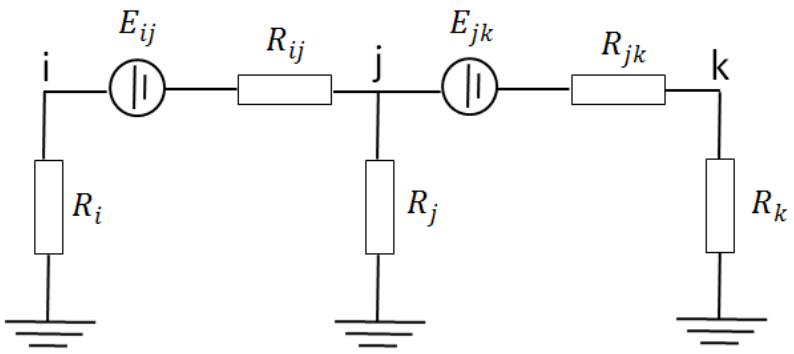

Figure 2.2 Three-bus network with induced electric field

Using Norton's theorem [68, 69], the electric field induced in line L_{ij} with resistance R_{ij} is converted to an equivalent current source h_{ij} in parallel with the admittance of the line y_{ij} as shown in Figure. 2.3. These are defined in equations 2.14 and 2.15.

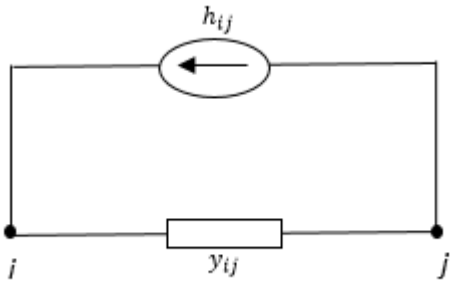

Figure 2.3 Norton's current equivalent

h_{ij} and y_{ij} in Figure 2.3 are defined as:

$$h_{ij} = \frac{E_{ij}}{R_{ij}} \tag{2.14}$$

$$y_{ij} = \frac{1}{R_{ij}} \tag{2.15}$$

Substituting equation 2.15 in equation 2.14, the current in line i_{ij} due to the induced electric field E_{ij}can be written as:

$$h_{ij} = E_{ij} y_{ij}. \tag{2.16}$$

The sum of all the currents at a node is derived using Kirchhoff's law for currents as:

$$i_i = \sum_{j=1}^{N} i_{ji} = -\sum_{j=1}^{N} i_{ij} \quad (2.17)$$

where N is the total number of nodes. The currents in line ij is:

$$i_{ij} = E_{ij}y_{ij} + y_{ij}(v_i - v_j). \quad (2.18)$$

Factoring the common term y_{ij} in equation 2.18 will yield:

$$i_{ij} = y_{ij}[E_{ij} + (v_i - v_j)], \quad (2.19)$$

and substituting equation 2.19 into equation 2.17 will yield:

$$i_i = -\sum_{j=1}^{N} y_{ij}[E_{ij} + (v_i - v_j)] \quad (2.20)$$

Assuming the path to ground from each node has zero resistance, the node voltages will be zero. Therefore, the current in the branches will be exactly equal to current sources. Hence, the sum of the current sources is equal to the current that flows to ground. This is given in equation 2.21 using Kirchhoff's' law currents:

$$J_i^e = -\sum_{j=1}^{N} E_{ij}y_{ij} \qquad i \neq j \quad (2.21)$$

Substituting equation 2.21 in equation 2.20 then gives:

$$i_i = J_i^e - \sum_{j=1}^{N}(v_i - v_j)y_{ij} \qquad i \neq j \quad (2.22)$$

And expanding equation 2.22 yields:

$$i_i = J_i^e - \sum_{j=1}^{N} v_i y_{ij} + \sum_{j=1}^{N} v_j y_{ij} \qquad i \neq j \quad (2.23)$$

The first summation in equation 2.23 represents the diagonal elements of a network admittance matrix:

$$Y_{ii}^{j} = \sum_{j=1}^{N} y_{ij} \qquad i \neq j \quad (2.24)$$

The second summation represents the dependence of the current i_i on all the other voltages and gives the off-diagonal elements of the network admittance matrix:

$$Y_{ij}^{j} = -y_{ij} \qquad i \neq j \quad (2.25)$$

Substituting equation 2.24 and 2.25 in equation 2.23 gives:

$$i_i = J_i^e - \sum_{j=1}^{N} v_j Y_{ij}^j \quad (2.26)$$

In matrix form, equation 2.26 can be written for all the nodes as:

$$[I^e] = [J^e] - \left[Y^j\right]\left[V^j\right] \quad (2.27)$$

Where the elements of the column matrix $[I^e]$ are the nodal currents, elements of the column matrix $\left[V^j\right]$ are the nodal voltages and $[J^e]$ is the column matrix of the current sources at each node.

The nodal voltage at each node can be derived as the product of the earthing impedance and the nodal current given in equation 2.28:

$$\left[V^j\right] = [Z^e][I^e] \quad (2.28)$$

where $[Z^e]$ is the earthing impedance matrix.

Substituting equation 2.28 in equation 2.27 gives:

$$[I^e] = [J^e] - \left[Y^j\right][Z^e][I^e] \quad (2.29)$$

Re-arranging equation 2.29 in terms of $[I^e]$ gives

$$[I^e]\left([1] + \left[Y^j\right][Z^e]\right) = [J^e] \quad (2.30)$$

where $[1]$ is a unit matrix.

Matrix $[I^e]$can be calculated by taking the inverse of $\left([1] + \left[Y^j\right][Z^e]\right)$ and multiplying the result by $[J^e]$ given in equation 2.31:

$$[I^e] = \left([1] + \left[Y^j\right][Z^e]\right)^{-1}[J^e] \quad (2.31)$$

The current in each node in $[I^e]$ is the GIC flowing through the node to ground.

2.2.1.1 Superposition

When the electric field induced in the network is decomposed into the eastern component and the northern component, $[J^e]$ in equation 2.21 will be calculated twice:

$$J^e_{i(x)} = -\sum_{j=1}^{N} E(x)_{ij} y_{ij} \qquad i \neq j \tag{2.32}$$

where $J^e_{i(x)}$ is the sum of the current source at a node due to the eastern component of the electric field, and:

$$J^e_{i(y)} = -\sum_{j=1}^{N} E(y)_{ij} y_{ij} \qquad i \neq j \tag{2.33}$$

where $J^e_{i(y)}$ is the sum of the current source at a node due to the northern component of the induced electric field.

Therefore, the nodal current as a result of the induced electric field will be:

$$[I^e] = \left([1] + \left[Y^j\right][Z^e]\right)^{-1}[J^e_x] + \left([1] + \left[Y^j\right][Z^e]\right)^{-1}\left[J^e_y\right] \tag{2.34}$$

For an electric field of 1 V/km in both eastern and northern components for node *i*:

$$a_i = \left([1] + \left[Y^j\right][Z^e]\right)^{-1}[J^e_x] \tag{2.35}$$

where a is nodal current corresponding to the eastern electric field of 1 V/km, and:

$$b_i = \left([1] + \left[Y^j\right][Z^e]\right)^{-1}\left[J^e_y\right] \tag{2.36}$$

where b is the nodal current corresponding to the northern electric field of 1 V/km.

This allows for equation 2.34 to re-written as:

$$[I^e] = [a_i]E_x + [b_i]E_y \tag{2.37}$$

Where E_x represents the induced electric field in the northern direction and E_y represents the electric field in the eastern direction.

Equation 2.35 and equation 2.36 are fixed network parameters for a specific network. Therefore once the a and b network parameters are calculated, the nodal currents can be calculated as shown in equation 2.37.

2.2.2 Nodal Admittance Matrix (NAM) method

For the network calculations, the electric field input can either be placed in series with the transmission lines or between the transformer and ground. As mentioned in the introduction, in 1998, Boteler and Pirjola [46] demonstrated that the GIC produced by a uniform electric field are the same, whether modelled in series with the transmission line or between the transformer and ground. In the NAM method, the electric field input, which is in series with the transmission line, is converted to its Norton equivalent circuit. In Figure 2.4, a two-bus network is used as an example. The induced electric field E_{ij} on the line R_{ij} is shown on the left Figure (2.4-a) while the Norton equivalent circuit which has the series admittance y_{ij} in parallel with the equivalent current h_{ij}, is shown on the right Figure (2.4-b).

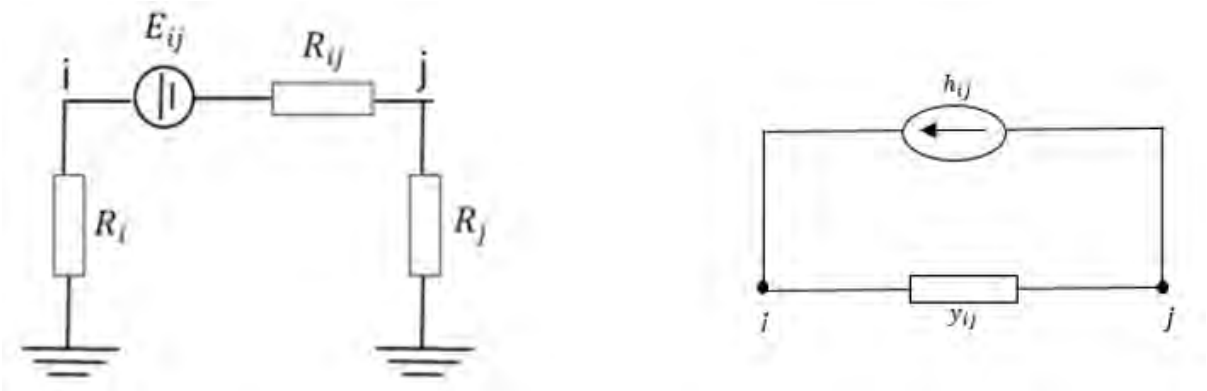

(a) Induced electric field **(b) Norton equivalent circuit**

Figure 2.4 Conversion of induced electric field to Norton equivalent

The nodal voltages are calculated by matrix inversion and multiplied by the nodal admittances [27]. The NAM method has been used extensively. In the development of a test case for calculating GIC by Horton *et al* [6], NAM was one of the methods used. The NAM method was compared with the Lehtinen - Pirjola method by Boteler and Pirjola and they

were found to be mathematically equivalent [26]. The derivation of the matrix equations are in section 3.3 of this thesis, where they are directly linked to the example that was used to derive the transformer time response equation.

2.3 CALCULATION AND MODELLING OF GIC IN POWER SYSTEMS

The aim of this section is to cover the techniques that have been used in software, to either calculate GIC or to model the effect of GIC on power systems. This section will not delve much into the half-wave saturation effects of GIC on power transformers because it has been extensively studied. The underlying assumptions in each of the programs will be discussed.

2.3.1 Koen

Koen wrote software in MATLAB to calculate GIC flowing through transformers in the Southern African power network, using the Lehtinen-Pirjola method and the uniform plane wave electric field model. The Earth's conductivity was assumed to be uniform and the effect of autotransformers was neglected. The GIC flowing through one of the transformers at Grassridge power station (South Africa) was calculated and compared with the measured GIC flowing through the same transformer. The profiles of the measured GIC and the calculated GIC were similar. In some instances, the difference between the measured GIC and calculated GIC was as low as 1 %, while on the other extreme, the difference between the measured and calculated GIC was up to 110 %. Some of the reasons cited for these discrepancies included the currents that flow through the autotransformer's series winding, GIC flow through connected reactors at the same substation, the actual ground resistivity at the substation and the location of the magnetometer site relative to Grassridge substation. To compensate for the difference between the measured and calculated GIC, a scaling factor was used to adjust the calculated results. The author gave no indication of the possibility that the transformer time response to changes in the magnetic field could influence the difference between the measured and calculated GIC [31].

2.3.2 PowerWorld Simulator

PowerWorld simulator is a power system simulation software, designed to simulate high voltage power systems in the time domain. It is equipped with the ability to incorporate the flow of GIC into its load flow calculation. However, the flow of GIC can be calculated without solving the load flow because it is generally considered as a DC problem. This software also models the additional reactive power demand due to GIC [70], by using a constant to relate GIC to the increase in reactive power lost in the transformer. This is done by adding a parallel reactance to the existing shunt magnetization reactance. The magnitude of the additional reactance is determined dynamically by the software.

In PowerWorld simulator, the induced electric field is modelled in series with the transmission line. It is assumed that the reactance of the transmission lines and transformers are negligible. The major system parameters that are used are the transmission line resistance, transformer winding resistance and substation grounding resistance. For auto-transformers the series winding resistance is required. The common winding resistance for auto-transformers is only required if it is grounded. In terms of geophysical calculations, the electric field can be entered either as a uniform plane wave or a non-uniform plane wave. For the former, the uniform electric field magnitude and angle are entered for the network. Using the longitude and latitude coordinates for the transmission line, the size of electric field induced on the transmission line is calculated. For the non-uniform electric field, the point of maximum electric field is chosen. From this point, it is assumed that the electric field taper linearly down to zero over the geographic area of the network. The electric fields induced on different segments of the transmission line as it transverses different regions, is calculated using the uniform plane wave approach [32], [71].

2.3.3 Boteler *et al*

The real-time simulator for GIC developed by Boteler *et al* for the Hydro One power transmission network in Ontario uses real-time measurements of the magnetic field from a magnetic observatory [36]. Based on the conventional uniform plane wave electric field calculation method, the Fast Fourier Transform (FFT) of the magnetic field in the frequency

domain is multiplied by the Earth surface impedance in the frequency domain followed by an inverse FFT to the time domain [36, 72]. This process requires that some magnetic field data be tapered off. Since this would not be suitable for real-time GIC calculations, the authors used another approach. In this approach, the Earth surface impedance in the frequency domain is transformed to give the impulse response of the Earth in the time domain. By applying convolution, the real-time magnetic data in the time domain is convolved with the impulse response of the Earth in the time domain to give the electric field in the time domain. In this simulator, a multi-layer Earth conductivity structure was used to determine the Earth's surface impedance. Figure 2.5 provides an overview of the model.

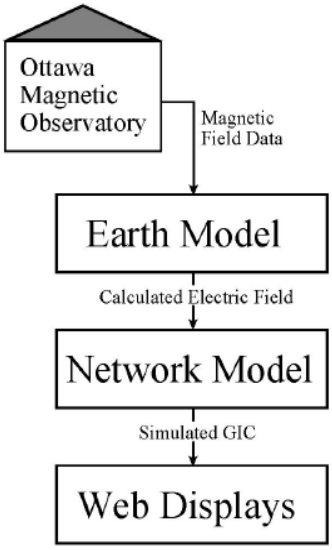

Figure 2.5 Overview of the real-time GIC simulator [36]

The NAM method discussed in section 2.2.2 was used to do the network calculations. In an earlier publication [72], the network was assumed to be purely resistive and therefore responded independently of frequency. While the software is a useful tool for GIC calculations, no mention is made of the various transformer types in the network and how these would respond to changing GIC magnitudes within the network.

2.3.4 Berge and Varma

The GIC simulator developed by Berge and Varma focuses on modelling aspects of the network, such as locating the termination points of transmission lines, autotransformers and the electric fields induced in the power system [29]. Where an autotransformer connects two buses, its winding resistance is divided between the coupling resistance and a resistance to the neutral terminal (if grounded) [8, 29]. In cases where an autotransformer connects more than one bus, the autotransformer is treated as a transmission line [29]. The NAM method [27, 57] was used for the network part of the GIC calculation. Although the assumption was made that the network could be treated as DC, the authors acknowledge that this is not *"strictly correct"* [29]. The main contributions by the authors are the elaborate method of locating transmission lines and the modelling of auto-transformers. As in other case studies, no mention was made of the transformer time response to GIC for different transformer core types.

2.4 SUMMARY OF GIC CALCULATION TECHNIQUES AND PROPOSED GIC CALCULATION TECHNIQUE

A review of calculation methods, software used for GIC calculation and comparisons of measured and calculated GIC was carried out to identify:

1. Some of the underlining assumptions about GIC calculation that have been made in the past;
2. Reasons for the differences between measured and calculated GIC;
3. Other factors which have not been rigorously investigated in the literature, that could contribute to the difference between measured and calculated GIC, and
4. The most suitable approach to be used for the method proposed in chapter 3.

The literature review pointed out the absence of any rigorous research into the effect of transformer time response, and how this varies by transformer core type, and transformer operation either as a GSU or a TT. To fill this gap in knowledge, a new method for calculating GIC is proposed in this thesis. This calculation method comprises the uniform plane wave

electric field model for deriving the electric field on the transmission line and the NAM method with the addition of the transformer time response. A uniform ground conductivity was assumed because it was used to calculate the electric field in the previous work to which the results in this thesis would be compared. Moreover for consistency in the analysis, to avoid distorting the analysis of the impact of the transformer time response to GIC, uniform ground conductivity is assumed.

CHAPTER 3

INTRODUCTION OF TRANSFORMER TIME RESPONSE INTO GIC CALCULATION

In the first section of this chapter, the formula for calculating the prospective GIC with transformer time response is derived, which takes into account the core type and operational mode (i.e. GSU or TT) of the transformer. This is followed by the derivation of the electric field induced in each transmission line and finally, a formula for calculating the prospective GIC without the transformer time response.

3.1 DERIVATION OF TRANSFORMER TIME RESPONSE

The induced electric field during geomagnetic storms causes GIC to flow through grounded transformers. Transformers are made up of primary windings, secondary windings and in some cases tertiary windings which are wound in a number of configurations. These configurations include [19]:

- Single-phase shell- or core-type
- Three-phase shell-type seven- limb core
- Three-phase shell-type conventional core
- Three-phase core-type five-limb core
- Three-phase core-form three-limb core

Figure 3.1 illustrates the flow of GIC in the transmission lines, grounded neutrals and windings or wye-connected transformers.

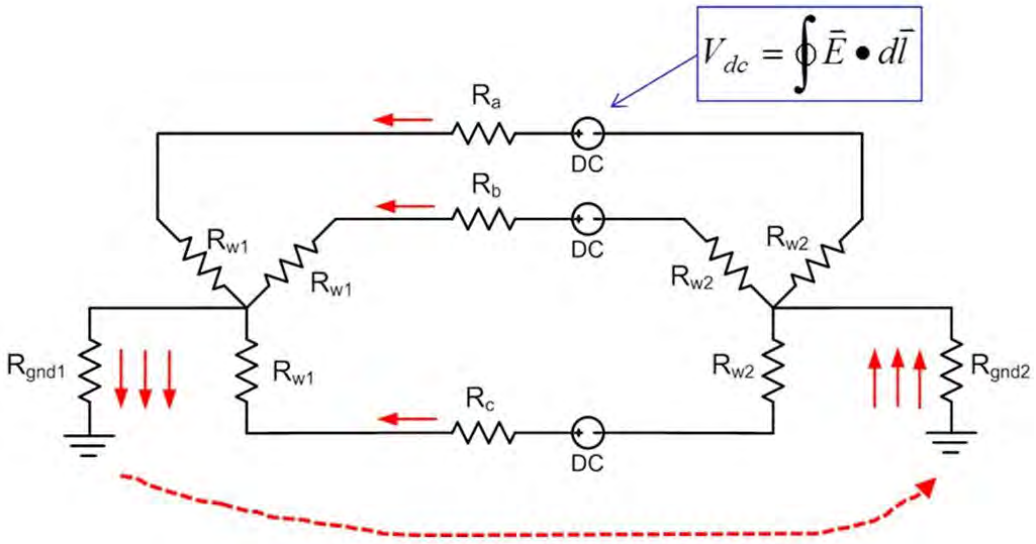

Figure 3.1 Illustration of GIC flow in transformers and transmission lines [73]

In Figure 3.1, R_w represents the transformer winding resistance, R_{gnd} represents the transformer grounding resistance: R_a, R_b, and R_c represent the resistance of each phase of the transmission line. *DC* represents the induced DC voltage in the transmission line. *E* represents the electric field and *l* represents the length of the transmission line.

Figure 3.2 illustrates the primary and secondary windings of a practical transformer. On the assumption that GIC flows through the primary side of the transformer, only the primary winding was considered. This is because GIC flow is found normally in high voltage networks. As a result, the secondary side of the transformer is either connected to a generator as a GSU by means of a delta connection or to a lower voltage network.

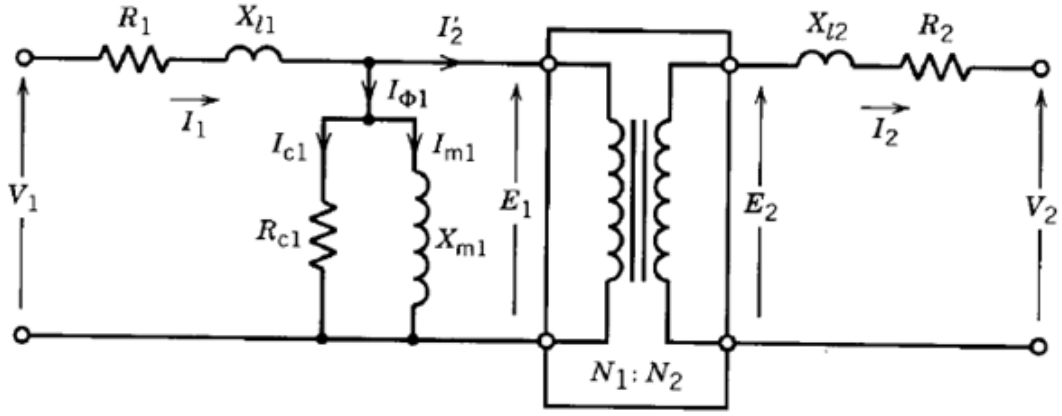

Figure 3.2 Non-ideal transformer model [74]

In Figure 3.2

V_1 = Voltage across the primary winding

X_{l1} = Leakage reactance of the primary winding

I_1 = Current in the primary winding

I_{c1} = Current due to core losses

I_{m1} = Magnetization current

X_{m1}= Magnetization reactance

R_{c1} = Core losses

V_2 = Voltage across the secondary winding

R_2 = Resistance of the secondary winding

X_{l2} = Leakage reactance of the secondary winding

I_2 = Current in the secondary winding

I'_2 = Current in the secondary winding refereed to the primary winding

R_1 = Resistance of the primary winding

If mutual inductance is neglected under GIC conditions, the secondary winding can be reduced to the self-inductance of the winding and the resistance of the winding as seen in Figure 3.3.

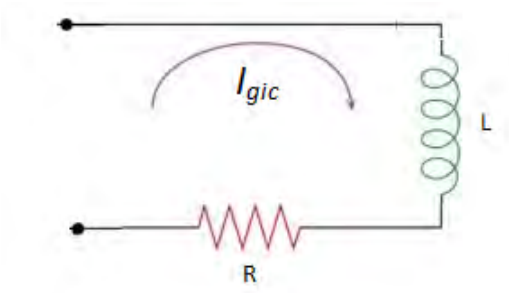

Figure 3.3 Reduced model of the primary winding

In this case of the transformer time response, the resistance *R* and *L* refers to the resistance and inductance of the transformer, respectively.

When voltage is induced in the winding on a transformer, current will flow. This flow of current is a function of the winding time constant. Equation 3.1 shows the sum of the voltages in the equivalent circuit to that in Figure 3.3 using Kirchhoff's voltage law.

$$V = RI_{gic} + L\frac{dI_{gic}}{dt} \tag{3.1}$$

Re-arranging equation 3.1 gives:

$$\frac{dI_{gic}}{dt} = \frac{-RI_{gic}+V}{L} \tag{3.2}$$

$$\frac{dI_{gic}}{dt} = \frac{-R}{L}\left(I_{gic} - \frac{V}{R}\right) \tag{3.3}$$

Multiplying both sides by dt

$$dI_{gic} = \frac{-R}{L}\left(I_{gic} - \frac{V}{R}\right)dt \tag{3.4}$$

Division of the L.H.S and R.H.S of equation 3.4 by $\left(I_{gic} - \frac{V}{R}\right)$ gives

$$dI_{gic}\left(\frac{1}{I_{gic}-\left(\frac{V}{R}\right)}\right) = \frac{-R}{L}dt \tag{3.5}$$

Integration of both sides using *x* and *y* as variables result in:

$$\int_{I_{gic(0)}}^{I_{gic(t)}}\left(\frac{1}{x-\left(\frac{V}{R}\right)}\right)dx = \frac{-R}{L}\int_0^t dy \tag{3.6}$$

$$ln\frac{I_{gic(t)-V/R}}{I_{gic(0)}-(V/R)} = \frac{-R}{L}t \tag{3.7}$$

$$\frac{I_{gic(t)}-(V/R)}{I_{gic(0)}-(V/R)} = e^{\left(\frac{-R}{L}\right)t} \tag{3.8}$$

Solving for $I_{gic(t)}$,

$$I_{gic(t)} = \frac{V}{R} + \left(I_{gic(0)} - \frac{V}{R}\right)e^{-\frac{R}{L}t} \tag{3.9}$$

If the initial GIC, $I_{gic(0)}$ is set to zero, then,

$$I_{gic(t)} = \frac{V}{R}\left(1 - e^{-\frac{R}{L}t}\right) \quad (3.10)$$

Let $\frac{L}{R} = \tau$,

If the prospective GIC without the transformer time response is $\frac{V}{R} = I_{gic(p)}$, then

$$I_{gic(t)} = I_{gic(p)}\left(1 - e^{-\frac{1}{\tau}t}\right) \quad (3.11)$$

The prospective GIC without the transformer time response is the maximum GIC that can be obtained for a transformer in a substation for a specific electric field induced in the transmission lines.

Using the transformer X/R ratio,

$$X/_R = \frac{2\pi fL}{R} \quad (3.12)$$

If the *X/R* ratio is represented by W,

then,

$$W = \frac{X}{R} = \frac{2\pi fL}{R} \quad (3.13a)$$

$$L = \frac{WR}{2\pi f} \quad (3.13b)$$

Figure 3.4 illustrates the relationship between the electric field and the prospective GIC without and with transformer time response.

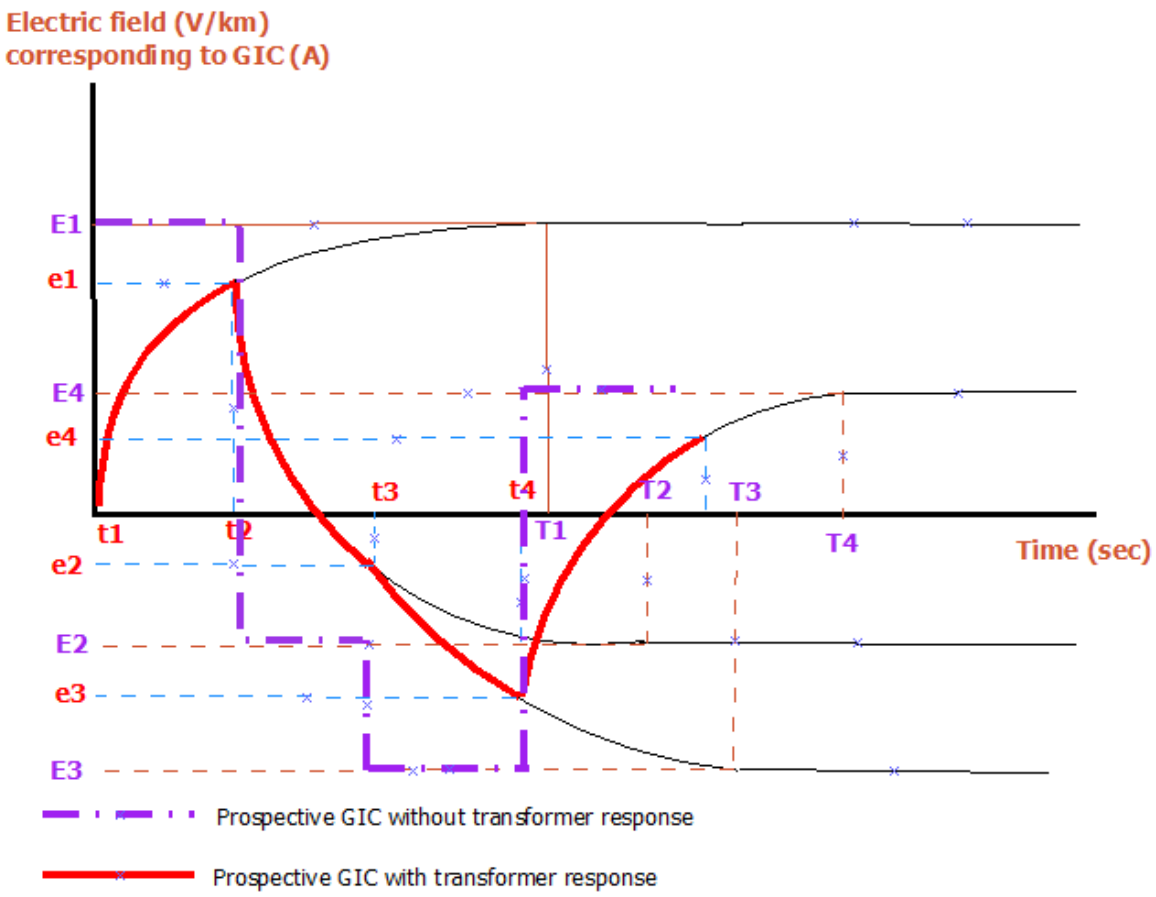

Figure 3.4 Different GIC values over time, transformer time response and the time when the GIC value changes

In Figure 3.4, *E* is the calculated induced nodal voltage across the transformer winding which corresponds to a prospective GIC value without the transformer time response flowing through the transformer after time *T,* which is the transformer response time. The prospective GIC calculated with the transformer time response at the time *t*, when the field changes, corresponds to *e*.

The purple curve in Figure 3.4 shows the prospective GIC profile through a transformer without taking the time response into account. The red curve shows the prospective GIC profile when the time response is taken into account in the calculation algorithm.

If *T> t* (*i.e., the transformer response time is greater than the* time at which the GIC value changes), then the GIC in the transformer will not get to its final value.

If *T< t* (*i.e. the transformer response time is less than the* time at which the GIC value changes), then the GIC in the transformer will always get to its final value over T.

As illustrated in Figure 3.4, actual GIC values are dependent upon past GIC values as a function of time. For example, at time = t_2, the GIC flowing through the transformer is the sum of the GIC at t_1 and the difference between the effect of the prospective GIC value at t_2 and the prospective GIC with transformer time response at t_1. This is summarized in equation 3.14.

$$I_{gic\_a(t)} = I_{gic\_a(t-1)} + \left[I_{gic\_p(t)} - I_{gic\_a(t-1)} \right] (1 - e^{\frac{-t_x}{T}}) \quad (3.14)$$

where $I_{gic\_a(t)}$ is the prospective GIC with transformer time response through substation *k* at time *t*, $I_{gic\_a(t-1)}$ is prospective GIC with transformer time response through substation *k* at time *t-1,* $I_{gic\_p(t)}$ is the prospective GIC without transformer time response at time *t,* t_x is the time difference between t_n and t_{n-1} . *T* is the transformer response time.

T is not necessarily equivalent to τ as is the case in a simple LR circuit. In this case, other networks factors may influence the value of T such as other transmission lines and transformers connected to the same bus. As *T* may not be readily available, laboratory tests and PSCAD simulations were used to derive empirical formulae for the response time of various transformer core structures and operational modes as a function of the magnitude of the prospective GIC as will be discussed in chapter 5 and 6.

3.2 DERIVATION OF THE MAGNITUDE OF ELECTRIC FIELD INDUCED ON THE TRANSMISSION LINE

The uniform plane wave electric field model described in chapter 2 gives the x and y components of the electric field induced on the network in V/km. This section describes the calculation of the magnitude of the electric field induced on a transmission line as a function of the transmission line alignment to the electric field. Figure 3.5 shows the induced electric field calculation for line L_{ij} between substation *i* and substation *j*.

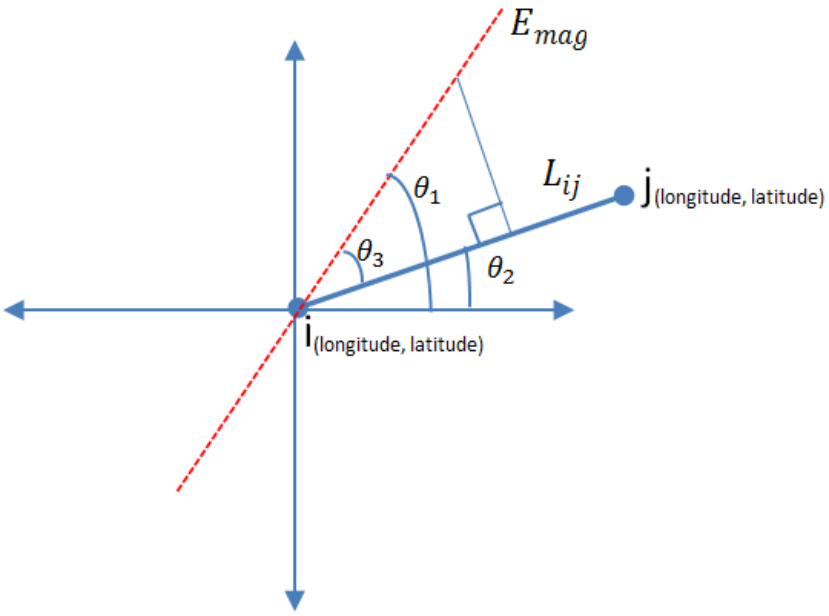

Figure 3.5 Calculation of the induced electric field on a transmission line

From Figure 3.5, the magnitude of the electric field is calculated from the *x* and *y* components as shown in equation 3.15.

$$E_{mag} = \sqrt[2]{{E_x}^2 + {E_y}^2} \tag{3.15}$$

E_{mag} is the magnitude of the electric field. θ_1 is the angle between the electric field and the reference axis, which is given as:

$$\theta_1 = \tan^{-1}\left[\frac{E_y}{E_x}\right] \tag{3.16a}$$

Using the GPS coordinates of the substation in WGS84 format [75], θ_2, the angle between the transmission line and the reference axis, is calculated by calculating the azimuth of point *j* from *i*. Although azimuths are generally calculated with north as the reference, here the reference is conveniently chosen as the horizontal (90^0). This is done because the angle difference between θ_2 and θ_1 is needed. The θ_2 angle is given as:

$$\theta_2 = cos^{-1}\left[\sin(i_{lat}) * \sin(j_{lat}) + \cos(i_{lat}) * \cos(j_{lat}) * \cos(j_{lon} - i_{lon})\right] * R \tag{3.16b}$$

where R = 6371 km is the radius of the Earth.

The absolute value of the difference between θ_1 and θ_2 is θ_3, which is the angle between the resultant electric field and the transmission line.

$$\theta_3 = |(\theta_2 - \theta_1)| \quad (3.17)$$

Therefore, the electric field E_{ij} induced on line L_{ij} is:

$$E_{ij} = E_{mag} * \cos\theta_3 \quad (3.18)$$

The induced voltage on the line is derived from the electric field as shown in equation 3.19.

$$V_{ij} = E_{ij} * l \quad (3.19)$$

Where l is the length of the line.

3.3 DERIVATION OF THE PROSPECTIVE GIC WITHOUT TRANSFORMER TIME RESPONSE

This prospective GIC value (the maximum GIC that can be obtained at a substation for a specific electric field induced on the network) may be calculated by means of the NAM method [26, 27].

To illustrate, a small three-bus network is shown in Figure 2.2 is reproduced here as Figure 3.6 for convenience. In the Figure, the induced electric fields on the lines are represented as E_{ij} and E_{jk}. The per-phase nodal resistances R_i, R_j and R_k represent the resistances at each substation per phase.

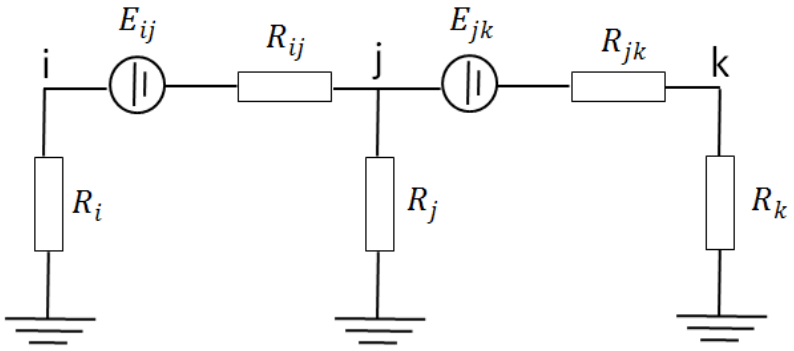

Figure 3.6 Three-bus network with induced electric field

Using Norton's theorem, the electric field (as calculated in equation 3.18) induced in line L_{ij} with resistance R_{ij} is converted to an equivalent current source h_{ij} in parallel with the admittance of the line y_{ij} as shown in Figure. 3.7. These are defined in equation 3.20 and 3.21.

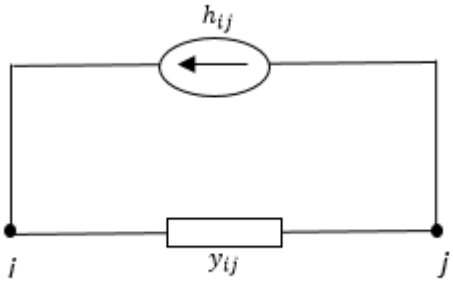

Figure 3.7 Norton's current equivalent

h_{ij} and y_{ij} in Figure 3.7 are defined as:

$$h_{ij} = \frac{E_{ij}}{R_{ij}} \tag{3.20}$$

$$y_{ij} = \frac{1}{R_{ij}} \tag{3.21}$$

The summation of the current equivalents at node$j$ is represented by equation 3.22.

$$H_j = \sum_{i \neq j}^{n} h_{ji} \tag{3.22}$$

From the equation above, summing up the equivalent currents at each node in Figure 3.6 are:

$$H_i = h_{ij}$$

$$H_j = h_{ji} + h_{jk} \quad (3.23)$$

$$H_k = h_{kj}$$

The total current flowing through line i, j is:

$$i_{ij} = h_{ij} + (v_i - v_j)y_{ij} \quad (3.24)$$

where v_i and v_j are the voltage at node i and node j respectively.

The total current flowing through node i is:

$$i_i = v_i . y_i \quad (3.25)$$

Since there is only one line that is connected to bus i, the nodal current at bus i is the same as the line current i_{ij} in equation 3.26.

$$i_i = i_{ij} \quad (3.26)$$

Substitution of the R.H.S of equation 3.24 into equation 3.26 gives:

$$i_i = h_{ij} + (v_j - v_i)y_{ij} \quad (3.27)$$

Similarly, at bus j, the sum of the line currents connected to it, is given in equation 3.28.

$$i_j = i_{ij+} i_{jk} \quad (3.28)$$

Substitution of the R.H.S of equation 3.24 and i_{jk} into equation 3.28 gives:

$$i_j = h_{ij} + (v_j - v_i)y_{ij} + h_{jk} - (v_j - v_k)y_{jk} \quad (3.29)$$

At bus k, the only current flowing through this node is the line current i_{jk} :

$$i_k = i_{jk} \quad (3.30)$$

Substituting for i_{jk}, gives:

$$i_k = h_{jk} - (v_k - v_j)y_{jk} \tag{3.31}$$

Replacement of the L.H.S of equation 3.27, 3.29 and 3.31 with the R.H.S of equation 3.25 gives:

$$v_i.y_i = h_{ij} + (v_j - v_i)y_{ij} \tag{3.32}$$

$$v_j.y_j = h_{ij} + (v_j - v_i)y_{ij} + h_{jk} - (v_j - v_k)y_{jk} \tag{3.33}$$

$$v_k.y_k = h_{jk} - (v_k - v_j)y_{jk} \tag{3.34}$$

Re-arranging the above three equations

$$h_{ij} = v_i.y_i - (v_j - v_i)y_{ij} \tag{3.35}$$

$$h_{ij} + h_{jk} = v_j.y_j - (v_j - v_i)y_{ij} + (v_j - v_k)y_{jk} \tag{3.36}$$

$$h_{jk} = v_k.y_k + (v_k - v_j)y_{jk} \tag{3.37}$$

The three equations above are written in matrix form as shown in equation 3.38

$$\begin{bmatrix} h_i \\ h_{ij} + h_{jk} \\ h_{jk} \end{bmatrix} = \begin{bmatrix} y_{i+}y_{ij} & -y_{ij} & 0 \\ -y_{ij} & y_j + y_{ij} + y_{jk} & -y_{jk} \\ 0 & -y_{jk} & y_{jk} + y_k \end{bmatrix} * \begin{bmatrix} v_i \\ v_j \\ v_k \end{bmatrix} \tag{3.38}$$

Equation 3.38 is summarised as shown in equation 3.39.

$$[H] = [Y][V] \tag{3.39}$$

where $[Y]$ is the network admittance matrix, $[V]$ is the nodal voltage matrix and $[H]$ is the matrix of Norton's currents (see Figure 3.7).

From the equation 3.39, the nodal voltage is determined as shown below,

$$[V] = [Y]^{-1}[H] \tag{3.40}$$

In equation 3.40, $[Y]^{-1}$ is the inverse of [Y] as is calculated as shown in equation 3.41.

$$[Y]^{-1} = \frac{1}{\det Y}(\text{adjoint of Y}) \tag{3.41}$$

When substituting equation 3.40 in equation 3.25, the nodal GIC current is derived as,

$$[i] = [y_0][Y]^{-1}[H] \tag{3.42}$$

$$= \left[I_{gic\_p}\right] \tag{3.43}$$

In equation 3.42, $[i]$ represents a matrix of the prospective GIC without the transformer time response (I_{gic_p}) at each node. When substituting equation 3.43 into equation 3.14, the prospective GIC taking into account the transformer time response at a substation as a function of time will be:

$$I_{gic\_a(t)} = I_{gic\_a(t-1)} + \left[I_{gic\_p(t)} - I_{gic\_a(t-1)}\right](1 - e^{\frac{-t_x}{T}}) \tag{3.44}$$

In the equation 3.44, t_x has been previously defined as the time difference between t_n and t_{n-1} in equation 3.14.

A significant input to equation 3.44 is *T* which is the response time of the transformers in a closed GIC loop. Laboratory test for the response time of various transformer core types to GIC is necessary to give an indicative value of *T*. Computer simulation with PSCAD was used to validate the transformer time response to GIC. Following this, the response time of larger power transformers in the MVA range to GIC was characterised, using piecewise linear equations discussed in section 6.3.

The following equations are used to derive the matrix format of equation 3.44 for a network of n substations and m GIC time steps.

Let the first term in equation 3.44 be represented by a column matrix $[F_1]$ with dimension $n\ x\ 1$, where $[\ I_{gic\_a(t-1)}]$ is a matrix with dimension $n\ x\ 1$ with elements defined in equation 3.45,

$$I_{gic\_a(t-1)_{(i,j)}} = \begin{cases} I_{gic\_a(i,(t-1)},\ 1 < i < n,\ 1 < t \leq m \\ 0,\ 1 < i < n,\ t = 1 \end{cases} \tag{3.45}$$

Let the second term $\left[I_{gic\_p(t)} - I_{gic\_a(t-1)} \right] (1 - e^{\frac{-t_x}{T}})$ in equation 3.44 be represented in matrix form by $([F_2] - [F_3]) \times [F_4]$.

where the elements of $[F_2]$ with dimension $n\ x\ 1$ are derived in equation 3.43, the elements of $[F_3]$ are defined in equation 3.45.

If the factor $(1 - e^{\frac{-t}{T}})$ in equation 3.44 is represented in matrix form as $[F_4]$, then:

$$[F_4] = [1] - [F_5] \tag{3.46}$$

where $[F_5]$ is a square matrix with dimension $n\ x\ n$ such that:

$$f_{5(i,j)t} = \begin{cases} e^{-\frac{t}{T_i}},\ i = j \\ 0,\ i \neq j \end{cases} \tag{3.47}$$

In the equation 3.47, i and j represents the row and column reference respectively. T_i represent the time response of the transformers in substation i . The dimension of the identity matrix $[1]$ in equation 3.46 is $n\ x\ n$. Therefore, the dimension of $[F_4]$ is $n\ x\ n$.

Therefore for a network with n substations, the prospective GIC with transformer time response can be derived as:

$$[I] = [F_1]^T + ([F_2]^T - [F_3]^T) \times [F_4] \tag{3.48}$$

where the superscript T means the transpose of the matrix.

CHAPTER 4

LABORATORY TEST PROTOCOL AND COMPUTER SIMULATION

In this chapter, the protocol that was used for the transformer time response test is outlined. The test protocol has two sections. The first part of the protocol was developed by Chisepo [76] as a standard procedure for testing transformer response to GIC in terms of reactive power, active power, harmonics and saturation. The second part of the test protocol describes the method to determine the range of DC current values that are injected into the transformer to emulate GIC. Tests were conducted on three types of transformer core structures namely, bank of single-phase transformers referred to as 3(1P-3L), three-phase three-limb referred to as 3P-3L and three-phase five-limb referred to as 3P-5L. These three core structures were selected to test the algorithm because they represent the most common types of transformers used in power networks.

Section 4.1 outlines the test protocol and describes the laboratory equipment that was used. The PSCAD simulations for both VA-rated and MVA-rated transformers are outlined in section 4.3.

4.1 TEST PROTOCOL

1. Determine the operating voltage at which the harmonics and distortion in the transformer complies with IEEE standard 1459 [77].

2. Determine the magnetization current (I_{mag}) of the transformer.

3. Determine the short circuit and open circuit parameters of the transformer.

   Tests conducted by Chisepo [76] on the same set of transformers determined these parameters. Tables 4.1 to 4.3 give the transformer ratings and parameters for the open and short circuit tests. The transformer inductance is calculated using equation 4.1.

$$L = \frac{X_{pu} \times V^2}{2 \times \pi \times f \times S} \quad (4.1)$$

   where L is the inductance, X is the reactance, V is the voltage, S is the power base (rating), f is the frequency (50 Hz).

4. Calculate the load current to DC current ratio k_{LD} given in equation 4.2.

$$k_{LD} = \frac{I_r}{I_m} \text{ (pu)} \quad (4.2)$$

   where I_r is the rated line current and I_m is the magnetization current.

5. Calculate the DC current in pu given in equation 4.3.

$$I_{pu} = \frac{I_{dc}}{I_m} \text{ (pu)}$$

   I_{dc} coupled with the AC current should not exceed the rating of the transformer.

6. Inject the DC current into the transformer neutral, such that the DC current per phase follows the inequality $1 \leq I_{pu} \leq k_{LD}$.

7. A NI data acquisition set was used to record the time taken for the DC current to rise from 0.5 pu to I_{pu}, and the time taken for the DC current to drop from $I_{pu}$to 0.5 pu. A value of 0.5 pu was chosen since it is relatively small compared to the value of the

magnetization current of the transformer. A sample of the NI record of the rise time is shown in Appendix P.

Table 4.1 Table showing the parameters of each of the transformer that formed the 3(1P-3L) transformer bank

Voltage rating	Power rating	Inductance	I_{mag}	Req	Xeq	No Load Losses
120/230 V	100 VA	15 mH	55 mA	0.0673 p.u.	0.0091 p.u	0.0229 p.u.

Table 4.2 Table showing the parameters of the 3P-3L transformer

Voltage rating	Power rating	Inductance	I_{mag}	Req	Xeq	No Load Losses
120/230V	100 VA	158 mH	80 mA	0.0009 p.u.	0.0328 p.u.	0.0094 p.u

Table 4.3 Table showing the parameters of the 3P-5L transformer

Voltage rating	Power rating	Inductance	I_{mag}	Req	Xeq	No Load Losses
120/230V	100 VA	74 mH	74 mA	0.0154 p.u.	0.0049 p.u	0.0208 p.u.

4.2 LABORATORY TEST SETUP

An induction generator was used as a three-phase power supply for the setup. It was chosen to provide galvanic isolation to the laboratory setup and to ensure that the quality of the AC supply was guaranteed. Bench scale source and load transformers were connected with copper wires rated at 10 A. The primary side of the source transformer was connected in delta to avoid the need for a neutral connection, while the transmission side of the source transformer and both sides of the load transformer were connected in wye with grounded neutrals. A programmable logic controller (PLC) unit was used to control the DC injection in

the transmission line through the neutrals of the transformer, while the NI data acquisition set was used to record the voltage and current signals in real time. A Yokogawa power meter was used to monitor all the system voltage and currents in real time to pick up faults, erroneous conditions and view the system response in real time. Figures 4.1 and 4.2 show the laboratory setup.

Figure 4.1 Laboratory setup outside the safety fence showing control and data logging systems

Figure 4.2 Laboratory setup inside the safely fence showing transformers and loads

4.2.1 Power supply

An induction generator supplied three-phase power to the source transformer.

4.2.2 Source and load transformers

The specifications of these transformers, manufactured by Ellof's transformers, are outlined in Table 4.1 to Table 4.3.

4.2.3 Load

The load connected to the secondary side of the load transformer depends on the operational mode of the transformer under test. For example, GSU transformers run at 95% load while transmission transformers operate at about 45% load. The load used in this test is purely resistive. Each resistor was rated at 100 W. During the test, a 230 V fan was used as a forced convection mechanism to cool the resistor banks.

4.2.4 Transformer

Three transformer core structures were investigated, 3(1P-3L), 3P-3L and 3P-5L. In each test, the source and load transformer had the same core structure. The ratings of the

transformers are in Tables 4.1 to 4.3. Figure 4.3 shows the three transformer core structures that were tested.

Figure 4.3 From left to right in order of appearance, single phase, three-phase five-limb and three-phase three-limb transformers [76]

4.2.5 Real-time data logging

Hall Effect current probes were used to measure the current. The voltage output signal from the current probes were connected to the NI 9225 32 bits C Series analog input module in the transformer neutral. From the range of data acquisition devices available, NI cDAQ - 9174 chassis was found suitable. It is a 32-bits 4-slot chassis designed for small portable, mixed-measurement test systems [78].

4.2.6 Timing control

A PLC, DVPEN01-SL manufactured by Delta Electronics [79] was used to control the time at which the DC current rises or fall from 0.5 pu to the set point. Specifications of the PLC are given in Appendix A.

4.2.7 DC Voltage source

A 12V / 7.2Ah DC battery and several 1.5 V DC touch cell batteries were used to supply the required DC voltage for each test.

4.3 PSCAD SIMULATION

PSCAD/EMTDC version X4 developed by Manitoba Hydro was used for the simulation. The purpose of the simulation was to:

1. Replicate the transformer time response to GIC laboratory test with PSCAD.
2. Compare the results obtained with PSCAD to those of the laboratory test.
3. Develop a relationship between the results with PSCAD and the laboratory test.
4. Scale up the test to the MVA-range using the results from 2 and 3 above.

The results of the transformer time response test in the MVA range are fed directly into the algorithm developed in chapter 3. This is described in chapter 7.

4.3.1 Saturation and transformer model in PSCAD

The DC current that will be injected in the transformers during the laboratory test and in the PSCAD simulation will range from values that will not drive the transformer into saturation to values that will see the transformer go into saturation. The general transformer model in PSCAD version X4 models saturation [80]. The model takes into consideration that as a transformer gets into saturation, the inductance of the windings reduces [81] while the magnetization current increases.

In most applications, saturation characteristics are modelled using piecewise linear inductance with two slopes, one for the linear region and the other for the air-core region with current injection at one terminal of the transformer [82]. However, when such a terminal is connected to a strong AC source, the secondary voltage is not distorted. When the saturation current is injected into the secondary winding, the distortion increase [80]. In PSCAD, saturation is modelled by current injection at both terminals of the transformer. The injected current in each terminal is calculated to be mathematically equivalent such that the effect is as though the current was only injected in the magnetisation branch in the transformer model. This approach not only retains computational efficiency but over comes some of the setbacks of only injecting the saturation current in either the primary or the secondary side of the transformer (see Figure 4.4) [80].

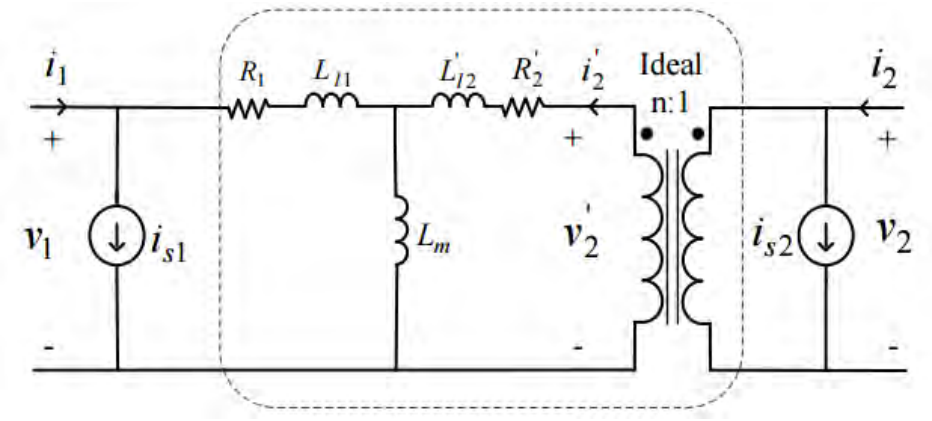

Figure 4.4 Mathematically equivalent model of transformer electric circuit [80]

In Figure 4.4, i refers to current, v refers to voltage, R refers to resistance, L refers to inductance. Subscript 1 refers to the primary side, 2 refers to the secondary side, s refers to saturation and m refers to magnetization. The transformer turns ratio is n. The primed variables are values referred to the primary side from the secondary side. Figure 4.5 shows the implementation in PSCAD, the complete mathematical model is available in [80].

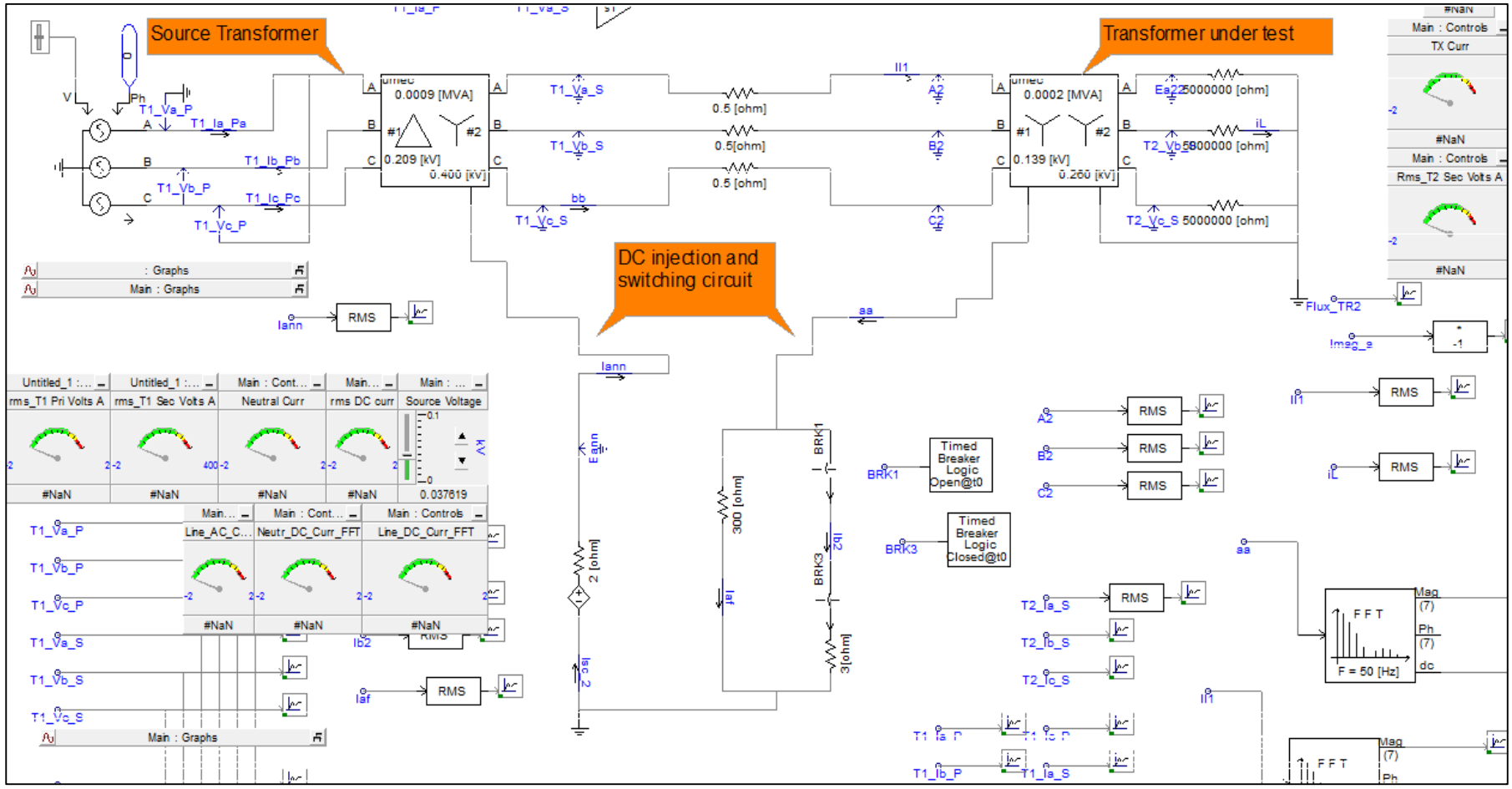

Figure 4.5 Transformer time response to GIC test circuit in PSCAD

CHAPTER 5

LABORATORY TEST FOR TRANSFORMER TIME RESPONSE

In this chapter, two major transformer categories were tested namely GSU and TT. The former is typically operated at full load, which in most cases is around 95 % of its rated capacity [83]. These transformers are built to carry full load continuously. On the other hand, TTs operate normally around 40 % to 45 % load as more than one transformer is usually connected in parallel. Each TT rating may go up to the power rating of the transmission line connected to it [83].

Based on specific application needs, each of these categories may contain the following core structures: 3(1P-3L), 3P-3L and 3P-5L.

In order to investigate the time response of these transformer core types, three load conditions were considered: 40 % load to represent the TTs, 80 % load to represent a GSU under light load conditions and 95 % load to represent GSUs under normal load conditions. The maximum value of the y-axis in all the graphs is fixed so that the graphs are easily compared.

5.1 BENCH SCALE 300 VA TRANSFORMER

To establish the initial time response of the transformer, a no-load test was conducted. During the no-load test, the transformer under test (TUT) was supplied by the source transformer. The secondary side of the TUT was disconnected from the load bank. Figure 5.1 shows the time response profile of the three core structures to the range of DC currents injected at no-load.

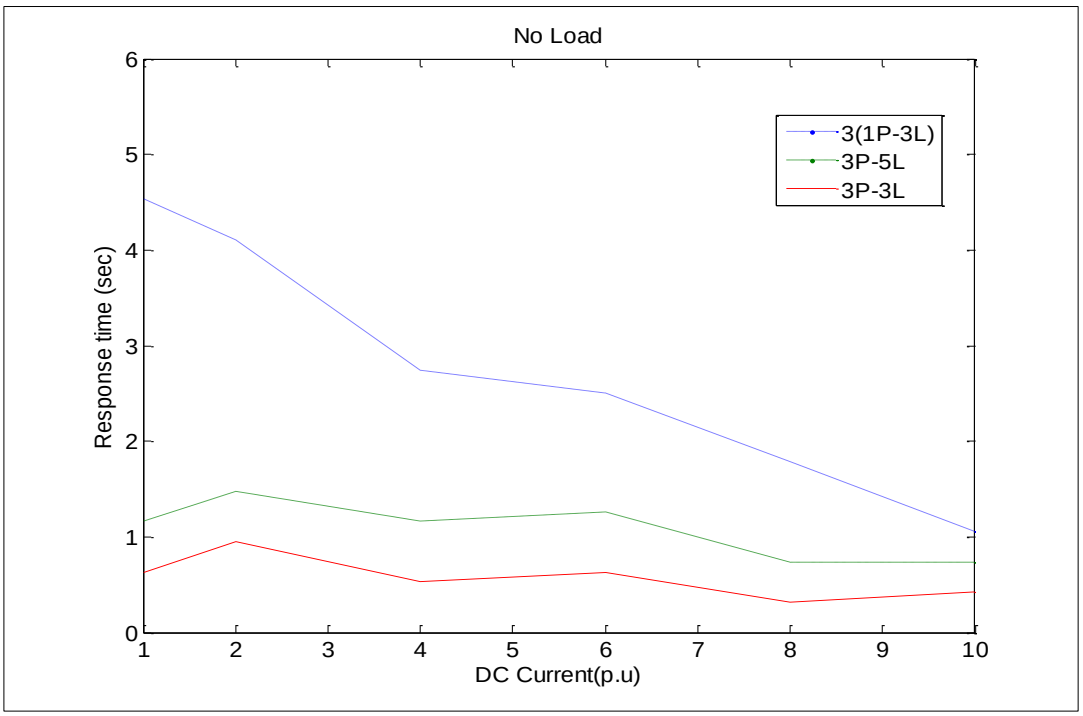

Figure 5.1 Response time by practical test of the transformers with no load

In this test, the 3P-3L transformer has the shortest response time, followed by the 3P-5L and the 3(1P-3L) transformer.

For the three cores, the longest response time was between 1.0 pu and 2.0 pu DC current. At 6.0 pu DC current, a second peak occurred which corresponded to a point where the response time was longer. This was again consistent for the three core structures.

The implication of these results is that the 3P-3L transformer will allow the flow of GIC through the windings of the transformer over a shorter length of time. During GMDs leading to higher GIC, the prospective GIC without or with the transformer time response will likely be the same.

Figure 5.2 shows the response time of the three core structures to the range of DC current injected at 40 % load.

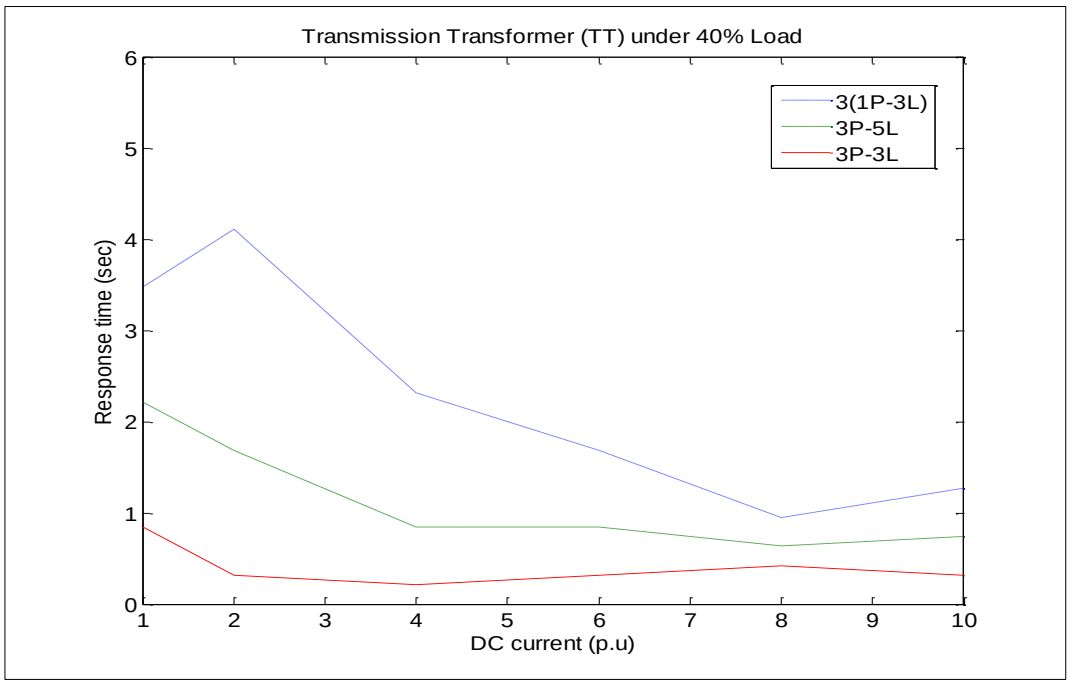

Figure 5.2 Response time of the transformer under 40 % load

In Figure 5.2, the response time for the 3P-3L and 3P-5L core decreased between 1.0 pu and 2.0 pu DC which is opposite to the trend in the case where the transformers were not loaded. However, between 2.0 pu and 10.0 pu, the trend in the response times for the three core structures remained fairly similar, except for the slight increase in response time in the 3(1P-3L) core type between 9.0 pu and 10.0 pu. For the 40 % load test, there is a 30 %, 17 % and 6 % average reduction in response time for the 3P-3L, 3(1P-3L) and 3P-5L transformers respectively. This implies that for transmission transformers the 3P-3L transformer core structure has the highest load sensitivity.

Figure 5.3 shows the response time of the three core structures to the range of DC injected at 80 % load representing GSUs under light load conditions. At 1.0 pu DC, the response time is longer than for the TT test. Above 1.0 pu, the response time is shorter than the response time of TTs. Only the 3(1P-3L) transformer had a second peak (corresponding to a long response time) at 6.0 pu DC.

Figure 5.4 shows the time response of the three core structures to the range of DC injected at 95 % load representing GSUs under full load conditions. In Figure 5.4, the core with the shortest response time is consistent with the initial condition test.

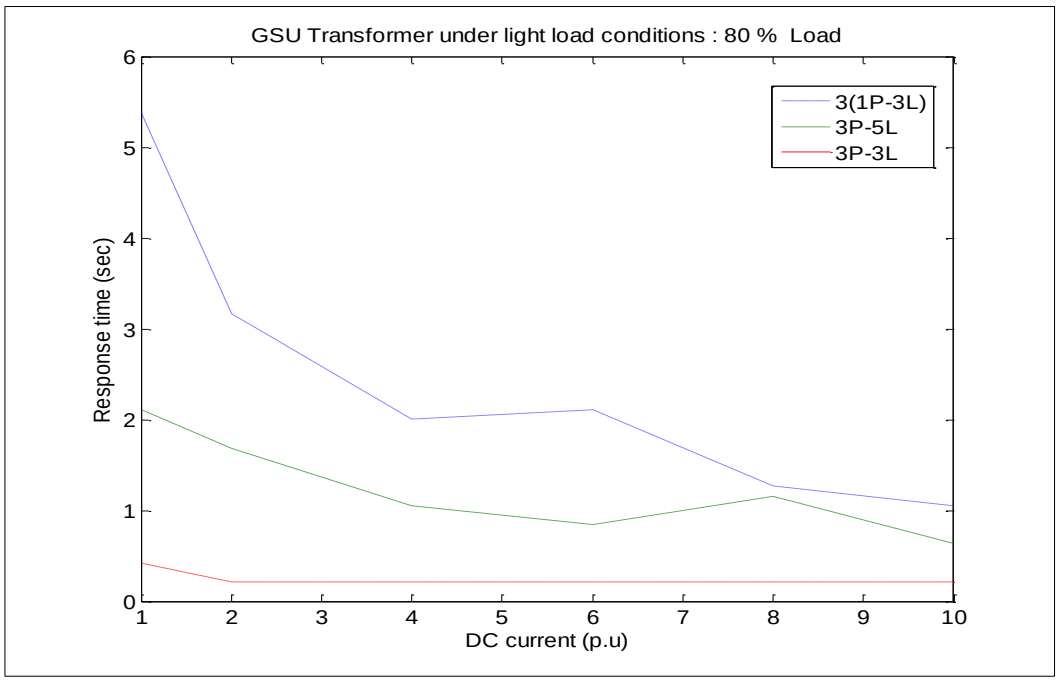

Figure 5.3 Response time for GSU transformer under light load conditions

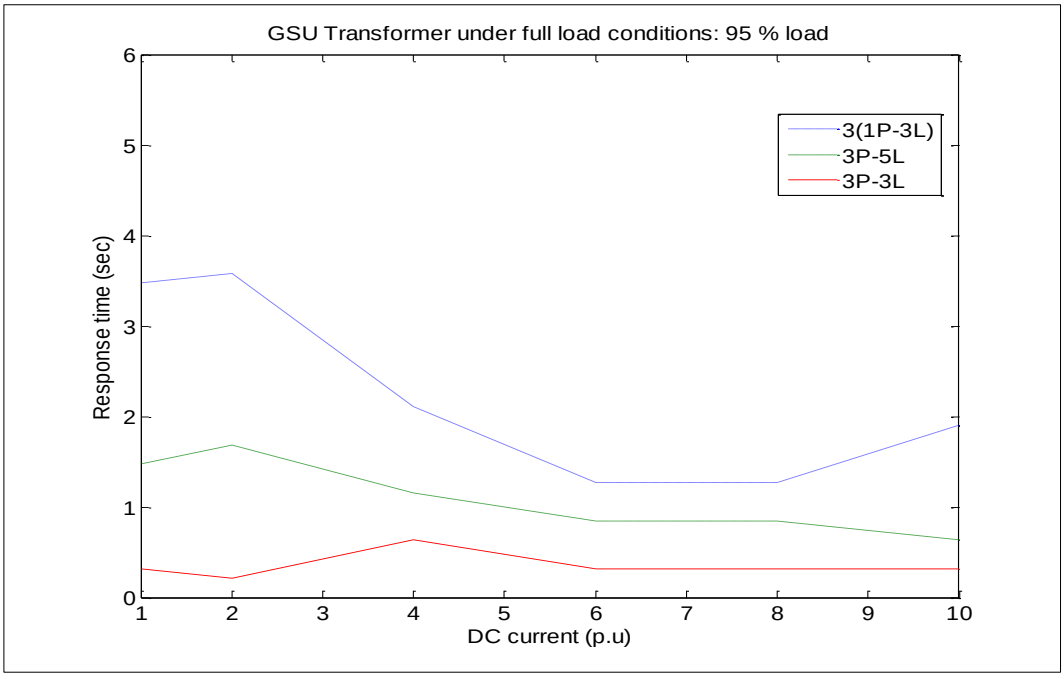

Figure 5.4 Response time for GSU transformer under full load conditions

This implies that the time taken for GIC to flow through the windings of a 3P-3L transformer at 95 % load will be shorter in comparison with the other transformer core structures.

Relating this to equation 3.40, the prospective GIC calculated with the transformer time response will be close to the prospective GIC without the transformer response in 3P-3L transformers. The variation in response time seems to be larger across the three cores for DC current values less than 4.0 pu. As the transformer is driven into deep saturation by the DC current, the response time of the 3P-3L transformer remains fairly constant while the response time of the 3(1P-3L) and 3P-5L transformers diverges between 8.5 pu and 10.0 pu.

Considering that the three core types have exactly the same power and voltage rating, the longer response time of the 3P-5L and 3(1P-3L) transformers may be attributed to the following reasons. 3P-3L transformers have lower magnetization impedance and higher magnetization current when compared to the 3P-5L and 3(1P-3L) transformers [84]. Furthermore, 3P-3L transformers do not provide a zero sequence flux path. Due to the absence of external limbs as is the case with shell type 3(1P-3L) and 3P-5L transformers, when the 3P-3L transformer gets into saturation, the leakage flux increases considerably when compared to the other two cores. This behaviour changes the inductance of the windings [85], in this case, it reduces the inductance of the windings [81].

The following can be inferred from the results presented in this chapter:

A 3P-3L transformer will permit the flow of GIC through the windings of the transformer over a shorter length of time. During GMDs leading to higher GIC, the difference between the prospective GIC with or without the transformer time response will be minimum.

At lower DC values, e.g. 1.0 pu, the flow of DC in GSU type transformers takes a shorter length of time when compared to transmission type transformers. This implies that the difference between the prospective GIC without or with the transformer time response in GIC loops around GSUs is more likely to be less than compared to TTs. Thus, for all three core structures, the transformer time response to GIC is dependent upon the mode of operation (either as a TT or GSU) and the core type. These new findings open the way for further research in this area. In fact, the response time should be an item that could be included in test protocols when tests are conducted on large transformers.

CHAPTER 6

PSCAD SIMULATION OF TRANSFORMER TIME RESPONSE TO GIC

In this chapter, section 6.1 presents results from the PSCAD simulation with the bench scale 300 VA transformer models. The aim of the PSCAD simulation is to investigate whether PSCAD can model the laboratory test setup to produce similar results. Section 6.2 compares results obtained in section 5.1 (laboratory test) and section 6.1 (PSCAD simulation) to determine how well the results from the PSCAD simulation correlate with the results of the laboratory test. The power transformer models in the PSCAD simulation are uprated to 500 MVA which is more representative of power transformers used in main transmission systems. The PSCAD simulation results for 500 MVA power transformers are presented in section 6.3. Finally, the response time for the three transformer types are compared in section 6.4.

6.1 BENCH SCALE 300 VA TRANSFORMERS

In PSCAD, modelling a bank of three single phase transformers can be achieved in one of two ways. Either by wiring three single-phase transformer models together 3(1P-3L) or using a single model called a three-phase bank. The former of the two options was used in this thesis because it best represents the test model in chapter 5. However, when the three-phase bank transformer models where used, the response time dropped significantly to between 0.15 and 0.3 second from an average of 10 seconds. This contradictory result indicates that both PSCAD models do not yield the same time response, although similar in terms of the saturation aspect that is included in both models as explained in section 4.3.1.

As in the laboratory test, the first simulation is the no-load (initial condition) test. This was followed by the, TT, GSU light load condition and GSU typical load condition tests. Although the laboratory test and PSCAD simulations were carried out with DC current values ranging

from 1 pu to 10 pu, a PSCAD simulation was run with DC current values ranging from 0 pu to 1 pu (see Figure 6.1). The aim was to investigate the response of the different transformer core types to DC current below the lower limit of the range of DC injections.

Only the results for the transmission transformer are shown here in Figure 6.1 because the results are similar to those of the GSU transformer. For a transmission level transformer presumably above 400 MVA, 400 kV and the assumption that its magnetization current is less than 1 % of its rated current, the magnetization current will be 6 A. GIC corresponding to 1 pu will then be 6 A, which is small compared to the rated transformer current. This result indicates that the lower end (i.e., 1.0 pu) of the range of DC currents injected in the transformers in determining the response time of the transformer core is adequate.

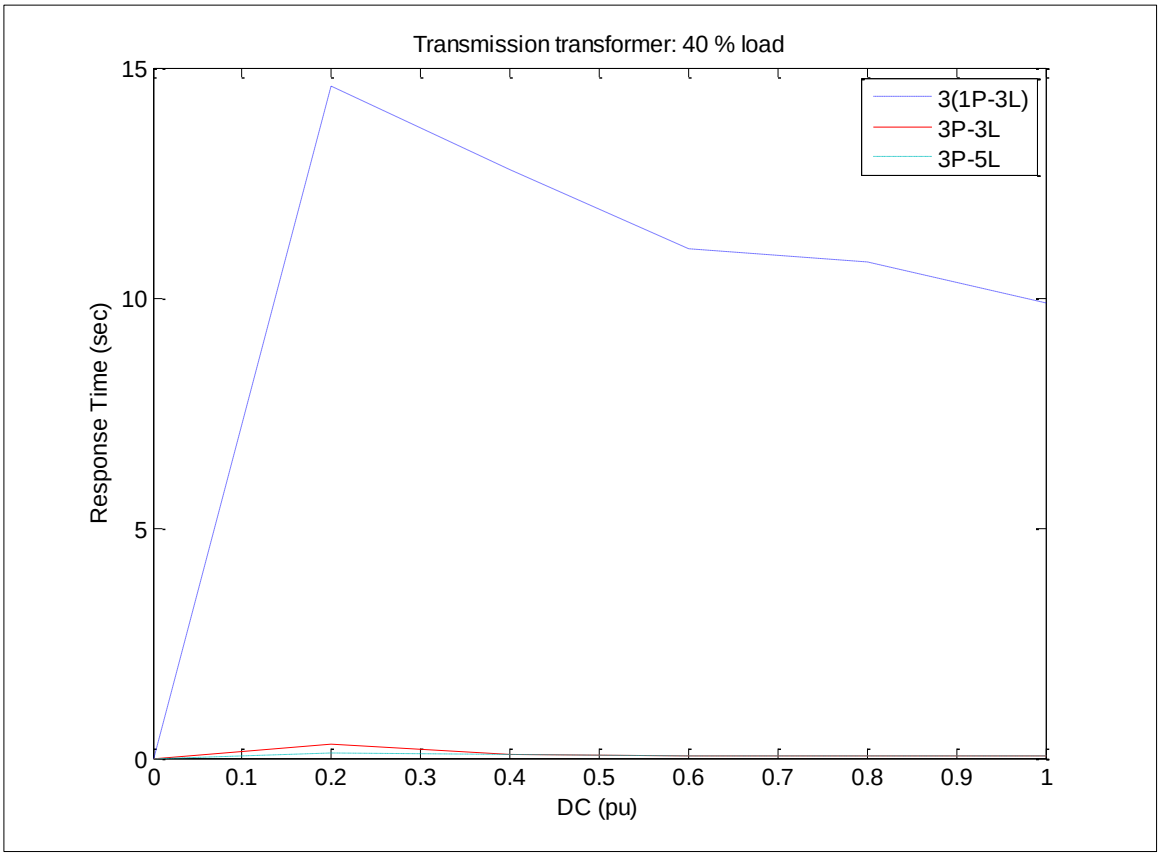

Figure 6.1 Profiles of the transformer time response to GIC between 0 pu and 1 pu for the three transformer core types under consideration.

From Figure 6.1, it can be seen that between 0 pu and 0.35 pu, there is a sudden raise in the transformer response time of the 3(1P-3L) transformer which gradually decreases as the

transformer gets into saturation. This is possibly linked to the increase in leakage flux already discussed in section 5.1. Between 0.35 pu and 1 pu, the response time settles to within values obtained for the lower limit DC current injection (1 pu) in the main simulations as shown in Figures 6.2 to Figure 6.5.

The transformer no-load response time to DC current for the three core structures in PSCAD is shown in Figure 6.2. While there is a high variation in the response time with varying DC current levels for the 3(1P-3L) transformer, there is an almost linear relationship between the response time of the 3P-3L and 3P-5L transformers to the DC current levels. In comparison with 3P-3L and 3P-5L transformers, the 3(1P-3L) transformer's response time is 25 to 85 times longer. When the transformers were loaded at 40%, 80% and 95%, the profiles of the transformer response time to DC current were very similar to the profiles at no-load condition. These results are shown in Figure 6.3 to Figure 6.5.

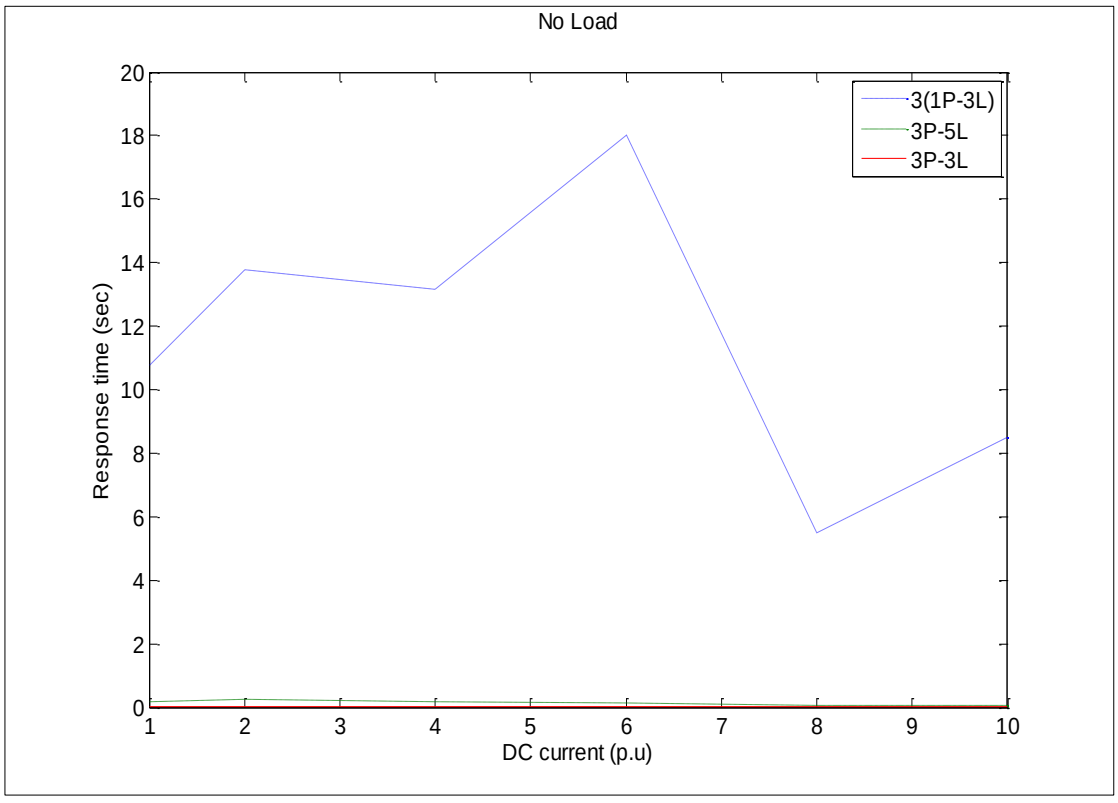

Figure 6.2 Initial condition test response time in PSCAD: 300 VA

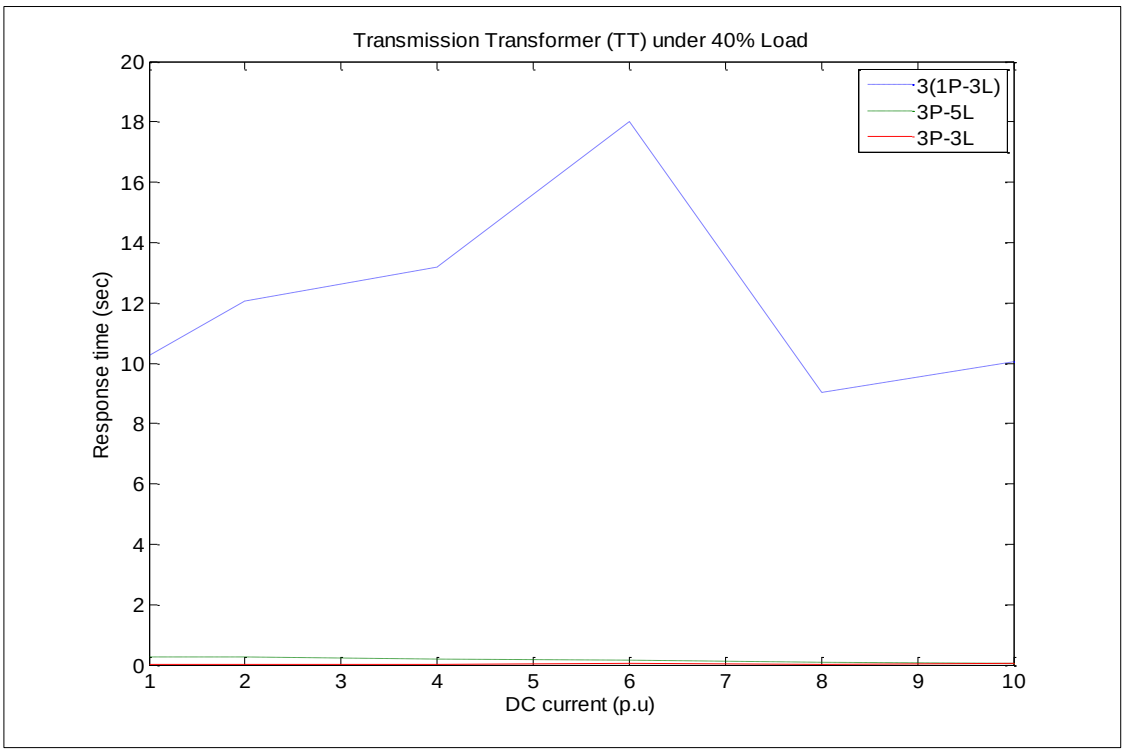

Figure 6.3 Response time of TT under 40 % load in PSCAD: 300 VA

Figure 6.4 Response time for GSU transformers at light load in PSCAD: 300 VA

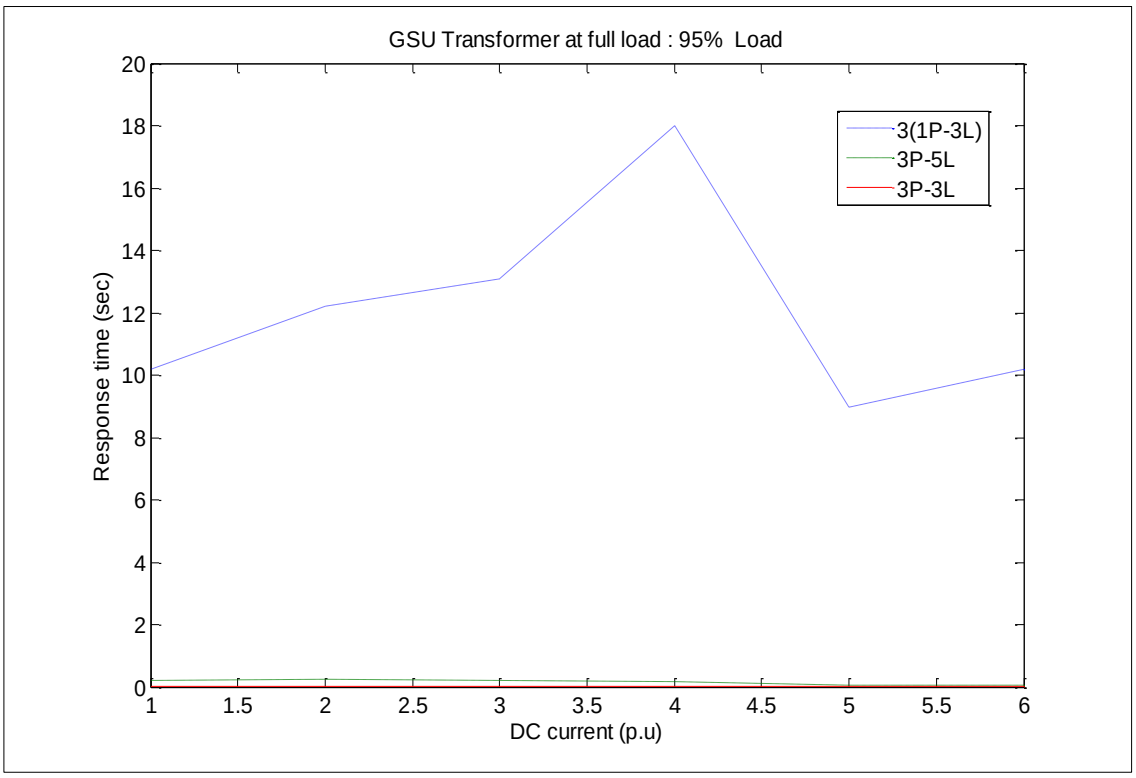

Figure 6.5 Response time for GSU transformer at full load in PSCAD: 300 VA

The results presented in Figures 6.2 to Figure 6.5 show that the responses of the 3P-3L and 3P-5L transformer model in PSCAD is on average about 48 times less than the average response time of the 3(1P-3L) transformer. In section 6.2, these results will be compared with the results from the laboratory test.

6.2 COMPARISON OF LABORATORY TEST AND PSCAD 300 VA TRANSFORMER SIMULATION RESULTS

Results from the PSCAD simulation and laboratory test indicated that, load has an impact on the response time variation with DC current levels. 3P-3L transformers are more likely to permit the flow of GIC through the windings of the transformer over a shorter span of time. As a result, during GMDs leading to higher GIC in the transmission network, the difference between the prospective GIC with and without transformer time response is minimum. The time response of the 300 VA 3P-3L and 3P-5L transformers in PSCAD is less sensitive to DC current (see Figure 6.4 and Figure 6.5) compared to the laboratory tests in section 5.1.

However, the time response of the 300 VA 3(1P-3L) transformer is more sensitive to the DC current in both PSCAD simulation and laboratory tests.

Although the response times followed a similar trend especially for the 3P-3L and 3P-5L transformer core types, the trend in the response time for the 3(1P-3L) was not consistent between the PSCAD results and the laboratory results. Nonetheless, what is clear is the indication that the core dependant transformer time response with respect to the flow of GIC is seen in both PSCAD simulation and laboratory tests. Simulations in PSCAD were run with 500 MVA transformers. Inference from the results of the 500 MVA transformers in PSCAD has to be made with caution as the results could not be compared with real large power transformers due to practical and laboratory limitations. The results from these simulations are discussed in section 6.3.

6.3 500 MVA POWER TRANSFORMER

At the end of this section, the piecewise linear equations which describe the transformer time response to GIC, *T*, are listed. For the three core structures under consideration, a 22 kV/400 kV 500 MVA transformer was chosen to represent large power transformers in main transmission systems. In chapter 4, it was established that the magnetization current forms the basis for the calculation of the DC current injected. Table 6.1 shows the magnetization current for the three core structures.

Table 6.1 Presented in this table are the magnetization currents in each phase for three transformer core structures

	Magnetization Current (A)		
Core structure	**Phase A**	**Phase B**	**Phase C**
3(1P-3L)	1.65	1.65	1.65
3P-3L	2.55	2.41	2.54
3P-5L	2.11	2.13	2.1

As in the 300 VA transformer simulation in section 6.1, the first simulation of the 500 MVA transformer is the no load (initial condition) test. This was followed by the TT typical load

condition test, the GSU light load condition test and GSU typical load condition test. The transformer response time to DC for the no load test is shown in Figure 6.6.

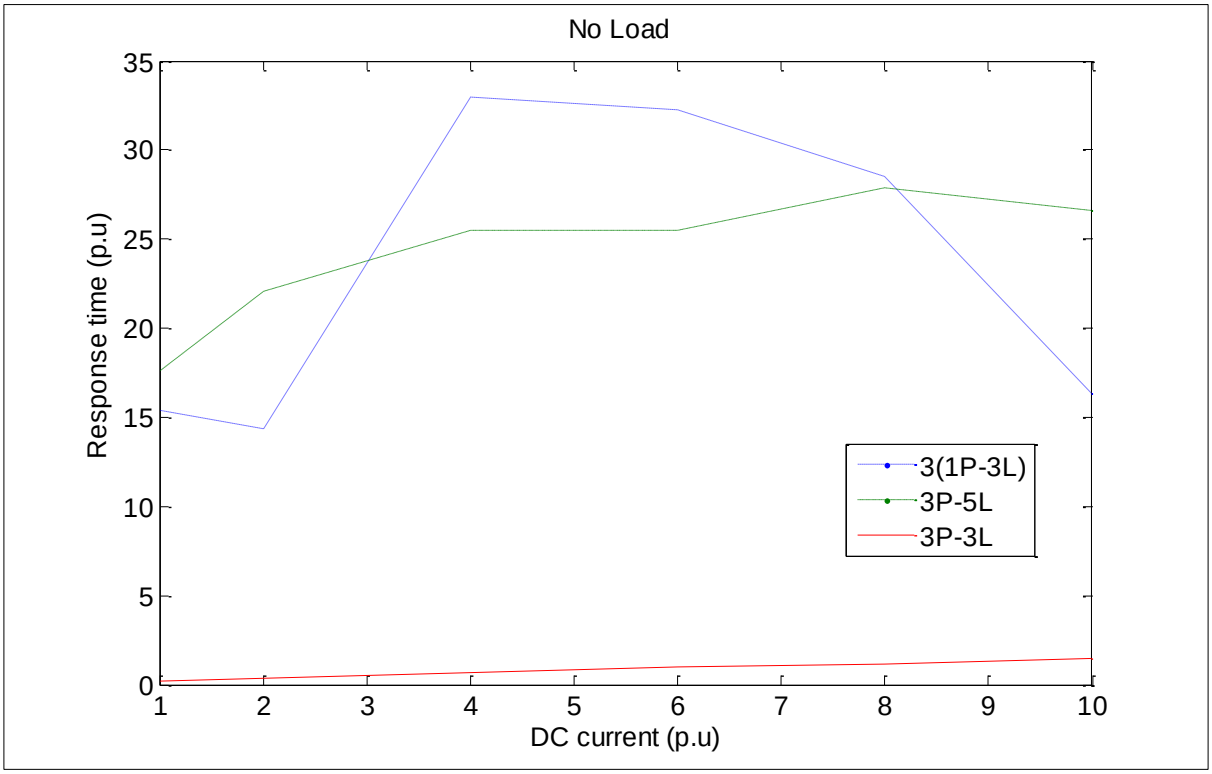

Figure 6.6 Response time for the initial condition test in PSCAD: 500 MVA

In Figure 6.6, the 3P-3L transformer had the shortest response time to DC current at 1.0 pu and the longest response time to DC current at 10.0 pu. The response time profile of the 3P-5L is similar in trend to that of the 3P-3L transformer, although not as linear as that of the 3P-3L transformer. The response time of the 3P-5L transformer is about 26 times longer than the 3P-3L transformer on average. The 3(1P-3L) transformer is not as linear as the other two transformer core types. The response time for the 3(1P-3L) transformer at 1.0 pu and 10.0 pu is the equal while it varies in between. This also shows the complexity in transformer time response to DC. Figure 6.7 shows the 500 MVA transformer response time to DC current for the TT with the three transformer cores.

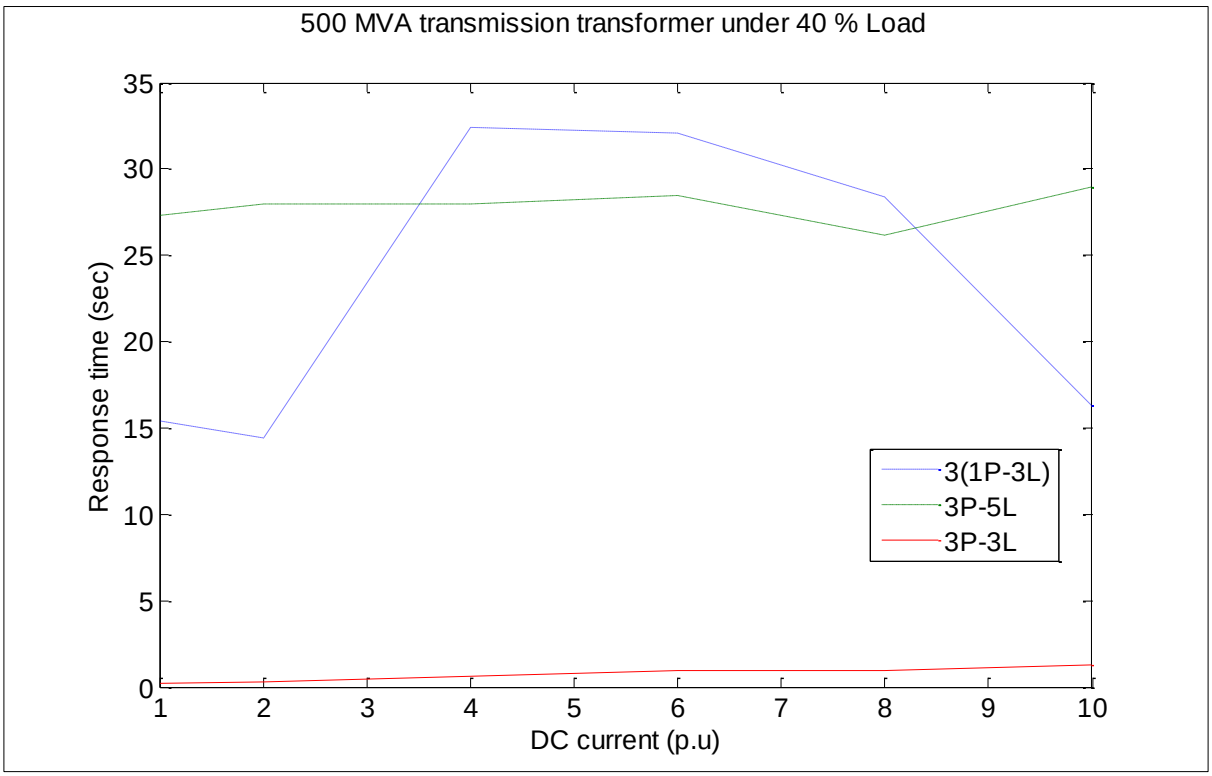

Figure 6.7 Response time for TT in PSCAD: 500 MVA

The response time profile for the three core types at 40 % load in Figure 6.7 is very similar to the no-load profile in Figure 6.6. At 1.0 pu, the 3(1P-3L) transformer in Figure 6.7 has a longer response time between 3.0 pu and 8.0 pu which is similar to the no-load simulation in Figure 6.6. In contrast to the 300 VA transformers, the 500 MVA 3(1P-3L) transformer response time to DC current between 3.0 pu and 8.0 pu in Figure 6.7 is longer than that of the 500 MVA 3P-5L transformer. This result is the same for the no-load and 40% load conditions (TT).

The transformer response times to DC current for the GSUs are shown in Figure 6.8 and Figure 6.9.

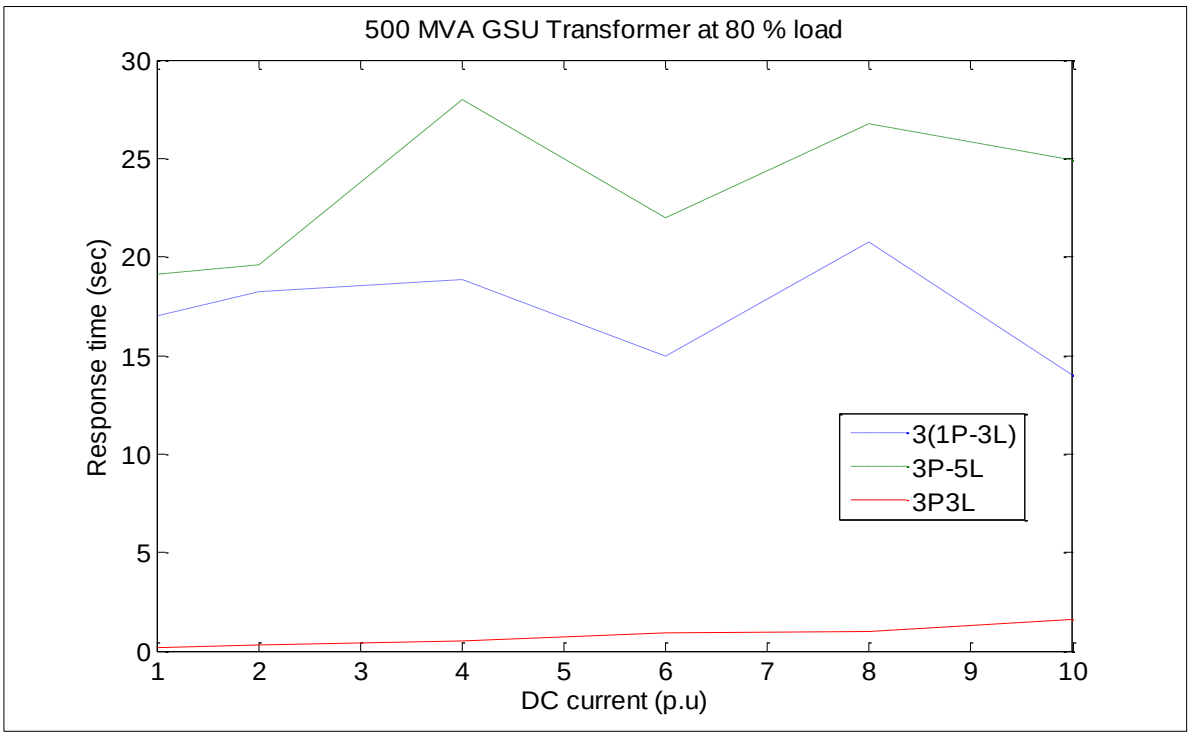

Figure 6.8 Response time for GSU under light load in PSCAD: 500 MVA

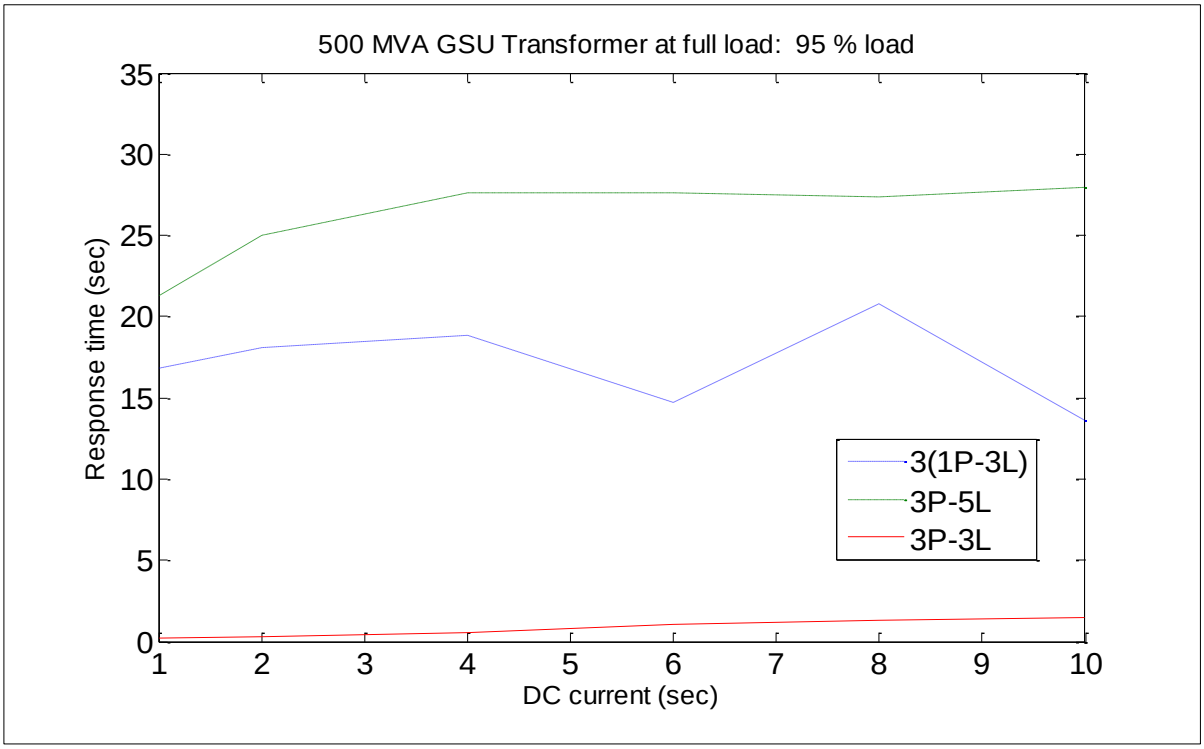

Figure 6.9 Response time for GSU under full load in PSCAD: 500 MVA

For the GSU-type transformers in Figure 6.8 and Figure 6.9, the response time of the 3P-5L transformers is consistently longer than that of the 3(1P-3L) transformer. This result differs from the 300 VA bench scale transformers and the 500 MVA TT. At full load the response time profile of the 3P-5L transformer is more linear when compared to the other conditions tested, as seen in Figure 6.9.

The response time for the GSU transformer is dependent on the level of the load. The average decrease in transformer response time at 95 % load is 10 % and 33% for the 3P-3L and 3P-5L transformer core structures respectively when compared to the no load condition. The 3(1P-3L) transformer showed a 5 % increase in response time. This suggests that when the 3P-3L and 3P-5L transformers are loaded, the time it takes for GIC to rise through the transformer windings is shorter.

According to the simulation results, the flow of GIC through the windings of a 3P-3L transformer takes the shortest length of time. This is consistent between the 300 VA and 500 MVA transformers.

From the results presented in Figures 6.7 to 6.9, piecewise linear equations were generated for the different transformer core structures and operational modes as shown in Tables 6.2 to 6.4. The DC current in per unit flowing through the winding of each transformer is represented as *z* in Tables 6.2 to 6.4.

Table 6.2 Time response equations derived for the 500 MVA TT (40% load) in PSCAD:

Core structure	Equation
3(1P-3L)	$t_r = \begin{cases} 14.90\ s & if\ \ 0 < z < 4 \\ 32.3\ s & if\ \ 4 \le z < 8 \\ 22.4\ s & if\ \ 8 \le z \le 10 \end{cases}$
3P-5L	$t_r = \begin{cases} 27.77\ s & if\ \ 0 < z < 6 \\ 28.48\ s & if\ \ 6 \le z < 8 \\ 26.18\ s & if\ \ 8 \le z < 10 \\ 28.98\ s & if\ 10 \le z \le 14 \end{cases}$
3P-3L	$t_r = \begin{cases} 0.23\ s & if\ \ 0 < z < 4 \\ 0.58\ s & if\ \ 4 \le z < 6 \\ 0.92\ s & if\ \ 6 \le z < 10 \\ 1.25\ s & if\ 10 \le z \le 15 \end{cases}$

Table 6.3 Transformer time response equations derived for the 500 MVA GSU under light load in PSCAD

Core structure	Equation
3(1P-3L)	$t_r = \begin{cases} 16.99\ s & if\ \ 0 < z < 2 \\ 18.56\ s & if\ \ 2 \le z < 6 \\ 14.99\ s & if\ \ 6 \le z < 8 \\ 20.79\ s & if\ 8 \le z \le 10 \\ 13.99\ s & if\ 10 \le z \le 15 \end{cases}$
3P-5L	$t_r = \begin{cases} 19.35\ s & if\ \ 0 < z < 4 \\ 27.98\ s & if\ \ 4 \le z < 6 \\ 21.96\ s & if\ \ 6 \le z < 8 \\ 25.83\ s & if\ 8 \le z \le 10 \\ 24.91\ s & if\ 10 \le z \le 15 \end{cases}$
3P-3L	$t_r = \begin{cases} 0.15\ s & if\ \ 0 < z < 2 \\ 0.29\ s & if\ \ 2 \le z < 4 \\ 0.53\ s & if\ \ 4 \le z < 6 \\ 0.96\ s & if\ \ 6 \le z \le 10 \\ 1.6\ s & if\ 10 \le z \le 15 \end{cases}$

Table 6.4 Transformer time response equations derived for the GSU under full load in PSCAD

Core structure	Equation
3(1P-3L)	$t_r = \begin{cases} 16.34\,s & if \;\; 0 < z < 2 \\ 18.49\,s & if \;\; 2 \leq z < 6 \\ 14.75\,s & if \;\; 6 \leq z < 8 \\ 20.79\,s & if \; 8 \leq z \leq 10 \\ 13.66\,s & if \; 10 \leq z \leq 15 \end{cases}$
3P-5L	$t_r = \begin{cases} 21.27\,s & if \;\; 0 < z < 2 \\ 25\,s & if \;\; 2 \leq z < 4 \\ 27.54\,s & if \;\; 4 \leq z < 10 \\ 27.95\,s & if \; 10 \leq z \leq 15 \end{cases}$
3P-3L	$t_r = \begin{cases} 0.26\,s & if \;\; 0 < z < 4 \\ 0.58\,s & if \;\; 4 \leq z < 6 \\ 1.19\,s & if \;\; 6 \leq z < 10 \\ 1.51\,s & if \; 10 \leq z \leq 15 \end{cases}$

The piecewise linear equations in Table 6.2 to Table 6.4 will be used to determine the transformer response time for the calculation of the prospective GIC in equation 3.40.

6.4 AVERAGE RESPONSE TIME RATIOS FOR CORE STRUCTURES

The response time for the 500 MVA transformer in PSCAD was in seconds. In real power transformers, the response time to DC excitation has been suggested to be between 10 – 30 seconds for star-connected transformers [86, 87]. The response time really depends on the size of the transformer and the core structure. This prompted the need to calculate the response time ratios between the various core structures of the 500 MVA transformer in PSCAD using an approach similar to the per unit system. Table 6.5 shows the average time response ratios of the 3(1P-3L) and 3P-5L transformer core structure. These empirical ratios were deduced from the curves in Figure 6.6 to Figure 6.9. To do this, the average response time across the DC levels for each transformer core structure and load condition was calculated. Since the response time of the 3P-3L transformer is the shortest, it was chosen as the base (common denominator). In column 2 of Table 6.5, the average response time of

the 3(1P-3L) transformer was divided by the average response time of the 3P-3L transformer. Similarly in column 3, the average response time of the 3P-5L transformer was divided by the average response time of the 3P-3L transformer.

These values indicate how much longer the time response is for a specific core structure when compared to the 3P-3L core structure. Column 2 in Table 6.6 shows the time response ratios for the 3P-5L and 3(1P-3L) transformers. These ratios are lower than the ratios in Table 6.5. This is because the comparison is between the 3P-5L and 3(1P-3L) transformer core types which are similar.

Table 6.5 Average time response ratios for 3(1P-3L) and 3P-5L with respect to 3P-3L for 500 MVA transformers.

	Time response ratios	
Transformer loading condition	**[3(1P-3L)] / [3P-3L]**	**[3P-5L] / [3P-3L]**
No Load	26.12	30.38
TT	31.14	37.39
GSU Transformer (light load)	24.17	34.00
GSU Transformer (full load)	18.99	28.75

Table 6.6 Average time response ratios for the 500 MVA 3P-5L and 3(1P-3L) core structures

	Time response ratios
	[3P-5L]/[3(1P-3L)]
No Load	1.16
Transmission Transformer	1.20
GSU Transformer (light Load)	1.41
GSU Transformer (full Load)	1.51

The ratios in Table 6.5 and Table 6.6 provide an indication of what the time response to DC would be in real large power transformers.

CHAPTER 7

TEST AND IMPLEMENTATION

The algorithm for calculating the prospective GIC without the transformer time response was tested in section 7.1 using the same input magnetic field data and network (see Figure 7.1) which Koen [31] used in 2002, to ensure that the same results are obtained. Unfortunately, the geo-magnetic data at the time from the Hermanus Magnetic Observatory (HER) for the severe storm on 13th March, 1989 [88] was only available at two-minute intervals. The transformer time response was implemented in section 7.2. In section 7.3, the effect of double the sampling time interval was investigated in relation to the transformer time response. This showed that an increased sampling time interval offsets the relevance of the transformer time response. In section 7.4 where the calculated GIC was compared with measured GIC at Grassridge (South Africa), the measured GIC was at two-second sampling interval whereas the magnetic field data was collected at one-minute intervals. In order to use both data sets with different sampling time intervals, an interpolation technique as discussed in this thesis was used to interpolate the magnetic field used to calculate GIC into a series of data sets with different sampling time intervals, ranging from two-second to 10-minute sampling intervals. The calculated GIC were compared with the measured GIC of the corresponding sampling time interval.

7.1 VALIDATING THE PROSPECTIVE GIC WITHOUT TRANSFORMER TIME RESPONSE

Koen used the magnetic data from the Hermanus Magnetic Observatory (HER) which is now called the Space Science Directorate of the South African National Space Agency (SANSA) to calculate the electric field. This data was only available at two-minute intervals for the severe storm on 13th March, 1989. The range of data he used was for a duration of 180

minutes [31]. The exact time was unavailable. Hence, the time axis in Figure 7.4 to Figure 7.15 shows the time from 0 min to 180 minutes. Figure 7.1 shows the test network with 10 substations and 13 transmission lines.

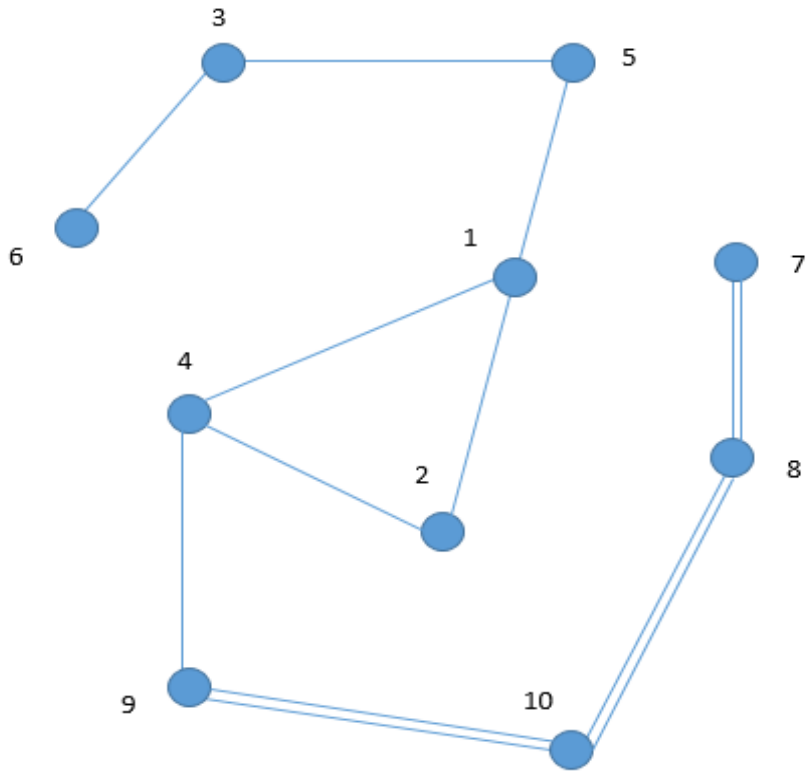

Figure 7.1 The test network used in section 7.1 to 7.3. It has 10 substations and 13 unique transmission lines

In this test case, before the prospective GIC was calculated using the same magnetic field data, the magnetic field data was processed with the FFT to determine the dominant frequencies in the magnetic field. Figure 7.2 shows the FFT of the magnitude of the magnetic field data which confirmed that magnetic field fluctuations leading to GIC typically have dominant frequencies which are less than 10 mHz [57], [89]. In this case, the frequencies are below 4.1 mHz.

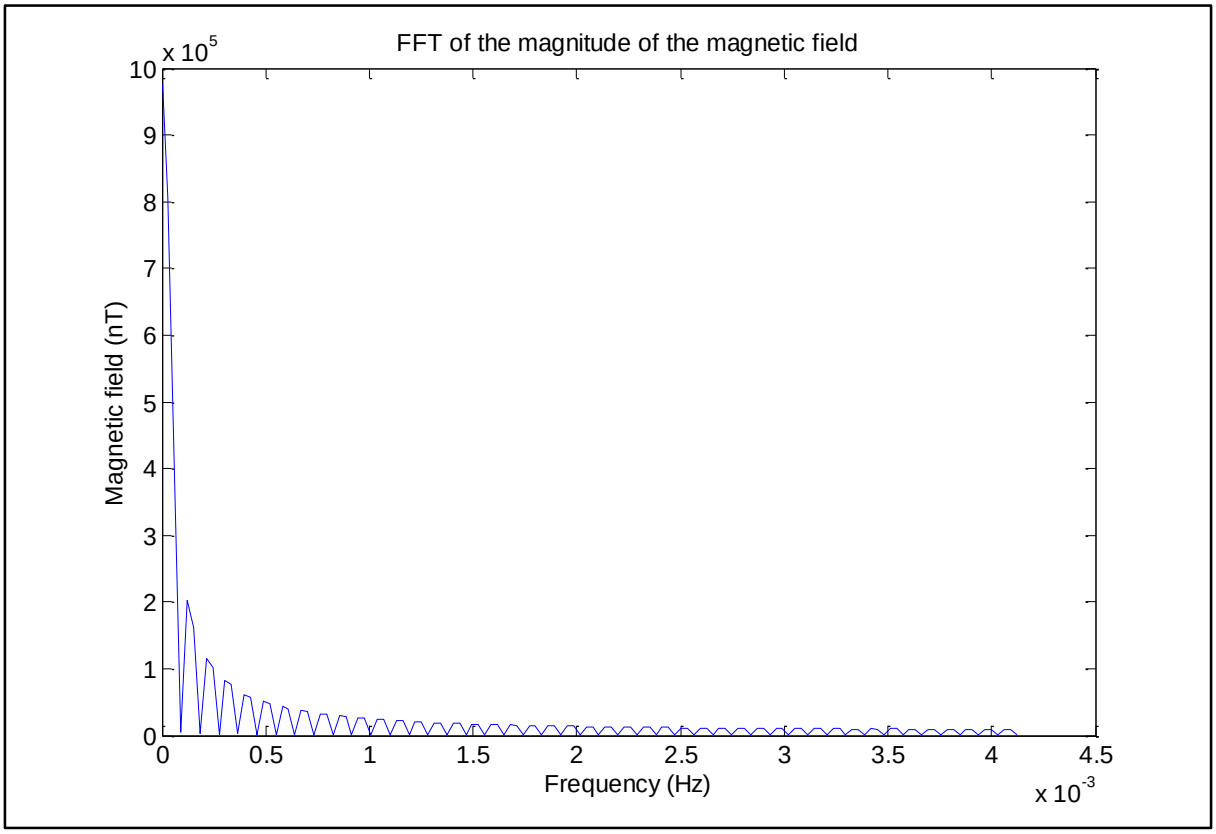

Figure 7.2 FFT of the magnitude of the magnetic field data used in chapter 7

A uniform ground conductivity value of 2.7 mS/m was chosen based on the conductivity profile at Grassridge, South Africa. The assumption of a uniform ground conductivity is reasonable when comparing GIC with and without transformer time response. When comparing modelled GIC with measured GIC, the use of single, multi-layer non uniform ground conductivity will change the profile of the electric field. Ground conductivity is an input to the electric field calculation. In this thesis, electric field was calculated by taking the inverse FFT of the product of the surface impedance and the geomagnetic field in the frequency domain. This has been explained in section 2.1.1 (See equations 2.8a, 2.8b and 2.8c). Figure 7.3 shows the x and y components of the measured magnetic field and the calculated electric field.

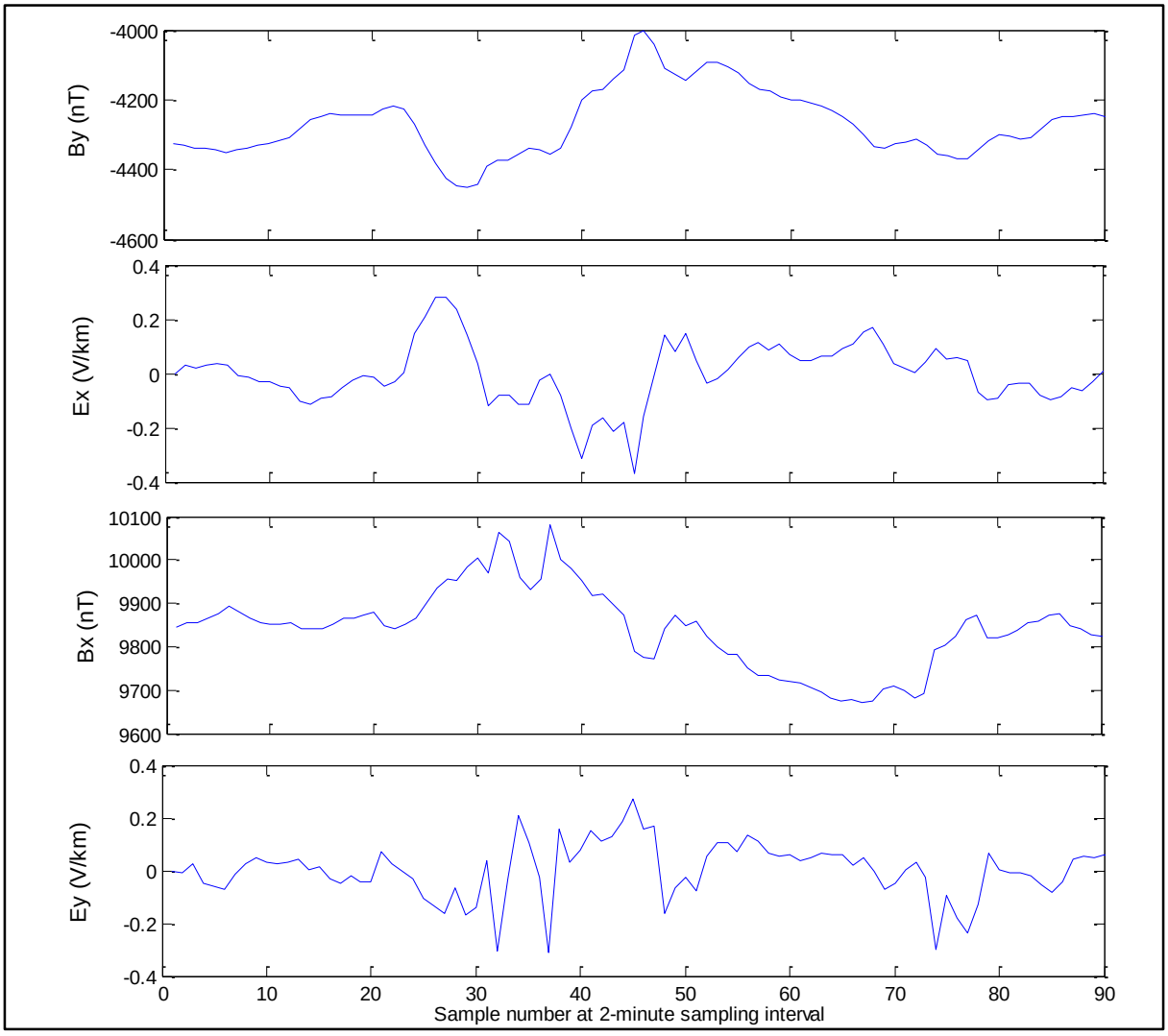

Figure 7.3 Magnetic and electric field profiles at Hermanus Magnetic Observatory (HMO) on 13 March 1989

Table 7.1 gives the transmission line data. For the purpose of validating the algorithm, it was assumed that the 10 substations have the same conductivity structure. The value of the ground resistance was set to 0.3 Ω as shown in column 2 of Table 7.2.

Table 7.1 Transmission line admittance, length and substation GPS coordinates of the test network

Line number	**Substation number**				**From Substation**		**To Substation**	
	From	To	Line admittance (S)	Line length (km)	Latitude (deg)	Longitude (deg)	Latitude (deg)	Longitude (deg)
1	6	3	0.34	130	-28.54	16.6	-29.6	17.18
2	3	5	0.57	76	-29.6	17.18	-29.63	17.88
3	5	1	0.44	99	-29.63	17.88	-29.3	18.8
4	1	2	0.66	196	-29.3	18.8	-29.49	20.79
5	1	4	0.09	337	-29.3	18.8	-26.54	18.12
6	2	4	0.36	420	-29.49	20.79	-26.54	18.12
7	4	9	0.34	446	-26.54	18.12	-22.59	17.37
8	4	9	0.06	446	-26.54	18.12	-22.59	17.37
9	9	10	1.01	29	-22.59	17.37	-22.52	17.08
10	9	10	1.09	29	-22.59	17.37	-22.52	17.08
11	10	8	0.19	163	-22.52	17.08	-21.5	16.03
12	10	8	0.19	165	-22.52	17.08	-21.5	16.03
13	8	7	0.16	524	-21.5	16.03	-17.4	14.22

Table 7.2 gives the number of transformers and reactors in each substation, the actual earthing resistance and the substation resistance data for the construction of the network admittance matrix.

Table 7.2 Substation transformer and reactor data used in the test network

Substation number	Actual grounding resistance (R_e)Ω	Number of transformers at substation (n_t)	Number of reactors at substation (n_r)	Calculated substation resistance per phase (R_i) Ω
1	0.3	1	0	0.8
2	0.3	2	1	0.8
3	0.3	1	0	0.8
4	0.3	2	1	0.8
5	0.3	1	0	0.8
6	0.3	1	0	0.8
7	0.3	2	1	0.8
8	0.3	1	0	0.8
9	0.3	2	1	0.8
10	0.3	1	0	0.8

The substation resistance per phase in Table 7.2 was calculated using equation 7.1. A more detailed explanation on how to calculate the substation resistances can be found in the research work published by Boteler and Pirjola [26].

$$R_j = {}^{r_t}/_{n_t} + {}^{r_r}/_{n_r} + 3R_e \quad (7.1)$$

where R_j is the substation resistance per phase

R_e is the substation grounding resistance

r_t is the transformer resistance per phase

r_r is the reactor resistance per phase

n_t is the number of transformers connected in parallel

$n_r$is the number of reactors connected in parallel

The inverse of R_j in equation 7.1 was used to calculate the shunt (nodal) admittances in the network.

$$y_j = \frac{1}{R_j} \quad (7.2)$$

To calculate the network admittance matrix $[Y]$, the diagonal and off-diagonal components were calculated separately. For the off-diagonal components, equation 7.3 was used.

$$Y_{ij} = -y_{ij} \quad (7.3)$$

where y_{ij} is the branch admittance between bus *i* and bus *j* which was obtained from Table 7.1. The diagonal components were calculated using equation 7.4.

$$Y_{ii} = y_i + \sum_{k=1,k\neq i}^{N} y_{ik} \quad (7.4)$$

where y_i is the nodal admittance at bus *i* and y_{ik} is the admittance between bus *i* and bus *k.*

The resultant network admittance matrix $[Y]$ is:

$$[Y] = \begin{bmatrix} 2.44 & -0.66 & 0.00 & -0.09 & -0.44 & 0.00 & 0.00 & 0.00 & 0.00 & 0.00 \\ -0.66 & 2.27 & 0.00 & -0.36 & 0.00 & 0.00 & 0.00 & 0.00 & 0.00 & 0.00 \\ 0.00 & 0.00 & 2.16 & 0.00 & -0.57 & -0.34 & 0.00 & 0.00 & 0.00 & 0.00 \\ -0.09 & -0.36 & 0.00 & 2.10 & 0.00 & 0.00 & 0.00 & 0.00 & -0.41 & 0.00 \\ -0.44 & 0.00 & -0.57 & 0.00 & 2.27 & 0.00 & 0.00 & 0.00 & 0.00 & 0.00 \\ 0.00 & 0.00 & -0.34 & 0.00 & 0.00 & 1.59 & 0.00 & 0.00 & 0.00 & 0.00 \\ 0.00 & 0.00 & 0.00 & 0.00 & 0.00 & 0.00 & 1.41 & -0.16 & 0.00 & 0.00 \\ 0.00 & 0.00 & 0.00 & 0.00 & 0.00 & 0.00 & -0.16 & 1.79 & 0.00 & -0.38 \\ 0.00 & 0.00 & 0.00 & -0.41 & 0.00 & 0.00 & 0.00 & 0.00 & 3.75 & -2.10 \\ 0.00 & 0.00 & 0.00 & 0.00 & 0.00 & 0.00 & 000 & -0.38 & -2.10 & 3.73 \end{bmatrix}$$

The next step was to develop the column matrix $[H]$, in equation 3.37. To do this, equation 3.19, 3.20 and 3.22 were used, resulting in $[H]$ given below:

$$[H] = \begin{bmatrix} 0.81 \\ -6.41 \\ -1.00 \\ -0.37 \\ -0.65 \\ 1.47 \\ 2.76 \\ -0.88 \\ 5.09 \\ -0.82 \end{bmatrix}$$

The unit for [H] is ampere. It should be noted that the electric field induced on each line was calculated using equations 3.15 to 3.18. The *Ex* and *Ey* used in equation 3.15 corresponds to the first set of *e*-field values given in Appendix B for the 1989 storm.

Inverting $[Y]$ and multiplying it by $[H]$ in equation 3.38 gives the nodal voltages in the network shown as $[V]$.

$$[V] = \begin{bmatrix} -0.61 \\ -3.06 \\ -0.48 \\ -0.40 \\ -0.53 \\ 0.83 \\ 1.95 \\ -0.16 \\ 1.72 \\ 0.73 \end{bmatrix}$$

The unit of [V] is volts. From equation 3.24, the prospective GIC flow in each node or substation was calculated, using the matrix of nodal voltages above and the admittance of each node. The prospective GIC flow, in each node for the first set of electric field data is shown below.

$$[i] = \begin{bmatrix} -0.76 \\ -3.82 \\ -0.60 \\ -0.49 \\ -0.66 \\ 1.03 \\ 2.43 \\ -0.21 \\ 2.15 \\ 0.91 \end{bmatrix}$$

The unit for [i] is ampere. Each row in the 1 x 10 matrix above represents the prospective GIC flow in each of the 10 nodes in the network. Negative GIC means the current is flowing into the ground while positive GIC means the current is flowing out of the ground. When the 90 electric field samples were used as inputs to the algorithm, 90 prospective GIC values were obtained for each node in the network. This result is shown in Table 7.3.

Table 7.3 Prospective GIC values calculated for the 10 substation network using 2-min sampling time interval magnetic field data

	Substation number									
Time (min)	1	2	3	4	5	6	7	8	9	10
2	-0.76	-3.82	-0.6	-0.49	-0.66	1.03	2.43	-0.21	2.15	0.91
4	-0.8	1.19	-0.89	-0.91	-0.54	0.05	0.55	-0.46	1.39	0.42
6	-0.24	-8.7	0.19	0.41	-0.43	1.82	3.66	0.29	1.94	1.06
8	-0.17	-9.71	0.32	0.56	-0.41	2	3.95	0.37	1.97	1.12
10	0.01	-10.7	0.55	0.81	-0.31	2.13	4.11	0.51	1.79	1.1
12	0.32	-1	0.38	0.4	0.2	0.09	-0.02	0.21	-0.47	-0.12
14	0.02	3.8	-0.17	-0.26	0.13	-0.76	-1.49	-0.17	-0.68	-0.4
16	0.22	7.86	-0.17	-0.36	0.39	-1.65	-3.31	-0.26	-1.77	-0.96
18	0.37	5.84	0.09	-0.06	0.44	-1.3	-2.72	-0.09	-1.72	-0.85
20	0.96	6.94	0.64	0.46	0.89	-1.72	-3.89	0.16	-3.07	-1.37
22	1.01	7.74	0.66	0.46	0.96	-1.9	-4.26	0.15	-3.32	-1.49

24	2.14	13.37	1.55	1.2	1.93	-3.43	-7.87	0.46	-6.52	-2.85
26	3.01	10.22	2.61	2.33	2.46	-3.11	-7.75	1.05	-7.71	-3.12
28	2.16	9.23	1.78	1.53	1.82	-2.61	-6.29	0.66	-5.86	-2.43
30	2.66	3.2	2.61	2.5	2	-1.58	-4.6	1.2	-5.84	-2.15
32	1.9	-1.25	2.04	2.05	1.33	-0.42	-1.92	1.02	-3.57	-1.17
34	0.86	-0.07	0.89	0.89	0.61	-0.29	-1.05	0.44	-1.69	-0.58
36	0.7	-4.29	0.95	1.05	0.38	0.61	0.76	0.56	-0.68	-0.04
38	0.91	-3.93	1.15	1.23	0.54	0.46	0.36	0.65	-1.15	-0.22
40	0.38	12.71	-0.25	-0.56	0.65	-2.67	-5.38	-0.41	-2.89	-1.57
42	0.51	5.51	0.25	0.11	0.53	-1.28	-2.77	0	-1.94	-0.92
44	-0.09	-0.45	-0.07	-0.06	-0.08	0.12	0.29	-0.03	0.26	0.11
46	-3.4	-16.14	-2.72	-2.29	-2.92	4.43	10.53	-0.97	9.49	4
48	-4.16	-29.28	-2.84	-2.08	-3.85	7.32	16.55	-0.73	13.21	5.87
50	-5.66	-39.37	-3.9	-2.88	-5.23	9.86	22.34	-1.02	17.91	7.94
52	-5.34	-42.7	-3.4	-2.3	-5.1	10.42	23.22	-0.7	17.83	8.07
54	-5.42	-27.08	-4.26	-3.55	-4.69	7.32	17.29	-1.47	15.34	6.51
56	-1.7	-31.41	-0.19	0.6	-2.15	6.88	14.27	0.61	8.69	4.41
58	0.8	-19.08	1.79	2.25	0.01	3.53	6.35	1.3	1.64	1.42
60	2.65	13.9	2.06	1.69	2.31	-3.71	-8.71	0.69	-7.62	-3.25
62	5.91	-28.91	7.6	8.24	3.38	3.68	3.67	4.36	-6.87	-1.07
64	2.54	2.98	2.49	2.39	1.91	-1.5	-4.37	1.15	-5.56	-2.05
66	0.37	33.68	-1.32	-2.14	1.26	-6.85	-13.45	-1.4	-6.42	-3.73
68	1.7	22.21	0.64	0.08	1.87	-5.03	-10.71	-0.19	-7.12	-3.45
70	0.99	-1.03	1.08	1.1	0.68	-0.15	-0.86	0.55	-1.8	-0.57
72	3.86	-36.22	5.84	6.69	1.7	5.87	9.08	3.66	-1.57	1.09
74	0.15	25.07	-1.1	-1.72	0.85	-5.06	-9.86	-1.1	-4.54	-2.69
76	4.94	20.59	4.1	3.54	4.16	-5.86	-14.19	1.54	-13.31	-5.51
78	7.33	35.03	5.85	4.91	6.29	-9.59	-22.77	2.07	-20.48	-8.63
80	3.18	33.79	1.6	0.74	3.28	-7.87	-17.05	0.02	-12.03	-5.67
82	2.94	26.48	1.72	1.04	2.89	-6.33	-13.92	0.24	-10.31	-4.74
84	4.05	32.66	2.56	1.72	3.87	-7.95	-17.71	0.51	-13.56	-6.14
86	2.48	36.7	0.73	-0.19	2.87	-8.21	-17.29	-0.47	-11.13	-5.49
88	6.46	62.75	3.54	1.94	6.49	-14.81	-32.36	0.32	-23.43	-10.9
90	2.13	31.69	0.62	-0.18	2.47	-7.08	-14.92	-0.41	-9.59	-4.73
92	-1.84	19.94	-2.92	-3.39	-0.73	-3.33	-5.36	-1.87	0.3	-0.79
94	-1.73	-30.87	-0.24	0.53	-2.15	6.77	14.08	0.58	8.65	4.37
96	-1.31	-14.59	-0.62	-0.25	-1.37	3.38	7.28	0.02	5.06	2.4
98	-3.63	-15.63	-2.99	-2.57	-3.07	4.41	10.62	-1.11	9.87	4.1
100	-0.35	-13.26	0.3	0.63	-0.65	2.77	5.56	0.45	2.94	1.61
102	0.31	9.06	-0.14	-0.36	0.49	-1.92	-3.88	-0.27	-2.14	-1.14
104	-0.84	13.82	-1.57	-1.9	-0.19	-2.46	-4.27	-1.08	-0.67	-0.85

106	-1.72	10.84	-2.34	-2.58	-0.91	-1.56	-2	-1.38	1.59	0.06
108	-2.49	3.43	-2.76	-2.81	-1.68	0.2	1.82	-1.42	4.36	1.35
110	-4.18	7.37	-4.71	-4.85	-2.78	0.01	2.44	-2.47	7.06	2.1
112	-4.43	3.13	-4.76	-4.79	-3.09	0.94	4.4	-2.4	8.29	2.72
114	-3.1	0.54	-3.25	-3.23	-2.21	0.99	3.71	-1.6	6.07	2.07
116	-3.61	-2.63	-3.62	-3.51	-2.66	1.8	5.58	-1.7	7.62	2.74
118	-2.5	1.21	-2.66	-2.66	-1.76	0.64	2.69	-1.32	4.76	1.59
120	-1.7	0.03	-1.77	-1.75	-1.22	0.6	2.14	-0.86	3.37	1.16
122	-1.9	1.57	-2.05	-2.07	-1.32	0.36	1.8	-1.04	3.51	1.14
124	-2.52	2.08	-2.72	-2.75	-1.74	0.48	2.38	-1.38	4.66	1.51
126	-2.42	1.47	-2.59	-2.6	-1.69	0.56	2.49	-1.3	4.56	1.51
128	-3.23	-0.82	-3.32	-3.27	-2.34	1.31	4.41	-1.6	6.57	2.3
130	-3.12	-6.53	-2.91	-2.72	-2.43	2.41	6.46	-1.28	7.31	2.81
132	-4.66	-7.7	-4.45	-4.21	-3.57	3.18	8.86	-2	10.56	3.99
134	-4.47	-15.05	-3.89	-3.48	-3.65	4.59	11.46	-1.56	11.44	4.62
136	-1.93	-17.67	-1.12	-0.66	-1.91	4.21	9.26	-0.15	6.83	3.15
138	-0.41	-8.77	0.02	0.24	-0.55	1.9	3.9	0.21	2.29	1.18
140	-0.55	-1.45	-0.5	-0.46	-0.44	0.48	1.26	-0.21	1.34	0.53
142	-0.41	3.2	-0.59	-0.66	-0.2	-0.49	-0.71	-0.36	0.28	-0.05
144	-0.73	-6.7	-0.43	-0.25	-0.73	1.6	3.51	-0.06	2.59	1.19
146	1.3	-42.68	3.5	4.53	-0.33	8.06	14.81	2.67	4.62	3.51
148	-0.22	-15.8	0.56	0.95	-0.63	3.23	6.38	0.63	3.11	1.78
150	0.76	-25.72	2.09	2.71	-0.21	4.87	8.95	1.6	2.82	2.13
152	1.69	-31.78	3.36	4.12	0.27	5.75	10.11	2.35	2	2.12
154	3.49	-9.24	4.1	4.29	2.23	0.61	-0.86	2.21	-5.39	-1.44
156	1.73	15.3	1.02	0.63	1.69	-3.67	-8.08	0.15	-6.01	-2.76
158	2.38	8.2	2.06	1.83	1.95	-2.48	-6.17	0.82	-6.11	-2.47
160	1.14	2.24	1.07	1.01	0.88	-0.85	-2.3	0.47	-2.64	-1.01
162	1.02	2.01	0.96	0.9	0.79	-0.76	-2.07	0.42	-2.37	-0.91
164	1.21	0.59	1.23	1.2	0.88	-0.55	-1.76	0.59	-2.5	-0.89
166	2.84	0.51	2.93	2.89	2.05	-1.11	-3.79	1.42	-5.74	-2
168	3.61	-1.71	3.84	3.84	2.54	-0.94	-3.91	1.91	-6.89	-2.3
170	2.8	1.92	2.81	2.74	2.06	-1.37	-4.28	1.33	-5.89	-2.12
172	0.77	9.31	0.33	0.1	0.83	-2.13	-4.57	-0.05	-3.11	-1.49
174	1.01	11.45	0.47	0.18	1.06	-2.64	-5.69	-0.03	-3.93	-1.87
176	0.15	8.24	-0.26	-0.47	0.35	-1.7	-3.36	-0.31	-1.68	-0.95
178	-0.97	6.09	-1.31	-1.45	-0.51	-0.87	-1.13	-0.78	0.9	0.03
180	-0.38	5.93	-0.7	-0.84	-0.1	-1.05	-1.8	-0.47	-0.24	-0.35

A comparison was made between the prospective GIC profiles using the NAM and the Lehtinen – Pirjola methods. Substations in the middle of the network with a number of interconnections were examined to see the similarities in the prospective GIC without transformer time response. In addition, substations at the fringes of the network were examined to determine whether the two GIC calculation methods yield similar results.

Substation 1 and substation 4 were considered, because they are the substations connected to the highest number of transmission lines within the network. Substation 6 and substation 7 were considered because they are on the edge of the network.

Figures 7.4, 7.5, 7.6 and 7.7 show the GIC profile at substation 1, 4, 6 and 7 respectively. These results indicate that both calculation methods produced exactly the same results.

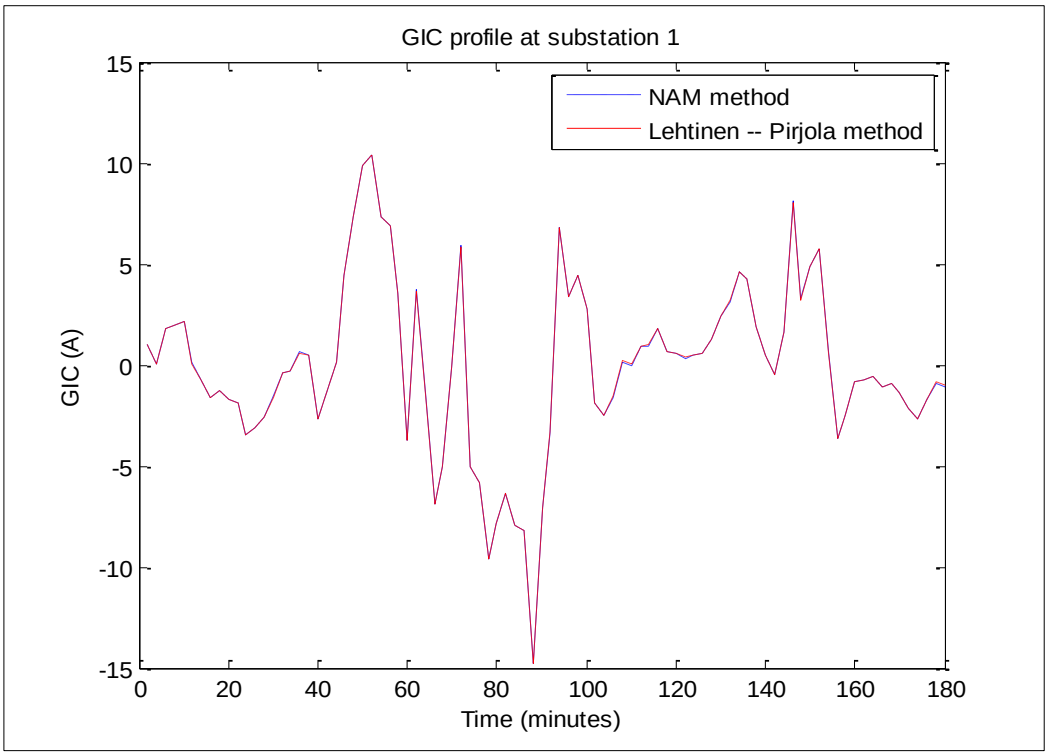

Figure 7.4 Substation 1: Comparison of GIC values obtained using NAM and Lehtinen-Pirjola methods

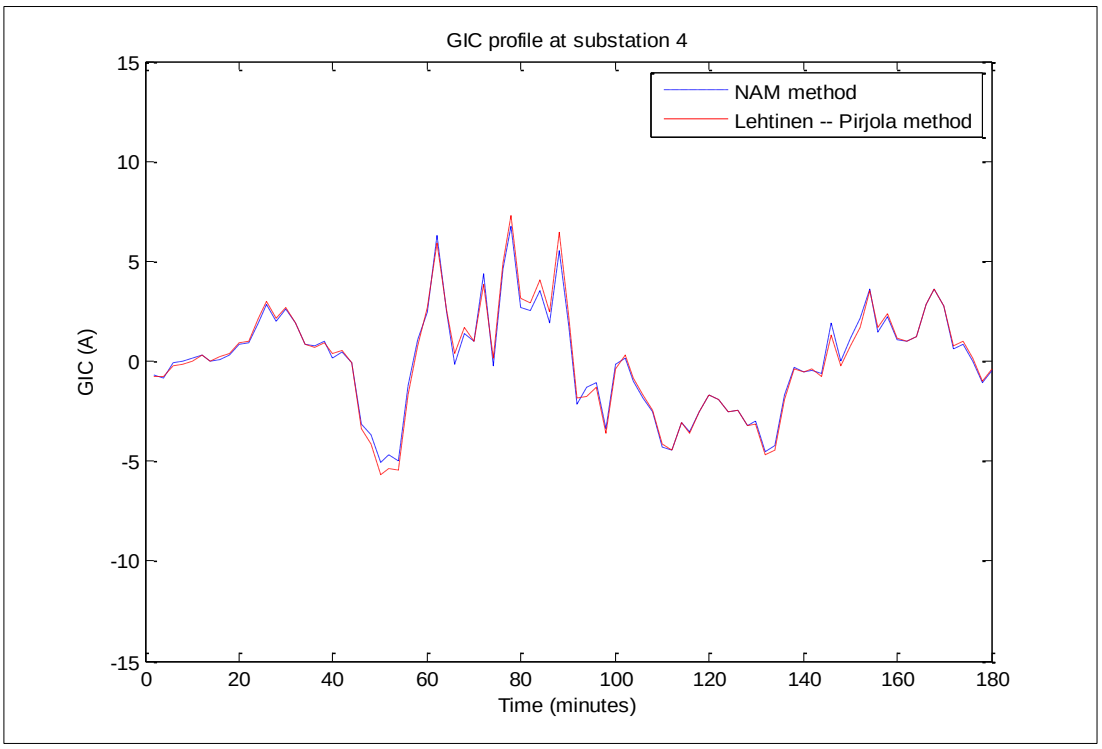

Figure 7.5 Substation 4: Comparison of GIC values obtained using NAM and Lehtinen-Pirjola methods

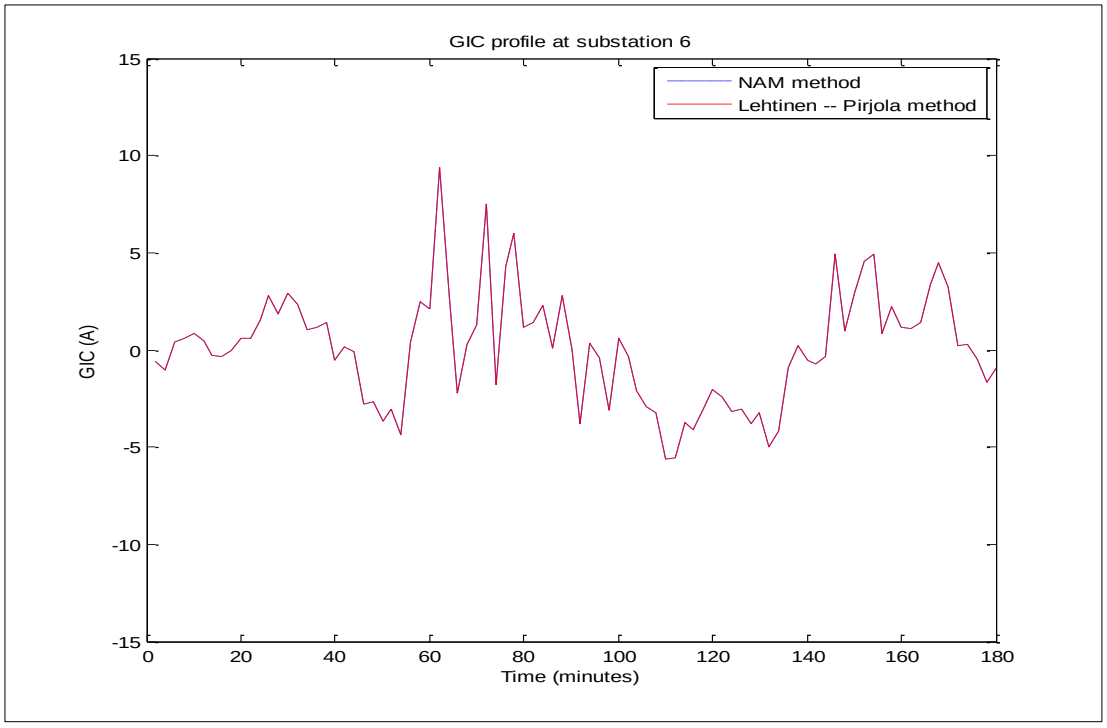

Figure 7.6 Substation 6: Comparison of GIC values obtained using NAM and Lehtinen-Pirjola methods

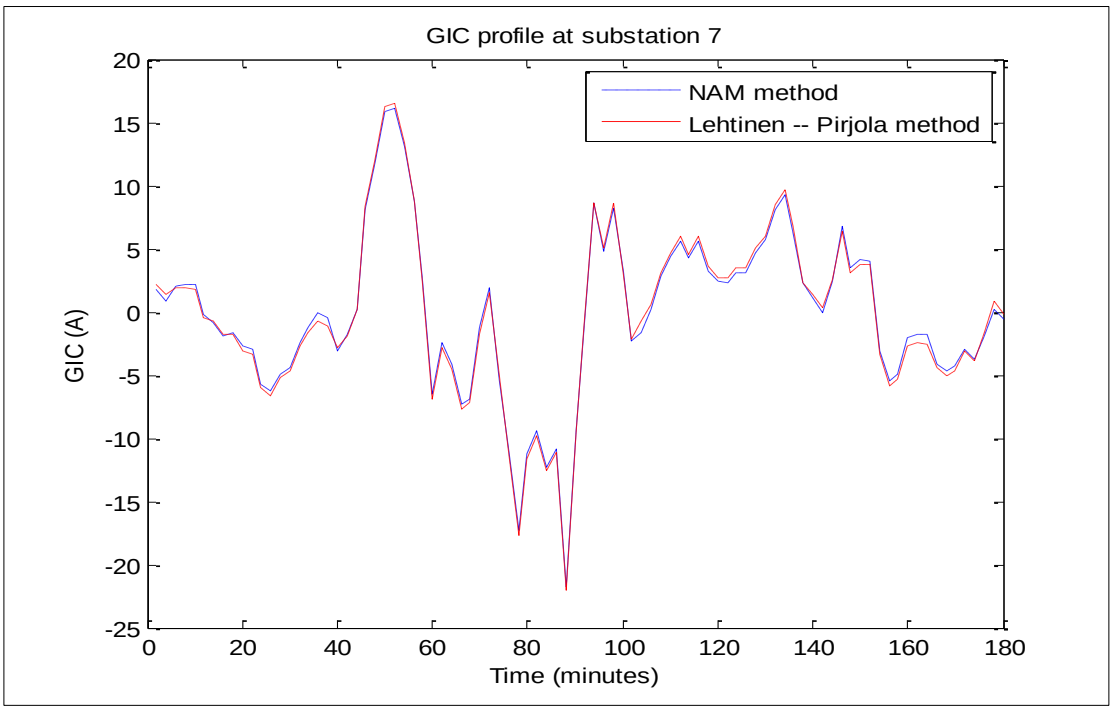

Figure 7.7 Substation 7: Comparison of GIC values obtained using NAM and Lehtinen-Pirjola methods

There are slight differences between the results from the two methods in substation 4 and substation 6. This is most likely due to the difference in software computations. However, for the purpose of comparing the results using both methods and validating the prospective GIC calculation approach, it can be concluded that the NAM method gives acceptable results. Comparison of the GIC profiles at the other six substations using the two methods are available in Appendix C. Having validated the prospective GIC calculation without transformer time response using the two methods, the transformer time response will be incorporated into the prospective GIC calculated with the NAM method in section 7.2. In a journal paper published by Boteler and Pirjola, both GIC calculation methods were validated to be mathematically equivalent [26].

7.2 INCORPORATING TRANSFORMER TIME RESPONSE

The incorporation of the transformer time response into the GIC calculation was done in two case studies. These case studies were structured to cover a combination of transformer types and modes of operation. The aim of these case studies was to show the variation in

transformer time response in a network with a variety of transformers. Incorporating the transformer time response allows for the calculation of the GIC at different times within any interval. This is of particular importance when the transformer response is relatively slow. Hence, in the case studies, values of the GIC at 1-second and 2-seconds will be calculated.

In case study 1, it was assumed that all the transformers in each substation had the same core structure and mode of operation, making it the most unlikely case. The 3P-5L transmission transformer was selected because it had the lowest time response ratio, as shown in Table 6.6.

In case study 2, 40 % of the transformers were 3P-5L, 20 % of the transformers were 3P-3L and 40 % of the transformers were 3(1P-3L). 30 % of the transformers operated GSUs, while 70 % operated as TTs.

7.2.1 Case 1: Calculated GIC in the test network with uniform transformer core structure using two-minute sampling time interval magnetic field data

Table 7.4 is a modified version of Table 7.2 with additional pseudo-data on the transformer core structure to suit the basis of case 1 as explained in the introduction to section 7.2.

Table 7.4 Substation data with additional data on the transformer core structure and operational state

Substation No.	Actual earthing resistance (R_e) Ω	Number of transformers at substation (n_t)	Transformer core structure	Operational state	Number of reactors at substation (n_r)	Calculated substation resistance per phase (R_j) Ω
1	0.3	1	3P-5L	Transmission	0	0.8
2	0.3	2	3P-5L	Transmission	1	0.8
3	0.3	1	3P-5L	Transmission	0	0.8
4	0.3	2	3P-5L	Transmission	1	0.8
5	0.3	1	3P-5L	Transmission	0	0.8
6	0.3	1	3P-5L	Transmission	0	0.8
7	0.3	2	3P-5L	Transmission	1	0.8
8	0.3	1	3P-5L	Transmission	0	0.8
9	0.3	2	3P-5L	Transmission	1	0.8
10	0.3	1	3P-5L	Transmission	0	0.8

Sample calculation for the prospective GIC with transformer time response at substation 7:

For substation 7 (at the fringe of the network) with two 500 MVA 3P-5L transmission transformers, the response time profile for each transformer was obtained from Table 6.2. The relevant equation in Table 6.2 is equation 7.5 given below as:

$$t_r = \begin{cases} 27.77\,s & if \quad 0 < z < 6 \\ 28.48\,s & if \quad 6 \le z < 8 \\ 26.18\,s & if \quad 8 \le z < 10 \\ 28.98\,s & if \ 10 \le z \le 14 \end{cases} \tag{7.5}$$

where z is the GIC in per unit of the transformer magnetization current and t_r is the transformer response time in seconds. The magnetization current for the transformer from the PSCAD simulation is 2.1 A. The prospective GIC through each transformer in substation 7 from the *i* matrix in section 7.1 is:

$$\frac{\text{substation prospective GIC}}{No\ of\ transformers} = \frac{2.43\ \text{A}}{2} = 1.22\ A \tag{7.6}$$

Therefore,

$$z = \frac{i}{i_{mag}} = \frac{1.22\ A}{2.1\ A} = 0.58 \tag{7.7}$$

Using $z = 0.58$ in equation 7.5, t_r is calculated as 27.77 seconds.

To initialize the calculation in equation 7.8, we set $I_{gic\_a(t-1)}$ = 0.

Taking the transformer response into consideration, the prospective GIC with transformer time response flowing through substation 7 is calculated using equation 7.8.

$$I_{gic\_a(t)} = I_{gic\_a(t-1)} + \left[I_{gic\_p(t)} - I_{gic\_a(t-1)} \right] (1 - e^{\frac{-t_x}{T}}) \tag{7.8}$$

In general LR circuitry, the response time (t_r) taken for current to reach its peak value is about 5 times its time constant [90]. Hence t_r is divided by 5 [91] .

$T = \frac{t_r}{5}$ = 5.55 seconds

From Table 7.3 in section 7.1, the first prospective GIC in substation 7 is 2.43 A.

From this, the first prospective GIC with transformer time response at one second is calculated as,

$I_{gic\_a(1)} = 0 + [2.43 - 0](1 - e^{-\frac{1}{5.55}}) = 0.39$ A, which is 84 % lower than the prospective without the transformer time response.

At t = 2 seconds,

$$I_{gic\_a(2)} = I_{gic\_a(1)} + \left[I_{gic\_p(1)} - I_{gic\_a(1)} \right] * (1 - e^{\frac{-2}{5.55}}) \quad (7.9)$$

$$= 0.39 + [2.43 - 0.39] * (0.30) \quad = 1.0\ A.$$

From the calculation of the prospective GIC with transformer response in substation 7 at two seconds, it can be seen that the transformer response time to GIC suppresses the prospective GIC, such that the difference between the prospective GIC with and without the transformer response is 59 %. It should be noted that when the time between two successive GIC samples are as long as two minutes, based on the time response profile of the transformer, the prospective GIC with and without the transformer time response may be the same. This is because the exponential term in equation 7.9 tends to zero with longer sampling time intervals.

Sample calculation for the prospective GIC with transformer time response at substation 4:

Substation 4 has 2 units of 500 MVA 3P-5L transmission transformers. The time response profile for each transformer is obtained from Table 6.2. The relevant equation in Table 6.2 is equation 7.5. The magnetization current for the transformer from the PSCAD simulation is 2.1 A. The prospective GIC through each transformer in substation 4, from Table 7.3 in section 7.1 is:

$$\frac{\text{substation prospective GIC}}{No\ of\ transformers} = \frac{-0.49\ \text{A}}{2} = -0.25\ A \quad (7.10)$$

Therefore,

$$z = \frac{i}{i_{mag}} \tag{7.11}$$

$$= \frac{-0.25\ A}{2.1\ A} = -0.12$$

Note that z can either be a positive or negative number as this depends on the polarity of the prospective GIC. For substation 4, z is negative.

Taking the absolute value of z as 0.12, in equation 7.5, t_r is 27.77 seconds for substation 4. To initialize the calculation in equation 7.12, we set $I_{gic\_a(t-1)}$ = 0.

Taking the transformer response into consideration, the prospective GIC flowing through substation 4 is calculated using equation 7.12.

$$I_{gic\_a(t)} = I_{gic\_a(t-1)} + \left[I_{gic\_p(t)} - I_{gic\_a(t-1)} \right] (1 - e^{\frac{-t_x}{T}}) \tag{7.12}$$

$$T = \frac{t_r}{5} = 5.55\ seconds$$

From Table 7.3 in section 7.1, the first prospective GIC $I_{gic\_p(1)}$ in substation 4 is - 0.49 A.

From this, the first prospective GIC with transformer time response at one second is calculated as,

$I_{gic\_a(1)} = 0 + [(-0.49) - 0](1 - e^{-\frac{1}{5.55}})$ = - 0.08 A, which is 84 % lower than the prospective without the transformer time response.

At *t* = 2 seconds,

$$I_{gic\_a(2)} = I_{gic\_a(1)} + \left[I_{gic\_p(1)} - I_{gic\_a(1)} \right] * (1 - e^{\frac{-2}{5.55}}) \tag{7.13}$$

$$= -0.08 + [-0.91 - (-0.08)] * (0.30) \quad = -0.33\ A.$$

From the calculation of the prospective GIC with transformer response in substation 4 at two seconds, it can be seen that the transformer response time to GIC suppresses the

prospective GIC, such that the difference between the prospective GIC with and without the transformer response is 33 %. In substation 7, the difference was 59 %. The values vary due to the dynamic characteristics of the transformer time response. By incorporating the transformer time response in GIC calculation, it is possible to calculate the GIC flowing at two seconds and any point in time.

Thus far, the calculation examples have demonstrated how the prospective GIC with transformer time response is calculated. This method was also used for calculating prospective GIC with transformer time response at the 10 substations. In this case, all the transformers in the network were set to 3P-5L transmission transformers. The profiles for substations 1 and 4 at the middle of the network and substation 6 and 7 at the edge of the network are shown in Figures 7.8 to Figure 7.11. The profiles for the other 6 substations are given in Appendix D.

The scale of the vertical axis in Figures 7.8 to 7.11 was chosen to match the scale of the substation with the highest GIC value, which is substation 7 in Figure 7.11.

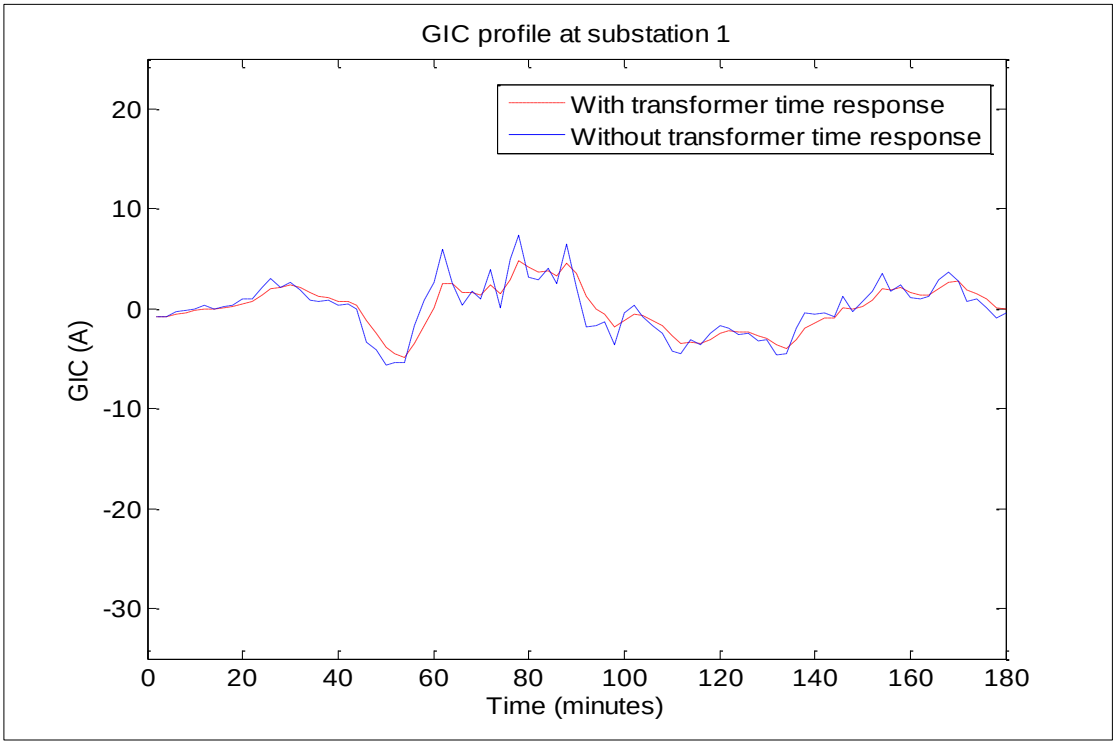

Figure 7.8 Prospective GIC profile with and without transformer time response at substation 1

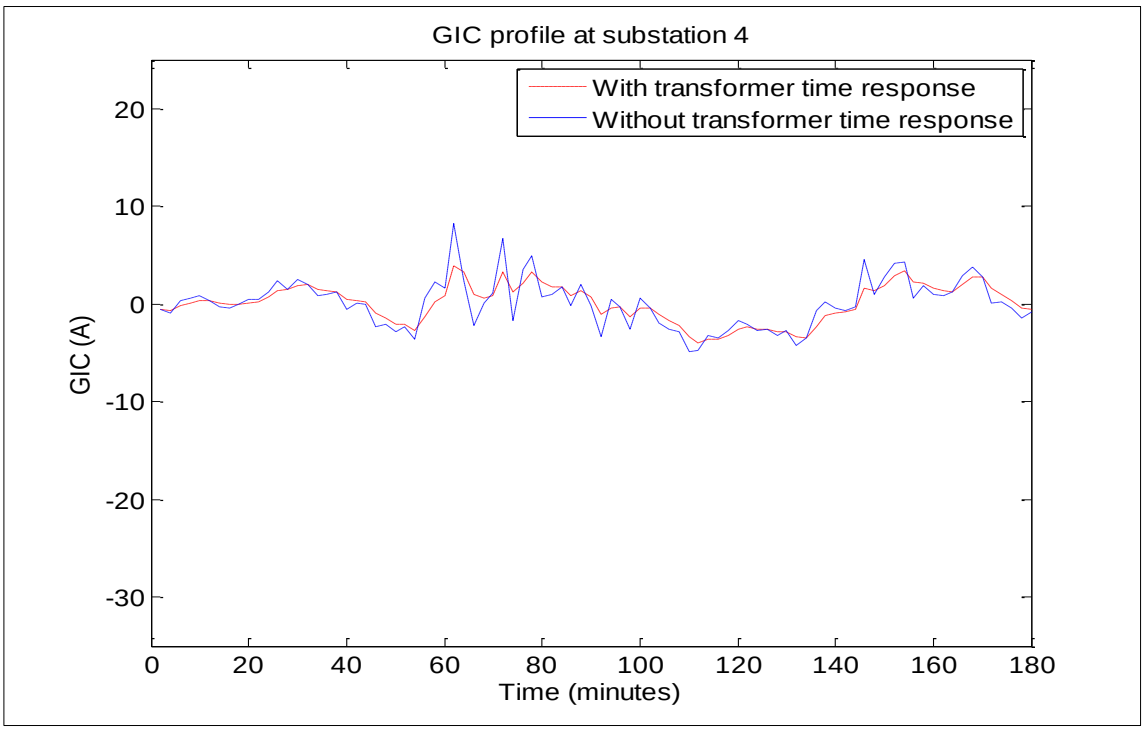

Figure 7.9 Prospective GIC profile with and without transformer time response at substation 4

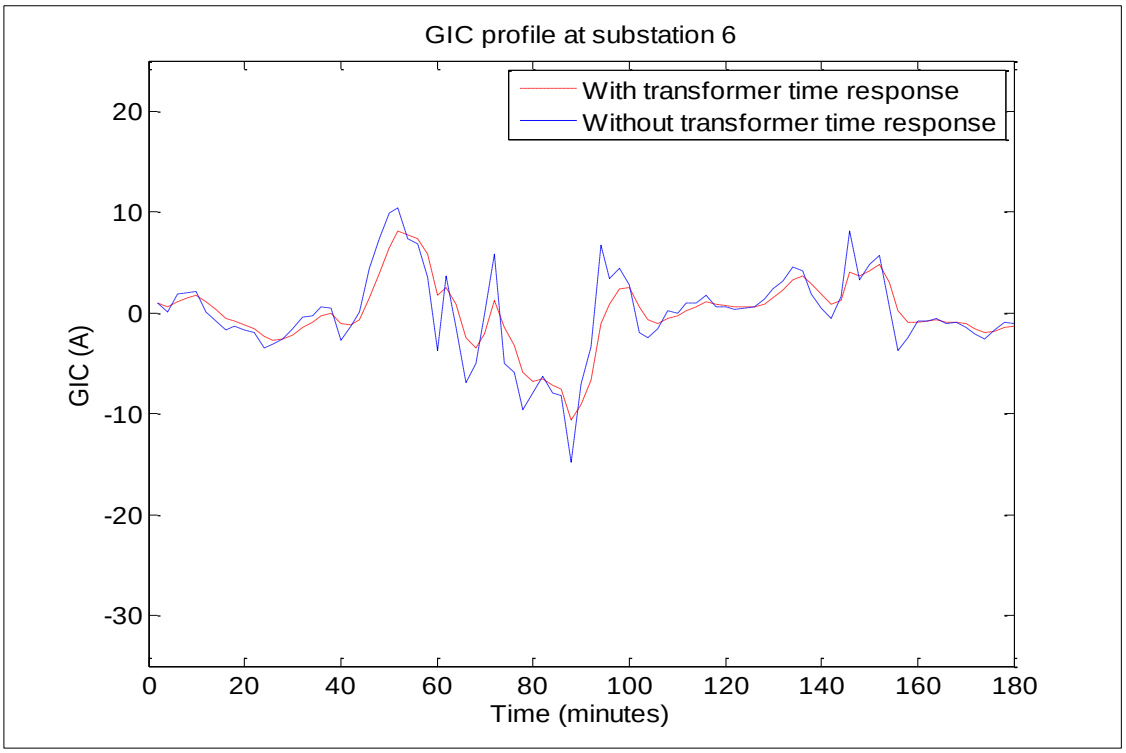

Figure 7.10 Prospective GIC profile with and without transformer time response at substation 6

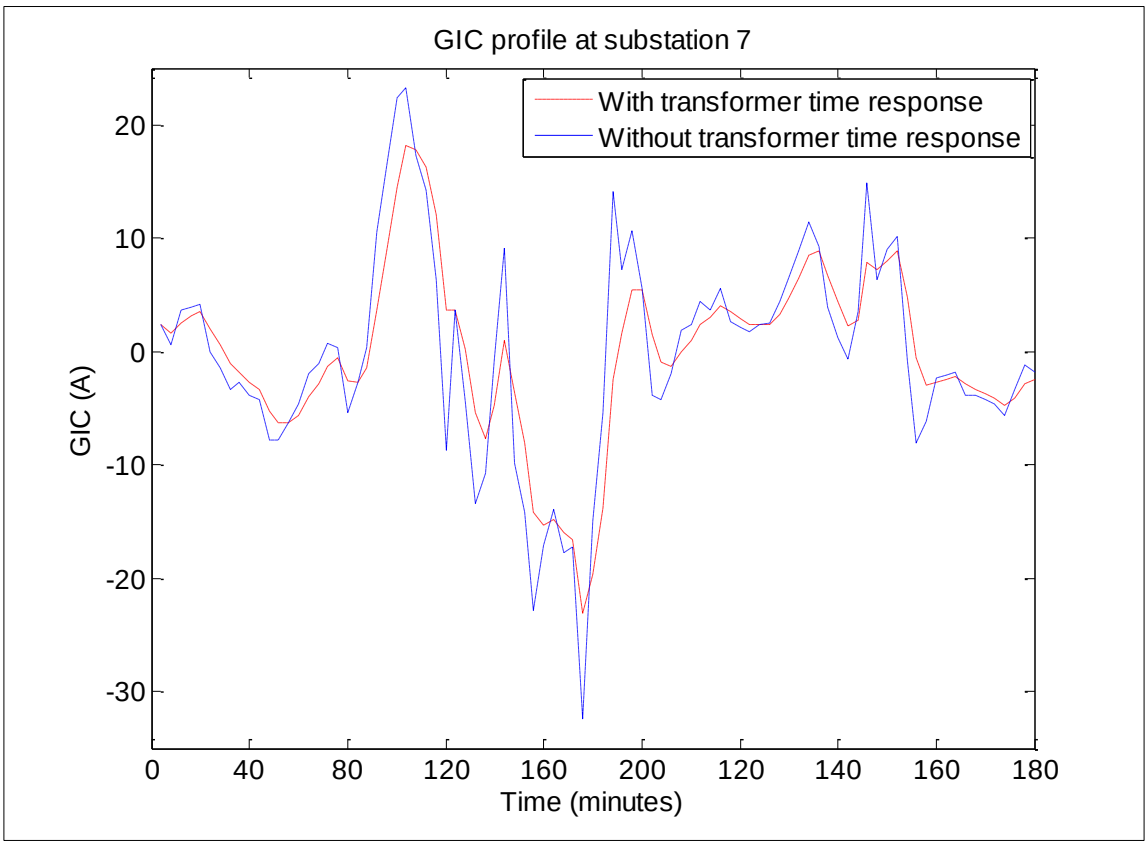

Figure 7.11 Prospective GIC profile with and without transformer time response at substation 7

There is no difference in the pattern of the transformer response time to DC between transformers at the middle of the network and transformers around the edge of the network. This can be seen by comparing Figures 7.8 and Figure 7.9 with Figure 7.10 and Figure 7.11. This is probably because in this case, all the transformers are the same in terms of the core structure and mode of operation as TTs. The prospective GIC calculated with the transformer time response is less than the prospective GIC calculated without the transformer time response on average, especially at the shorter peaks. This profile is based on the equation of the transformer time response to GIC and the sampling time interval of the magnetic field.

7.2.2 Case 2: Calculated GIC in the test network with a variety of transformer core structures using two-minute sampling time interval magnetic field data

In this case study, 40 % of the transformers were 3P-5L, 20 % of the transformers were 3P-3L and 40 % of the transformers were 3(1P-3L). 30 % were operating as GSUs, while 70 % were operating as TTs. Table 7.5 is a modified version of Table 7.2 with additional pseudo-data on the transformer core structure and operational state.

Table 7.5 Substation data with additional data on the transformer core structure and operational state. In this case, the transformer core structure is not the same across the network

Substation No.	Actual earthing resistance (R_e) Ω	Number of transformers at substation (n_t)	Transformer core structure	Operational state	Number of reactors at substation (n_r)	Calculated substation resistance per phase (R_i) Ω
1	0.3	1	3P-5L	Transmission	0	0.8
2	0.3	2	3(1P-3L)	GSU	1	0.8
3	0.3	1	3(1P-3L)	Transmission	0	0.8
4	0.3	2	3P-3L	Transmission	1	0.8
5	0.3	1	3P-3L	GSU	0	0.8
6	0.3	1	3P-5L	Transmission	0	0.8
7	0.3	2	3(1P-3L)	GSU	1	0.8
8	0.3	1	3P-5L	Transmission	0	0.8
9	0.3	2	3(1P-3L)	Transmission	1	0.8
10	0.3	1	3P-5L	Transmission	0	0.8

Sample calculations of the GIC flow through substation 4 and substation 7 are shown in Appendix M. The procedure for this calculation was outlined in case 1. The relevant transformer response time equation for substation 7, with two 500 MVA 3(1P-3L) GSUs, is given in equation 7.14 and that of substation 4, with two 500 MVA 3P-3L TTs is given in equation 7.15.

$$t_r = \begin{cases} 16.34\ s & if \quad 0 < z < 2 \\ 18.49\ s & if \quad 2 \leq z < 6 \\ 14.75\ s & if \quad 6 \leq z < 8 \\ 20.79\ s & if\ 8 \leq z \leq 10 \\ 13.66\ s & if\ 10 \leq z \leq 14 \end{cases} \tag{7.14}$$

$$t_r = \begin{cases} 0.23\,s & if \quad 0 < z < 4 \\ 0.58\,s & if \quad 4 \leq z < 6 \\ 0.92\,s & if \quad 6 \leq z < 10 \\ 1.25\,s & if \; 10 \leq z \leq 14 \end{cases} \tag{7.15}$$

From the calculation of the prospective GIC with transformer time response at substation 7, it can be seen that the transformer response suppresses the prospective GIC, such that the difference between the prospective GIC with and without transformer time response is 74 %. This difference at two seconds is 35 %. For substation 4, the results show that the prospective GIC with and without transformer time response are the same. This is primarily because of the relatively shorter response time of the 3P-3L transformer.

This example demonstrates that the prospective GIC with and without transformer time response may be equal, especially in 3P-3L transformers.

The next step was to calculate the prospective GIC with transformer time response at the 10 substations. The time between each electric field sample was set to two minutes, because the magnetic field data has a two-minute sampling time interval. 40 % of the transformers were 3P-5L, 20 % of the transformers were 3P-3L and 40 % of the transformers were 3(1P-3L). 30 % of the transformers were operating as GSUs, while 70 % were operating as TTs. The profiles for substations 1 and 4 at the middle of the network and substations 6 and 7 at the edge of the network are shown in Figures 7.12 to 7.13. The profiles for the other 6 substations are given in Appendix E.

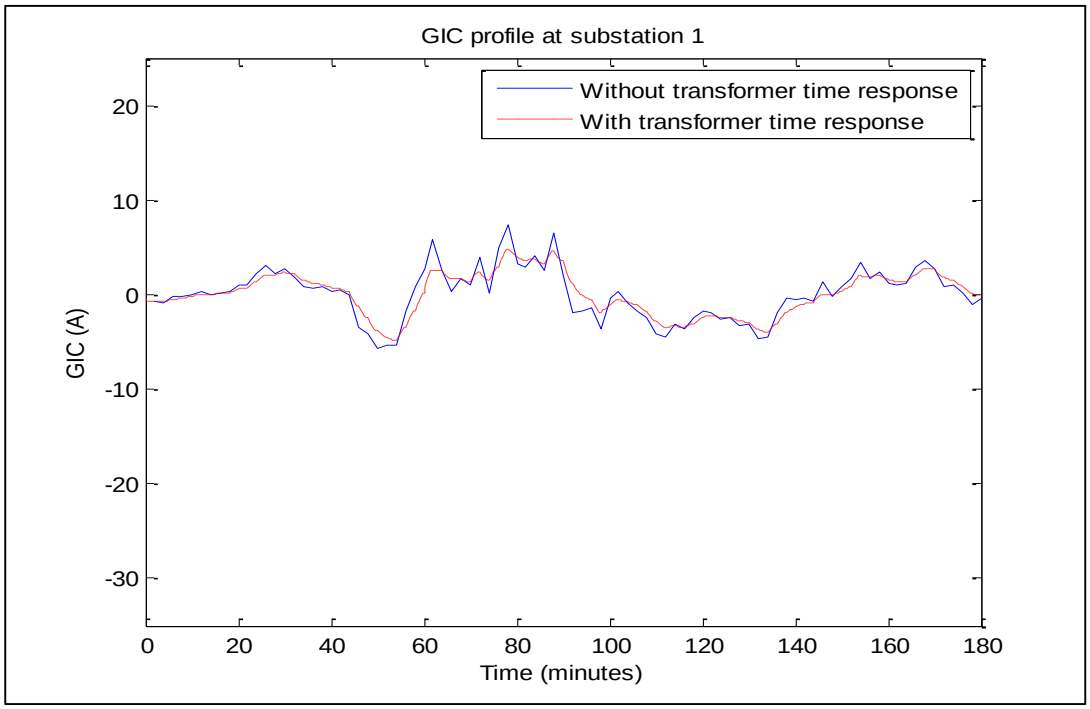

Figure 7.12 Case 2: Prospective GIC profile with and without transformer time response at substation 1

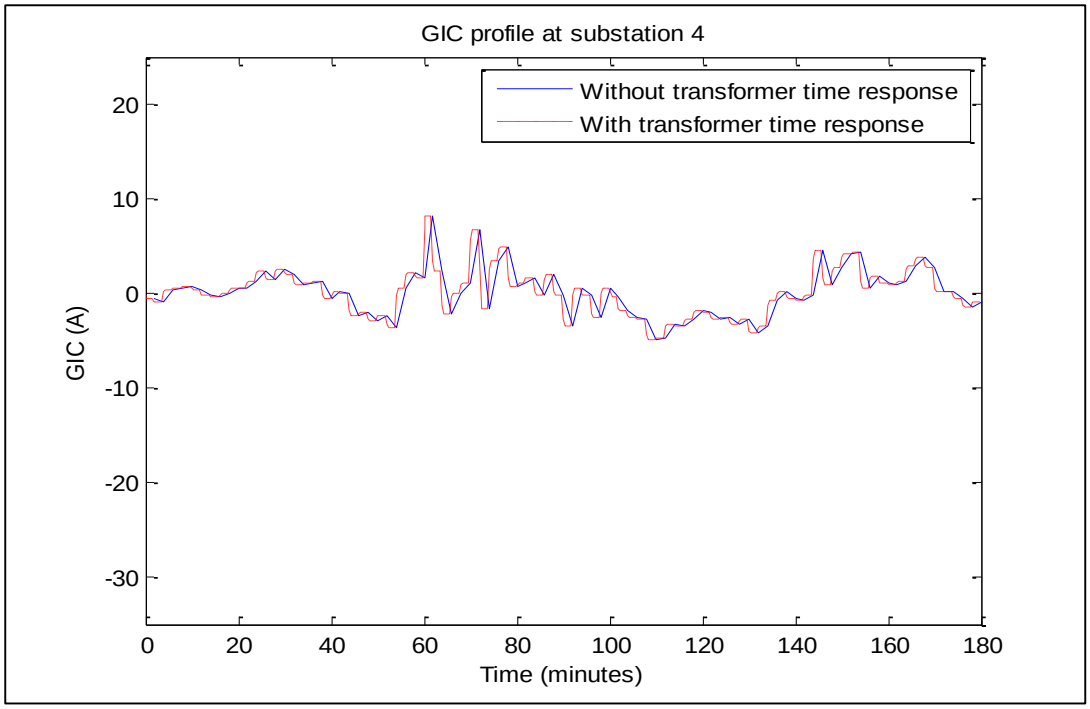

Figure 7.13 Case 2: Prospective GIC profile with and without transformer time response at substation 4

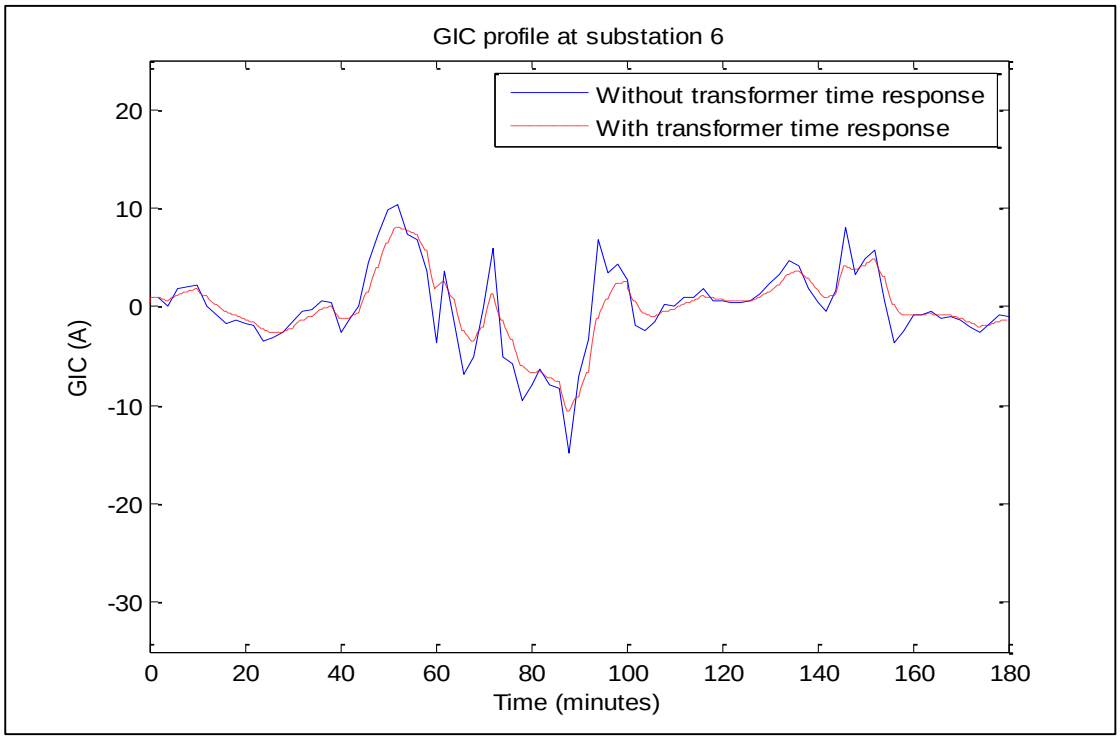

Figure 7.14 Case 2: Prospective GIC profile with and without transformer time response at substation 6

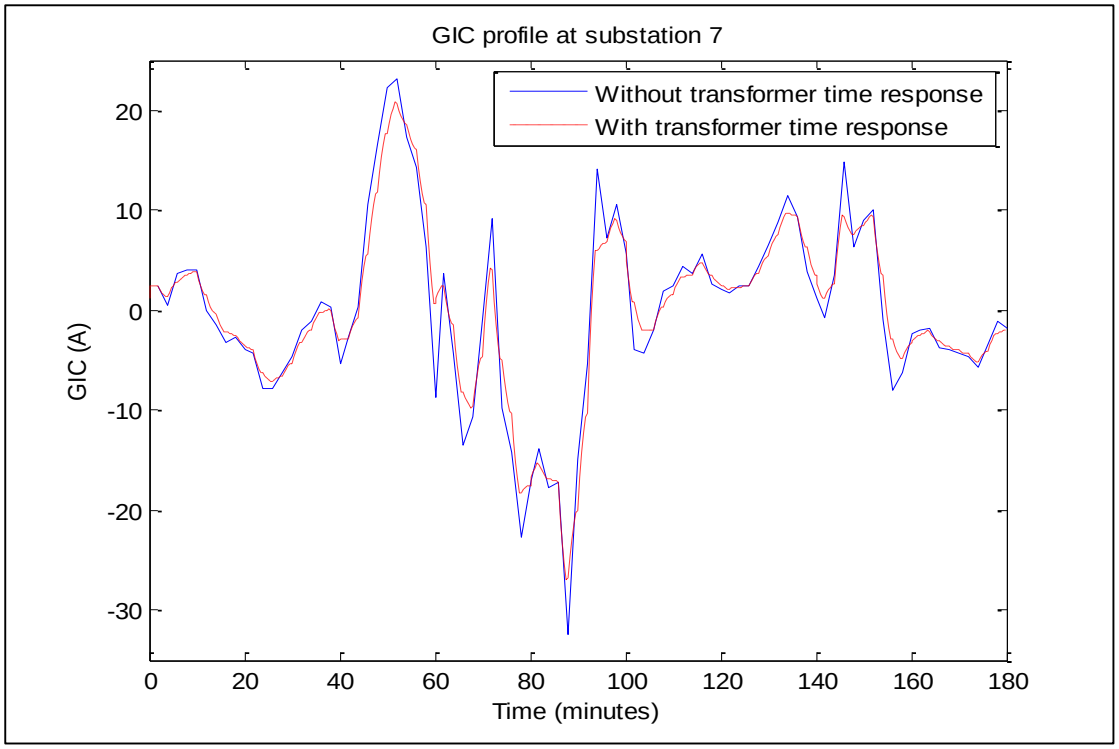

Figure 7.15 Case 2: Prospective GIC profile with and without transformer time response at substation 7

The difference in the profiles of the prospective GIC with and without transformer time response for substation 4 is reduced when compared with substation 7. This is attributed to the short response time to GIC of the 3P-3L transformers in substation 4. Substation 7 shows a larger difference between the two GIC profiles which stems from the longer time response of the 3(1P-3L) GSU transformers in substation 7. In the next section the effect of using interpolated magnetic field data on the magnitude of the prospective GIC with and without transformer time response is investigated.

7.3 EFFECT OF INCREASED MAGNETIC FIELD SAMPLING TIME INTERVAL ON THE MAGNITUDES OF THE PROSPECTIVE GIC WITH AND WITHOUT TRANSFORMER TIME RESPONSE

In chapter 3, where the transformer time constant was introduced, it was mentioned that if the magnetic field sampling interval is chosen such that it is longer than the average transformer response time to GIC, the prospective GIC with and without the transformer time response will be similar. In section 7.1 and section 7.2, the sampling time interval of the magnetic field data used to calculate the electric field was two minutes. In this, section, the magnetic field sampled at two-minute interval was interpolated at four-minute intervals in order to determine the effect that doubling the magnetic field sampling interval has on the prospective GIC, taking the transformer time response into account.

Two case studies, cases 3 and 4 were done. These case studies are similar to case 1 and case 2 in section 7.2. The only difference is that the magnetic field data was interpolated at 4-minute sampling intervals.

7.3.1 Case 3: Calculated GIC in the test network with uniform transformer core structure using 4-minute sampling time interval magnetic field data

The procedure for calculating the prospective GIC without the transformer time response was sufficiently explained in section 7.1. Thus, only the table of these values are shown. Table 7.6 shows the prospective GIC values without transformer time response at the 10 substations with four-minute sampling time interval magnetic field data.

Table 7.6 Prospective GIC values without transformer time response calculated for the 10 substation network with four-minute sampling time interval magnetic field data

	Substation number									
Sample	1	2	3	4	5	6	7	8	9	10
1	-0.78	-1.32	-0.74	-0.70	-0.60	0.54	1.49	-0.33	1.77	0.67
2	-0.20	-9.20	0.25	0.48	-0.42	1.91	3.80	0.33	1.96	1.09
3	0.16	-5.85	0.47	0.61	-0.06	1.11	2.05	0.36	0.66	0.49
4	0.12	5.83	-0.17	-0.31	0.26	-1.21	-2.40	-0.21	-1.22	-0.68
5	0.66	6.39	0.37	0.20	0.66	-1.51	-3.30	0.03	-2.39	-1.11
6	1.58	10.56	1.11	0.83	1.44	-2.67	-6.07	0.30	-4.92	-2.17
7	2.59	9.72	2.20	1.93	2.14	-2.86	-7.02	0.85	-6.78	-2.78
8	2.28	0.98	2.32	2.27	1.67	-1.00	-3.26	1.11	-4.70	-1.66
9	0.78	-2.18	0.92	0.97	0.49	0.16	-0.15	0.50	-1.18	-0.31
10	0.65	4.39	0.45	0.33	0.59	-1.10	-2.51	0.12	-2.02	-0.90
11	0.21	2.53	0.09	0.02	0.22	-0.58	-1.24	-0.01	-0.84	-0.40
12	-3.78	-22.71	-2.78	-2.19	-3.38	5.87	13.54	-0.85	11.35	4.93
13	-5.50	-41.04	-3.65	-2.59	-5.16	10.14	22.78	-0.86	17.87	8.00
14	-3.56	-29.25	-2.23	-1.47	-3.42	7.10	15.78	-0.43	12.02	5.46
15	1.73	-2.59	1.92	1.97	1.16	-0.09	-1.18	1.00	-2.99	-0.92
16	4.23	-12.96	5.05	5.32	2.65	1.09	-0.35	2.75	-6.22	-1.56
17	1.03	27.95	-0.34	-1.03	1.57	-5.94	-12.08	-0.79	-6.77	-3.59
18	2.43	-18.63	3.46	3.89	1.19	2.86	4.11	2.11	-1.68	0.26
19	2.55	22.83	1.50	0.91	2.50	-5.46	-12.03	0.22	-8.92	-4.10
20	5.25	34.41	3.72	2.83	4.79	-8.73	-19.91	1.04	-16.26	-7.15
21	3.49	29.57	2.14	1.38	3.38	-7.14	-15.82	0.38	-11.93	-5.44
22	4.47	49.72	2.14	0.88	4.68	-11.51	-24.82	-0.07	-17.28	-8.19
23	0.14	25.82	-1.15	-1.78	0.87	-5.21	-10.14	-1.14	-4.65	-2.76
24	-1.52	-22.73	-0.43	0.14	-1.76	5.07	10.68	0.30	6.85	3.38
25	-1.99	-14.45	-1.34	-0.97	-1.86	3.59	8.09	-0.33	6.40	2.86
26	-0.27	11.44	-0.85	-1.13	0.15	-2.19	-4.08	-0.67	-1.40	-1.00
27	-2.10	7.14	-2.55	-2.70	-1.30	-0.68	-0.09	-1.40	2.98	0.71
28	-4.31	5.25	-4.74	-4.82	-2.93	0.48	3.42	-2.43	7.68	2.41
29	-3.35	-1.04	-3.43	-3.37	-2.43	1.39	4.64	-1.65	6.84	2.40
30	-2.10	0.62	-2.21	-2.20	-1.49	0.62	2.41	-1.09	4.07	1.37
31	-2.21	1.82	-2.39	-2.41	-1.53	0.42	2.09	-1.21	4.08	1.33
32	-2.83	0.32	-2.95	-2.93	-2.02	0.94	3.45	-1.45	5.57	1.90
33	-3.89	-7.11	-3.68	-3.47	-3.00	2.80	7.66	-1.64	8.93	3.40
34	-3.20	-16.36	-2.50	-2.07	-2.78	4.40	10.36	-0.85	9.13	3.88

35	-0.48	-5.11	-0.24	-0.11	-0.50	1.19	2.58	0.00	1.82	0.86
36	-0.57	-1.75	-0.51	-0.46	-0.46	0.55	1.40	-0.21	1.44	0.57
37	0.54	-29.24	2.03	2.74	-0.48	5.65	10.59	1.65	3.87	2.65
38	1.23	-28.75	2.73	3.42	0.03	5.31	9.53	1.98	2.41	2.12
39	2.61	3.03	2.56	2.46	1.96	-1.53	-4.47	1.18	-5.70	-2.10
40	1.76	5.22	1.56	1.42	1.42	-1.66	-4.24	0.65	-4.38	-1.74
41	1.12	1.30	1.09	1.05	0.84	-0.65	-1.91	0.50	-2.44	-0.90
42	3.23	-0.60	3.38	3.36	2.30	-1.02	-3.85	1.66	-6.32	-2.15
43	1.79	5.62	1.57	1.42	1.45	-1.75	-4.43	0.64	-4.50	-1.80
44	0.58	9.85	0.10	-0.15	0.70	-2.17	-4.52	-0.17	-2.81	-1.41
45	-0.68	6.01	-1.01	-1.15	-0.31	-0.96	-1.46	-0.63	0.33	-0.16

Table 7.7 shows the data on transformer core structure which suits the basis of case 3, as explained in the introduction to section 7.3.

Table 7.7 Substation data with additional data on the transformer core structure and operational state. In this case study, all the transformer core structure and operational state are the same

Substation No.	Actual earthing resistance (R_e) Ω	Number of transformers at substation (n_t)	Transformer core structure	Operational state	Number of reactors at substation (n_r)	Calculated substation resistance per phase (R_j) Ω
1	0.3	1	3P-5L	Transmission	0	0.8
2	0.3	2	3P-5L	Transmission	1	0.8
3	0.3	1	3P-5L	Transmission	0	0.8
4	0.3	2	3P-5L	Transmission	1	0.8
5	0.3	1	3P-5L	Transmission	0	0.8
6	0.3	1	3P-5L	Transmission	0	0.8
7	0.3	2	3P-5L	Transmission	1	0.8
8	0.3	1	3P-5L	Transmission	0	0.8
9	0.3	2	3P-5L	Transmission	1	0.8
10	0.3	1	3P-5L	Transmission	0	0.8

Sample calculations of the GIC flow through substation 4 and substation 7 are shown in Appendix N. The relevant transformer response equation for substations 4 and 7, each with two 500 MVA 3P-5L transmission transformers is given in equation 7.16.

$$t_r = \begin{cases} 27.77\ s & if \quad 0 < z < 6 \\ 28.48\ s & if \quad 6 \leq z < 8 \\ 26.18\ s & if \quad 8 \leq z < 10 \\ 28.98\ s & if\ 10 \leq z \leq 14 \end{cases} \tag{7.16}$$

For substation 7, at one second, the prospective GIC with transformer time response was 49 % lower than the prospective GIC without transformer response. For substation 4, at one second, the prospective GIC with transformer time response was 83 % lower than the prospective GIC without transformer time response. At two seconds, this was 79 %. The percentage differences are to be expected due the dynamic characteristics of the transformer time response to GIC.

The profiles for substations 1 and 4 at the middle of the network and substations 6 and 7 at the edge of the network are shown in Figures 7.16 to 7.19. The profiles for the other 6 substations are given in Appendix F.

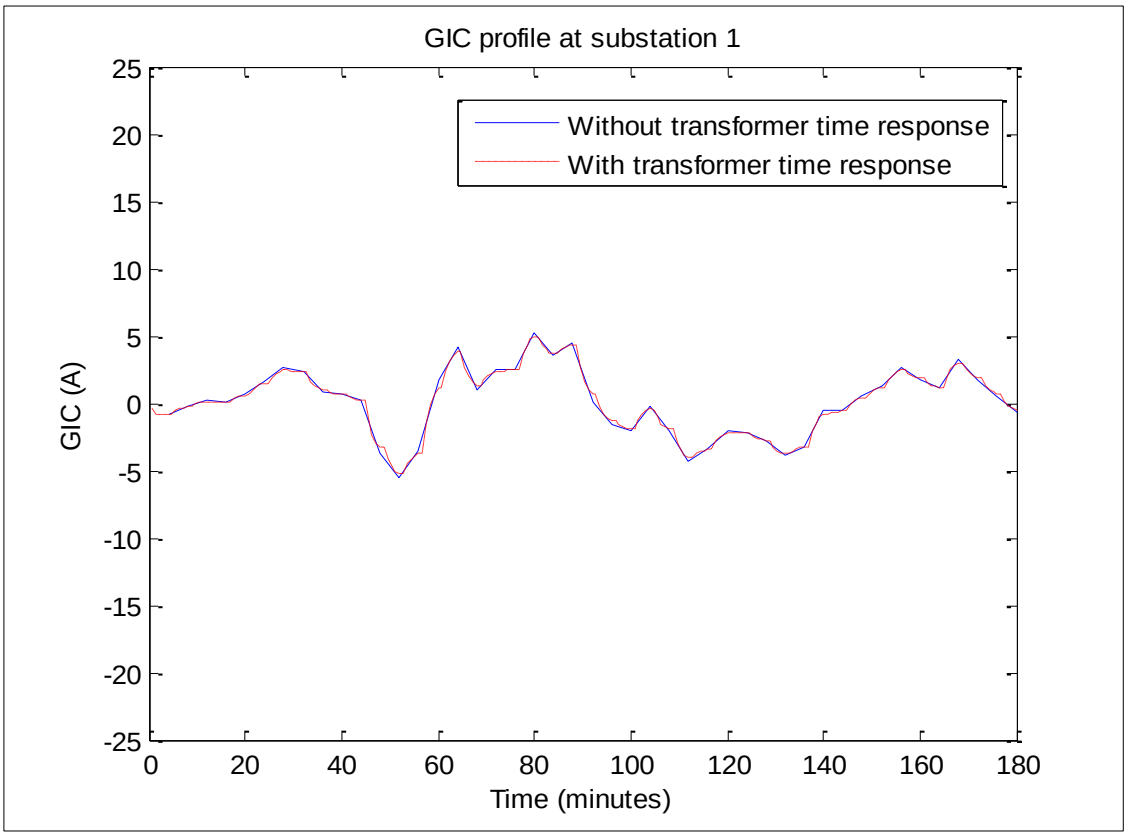

Figure 7.16 Prospective GIC profile with and without transformer time response at substation 1

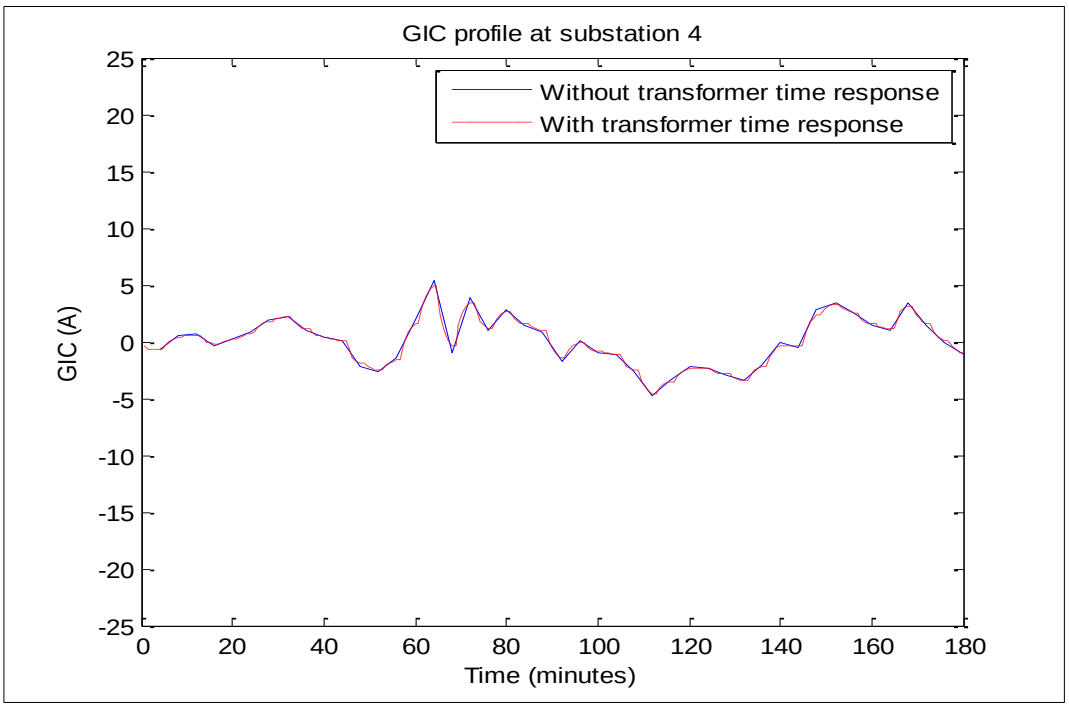

Figure 7.17 Prospective GIC profile with and without transformer time response at substation 4

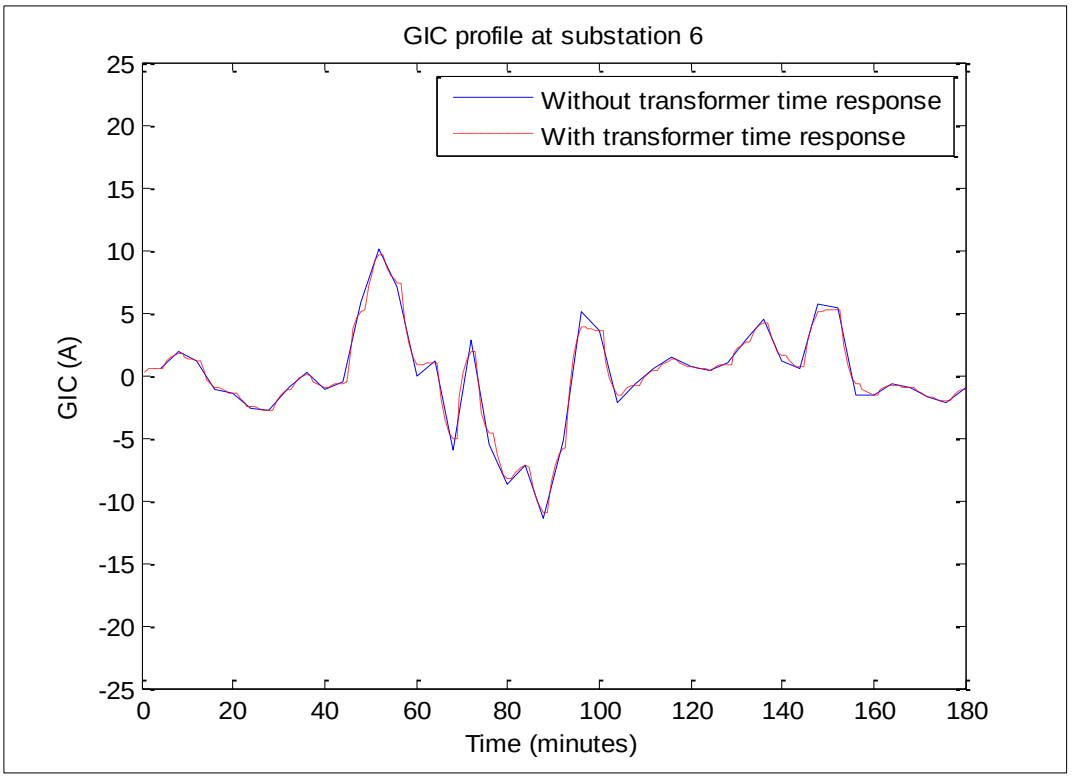

Figure 7.18 Prospective GIC profile with and without transformer time response at substation 6

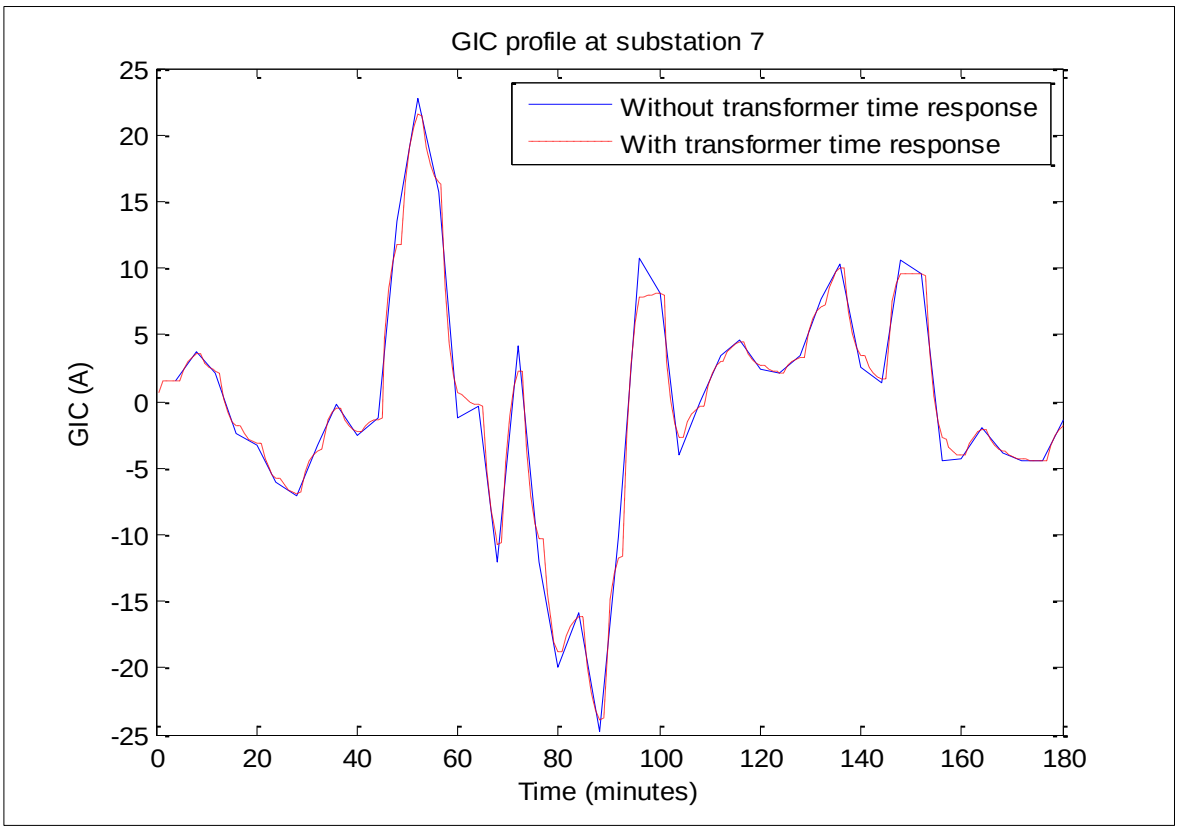

Figure 7.19 Prospective GIC profile with and without transformer time response at substation 7

The results of this case study show that with the four-minute sampling interval, the prospective GIC with and without transformer time response are similar, offsetting the relevance of the transformer time response. In the next case study, a variety of transformers structures are considered in order to determine the effect of the doubled magnetic field sampling time interval on the prospective GIC with transformer time response at the substations with different transformer core structures and mode of operation.

7.3.2 Case 4: Calculated GIC in the test network with a variety of transformer core structure using four-minute sampling time interval magnetic field data

The step-by-step calculation of the prospective GIC with transformer time response in substation 4 and substation 7 are not shown here, but is available in Appendix O. Table 7.8

shows the substation data and the transformer core structures which suit the basis of case 4, as explained in the introduction to section 7.3.

Table 7.8 Substation data with additional data on the transformer core structure and operational state. In this case, the transformer core structure is not the same across the network

Substation No.	Actual earthing resistance (R_e) Ω	Number of transformers at substation (n_t)	Transformer core structure	Operational state	Number of reactors at substation (n_r)	Calculated substation resistance per phase (R_j) Ω
1	0.3	1	3P-5L	Transmission	0	0.8
2	0.3	2	3(1P-3L)	GSU	1	0.8
3	0.3	1	3(1P-3L)	Transmission	0	0.8
4	0.3	2	3P-3L	Transmission	1	0.8
5	0.3	1	3P-3L	GSU	0	0.8
6	0.3	1	3P-5L	Transmission	0	0.8
7	0.3	2	3(1P-3L)	GSU	1	0.8
8	0.3	1	3P-5L	Transmission	0	0.8
9	0.3	2	3(1P-3L)	Transmission	1	0.8
10	0.3	1	3P-5L	Transmission	0	0.8

For substation 4, the relevant transformer response equation for the 500 MVA 3P-3L transmission transformers is given in equation 7.17 and that of substation 7 with two 500 MVA 3P-3L GSU transformers is given in equation 7.18.

$$t_r = \begin{cases} 0.23\ s & if \quad 0 < z < 4 \\ 0.58\ s & if \quad 4 \leq z < 6 \\ 0.92\ s & if \quad 6 \leq z < 10 \\ 1.25\ s & if\ 10 \leq z \leq 14 \end{cases} \tag{7.17}$$

$$t_r = \begin{cases} 16.34\ s & if \quad 0 < z < 2 \\ 18.49\ s & if \quad 2 \leq z < 6 \\ 14.75\ s & if \quad 6 \leq z < 8 \\ 20.79\ s & if\ 8 \leq z \leq 10 \\ 13.66\ s & if\ 10 \leq z \leq 14 \end{cases} \tag{7.18}$$

The calculations in Appendix O show that for substation 7, the prospective GIC with transformer time response is 74% lower than the prospective GIC without the transformer time response at one second. At two seconds, this is 52% lower. For substation 4, the prospective GIC with transformer time response is 1 % lower than the prospective GIC without the transformer time response at one second. At two seconds, both prospective GIC values are equivalent. The similarity between the prospective GIC with and without transformer time response in the 3P-3L transformer is due to its relatively shorter response time. The profiles for substations 1 and 4 at the middle of the network and substations 6 and 7 at the edge of the network are shown in Figures 7.20 to 7.23. The profiles for the other 6 substations are given in Appendix F.

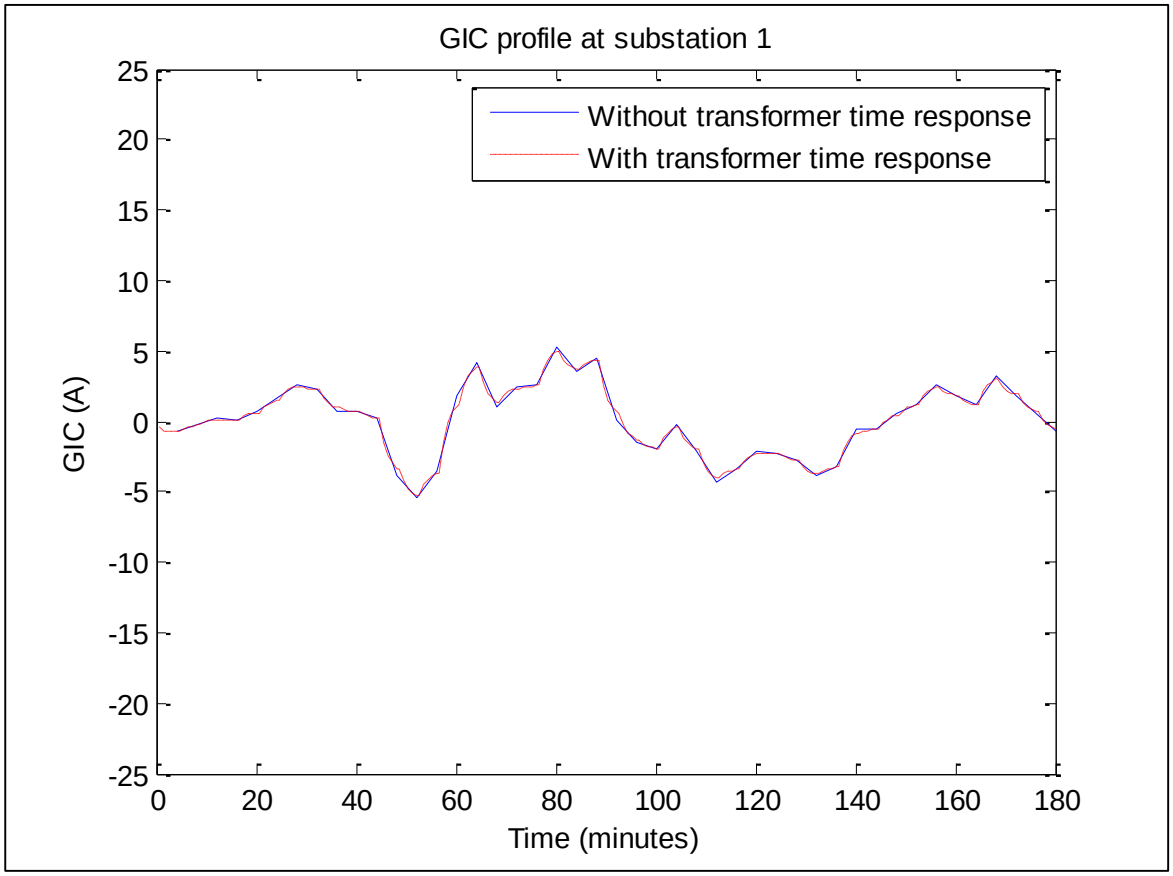

Figure 7.20 Prospective GIC profile with and without transformer time response at substation 1

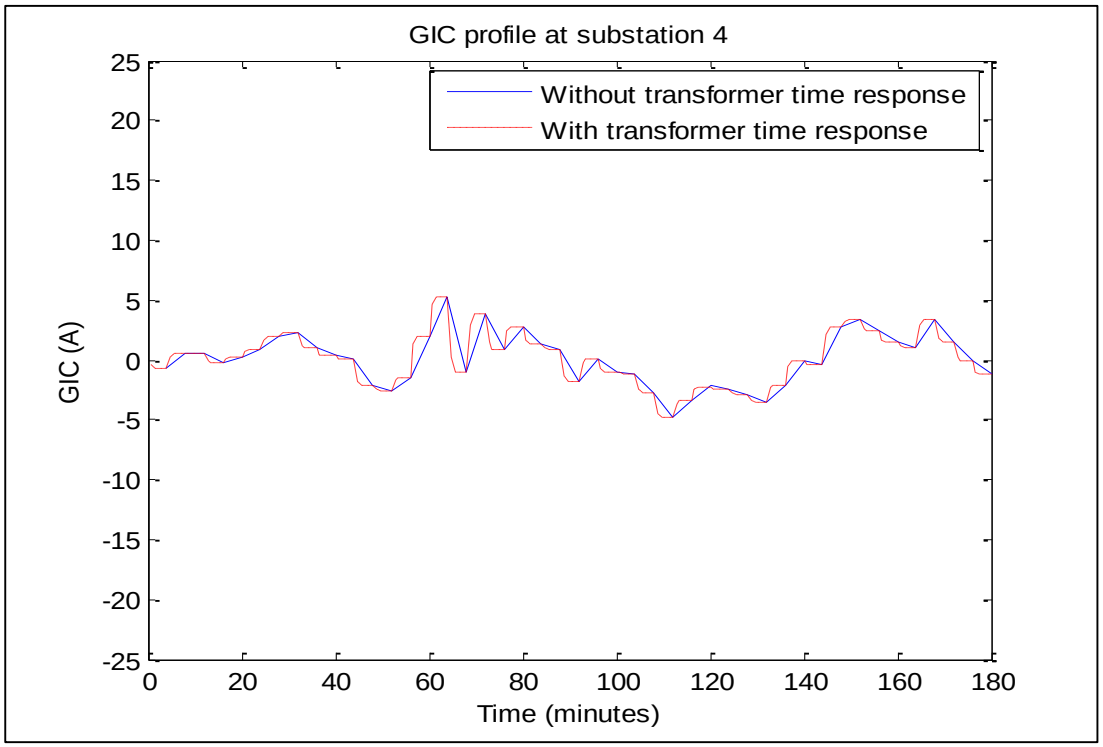

Figure 7.21 Prospective GIC profile with and without transformer time response at substation 4

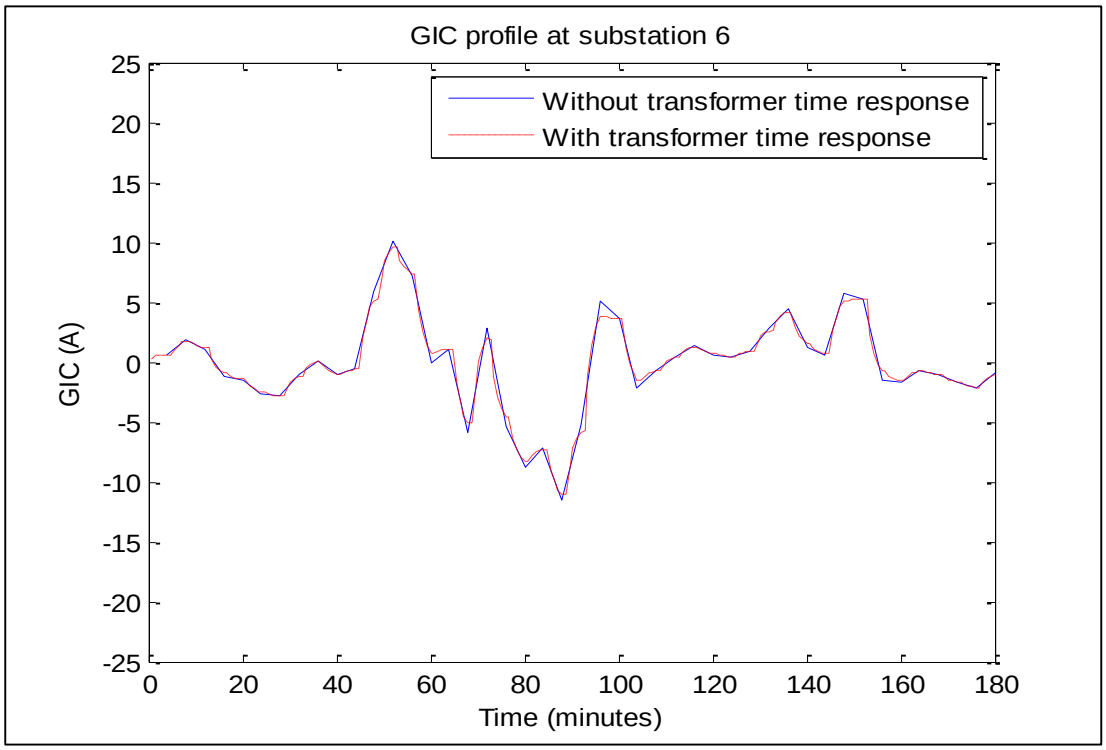

Figure 7.22 Prospective GIC profile with and without transformer time response at substation 6

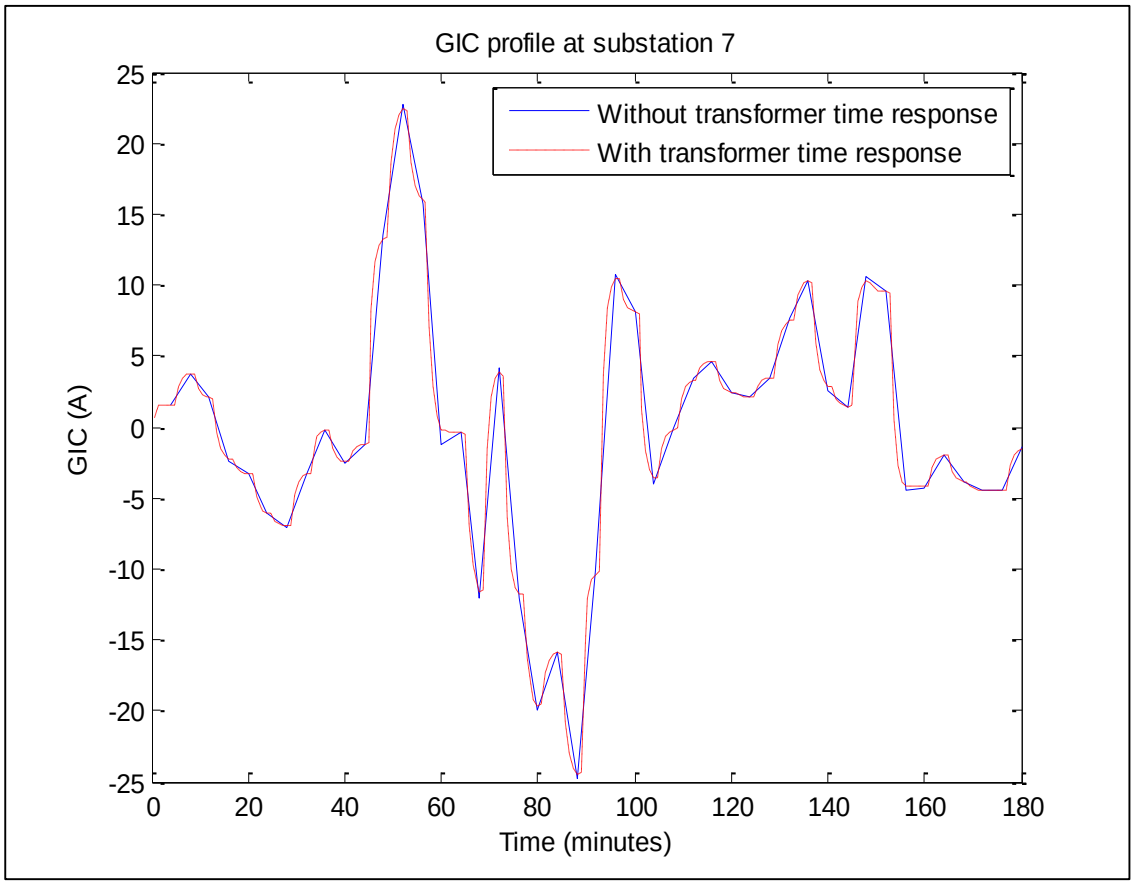

Figure 7.23 Prospective GIC profile with and without transformer time response at substation 7

The profiles in Figures 7.20 to 7.23, show no significant difference between the transformer time response to GIC for transformers at the middle of the network and transformers around the edge of the network with the four-minute sampling time interval magnetic field data.

However, one major difference between the GIC profiles in this case and case 2 is that in 90 % of all the substations, the prospective GIC profile with and without the transformer time response are exactly the same, despite the variation of transformer core structure and mode of operation. This is mainly due to the increased length of the sampling time interval of the magnetic field data.

7.4 COMPARISON BETWEEN MEASURED GIC AND CALCULATED GIC

During the Halloween storm of 2003, between 29 and 31 October, the GIC flow through Grassridge substation, South Africa was recorded at two-second time intervals. The geomagnetic field data at the closest INTERMAGNET observatory, Hermanus, was recorded at one-minute time intervals. The geomagnetic field data was interpolated using the Brownian (i.e., stochastic) method from one-minute intervals to two-second intervals, so that both the measured GIC and the geomagnetic field data will have the same time interval. This allowed for the comparison of the measured GIC against the prospective GIC with transformer time response.

Interpolating the one-minute sampling interval geomagnetic field data to two-second intervals may result in the loss of higher frequency components in the geomagnetic field data. However, since the frequencies of concern are very low, typically well below 1 Hz, interpolating the geomagnetic field data was considered acceptable. The effect of interpolating the geomagnetic field data from one-minute intervals to two-second intervals and GIC data sampled at two-second interval to one-minute intervals was investigated.

The results of the investigation showed that higher frequency components between 8 mHz and 250 mHz were lost. Considering GIC frequencies are very low frequencies, this interpolated data was considered valid, Both geomagnetic field data and measured GIC were then interpolated to four-second, 10-second, 30-second, one-minute, two-minute, four-minute and 10-minute sampling time intervals, so that the transformer response could be analysed extensively. In literature, it is not clear which sampling time interval is most adequate for measuring GIC and geomagnetic data for GIC calculation. Hence, these intervals were chosen as multiples of the one-second and one-minute sampling time intervals that are commonly used, to allow for the extensive analysis of the data and to show the impact of different sampling time intervals on the time response based GIC calculation.

This is not linked to “M” which is the ratio of the integral duration for the discretization of the electric field and the sampling time interval of the magnetic field. In general, this integral duration has been suggested to be 20 minutes. Hence for magnetic field data

sampled at one-minute intervals, M=20, for a one-second sampling interval, M=1200 which means that 1200 previous magnetic field data are needed to calculate the electric field.

The corresponding electric fields to each data set of interpolated magnetic field data in the time domain was calculated using the inverse Fourier transform of the ratio of the geomagnetic field and the Earth's surface impedance in the frequency domain. These electric field data together with the 400 kV network data for South Africa as in 2002 were then used to calculate the GIC at Grassridge.

In the first part of this section, the measured GIC at Grassridge interpolated to the different time intervals was compared with the prospective GIC without transformer time response, using the magnetic field data for the corresponding time interval. Based on the results of this comparison, the prospective GIC with transformer time response was calculated using a number of sampling time intervals in section 7.4.2.

7.4.1 Case 5: Comparison between measured GIC and prospective GIC without transformer response

The comparison of measured GIC and prospective GIC without transformer time response using magnetic field data extrapolated to four-second, 10-second, 30-second, one-minute, two-minute, four-minute and 10-minute time intervals is presented in Figures 7.24 to 7.31. The conclusions drawn from analysing these results led to the selection of the sampling time interval used in case 6.

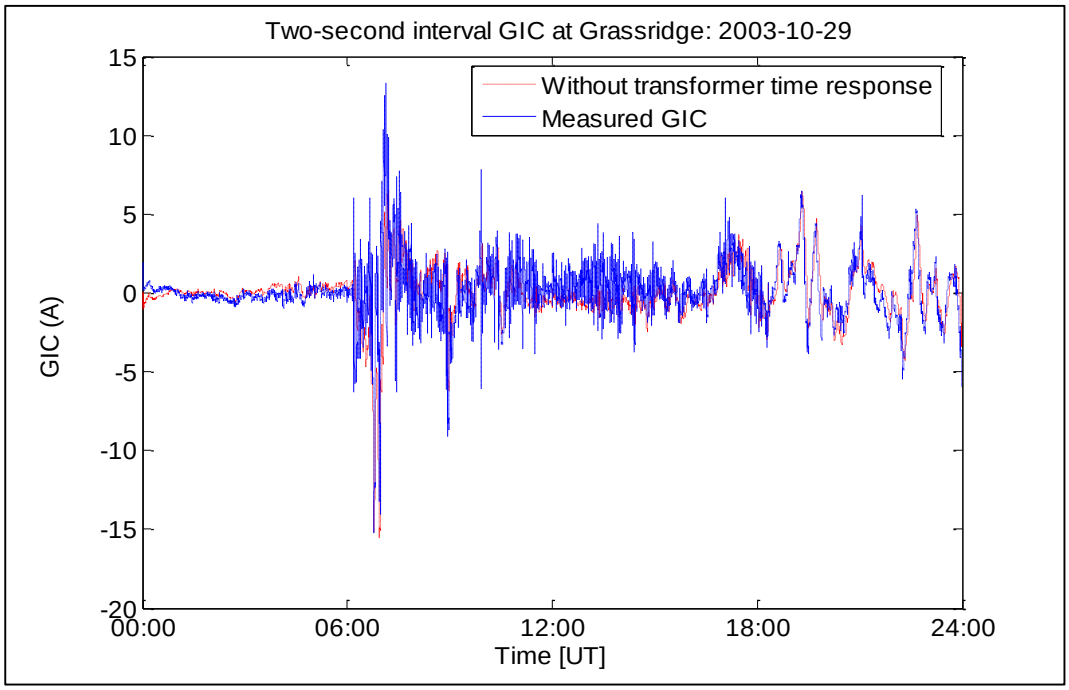

Figure 7.24: Comparison between the prospective GIC without transformer time response and the measured GIC at Grassridge using two-second sampling time interval data

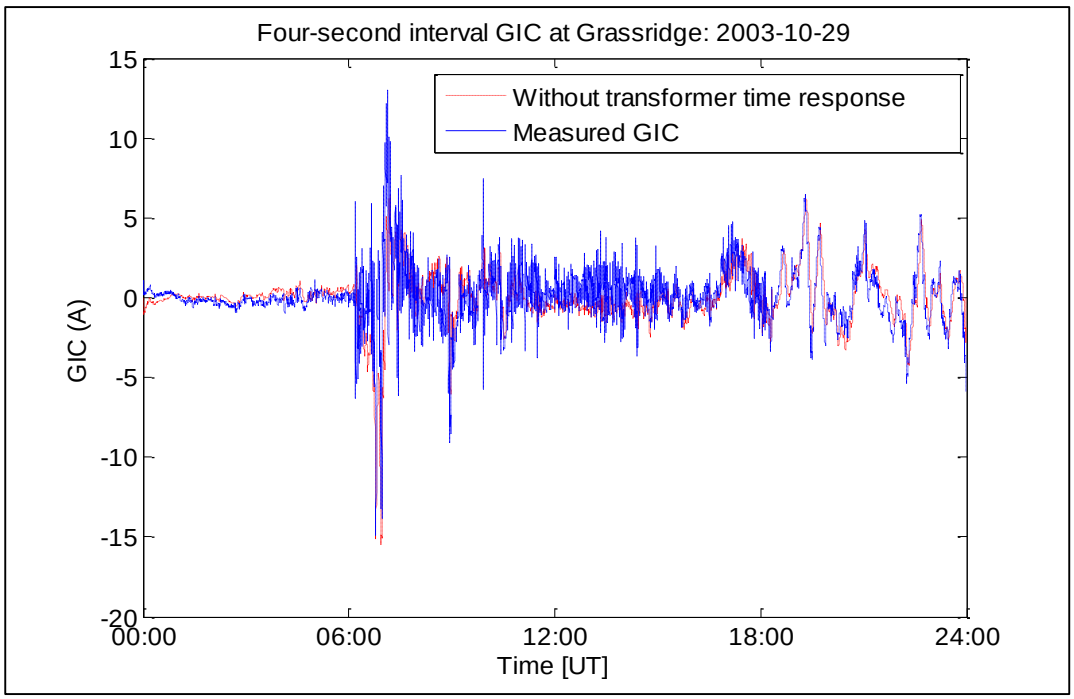

Figure 7.25 Comparison between the prospective GIC without transformer time response and the measured GIC at Grassridge using four-second sampling time interval data

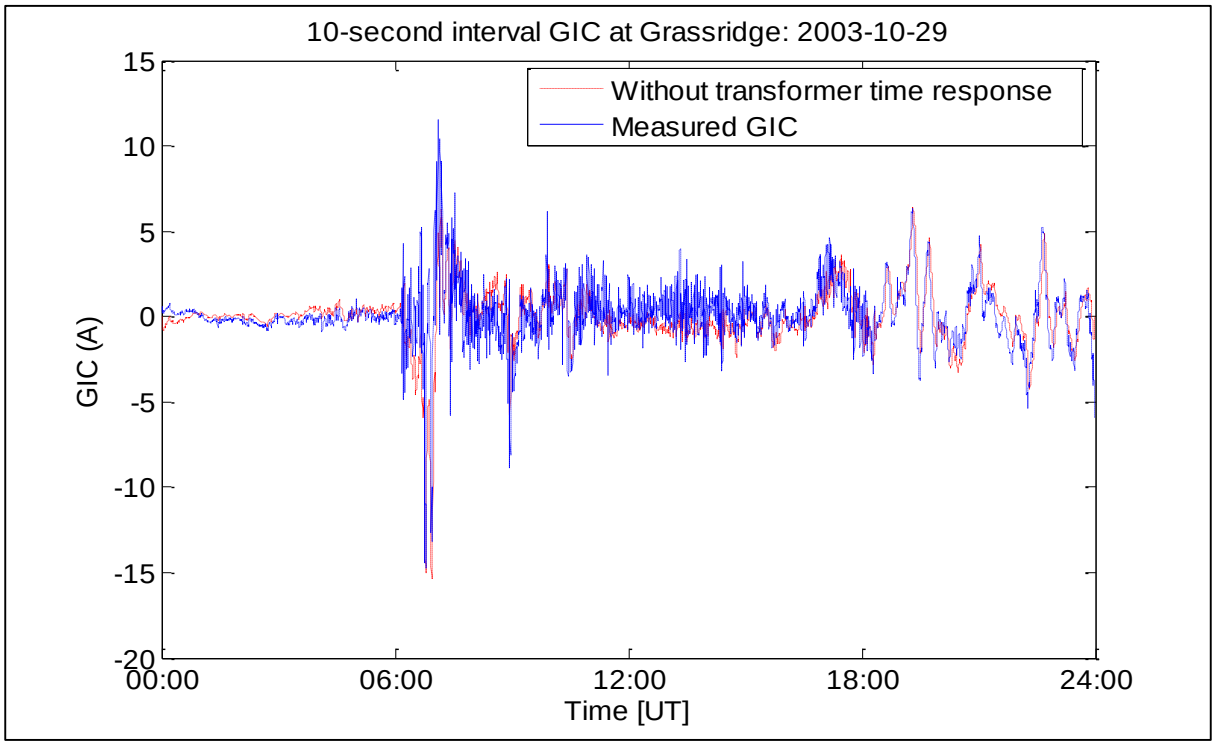

Figure 7.26 Comparison between the prospective GIC without transformer time response and the measured GIC at Grassridge using 10-second sampling time interval data

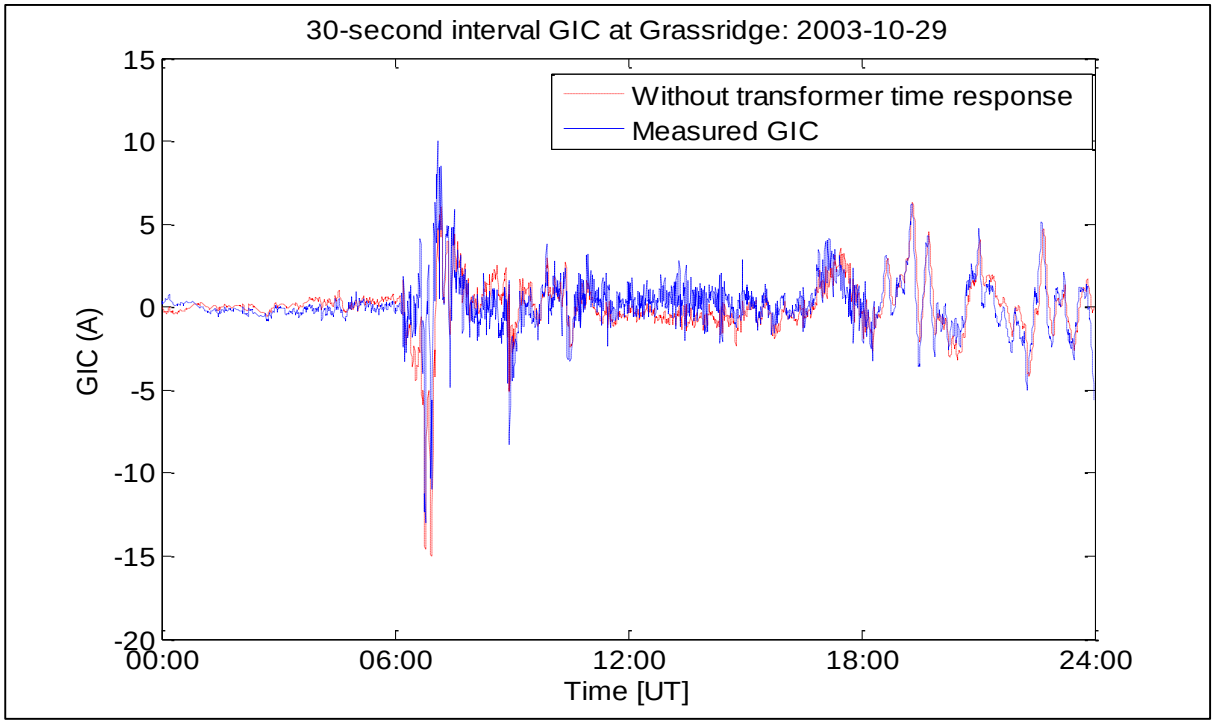

Figure 7.27 Comparison between the prospective GIC without transformer time response and the measured GIC at Grassridge using 30-second sampling time interval

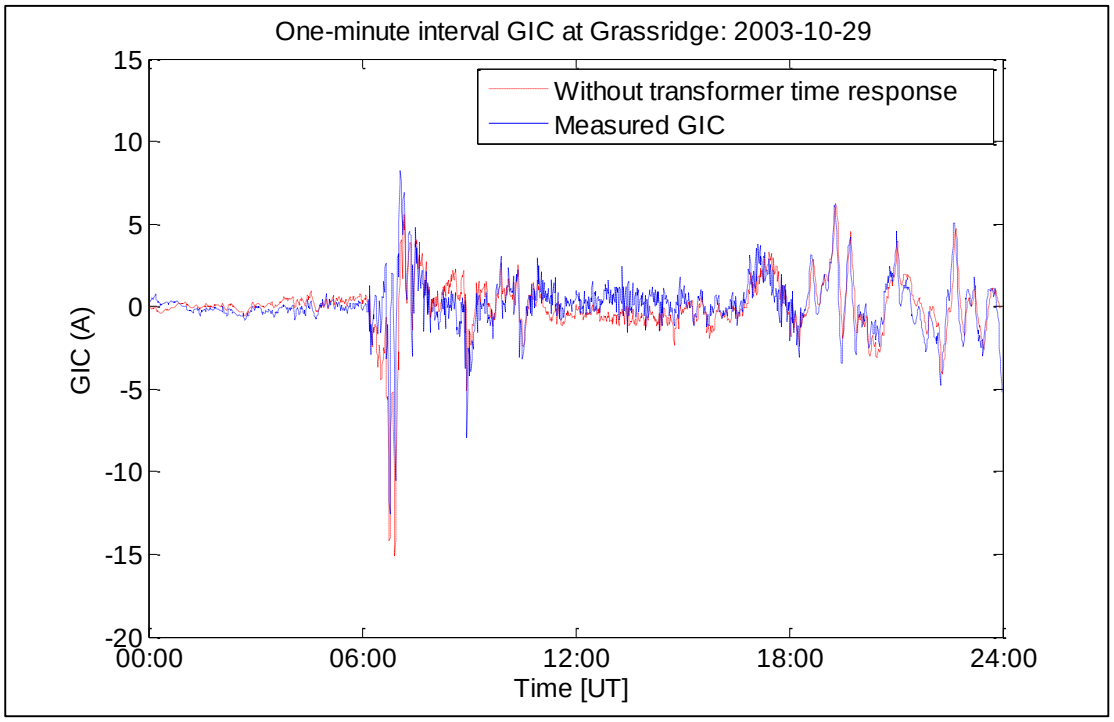

Figure 7.28 Comparison between the prospective GIC without transformer time response and the measured GIC at Grassridge using one-minute sampling time interval data

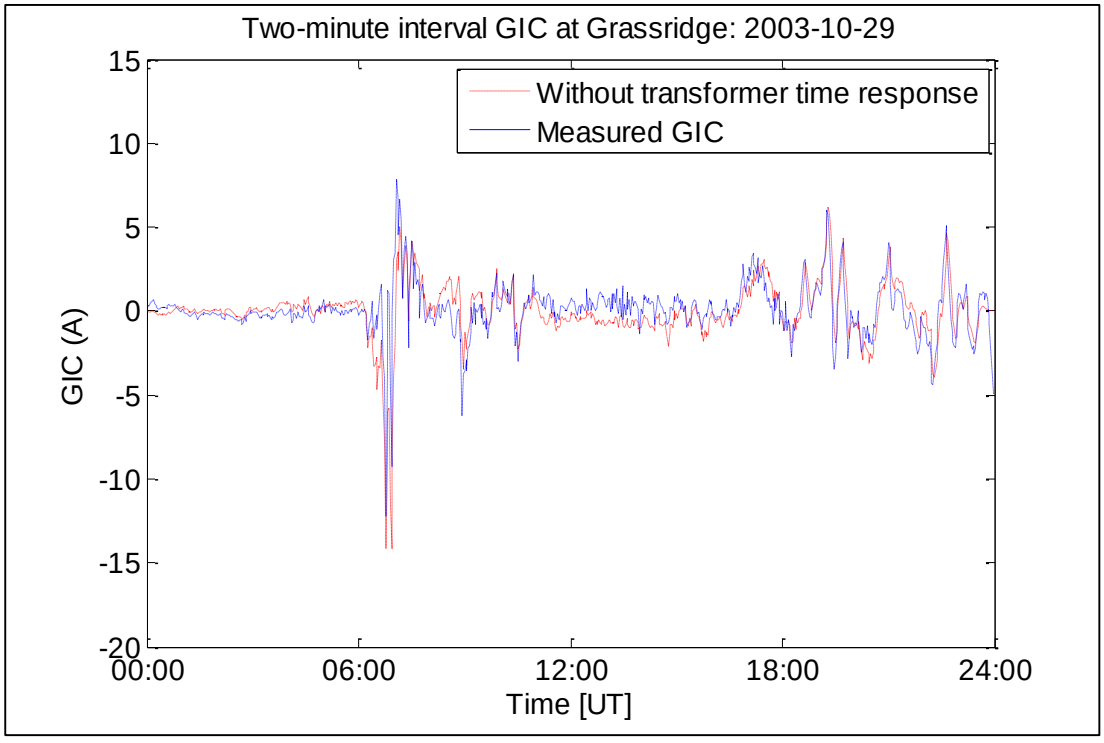

Figure 7.29 Comparison between the prospective GIC without transformer time response and the measured GIC at Grassridge using two-minute sampling time interval data

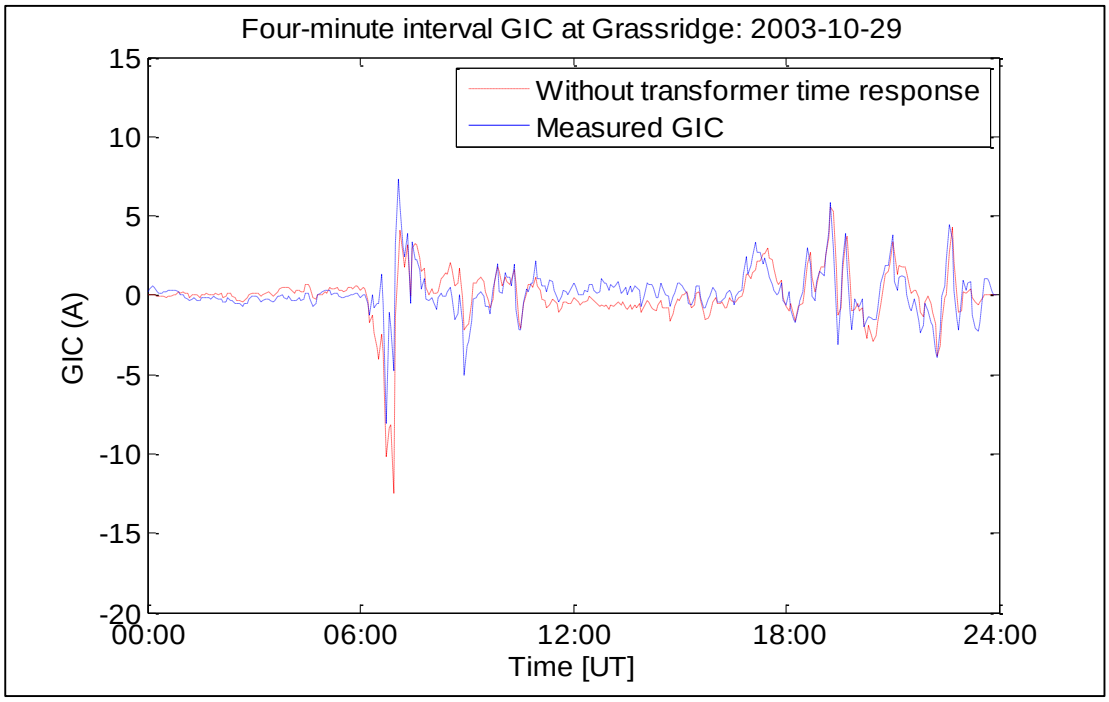

Figure 7.30 Comparison between the prospective GIC without transformer time response and the measured GIC at Grassridge using four-minute sampling time interval data

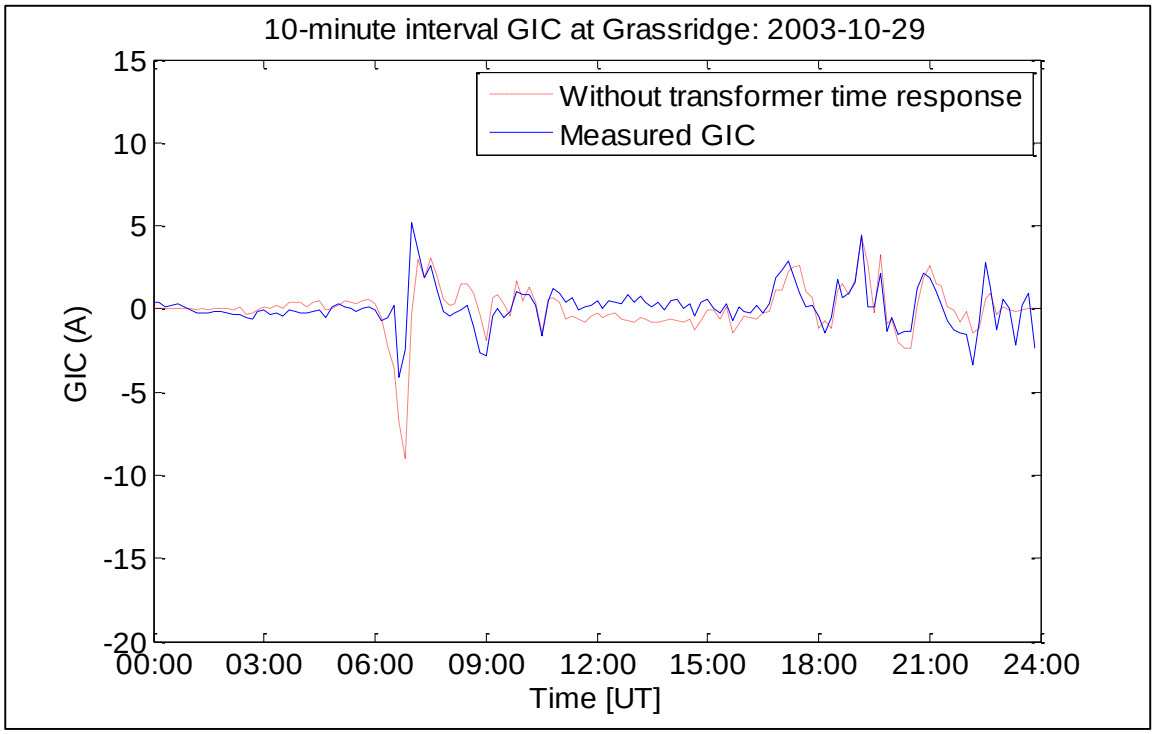

Figure 7.31 Comparison between the prospective GIC without transformer time response and the measured GIC at Grassridge using 10-minute sampling time interval data

When the calculated and measured GIC profiles are compared in Figures 7.24 to 7.31, there seems to be a polarity reversal after the sudden storm commencement (SSC) between 11:00 and 17:00. During this time interval, the variation in magnetic field was low compared to during the SSC around 06:40.

The results in Figures 7.24 to 7.31 show that as the sampling time increases, the difference between the measured GIC and the prospective GIC without transformer time response increases. The percentage difference between the prospective GIC without transformer time response and measured GIC during the SSC at about 06:45 for each of the sampling time interval was calculated and is shown in Figure 7.32. From a two-second sampling time interval to 10-minute sampling time interval, the percentage difference between the measured and prospective GIC without transformer time response increased from 0.1 % to 54 %. Between two-second and 10-second sampling intervals, the percentage change between measured and calculated GIC is less than 2.5 %.

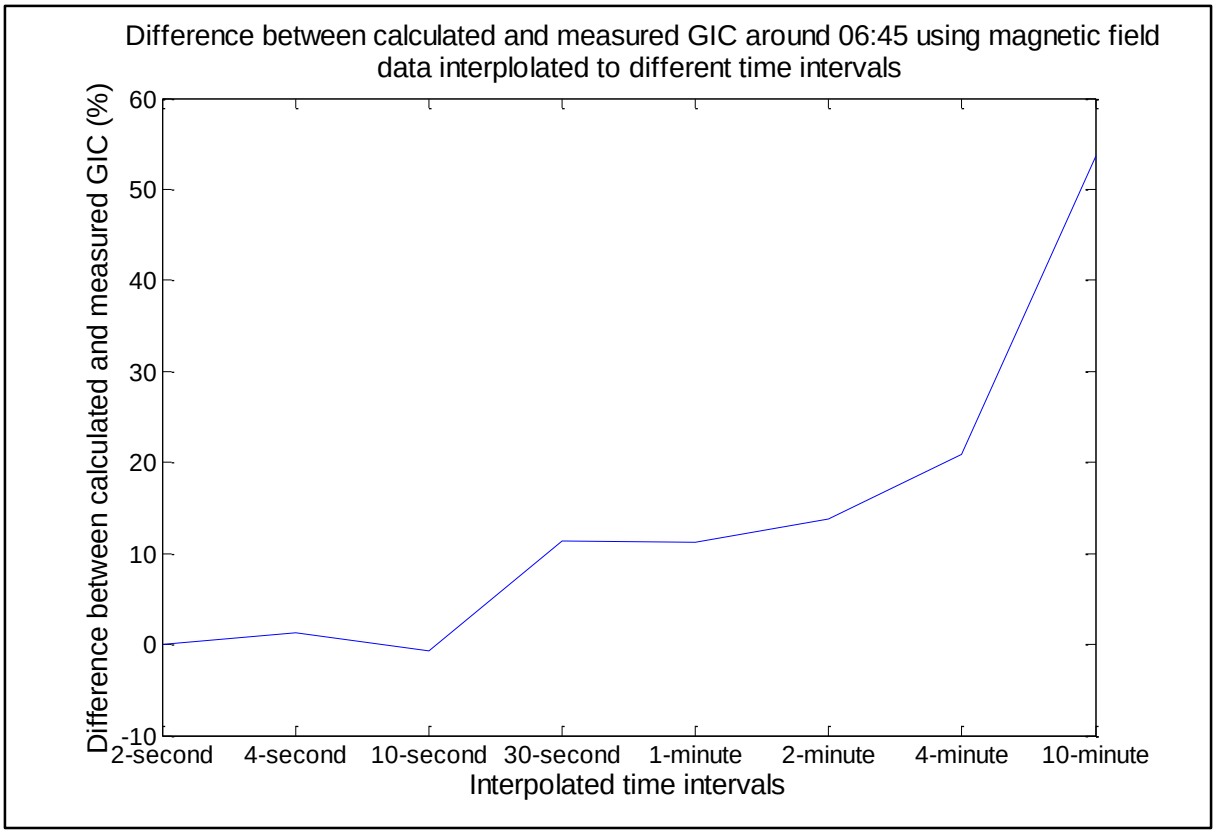

Figure 7.32 Difference between calculated and measured GIC during SSC (06:45 UT)

The percentage difference between the prospective GIC without transformer response and measured GIC at about 21:00 - which was not during the SSC - for each of the sampling time intervals was calculated and is shown in Figure 7.33. From a two-second sampling time interval to 10-minute sampling time interval, the percentage difference between the prospective GIC without transformer time response and measured GIC increased from -12 % to 18 %. The negative percentages in Figure 7.33 imply that the measured GIC value was higher than the prospective GIC without transformer time response. For all the sampling time intervals considered, the measured GIC value was higher in magnitude than the prospective GIC value, except for the 10-minute sampling time interval data set.

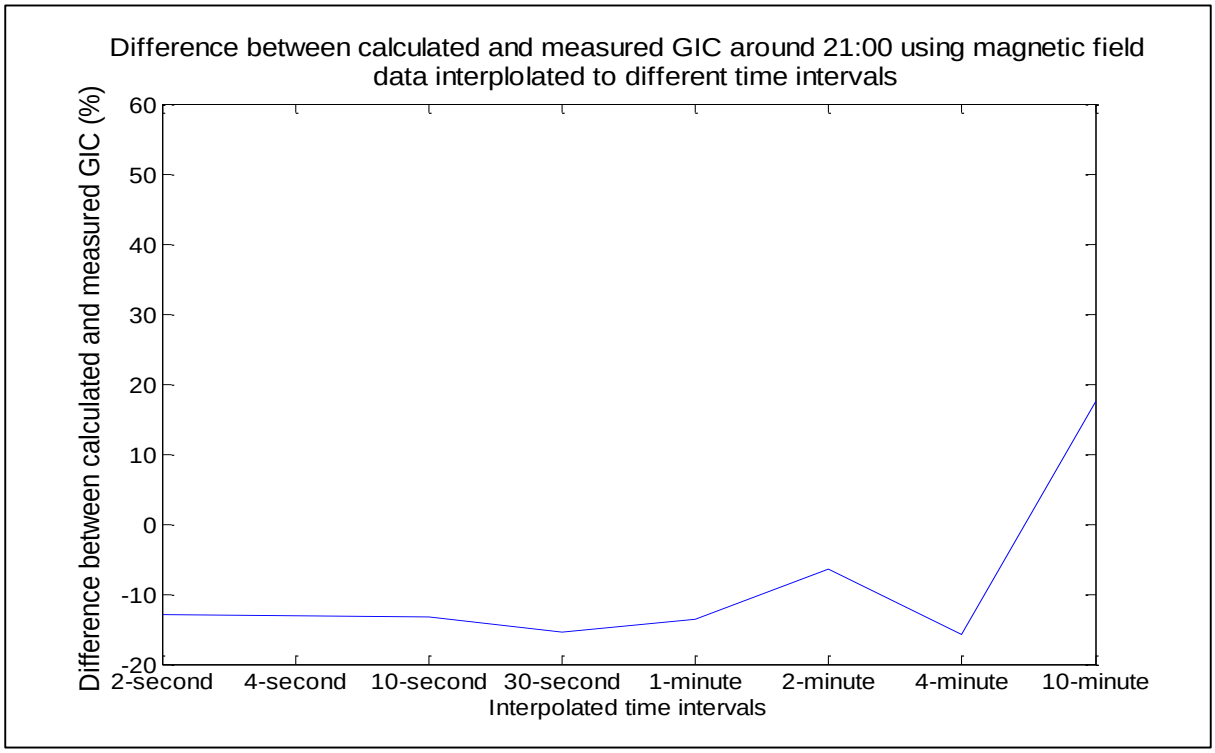

Figure 7.33 Difference between calculated and measured GIC around 21:00

Based on the results in Figure 7.32 and Figure 7.33, the transformer time response was incorporated into the GIC calculation algorithm using a selection of three data sets corresponding to two-second, two-minute, and 10-minute sampling time intervals. These

three sampling time intervals were chosen such that the effect of the sampling time interval on the prospective GIC with transformer time response can be investigated.

The results indicated that sampling at intervals above 10 seconds results in an increased discrepancy between measured and calculated GIC. In addition to this, sampling above 10-second intervals is not sufficient to correctly capture the profile of the GIC. See Figures 7.32 and 7.33.

7.4.2 Case 6: Comparison between measured GIC, prospective GIC with and without transformer response

The comparison between measured GIC and calculated GIC interpolated to two-second, two-minute and 10-minute sampling time interval data is shown in Figures 7.34 to 7.42. Due to the large number of data points (43,200 for 2-second sampling time intervals and 720 for two-minute sampling time interval), the two-second and two-minute sampling time interval graphs were split into four sections for clarity. Section A shows the GIC pre-SSC; section B shows the GIC during the SSC and sections C and D show the GIC post-SSC. The vertical axis for each section is different because the amplitude of the GIC in each section is different.

Two-second sampling time interval

Figure 7.34 shows the measured and calculated GIC using two-second sampling time interval data.

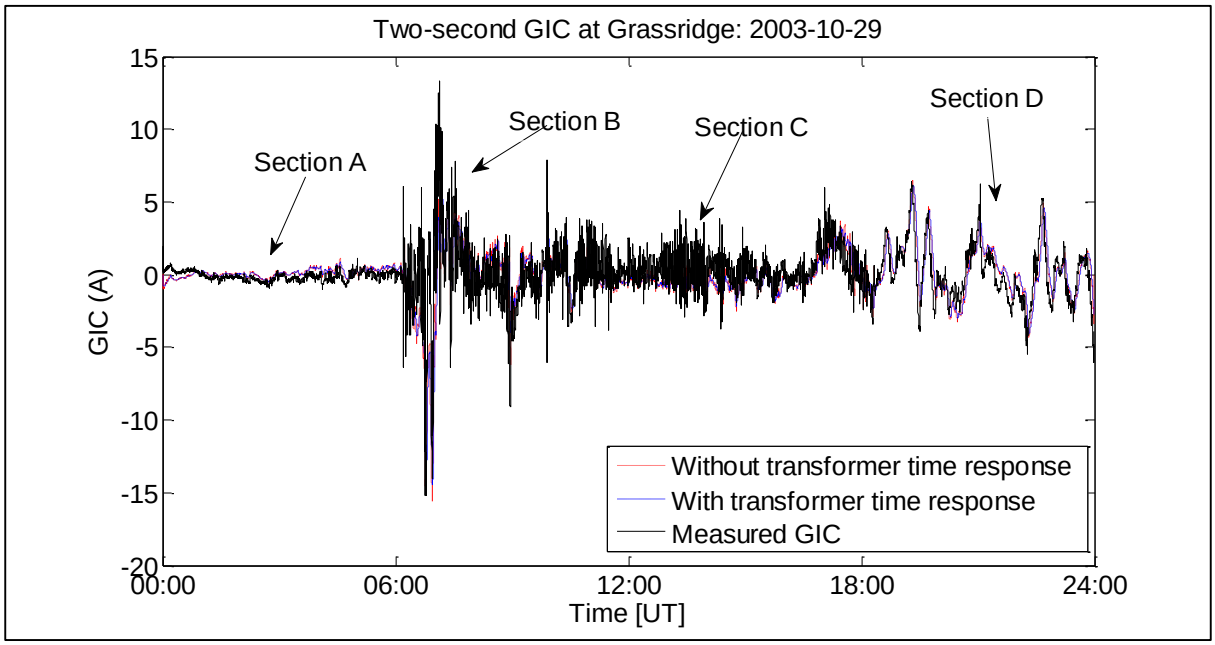

Figure 7.34 Comparison between the prospective GIC with and without transformer time response with the measured GIC using two-second sampling time interval data

Figures 7.35 to 7.37 show the zoomed version of section A, section B and section C respectively.

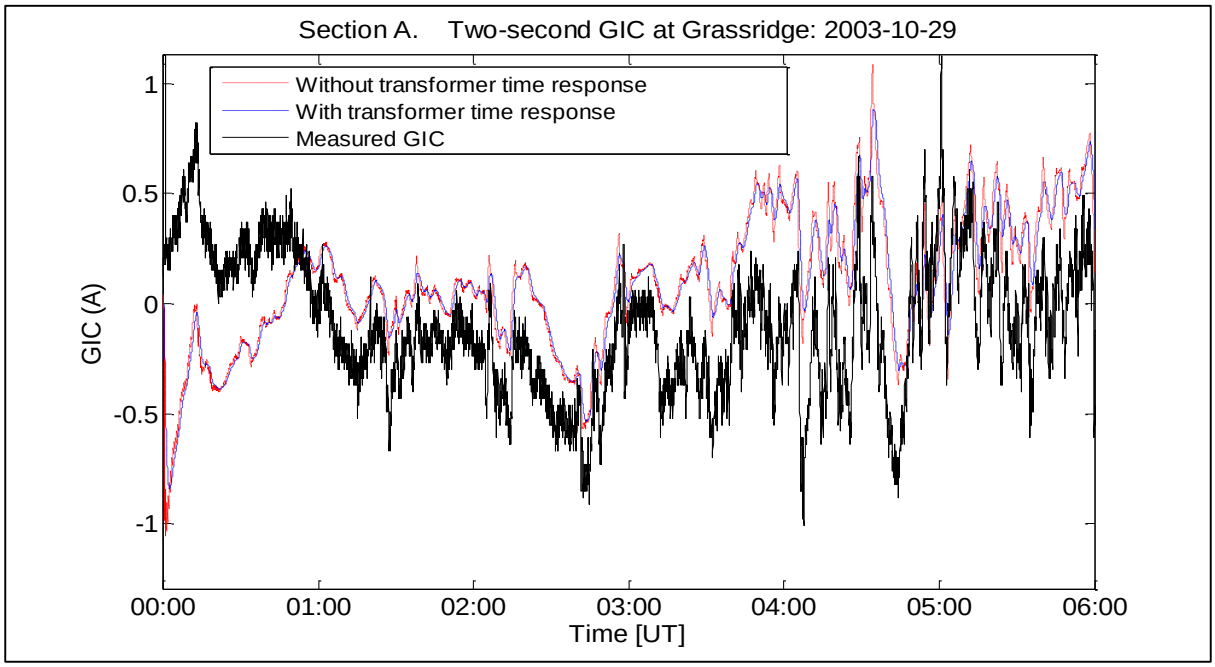

Figure 7.35 Section A Zoomed: Comparison between the prospective GIC with and without transformer time response with the measured GIC using two-second sampling time interval data

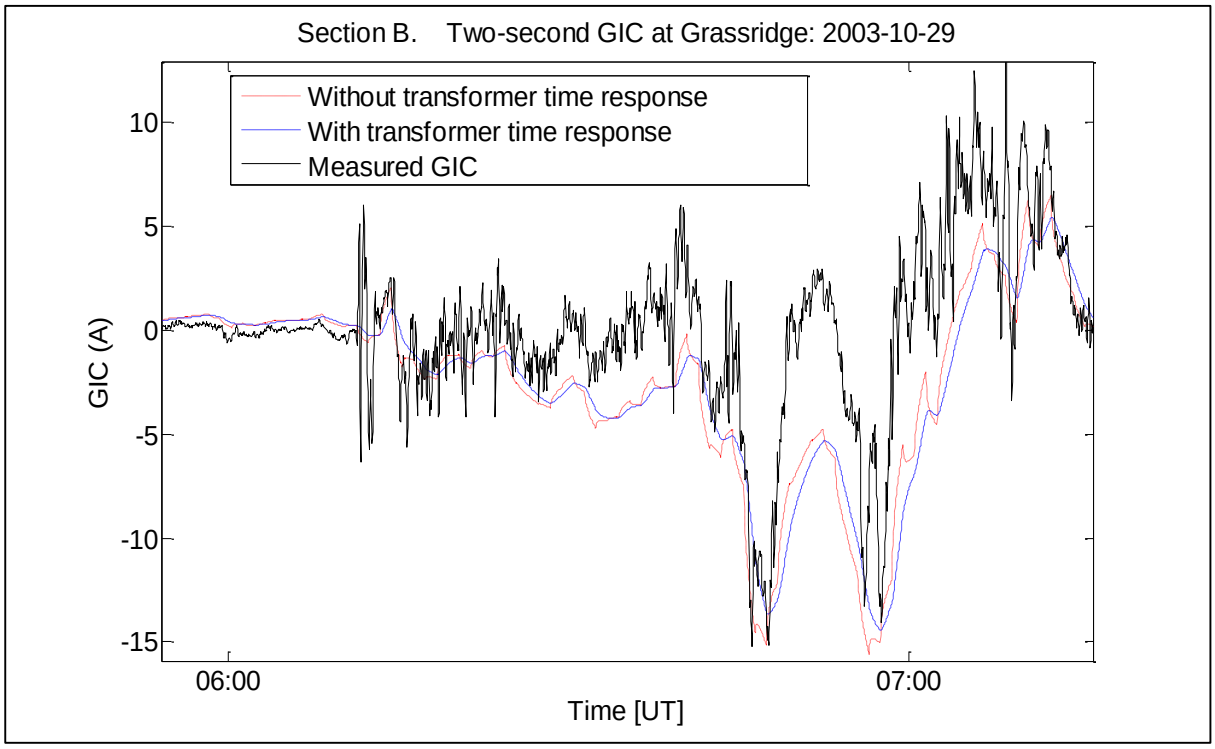

Figure 7.36 Section B Zoomed: Comparison between the prospective GIC with and without transformer time response with the measured GIC using two-second sampling time interval data

Section A between 00:00 UT and 6:00 UT in Figure 7.35 shows the measured and calculated GIC before the SSC commenced around 6:40 UT.

Section B between 6:00 UT and 7:20 UT in Figure 7.36 shows the measured and calculated GIC 40 minutes before the SSC and 40 minutes after the SSC. This section of the graph was zoomed and as a result the scale of the vertical axis changed.

Section C between 07:20 UT and 18:00 UT in Figure 7.37 shows the measured and calculated GIC. This was after the SSC when the variation of the magnetic field was low, but higher than it was in section A.

Section D between 18:00 UT and 24:00 UT in Figure 7.38 shows the measured and calculated GIC during the last 6 hours of the day.

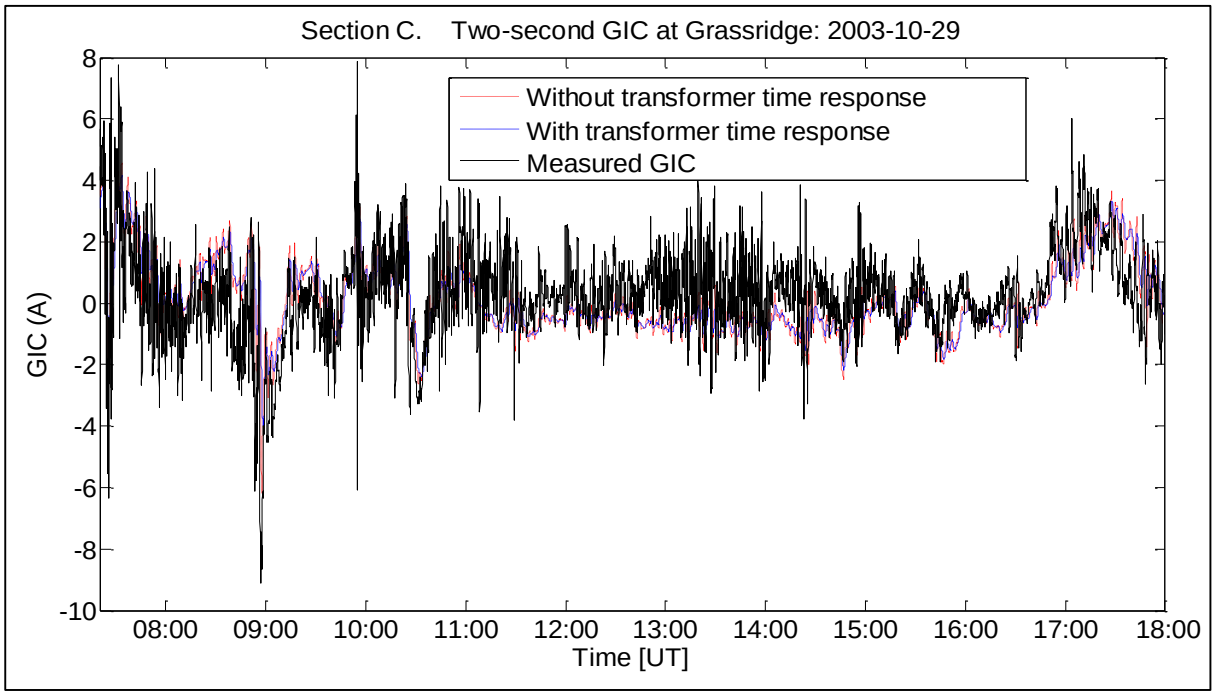

Figure 7.37 Section C Zoomed: Comparison between the prospective GIC with and without transformer time response with the measured GIC using two-second sampling time interval data

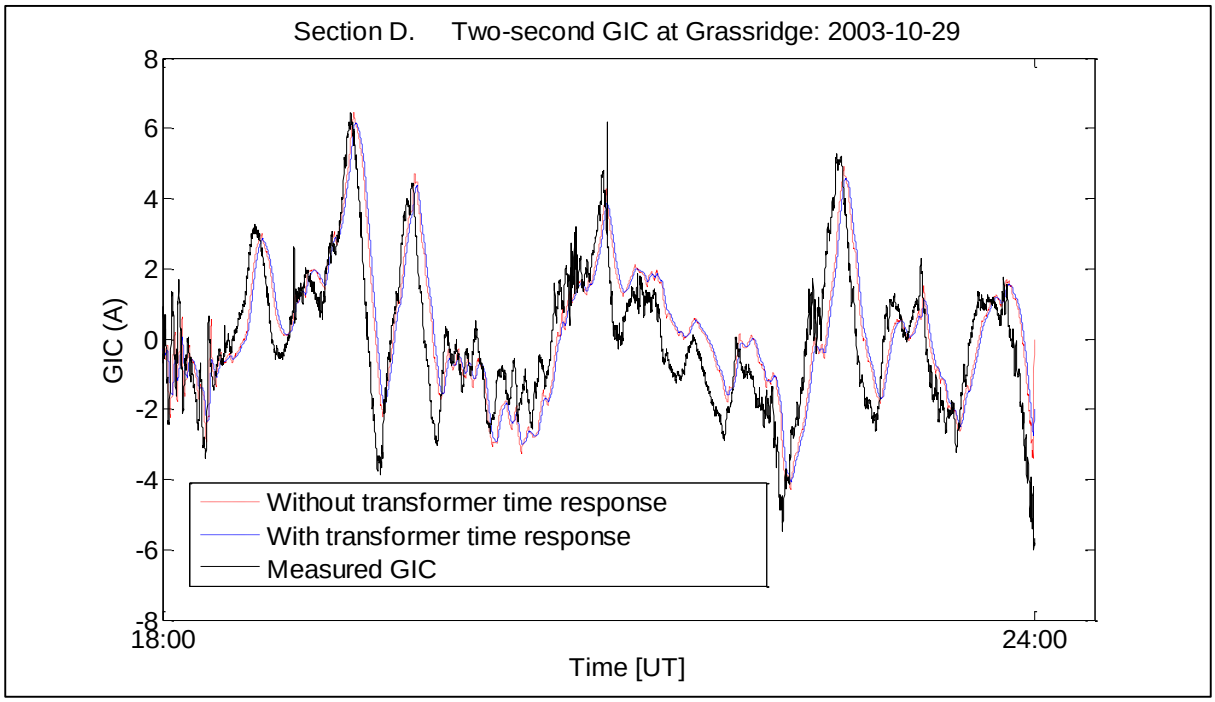

Figure 7.38 Section D Zoomed: between the prospective GIC with and without transformer time response with the measured GIC using two-second sampling time interval data

The number of instances in each section, where the prospective GIC with transformer time response is closer to the measured GIC, when compared to the prospective GIC without transformer time response was calculated and is shown in Table 7.9. In these instances, the inclusion of the transformer time response in the calculation of GIC improved the difference between the measured GIC and calculated GIC.

Table 7.9 Improvement in GIC calculation with transformer time response included using two-second sampling time interval data

	Number of sampling points with improvement	Total number of sampling points
Section A	5062	10801
Section B	1154	2401
Section C	9379	19199
Section D	5481	10807

Using Table 7.9, the probability that the transformer response improved the correlation between measured and calculated GIC for each section was calculated by dividing column 2 by column 3.

$P_A = \frac{5062}{10801} = 0.47$

Similarly in section B, this probability is: $P_B = \frac{1154}{2401} = 0.48$

In section C, this probability is: $P_C = \frac{9379}{19199} = 0.49$

In section D, this probability is: $P_D = \frac{5481}{10807} = 0.51$

The total probability P_T that included the transformer response, improved the correlation between the measured and calculated GIC for the whole profile, is calculated by dividing the sum of column 2 by the sum of column 3.

$P_T = \frac{21076}{43200} = 0.49$

Therefore, with two-second sampling intervals, incorporating the transformer time response into the calculation of the GIC was most effective in section D (i.e. about 12 hours after the SSC) and least effective during the six hours before the SSC in section A.

Two-minute sampling time interval

Figure 7.39 shows the measured and calculated GIC using two-minute sampling time interval data. Figure 7.40, Figure 41, Figure 7.42 and Figure 7.43 show the zoomed version of section A, section B, section C and section D, respectively. Section A between 00:00 UT and 06:00 UT in Figure 7.40 shows the measured and calculated GIC before the SSC commenced around 06:40 UT.

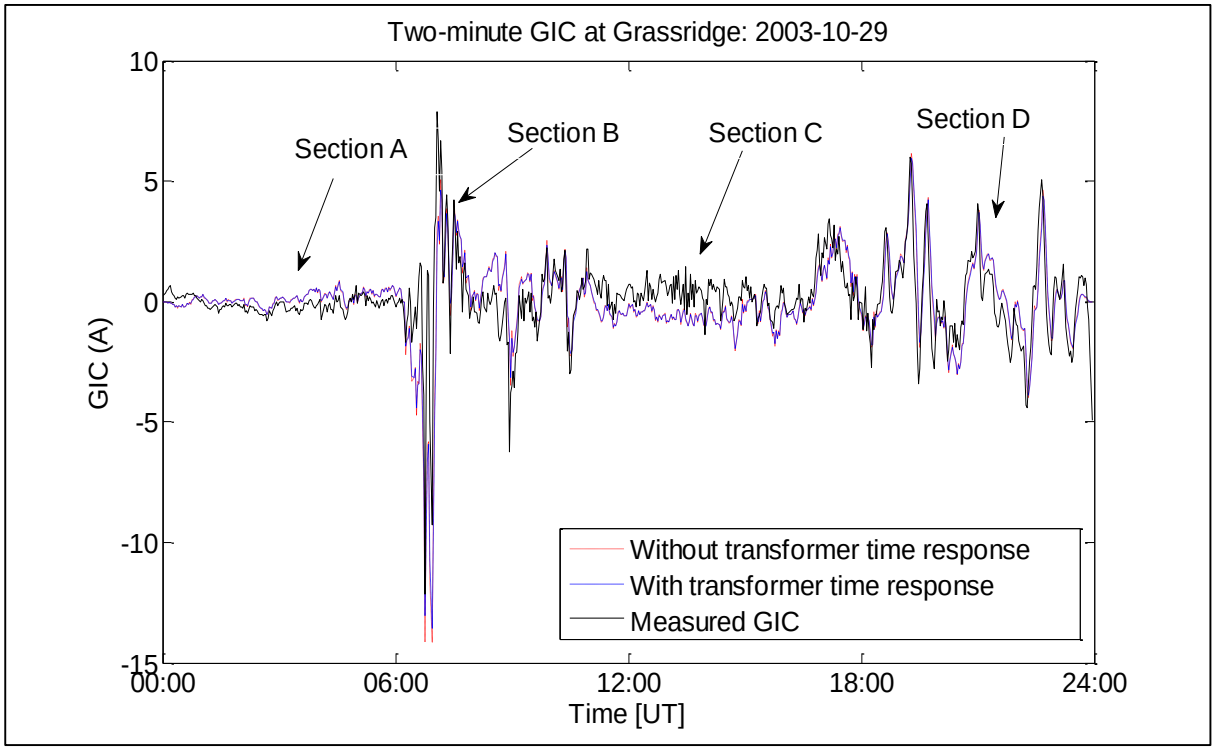

Figure 7.39 Comparison between the prospective GIC with and without transformer time response with the measured GIC using two-minute sampling time interval data

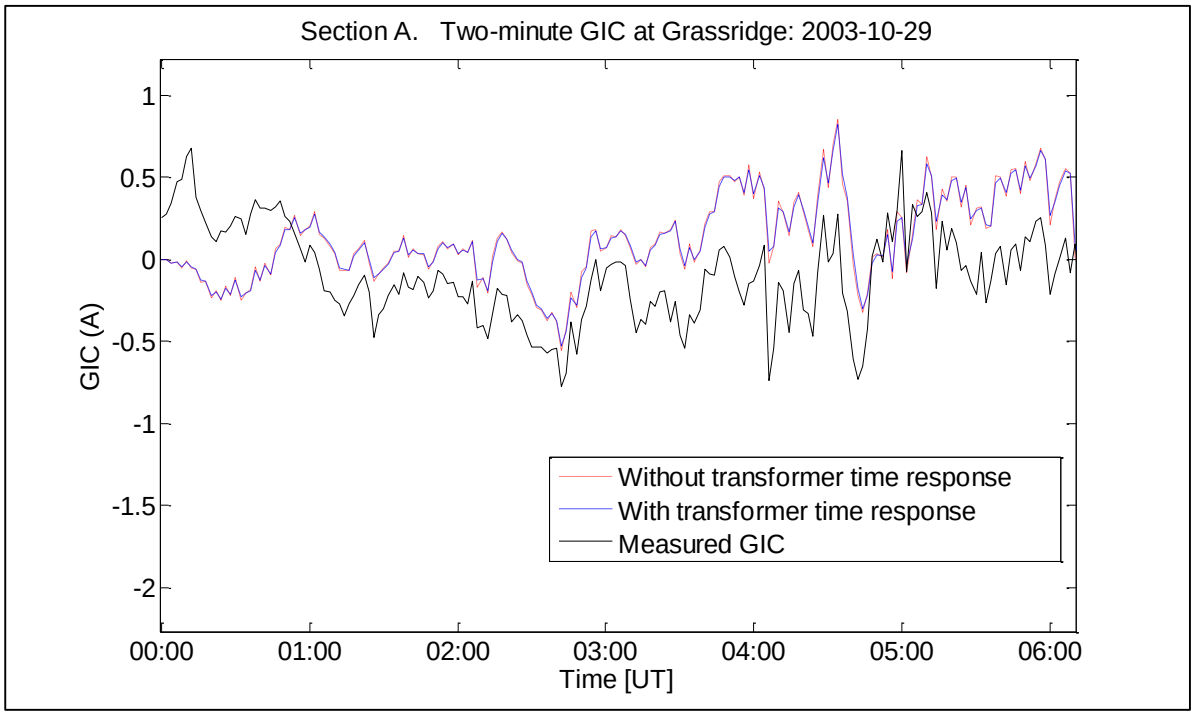

Figure 7.40 Section A Zoomed: Comparison between the prospective GIC with and without transformer time response with the measured GIC using two-minute sampling time interval data

Section B between 06:00 UT and 07:20 UT in Figure 7.41 shows the measured and calculated GIC 40 minutes before the SSC and 40 minutes after the SSC. Section C between 7:20 UT and 18:00 UT in Figure 7.42 shows the measured and calculated GIC. This was after the SSC when the variation of the magnetic field was low, but higher than it was in section A. Section D between 18:00 UT and 24:00 UT in Figure 7.43 shows the measured and calculated GIC during the last 6 hours of the day.

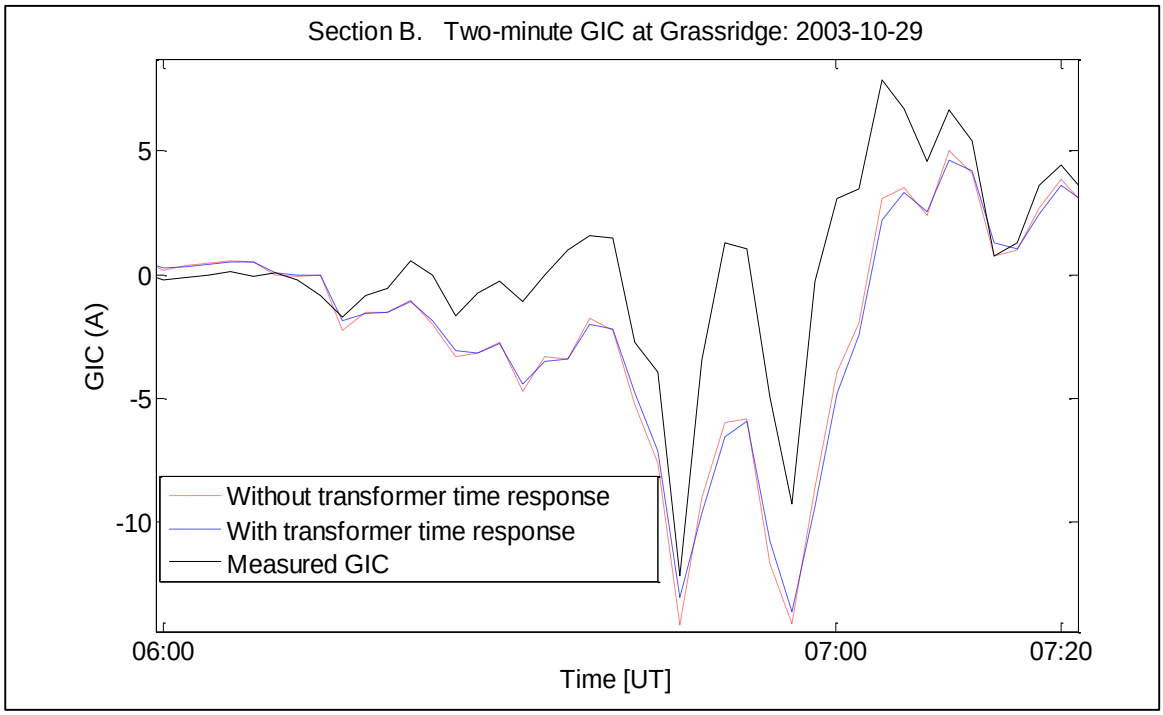

Figure 7.41 Section B Zoomed: Comparison between the prospective GIC with and without transformer time response with the measured GIC using two-minute sampling time interval data

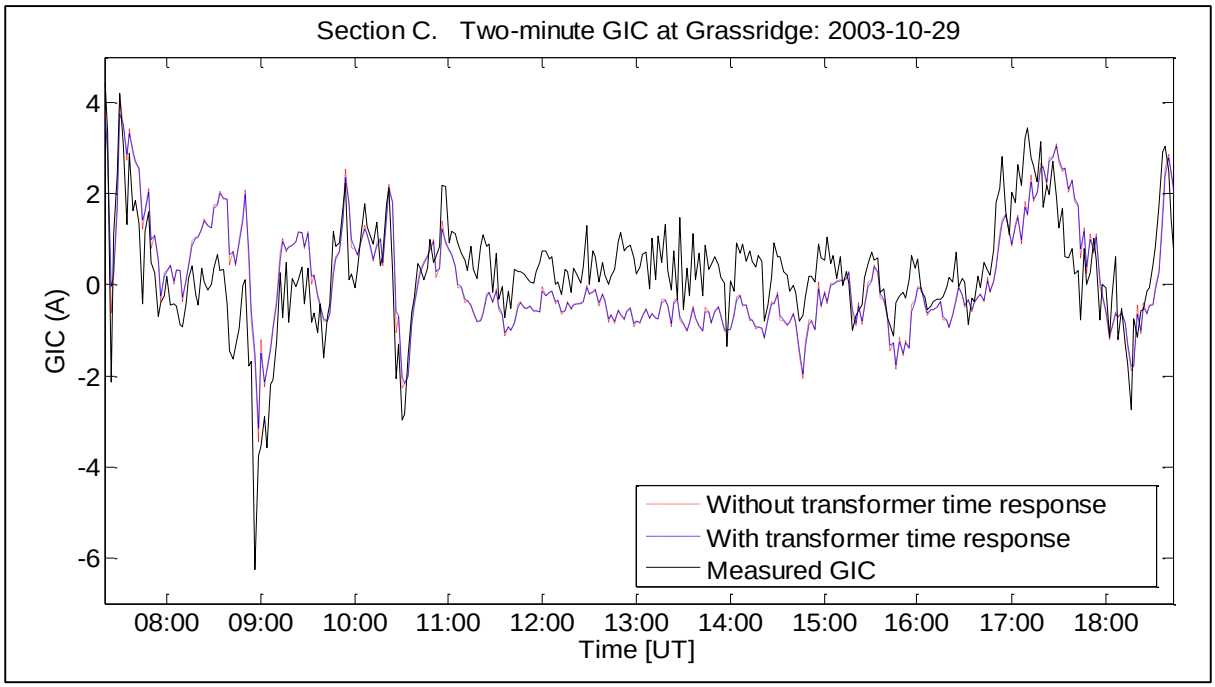

Figure 7.42 Section C Zoomed: Comparison between the prospective GIC with and without transformer time response with the measured GIC using two-minute sampling time interval data

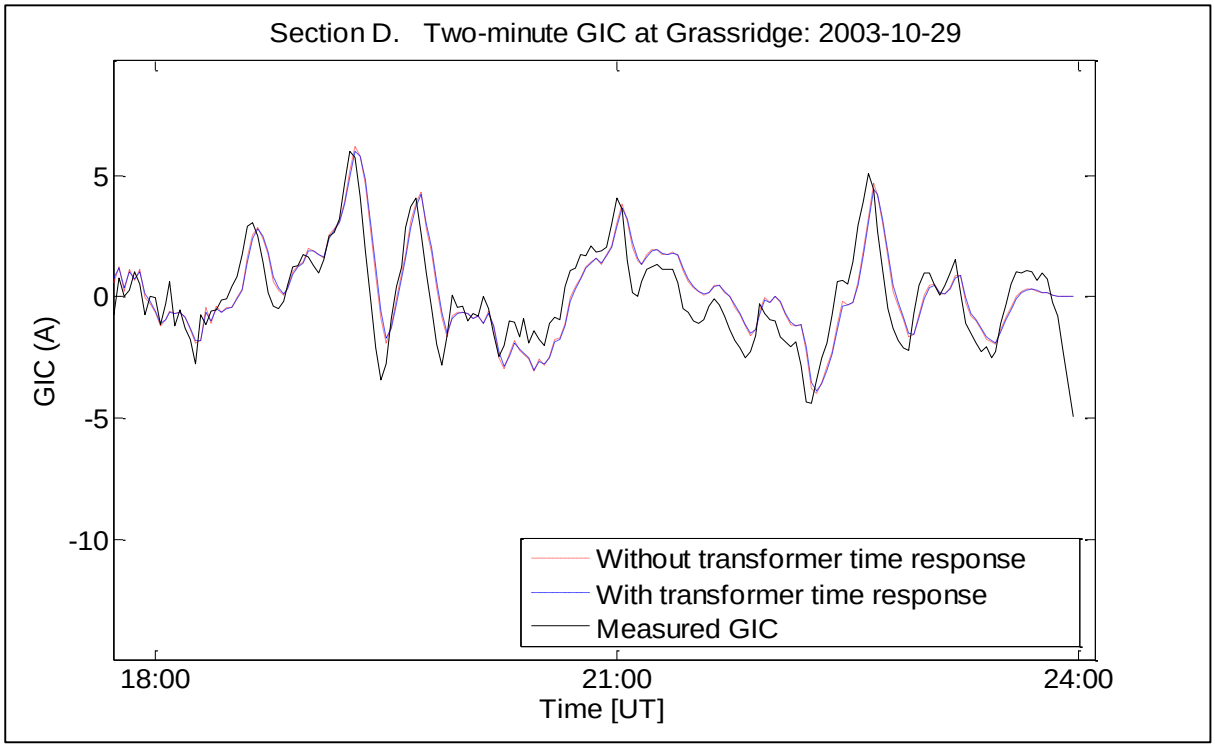

Figure 7.43 Section D Zoomed: Comparison between the prospective GIC with and without transformer time response with the measured GIC using two-minute sampling time interval data

From these results, the number of instances in each section when the transformer time response reduced the difference between the measured GIC and the prospective GIC was calculated and is shown in Table 7.10.

Table 7.10 Improvement in GIC calculation with transformer time response using two-minute sampling interval data

	Number of sampling points with improvement	Total number of sampling points
Section A	84	181
Section B	20	41
Section C	151	321
Section D	87	177

From Table 7.10, the following probabilities were calculated.

$P_A = \frac{84}{181} = 0.47$

Similarly in section B, this probability is: $P_B = \frac{20}{41} = 0.49$

In section C, this probability is: $P_C = \frac{151}{321} = 0.47$

In section D, this probability is: $P_D = \frac{87}{177} = 0.49$

$P_T = \frac{342}{720} = 0.48$

Therefore, with a two-minute sampling interval, incorporating the transformer time response to calculate the GIC was most effective in section B and D and least effective during the 6 hours before the SSC in section A and C.

10-minute sampling time interval

Figure 7.44 shows the measured and calculated GIC using 10-min sampling time interval data.

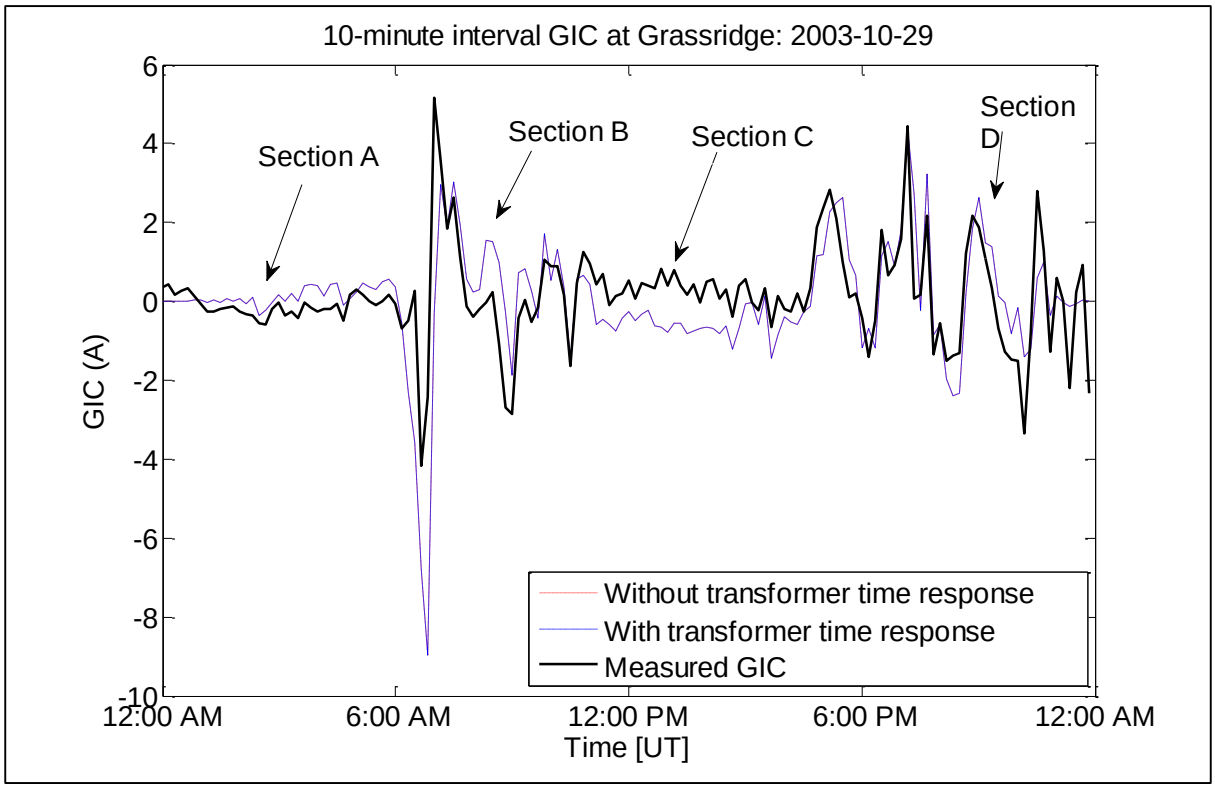

Figure 7.44 Comparison between the prospective GIC with and without transformer time response with the measured GIC using 10-minute sampling time interval data

Due to the reduced number of data points in the curves in Figure 7.44, sections A, B, C and D were not separated into different graphs. The number of instances in which the transformer time response improved the difference between the measured GIC and the calculated GIC is shown in Table 7.11.

Table 7.11 Improvement in GIC calculation with transformer time response using 10-minute sampling time interval data

	Number of sampling points with improvement	Total number of sampling points
Section A	16	37
Section B	6	9
Section C	33	65
Section D	16	33

From Table 7.11, the following probabilities were calculated.

$P_A = \frac{16}{37} = 0.43$

Similarly in section B, this probability is: $P_B = \frac{6}{9} = 0.67$

In section C, this probability is: $P_C = \frac{33}{65} = 0.51$

In section D, this probability is: $P_D = \frac{16}{33} = 0.49$

$P_T = \frac{71}{144} = 0.49$

Therefore, with a 10-minute sampling interval, incorporating the transformer time response into the calculation of the GIC was most effective in section B and least effective during the 6 hours before the SSC in section A. An extensive discussion on comparison between the different sections of the storm using the different sampling time interval is given in section 8.2.6.

7.4.3 Transformer time response and the error between measured GIC and calculated GIC

Determining the error is aimed at investigating whether or not including the transformer time response reduced the error between measured and calculated GIC. Storm characteristics vary from storm to storm, so does the characteristics of a segment of a storm differ from other segments within the same storm. Further to this, as the profile of the transformer core structures across the network changes, results of the error analysis may change. These implicitly suggests that the information deduced from the error analysis is unique to the specific GIC and geomagnetic data.

Before the impact of the transformer time response on the error between measured and calculated GIC is considered, it is vital to mention some of the underlying issues that might have contributed to the discrepancies between measured GIC and calculated GIC. These include:

i. Possible filtering in the measurement of GIC.
ii. The impact of temperature variation on the GIC measurement device.
iii. The INTERMAGNET site (Hermanus) at which the geomagnetic data was logged is about 800 km from Grassridge, the site where the GIC was measured.
iv. The assumption of uniform ground conductivity based on the limited data available.

The conductivity value is linked to the calculation of the electric field from the magnetic field. The calculated electric field is one of the inputs to the prospective GIC calculation. Hence, changing the conductivity value does not increase or decrease the variance between the prospective GIC with transformer time response and the prospective GIC without transformer time response.

Taking the aforementioned issues into consideration, error analysis is conducted on three sets of data used in chapter 7.4.2. These are two-seconds, two-minute and 10-minutes sampling intervals.

Two methods are used to determine the performance of the time response based model used to calculate the prospective GIC. These methods are the mean absolute error (MAE) and Variance.

Mean absolute error (MAE)

Mean absolute error is a measure of error which takes the mean of the absolute difference between measured and predicted values. MAE is considered to be a dimensioned measure of error, because it expresses average model-prediction error in the units of the variable of interest. In contrast to other measures of average error such as Root Means Square Error (RMSE), which is based on the sum of square errors with the setback that it inadvertently does not describe average error alone, MAE has been shown in literature to be an unambiguous measure of average error magnitude [92], [93].

Chai and Draxler [92] argues that the singular advantage of RMSE over MAE is that RMSE does not use absolute values. However, this may not be satisfactory in some applications where gradients are calculated as an example. Moreover, the sensitivity of RMSE to outliers

is the most reported concern with its use. This setback can be circumvented by the removal of outlier data points which may not be suitable in application to the specific GIC model under consideration. This is because all the GIC values calculated or measured during any segments of a storm is of particular significance in the understanding of the transformer response.

The mean absolute error [93] is defined by equation 7.19 as:

$$MAE = \frac{1}{n}\sum_{d=1}^{n}|m_d - c_d| \quad (7.19)$$

Where d is an integer, n is the number of samples points, m_d is the measured GIC, c_d is the calculated prospective GIC without or with transformer time response. MAE is typically used to determine the performance of prediction models [93]. The MAE is computed between the measured GIC and the prospective GIC without transformer time response and compared with the MAE between the measured GIC and the prospective GIC with the transformer time response.

The MAE was calculated with GIC data over a period of 24 hours, sampled at two-second intervals using equation 7.16. The MAE between the measured GIC and the prospective GIC with transformer time response using equation 7.19 is 1.01, while the MAE computed between the measured GIC and the prospective GIC without the transformer time response is 0.92. This implies that including the transformer time response increased the overall MAE.

However, when the MAE is calculated for moving blocks of 10-minutes as shown in Figure 7.45, it is evident that the MAE is lower with the transformer time response in certain segments of the profile. To determine this, the MAE was calculated for 10-minute unique block intervals. The intervals in which the MAE was reduced due to the transformer time response were assigned to “8” while the converse were assigned to “0” and plotted in Figure 7.45.

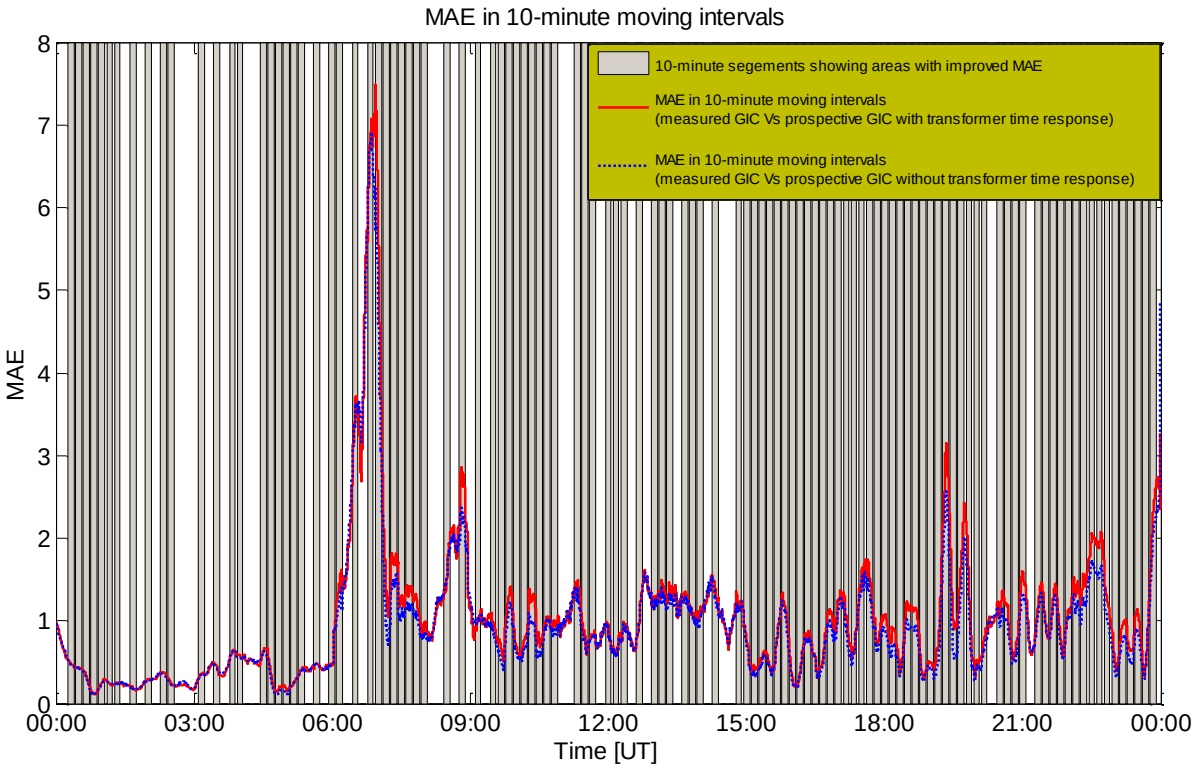

Figure 7.45 The curves in the graph compares the mean absolute error (MAE) calculated in 10-minute moving intervals between the measured GIC versus the prospective GIC without transformer time response and the MAE between the measured GIC versus the prospective GIC with transformer time response. The grey blocks show the 10-minute block interval where the MAE was improved due to the incorporation of the transformer time response.

A time correlation between the curves and the grey blocks indicates that, most of the segments with relatively high MAE correlated to an improvement in the MAE by the transformer time response, which also corresponds to segments with high magnitudes of GIC.

Variance

Variance [94] is the second tool used to determine the effect of the transformer time response on the error between the measured GIC and the prospective GIC. In the context of this research, error is determined by calculating the difference between the variance profiles of the measured GIC versus the calculated GIC with the transformer time response,

as well as the variance profile of the measured GIC versus the calculated GIC without the transformer time response.

The profile for 24 hours as shown in Figure 7.46 is divided into different segments. The first of which is the quiet time in Figure 7.47. The next segment between 06:00 and 12:00 shown in Figure 7.48 covers the period leading to the SSC while Figures 7.49 and 7.50 show the rest of the GIC profile between 12:00 and 00:00.

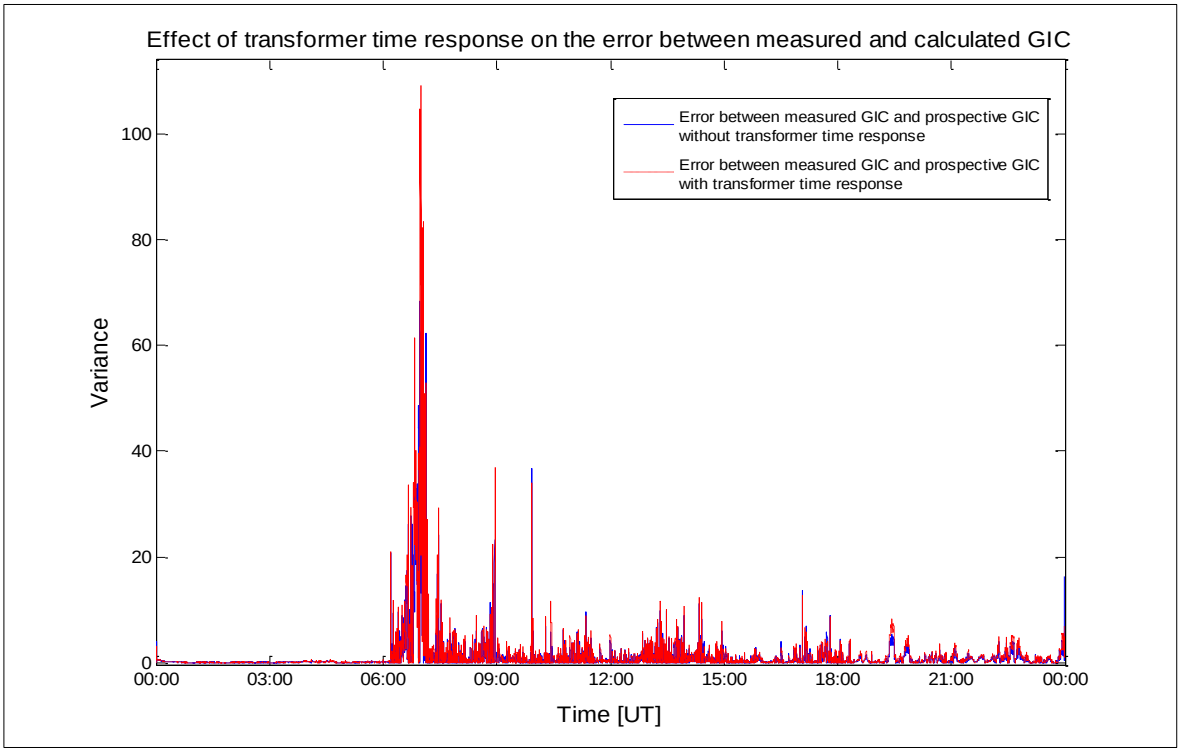

Figure 7.46 Comparison between the variance profile of the measured GIC versus the calculated GIC with the transformer time response and the variance profile of the measured GIC versus the calculated GIC without the transformer time response.

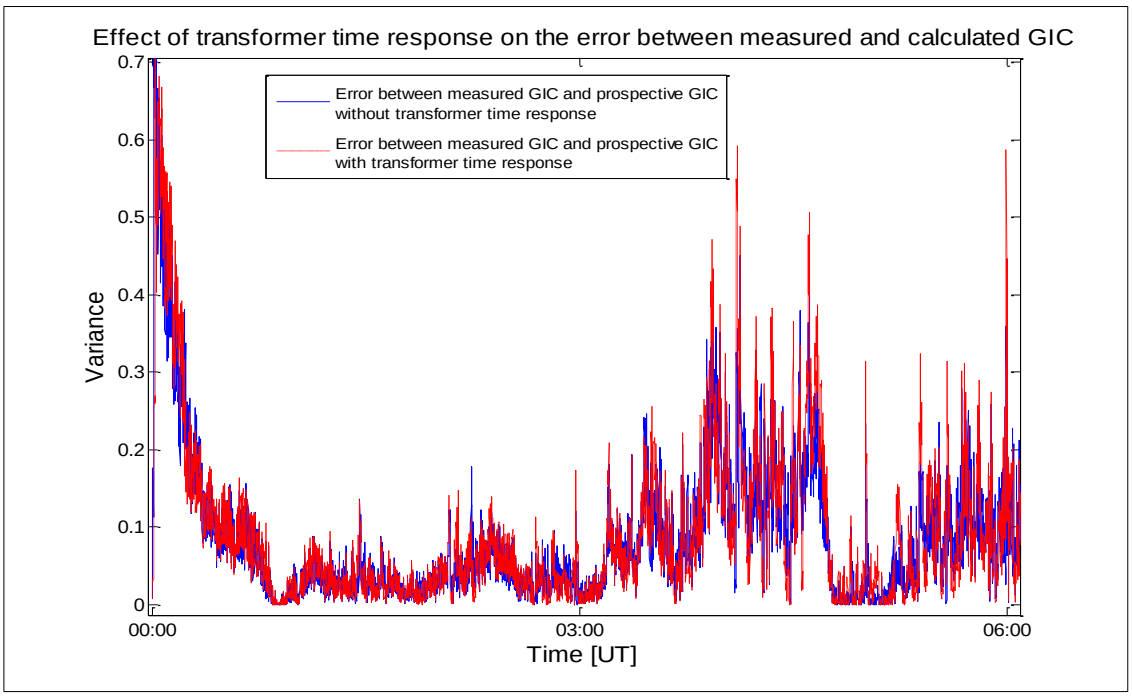

Figure 7.47 Quiet time: Comparison between the variance profile of the measured GIC versus the calculated GIC with the transformer time response and the variance profile of the measured GIC versus the calculated GIC without the transformer time response.

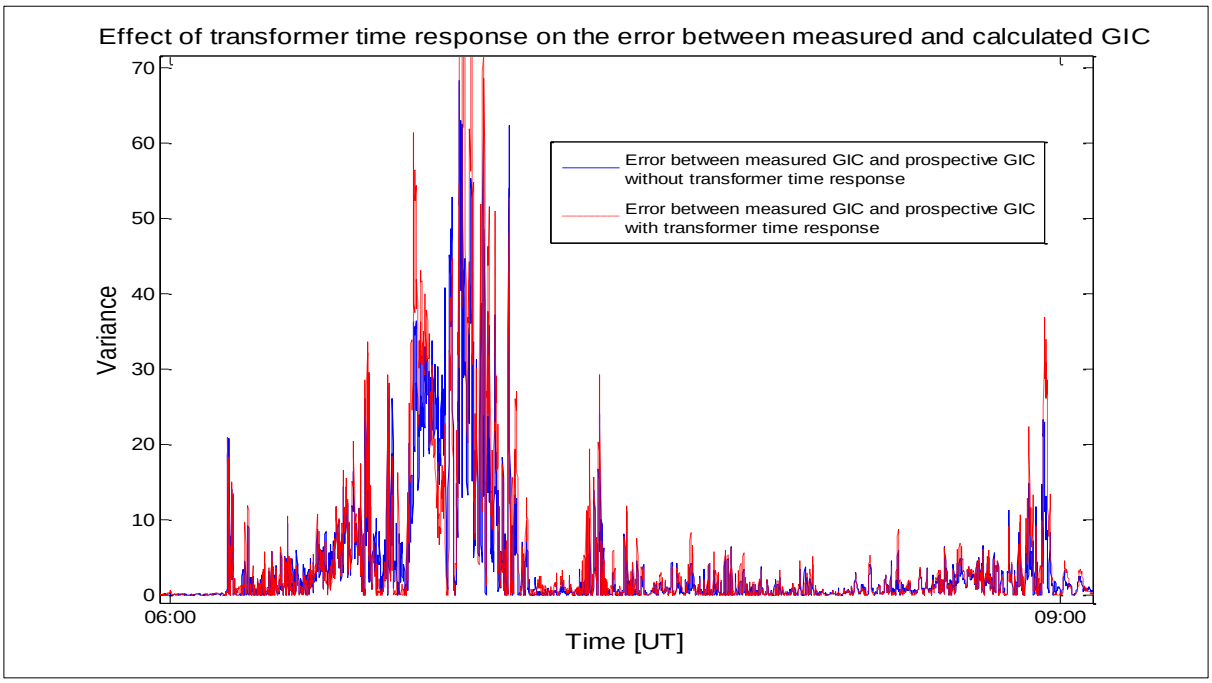

Figure 7.48 Pre-SSC, SSC: Comparison between the variance profile of the measured GIC versus the calculated GIC with the transformer time response and the variance profile of the measured GIC versus the calculated GIC without the transformer time response.

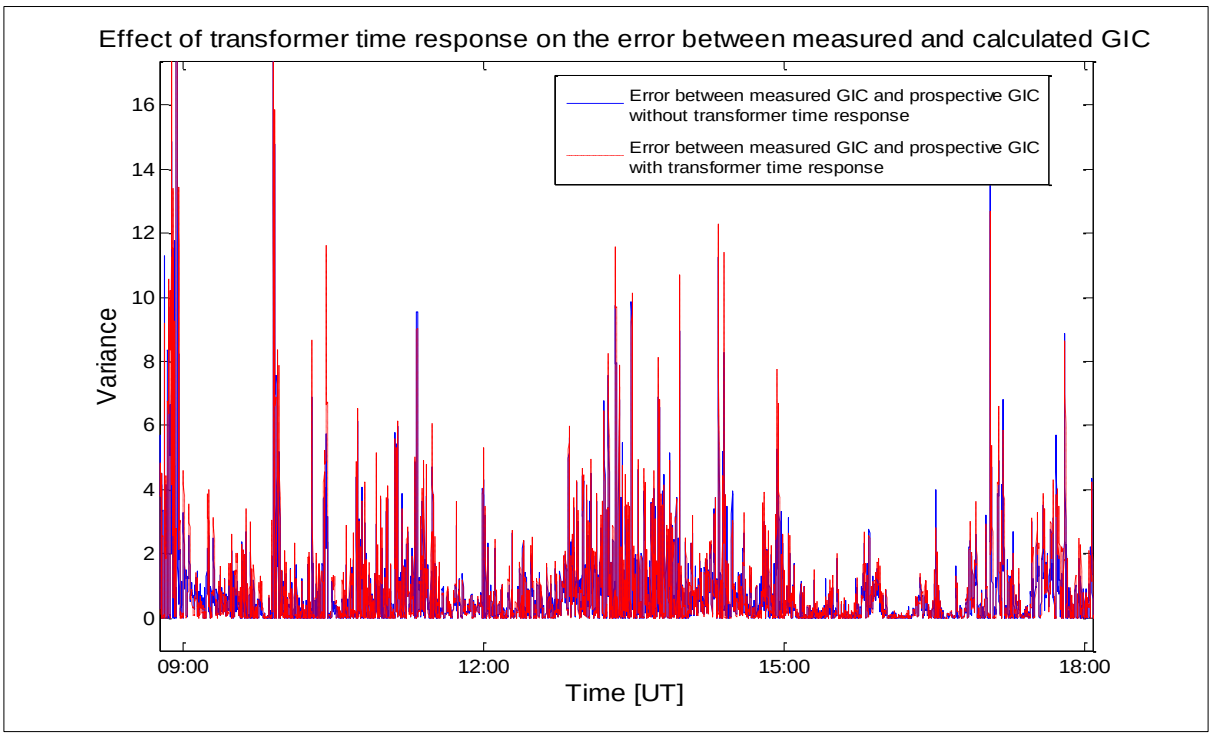

Figure 7.49 Period of reduced geomagnetic activity: Comparison between the variance profile of the measured GIC versus the calculated GIC without the transformer time response and the variance profile of the measured GIC versus the calculated GIC with the transformer time response.

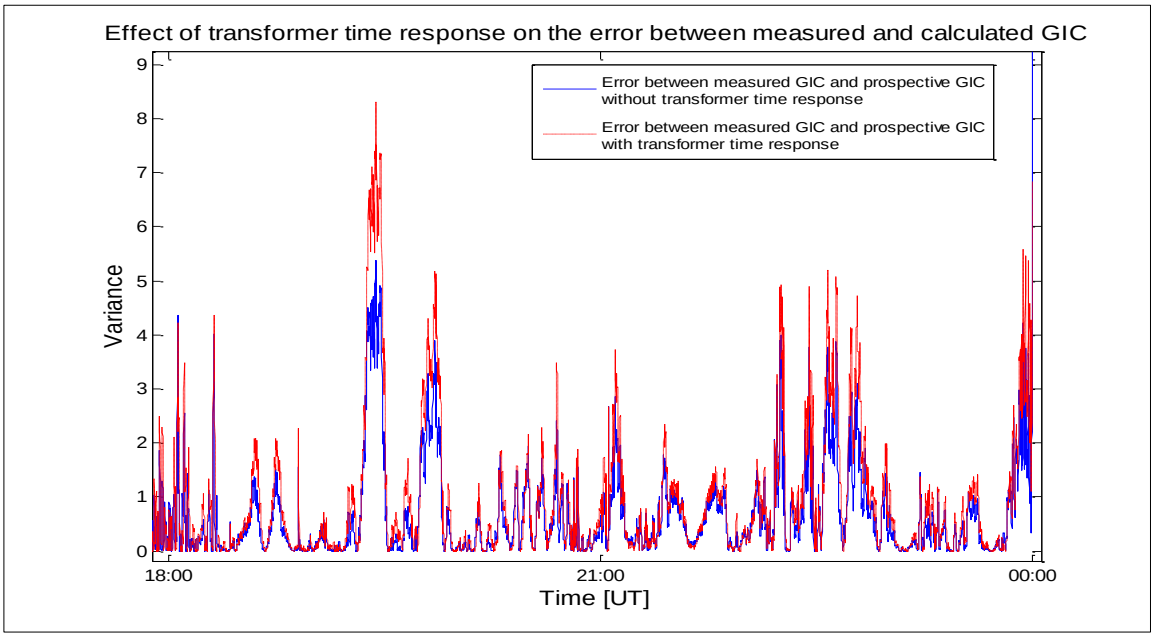

Figure 7.50 Period of low geomagnetic activity: Comparison between the variance profile of the measured GIC versus the calculated GIC without the transformer time response and the variance profile of the measured GIC versus the calculated GIC with the transformer time response.

In the graphs shown in Figures 7.45 to 7.50, the effect of the transformer time response is less prominent during high peaks in the GIC profile. This is because the variance between the measured GIC and the prospective GIC with transformer time response increased. From the probabilities calculated in case 6 (section 7.4.2) and the analysis using the MAE and variance, the following can be deduced:

- The average probability the transformer time response improves GIC calculation is about 0.5 which means that in general, calculating GIC with or without the transformer time response is equally good.
- The MAE increases during high GIC and so does the variance between the measured GIC and the calculated GIC. However, when 10-minutes segments are considered, the transformer time response reduces the MAE even during segments with relatively high GIC. This corroborates the first point that the impact of the transformer time response could be pronounced during smaller time intervals.

CHAPTER 8

ASSUMPTIONS ON WHICH THE RESEARCH IS BASED AND DISCUSSIONS

In this chapter, the assumptions made in this thesis are presented, followed by a discussion of the results of the research.

8.1 ASSUMPTIONS

A number of assumptions were made in the effort to calculate GIC using the developed algorithms explained in chapter 3.

8.1.1 Imaginary location of the voltage source

Some sources in the literature [95-98] mention that the imaginary location of the voltage source due to a geomagnetic disturbance (GMD) is in series with the transmission lines. This gives rise to the flow of GIC in transmission lines connected to wye-connected transformers with grounded neutrals. In this configuration, the Earth serves as a parallel path for the GIC. This approach was chosen to place the induced electric field in the model used for calculation.

8.1.2 Time-dependent flow of GIC in transformer windings

The assumption was made that the maximum expected GIC (referred to as the prospective GIC without transformer time response) that flows through a transformer is a function of time.

8.1.3 Flow of GIC in a three-phase four-wire system

The assumption was made that the GIC flow in the different phases of a three-phase transmission line and transformer are the same. Furthermore, the GIC in the grounded

neutral of the transformer was assumed to be the algebraic sum of the GIC in the three phases.

8.1.4 Line inductance should not be considered in GIC calculations

When calculating the GIC in transmission networks, the inductance of the line is neglected at GIC frequencies (< 1 Hz). This is because the frequency is regarded as quasi-DC (less than 1 Hz). Therefore, only the line resistance is taken into account.

8.2 DISCUSSIONS

8.2.1 Introduction of prospective GIC with and without transformer response calculations

One of the key findings in this thesis is that there is a difference between the prospective GIC with transformer time response and the prospective GIC without transformer time response. The time response being the distinguishing factor which affects the flow of GIC through a transformer. This difference is based on the characteristics of the transformer among others and the transformer's time response to changing GIC magnitudes. The equations derived in chapter 3 showed the difference between the prospective GIC without and with the transformer response.

The Lehtinen - Pirjola method has been widely used for calculating GIC. There was a strong correlation when the GIC values calculated using this method were compared to the GIC values calculated using the NAM methods. Therefore the similarity in the results validated the code that was written in MATLAB for this calculation.

For the calculation of the prospective GIC with transformer time response, the transformer core type and the GIC flow through the transformer was taken into account to determine the transformer response time to GIC. Only three transformer core structures were tested: 3(1P-3L), 3P-3L and 3P-5L. While the results of the test could not confirm that all transformer designs with the same core structure have the same time response to GIC, the results indicated that different core structures respond differently to GIC. This conclusion contributes greatly to the improvement of GIC calculations.

All the previous calculation algorithms did not take into account the core-dependant transformer time response to GIC.

8.2.2 Differential transformer core time response to GIC

Laboratory tests were conducted on 300 VA 3(1P-3L), 3P-3L and 3P-5L transformer core structures to determine their time response to DC. To validate the laboratory tests, corresponding simulations in PSCAD were done. In both cases, the results showed that load had an impact on the response time variation with DC current injected. The major difference was that the time response to DC current of the 300 VA 3P-3L and 3P-5L transformers modelled in PSCAD was less than when tested in the laboratory.

The 3P-3L transformer was more likely to permit the flow of GIC through the windings of the transformer over a shorter length of time in comparison to the other two core types. The 300 VA transformers were uprated to 500 MVA to represent power transformers in main transmission systems. The 500 MVA 3P-3L transformer core type had the shortest response time to GIC, followed by the 3(1P-3L) and the 3P-5L transformers. Figure 8.1 shows the average time response profile for the three core structures under no-load and load conditions.

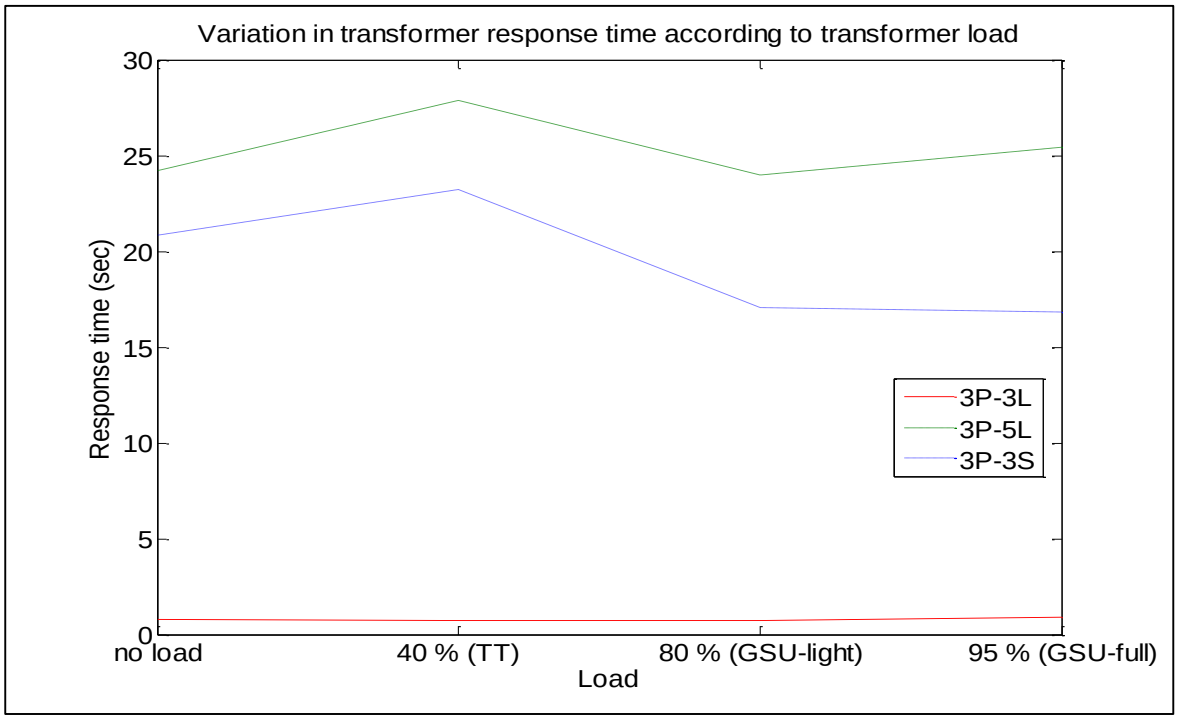

Figure 8.1 Profile of the average response time for the three transformer core structures

Table 6.5 and 6.6 in chapter 6 shows the ratios in response times. The hypothesis states that:

> ***The integration of transformer core characteristics and time response to GIC into GIC calculations improves the modelling of GIC as indicated by reduced differences between measured GIC and calculated GIC, and helps to improve the understanding of the transformer response to GIC.***

It was expected that the three transformer core structures would have different response times to the DC current. To a large extent, the results backed the expectation. Laboratory and PSCAD tests with the 300 VA transformer indicated that the 3(1P-3L) transformer has the longest response time in comparison to the 3P-3L and 3P-5L transformers.

In fact, the PSCAD simulation of the 500 MVA 3(1P-3L) power transformers yielded similar trends for both conditions of operation, namely either TT or GSU. This is attributed to the reduced leakage flux, high magnetization impedance and the higher winding inductance due to the lower leakage flux in 3(1P-3L) transformers [81], [99] and [100]. This implies that the results are consistent with the expected relative time response of the three transformer cores tested.

8.2.3 Limitations with scaling up transformer size from 300 VA to 500 MVA

Sometimes when test systems are scaled up, the results may not always be the same under similar conditions. This was found to be the case in this research. The 500 MVA 3(1P-3L) transformer's response time to DC between 3.0 pu and 8.0 pu was longer in comparison to the 500 MVA 3P-5L transformer. This was the same for the no-load and 40 % load condition, representing TTs.

Another difference between the 300 VA and 500 MVA transformers was that, during operation under the GSU conditions, the response time of the 500 MVA 3(1P-3L) transformer was less than the 500 MVA 3P-5L, while the opposite was true for the 300 VA transformer under the same GSU conditions.

8.2.4 Incorporating the transformer time response piecewise linear equations into the GIC calculation: 10 substation test network

The piecewise linear equations derived from the PSCAD simulation of the 500 MVA transformers represent the specific transformer core type under test. These equations are listed in section 6.3. While these equations may not fully reflect the exact time response profiles for real larger power transformers, such as 1,000 MVA, or a medium-sized power transformer, such as 500 MVA, the results brought to light the expected response time profile of power transformers. In so doing, they provide a platform upon which further research can be done.

The calculation examples with the test network in chapter 7 demonstrate how the GIC with transformer response is calculated. For each substation, this was calculated initially for a case where all the transformers in the network have the same core structure and later for a case where the transformer core structures as well as mode of operation differed.

In line with the results of the PSCAD simulations and the laboratory tests, the 3P-3L transformer had the smallest percentage difference in prospective GIC with transformer time response when compared to the prospective GIC without transformer time response.

This is based on the fact that the 3P-3L transformer has the shortest response time to DC current.

An investigation was done to determine whether the location of a transformer in the network has an impact on the profile of the prospective GIC with transformer time response. The investigation showed that the location of the transformer within the power network does not determine its response time to GIC but rather the core characteristics of the transformer.

8.2.5 Effect of interpolation on peak GIC

Interpolation was used to obtain the magnetic field data sets for the various sampling time intervals. For each set, the magnetic field data was used to calculate the corresponding electric field as an input to the GIC calculation. To quantify the effect of the interpolation method on the GIC calculation, the measured GIC interpolated to a series of sampling time intervals and the corresponding prospective GIC with and without transformer time response were compared. The outcome shows that the absolute peak values of measured and calculated GIC decrease as the sampling time interval increases as shown in Figure 8.2. The absolute peak values of the measured and calculated GIC in Figure 8.2 are not necessarily exactly time correlated with the same polarity. The monotonic shape of all the curves illustrates that the effects of averaging over longer periods are consistent for the whole range.

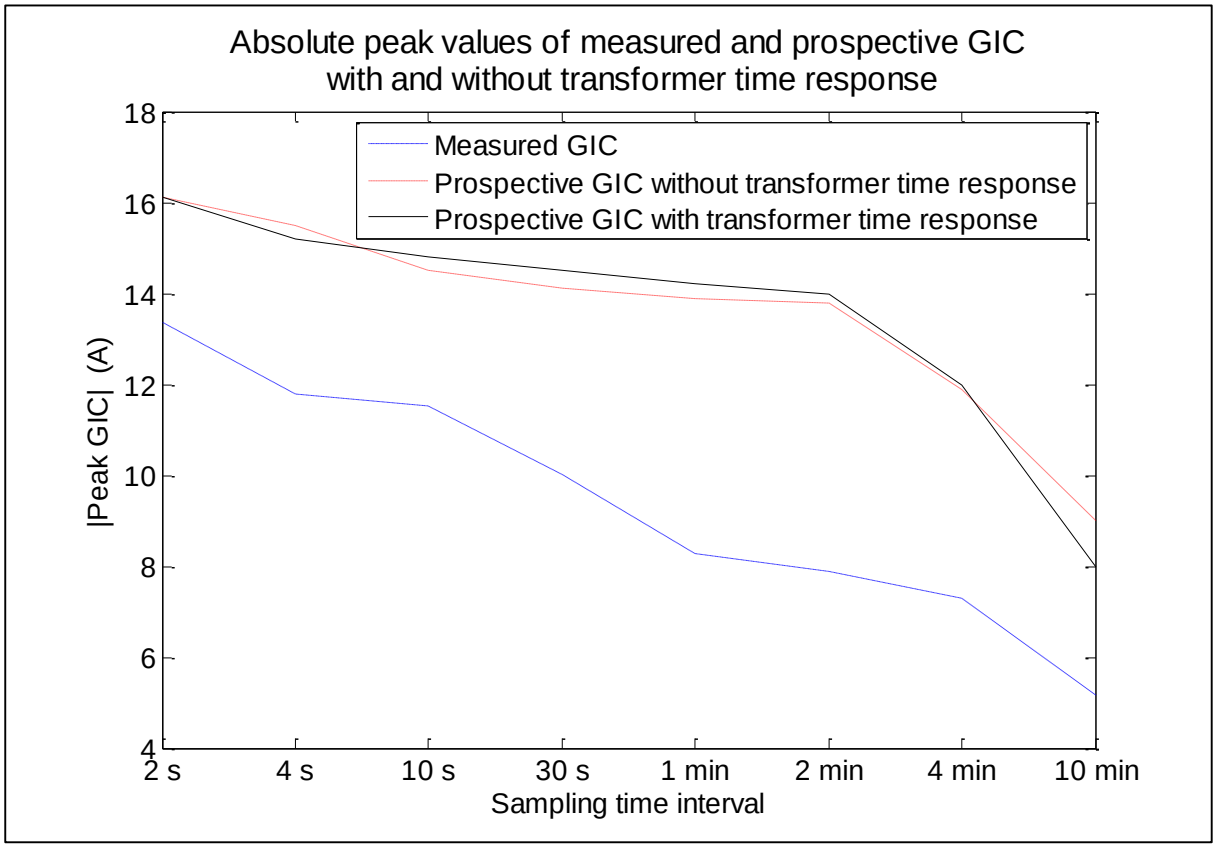

Figure 8.2 Comparison between the peak values of measured and calculated GIC using different sampling time intervals

This result when analysed in conjunction with the results in Figures 7.32 and 7.33 indicates that using two-second to 10-second intervals to sample the geomagnetic field used for GIC calculation produces acceptable results. The same applies for logging GIC in the grounded neutral of wye-connected transformers. Using two-second to 10-second intervals for logging GIC should sufficiently capture the GIC profile.

8.2.6 Effect of transformer time response on measured GIC and calculated GIC

Table 8.1 gives a summary of the probabilities that the transformer time response improves GIC calculation by reducing the difference between the calculated and measured GIC.

Table 8.1 Probabilities of improved GIC calculation using variable time intervals to sample the magnetic field

GIC Profile section	two-second	two-minute	10-minute
Section A	0.47	0.47	0.43
Section B	0.48	0.49	0.67
Section C	0.49	0.47	0.51
Section D	0.51	0.49	0.49
Total profile	0.49	0.48	0.49

The probability that the transformer time response reduced the difference between calculated and measured GIC using data sampled at two-second, two-minute and 10-minute time intervals is between 0.47 and 0.51, with the exception of two cases.

The first exception was in section A of the GIC profile using a 10-minute sampling time interval, where the probability of an improvement in the GIC calculation was 0.43. This was a result of the lower variations in the magnetic field and the larger sampling interval.

The second exception was in section B of the GIC profile using a 10-min sampling time interval, where the probability of an improvement in the GIC calculation was the highest at 0.67. This section of the GIC profile contains large fluctuations in the GIC during the SSC. As a result, the effect of the transformer time response is greater.

In conjunction with the MAE and variance analysis in section 7.4.3, the discussion thus far indicates that not only does the transformer response time differ for different transformer core structures, the average probability that the transformer time response improves GIC calculation is about 0.5. This means that both methods are almost equally good. The MAE increases during high GIC so does the variance between the measured GIC and the calculated GIC. However, when 10-minutes segments are considered, the transformer time response reduces the MAE even during segments with relatively high GIC.

CHAPTER 9

CONCLUSIONS

The research conducted for this thesis was aimed at developing a method for incorporating the transformer time response to GIC into GIC calculations, and to determine whether this will reduce the discrepancies between measured and calculated GIC. To this effect, several areas contiguous to transformer time response to GIC were developed. In this chapter, conclusions are drawn about each of these areas.

9.1 DIFFERENTIAL TRANSFORMER CORE RESPONSE TIME TO GIC

The transformer response time to DC current was not the same for the different transformer cores tested namely, 3P-3L, 3P-5L and 3(1P-3L). The response time for the 300 VA transformers increased in the following order: 3P-3L, 3P-5L, 3(1P-3L) and increased in the following order for the 500 MVA transformers in PSCAD: 3P-3L, 3(1P-3L), 3P-5L.

9.2 EFFECT OF LOAD ON TRANSFORMER RESPONSE TIME TO GIC

The laboratory test and PSCAD simulations showed that the response time to GIC for the 3P-3L, 3P-5L and 3(1P-3L) transformer core types are load dependant. From the average time response to DC for the three transformer cores shown in Figure 8.1, it was concluded that 3(1P-3L) and 3P-5L transformers operating as TT's have the longest response time to GIC.

The shortest response time to GIC was at GSU (light load), which was consistent across the three transformer cores. This correlates well with the notion that power transmission networks would stand a better chance of surviving a high GMD when all generating units and loads are online.

9.3 CHARACTERISING TRANSFORMER TIME RESPONSE TO GIC

Piecewise linear equations are suitable for characterising the response time of different transformer core structures at different load levels to different levels of GIC. This promotes a more detailed understanding and analysis of GIC flow through large power transformers with different core structures.

9.4 ANSWERS TO RESEARCH QUESTIONS

Five research questions were posed in chapter 1 to probe the hypothesis. This section summarises the answers to these questions. These answers are based on the results of the laboratory test and PSCAD simulations.

1. **How is the network part of GIC calculations affected by the transformer response to changing electric fields?**

The sampling time interval of the geomagnetic field influences the peak values of the geomagnetic field. This in turn is linked to the peak values of the calculated electric field. Since the rate of change of the magnetic field may vary during any time frame under consideration, the prospective GIC with transformer time response approach is a preferred method, as it presents a better understanding of the exact GIC flow through the transformer during a storm. This is because the transformer response time determines whether or not the prospective GIC flow through the transformer in the network will be reached as the electric field changes.

2. **What is the response of transformers to changing electric fields imposed at low frequencies and how does it vary with transformer core type?**

The response of transformers to GIC - like frequencies is such that the prospective GIC with and without transformer response are not always the same. This is attributed to the varying transformer response time.

3. Why was the time response of transformers neglected in the past? Are the reasons valid?

In the past, the time response of transformers was neglected because it was assumed that the contribution of the transformer time response to GIC was insignificant. This assumption now proves to be inaccurate, since it has been established that transformer's time response to GIC is core type and load dependent.

Taking into account that the transformer time response reduces the difference between the measured GIC and the calculated GIC. This would prevent an overestimation of the maximum GIC expected to flow through the substation. As a result, it will be possible to plan a more appropriate contingency measure to mitigate possible network problems anticipated during severe GMDs.

4. To what extent can the modelled and tested transformers represent all transformers?

The three main core structures were modelled with a variety of DC current levels and load conditions, both in PSCAD and in the laboratory. Therefore, while these results are unique to these transformer models, they provide an indication that it is incorrect to lump the transformer response of all transformers.

5. How does the sampling interval of the magnetic field and measured GIC affect GIC calculations?

As the sampling interval increases, the difference between the measured and calculated GIC increases. However, the difference between the peaks of the measured and calculated GIC is less than 2 %, when the sampling time interval is either two-second, four-second or 10-second. Therefore, the sampling between two-second and 10-second intervals is the recommended sampling time interval for GIC studies. This will increase the amount of data that can be stored in a given storage and still capture sufficient data for GIC analysis.

9.5 VALIDITY OF HYPOTHESIS

The background to this research work and the objectives as laid out in chapter 1 led to the hypothesis which states that:

> ***The integration of transformer core characteristics and time response to GIC into GIC calculations improves the modelling of GIC as indicated by reduced differences between measured GIC and calculated GIC, and helps to improve the understanding of the transformer response to GIC.***

The results in chapter 5, 6 and 7 as well as the discussions in chapter 8, which improved the understanding of transformer response to GIC, prove that the hypothesis is valid.

This research lays a foundation for further work on the transformer time response in GIC calculations.

List of References

[1] T. Forbes, "A review on the genesis of coronal mass ejections," *Journal of Geophysical Research: Space Physics (1978–2012),* vol. 105, pp. 23153-23165, 2000.

[2] J. T. Gosling, D. J. McComas, J. L. Phillips, V. J. Pizzo, B. E. Goldstein, R. J. Forsyth and R. P. Lepping, "A CME-driven solar wind disturbance observed at both low and high heliographic latitudes," *Geophys. Res. Lett.,* vol. 22, pp. 1753-1756, 1995.

[3] A. Viljanen, H. Nevanlinna, K. Pajunpää and A. Pulkkinen, "Time derivative of the horizontal geomagnetic field as an activity indicator," in *Annales Geophysicae,* 1999, pp. 1107-1118.

[4] J. A. Jacobs, *Geomagnetism.* Elsevier, 2013.

[5] A. J. Dessler and E. N. Parker, "Hydromagnetic theory of geomagnetic storms," *Journal of Geophysical Research,* vol. 64, pp. 2239-2252, 1959.

[6] R. Horton, D. Boteler, T. J. Overbye, R. Pirjola and R. C. Dugan, "A test case for the calculation of geomagnetically induced currents," *Power Delivery, IEEE Transactions on,* vol. 27, pp. 2368-2373, 2012.

[7] E. Bernhardi, P. Cilliers and C. Gaunt, "Improvement in the modelling of geomagnetically induced currents in southern Africa," *S. Afr. J. Sci.,* vol. 104, pp. 265-272, 2008.

[8] V. Albertson, B. Bozoki, W. Feero, J. Kappenman, E. Larsen, D. Nordell, J. Ponder, F. Prabhakara, K. Thompson and R. Walling, "Geomagnetic disturbance effects on power systems," *IEEE Trans. Power Del.,* vol. 8, pp. 1206-1216, 1993.

[9] C. T. Gaunt, "Reducing uncertainty–responses for electricity utilities to severe solar storms," *Journal of Space Weather and Space Climate,* vol. 4, pp. A01, 2014.

[10] K. Zheng, D. Boteler, R. J. Pirjola, L. Liu, R. Becker, L. Marti, S. Boutilier and S. Guillon, "Effects of system characteristics on geomagnetically induced currents," *Power Delivery, IEEE Transactions on,* vol. 29, pp. 890-898, 2014.

[11] W. Radasky and J. Kappenman, "Impacts of geomagnetic storms on EHV and UHV power grids," in *Electromagnetic Compatibility (APEMC), 2010 Asia-Pacific Symposium on,* 2010, pp. 695-698.

[12] H. Lundstedt, "The sun, space weather and GIC effects in Sweden," *Advances in Space Research,* vol. 37, pp. 1182-1191, 2006.

[13] K. Zheng, L. Trichtchenko, R. J. Pirjola and L. Liu, "Effects of geophysical parameters on GIC illustrated by benchmark network modeling," *Power Delivery, IEEE Transactions on,* vol. 28, pp. 1183-1191, 2013.

[14] V. D. Albertson, J. Thorson, R. Clayton and S. Tripathy, "Solar-induced-currents in power systems: cause and effects," *Power Apparatus and Systems, IEEE Transactions on,* pp. 471-477, 1973.

[15] J. G. Kappenman, "Geomagnetic storms and their impact on power systems," *IEEE Power Engineering Review,* vol. 16, 1996.

[16] D. Boteler. "Chapter 4. The impact of space weather on the electric power grid," in (1st ed.), C. J. Schrijver, F. Bagenal and J. J. Sojka, Eds. 2014, [Online].

[17] B. Bozoki, S. Chano, L. Dvorak, W. Feero, G. Fenner, E. Guro, C. Henville, J. Ingleson, S. Mazumdar and P. McLaren, "The effects of GIC on protective relaying," *Power Delivery, IEEE Transactions on,* vol. 11, pp. 725-739, 1996.

[18] L. Marti, J. Berge and R. K. Varma, "Determination of Geomagnetically Induced Current Flow in a Transformer from Reactive Power Absorption," *Power Delivery, IEEE Transactions on,* vol. 28, pp. 1280-1288, 2013.

[19] T. S. Molinski, "Why utilities respect geomagnetically induced currents," *J. Atmos. Solar Terr. Phys.,* vol. 64, pp. 1765-1778, 2002.

[20] J. Kappenman, S. Norr, G. Sweezy, D. Carlson, V. Albertson, J. Harder and B. Damsky, "GIC mitigation: a neutral blocking/bypass device to prevent the flow of GIC in power systems," *Power Delivery, IEEE Transactions on,* vol. 6, pp. 1271-1281, 1991.

[21] L. Bolduc, M. Granger, G. Paré, J. Saintonge and L. Brophy, "Development of a DC current-blocking device for transformer neutrals," *Power Delivery, IEEE Transactions on,* vol. 20, pp. 163-168, 2005.

[22] R. J. Pirjola and A. Viljanen, "Research of geomagnetically induced currents (gic) in finland," in *Electromagnetic Compatibility and Electromagnetic Ecology, 2007 7th International Symposium on,* 2007, pp. 269-272.

[23] A. W. Thomson, C. Gaunt, P. Cilliers, J. Wild, B. Opperman, L. McKinnell, P. Kotze, C. M. Ngwira and S. I. Lotz, "Present day challenges in understanding the geomagnetic hazard to national power grids," *Advances in Space Research,* vol. 45, pp. 1182-1190, 2010.

[24] I. A. Erinmez, J. G. Kappenman and W. A. Radasky, "Management of the geomagnetically induced current risks on the national grid company's electric power transmission system," *J. Atmos. Solar Terr. Phys.,* vol. 64, pp. 743-756, 2002.

[25] M. Lehtinen and R. Pirjola, "Currents produced in earthed conductor networks by geomagnetically-induced electric fields," in *Annales Geophysicae,* 1985, pp. 479-484.

[26] D. Boteler and R. Pirjola, "Comparison of methods for modelling geomagnetically induced currents," in *Annales Geophysicae,* 2014, pp. 1177-1187.

[27] A. A. Trichtchenko, D. H. Boteler and A. Foss, "GIC modelling for an overdetermined system," in *Electrical and Computer Engineering, 2006. CCECE'06. Canadian Conference on,* 2006, pp. 394-397.

[28] D. Boteler, "Methodology for simulation of geomagnetically induced currents in power systems," *Journal of Space Weather and Space Climate,* vol. 4, pp. A21, 2014.

[29] J. Berge and R. K. Varma, "A software simulator for geomagnetically induced currents in electrical power systems," in *Electrical and Computer Engineering, 2009. CCECE'09. Canadian Conference on,* 2009, pp. 695-700.

[30] J. Koen and T. Gaunt, "Geomagnetically induced currents in the southern african electricity transmission network," in *Power Tech Conference Proceedings, 2003 IEEE Bologna,* 2003, pp. 7 pp. Vol. 1.

[31] J. Koen, "Geomagnetically induced currents in the Southern African electricity transmission network," *University of Cape Town, South Africa,* 2002.

[32] (2014, February 06). *Modeling Geomagnetically Induced Currents in PowerWorld Simulator*. Available: http://www.powerworld.com/files/GICModeling.pdf.

[33] M. Wik, A. Viljanen, R. Pirjola, A. Pulkkinen, P. Wintoft and H. Lundstedt, "Calculation of geomagnetically induced currents in the 400 kV power grid in southern Sweden," *Space Weather,* vol. 6, pp. S07005, 2008.

[34] C. Barbosa, K. Pinheiro, G.A. Hartmann, R.I.F. Trindade, "Numerical model test of geomagnetic induced currents in Brazil," *Latinmag Letters,* vol. Volume 3, 2013.

[35] T. J. Overbye, T. R. Hutchins, K. Shetye, J. Weber and S. Dahman, "Integration of geomagnetic disturbance modeling into the power flow: A methodology for large-scale system studies," in *North American Power Symposium (NAPS), 2012,* 2012, pp. 1-7.

[36] D. Boteler, L. Trichtchenko, R. Pirjola, J. Parmelee, S. Souksaly, A. Foss and L. Marti, "Real-time simulation of geomagnetically induced currents," in *Electromagnetic Compatibility and Electromagnetic Ecology, 2007 7th International Symposium on,* 2007, pp. 261-264.

[37] R. Walling and A. Khan, "Characteristics of transformer exciting-current during geomagnetic disturbances," *Power Delivery, IEEE Transactions on,* vol. 6, pp. 1707-1714, 1991.

[38] L. Bolduc, "GIC observations and studies in the Hydro-Québec power system," *J. Atmos. Solar Terr. Phys.,* vol. 64, pp. 1793-1802, 2002.

[39] D. H. Boteler, R. J. Pirjola and H. Nevanlinna, "The effects of geomagnetic disturbances on electrical systems at the Earth's surface," *Advances in Space Research,* vol. 22, pp. 17-27, 1998.

[40] A. Pulkkinen, S. Lindahl, A. Viljanen and R. Pirjola, "Geomagnetic storm of 29–31 October 2003: Geomagnetically induced currents and their relation to problems in the Swedish high-voltage power transmission system," *Space Weather,* vol. 3, 2005.

[41] T. J. Overbye, K. S. Shetye, T. R. Hutchins, Q. Qiu and J. D. Weber, "Power grid sensitivity analysis of geomagnetically induced currents," *Power Systems, IEEE Transactions on,* vol. 28, pp. 4821-4828, 2013.

[42] A. McNish, "Magnetic storms," *Edison Electric Institute Bulletin,* 1940.

[43] P. J. Kellogg, "Terrestrial effects of solar activity," in *Proceedings Minn. Power Systems Conf.,* Minnesota, 1966,.

[44] V. D. Albertson and J. A. Van Baelen, "Electric and magnetic fields at the earth's surface due to auroral currents," *Power Apparatus and Systems, IEEE Transactions on,* pp. 578-584, 1970.

[45] J. Koen and C. Gaunt, "Disturbances in the Southern African power network due to geomagnetically induced currents," *Cigré Session,* pp. 206, 2002.

[46] D. Boteler and R. Pirjola, "Modelling geomagnetically induced currents produced by realistic and uniform electric fields," *Power Delivery, IEEE Transactions on,* vol. 13, pp. 1303-1308, 1998.

[47] A. Pulkkinen, O. Amm and A. Viljanen, "Ionospheric equivalent current distributions determined with the method of spherical elementary current systems," *Journal of Geophysical Research,* vol. 108, pp. 1053, 2003.

[48] O. Amm and A. Viljanen, "Ionospheric disturbance magnetic field continuation from the ground to the ionosphere using spherical elementary current systems," *Earth, Planets and Space,* vol. 51, pp. 431-440, 1999.

[49] O. AMM, "Ionospheric elementary current systems in spherical coordinates and their application," *Journal of Geomagnetism and Geoelectricity,* vol. 49, pp. 947-955, 1997.

[50] S. Watari, M. Kunitake, K. Kitamura, T. Hori, T. Kikuchi, K. Shiokawa, N. Nishitani, R. Kataoka, Y. Kamide and T. Aso, "Measurements of geomagnetically induced current in a power grid in Hokkaido, Japan," *Space Weather,* vol. 7, 2009.

[51] A. Viljanen, "Relation of geomagnetically induced currents and local geomagnetic variations," *Power Delivery, IEEE Transactions on,* vol. 13, pp. 1285-1290, 1998.

[52] L. Trichtchenko and D. Boteler, "Effects of recent geomagnetic storms on power systems," in *Electromagnetic Compatibility and Electromagnetic Ecology, 2007 7th International Symposium on,* 2007, pp. 265-268.

[53] A. Viljanen, R. Pirjola, M. Wik, A. Ádám, E. Prácser, Y. Sakharov and J. Katkalov, "Continental scale modelling of geomagnetically induced currents," *Journal of Space Weather and Space Climate,* vol. 2, 2012.

[54] W. McNutt, "The effect of GIC on power transformers," in *IEEE PES Summer Meeting July,* 1990, pp. 32-37.

[55] J. Berge, L. Marti and R. K. Varma, "Modeling and mitigation of geomagnetically induced currents on a realistic power system network," in *Electrical Power and Energy Conference (EPEC), 2011 IEEE,* 2011, pp. 485-490.

[56] N. Takasu, T. Oshi, F. Miyawaki, S. Saito and Y. Fujiwara, "An experimental analysis of DC excitation of transformers by geomagnetically induced currents," *Power Delivery, IEEE Transactions on,* vol. 9, pp. 1173-1182, 1994.

[57] D. Boteler, "Geomagnetically induced currents: present knowledge and future research," *Power Delivery, IEEE Transactions on,* vol. 9, pp. 50-58, 1994.

[58] R. Pirjola, "Review on the calculation of surface electric and magnetic fields and of geomagnetically induced currents in ground-based technological systems," *Surv. Geophys.,* vol. 23, pp. 71-90, 2002.

[59] A. Pulkkinen, A. Thomson, E. Clarke and A. McKay, "April 2000 geomagnetic storm: Ionospheric drivers of large geomagnetically induced currents," in *Annales Geophysicae,* 2003, pp. 709-717.

[60] A. Viljanen, A. Pulkkinen, O. Amm, R. Pirjola and T. Korja, "Fast computation of the geoelectric field using the method of elementary current systems and planar earth models," in *Annales Geophysicae,* 2004, pp. 101-113.

[61] A. Viljanen and R. Pirjola, "Statistics on geomagnetically-induced currents in the Finnish 400 kV power system based on recordings of geomagnetic variations," *Journal of Geomagnetism and Geoelectricity,* vol. 41, pp. 411-420, 1989.

[62] R. Pirjola, "Geomagnetically induced currents during magnetic storms," *Plasma Science, IEEE Transactions on,* vol. 28, pp. 1867-1873, 2000.

[63] C. Liu, L. Liu, R. Pirjola and Z. Wang, "Calculation of geomagnetically induced currents in mid-to low-latitude power grids based on the plane wave method: A preliminary case study," *Space Weather,* vol. 7, 2009.

[64] T. A. Tjimbandi, "Geomagnetically Induced Currents in South Africa," *BSc Elec Eng Thesis, University of Cape Town.,* 2007.

[65] H. Vanhamäki, A. Viljanen, R. Pirjola and O. Amm, "Deriving the geomagnetically induced electric field at the Earth's surface from the time derivative of the vertical magnetic field," *Earth, Planets and Space,* vol. 65, pp. 997-1006, 2013.

[66] R. Pirjola and A. Viljanen, "Complex image method for calculating electric and magnetic fields produced by an auroral electrojet of finite length," in *Annales Geophysicae,* 1998, pp. 1434-1444.

[67] R. Pirjola, A. Viljanen, A. Pulkkinen and O. Amm, "Space weather risk in power systems and pipelines," *Physics and Chemistry of the Earth, Part C: Solar, Terrestrial & Planetary Science,* vol. 25, pp. 333-337, 2000.

[68] P. A. Tipler and G. Mosca, *Physics for Scientists and Engineers.* Macmillan, 2007.

[69] P. E. Gray and C. L. Searle, *Electronic Principles: Physics, Models, and Circuits.* Wiley, 1969.

[70] K. S. Shetye, T. J. Overbye, Q. Qiu and J. Fleeman, "Geomagnetic disturbance modeling results for the AEP system: A case study," in *Power and Energy Society General Meeting (PES), 2013 IEEE,* 2013, pp. 1-5.

[71] J. D. Glover, M. S. Sarma and T. J. Overbye, *Power System Analysis and Design.* CengageBrain. com, 2011.

[72] L. Trichtchenko and D. H. Boteler, "Modeling geomagnetically induced currents using geomagnetic indices and data," *Plasma Science, IEEE Transactions on,* vol. 32, pp. 1459-1467, 2004.

[73] (8th January, 2014). *GIC flow in power systems*. Available: http://www.powerworld.com/files/GICGroundLoop.jpg.

[74] P. C. Sen, *Principles of Electric Machines and Power Electronics.* John Wiley & Sons, 2007.

[75] National Imagery and Mapping Agency (NIMA), "Department of defence world geodetic system 1984," NIMA/Geodesy and Geophysics Department, Tech. Rep. NIMA TR8350.2, 2000.

[76] H. K. Chisepo, "The Response of Transformers to Geomagnetically Induced-like Currents," *MSc Dissertation. University of Cape Town,* 2014.

[77] A. E. Emanuel, "Summary of IEEE standard 1459: definitions for the measurement of electric power quantities under sinusoidal, nonsinusoidal, balanced, or unbalanced conditions," *Industry Applications, IEEE Transactions on,* vol. 40, pp. 869-876, 2004.

[78] (). *NI 9225 3-Channel, 300 Vrms Analog Input Module*. Available: http://sine.ni.com/nips/cds/view/p/lang/en/nid/208795.

[79] (). *PLC: DVPEN01-SL*. Available: http://www.delta.com.tw/product/em/control/cm/download/manual/DVPEN01-SL_O_EN_20090721.pdf.

[80] M. Salimi, A. Gole and R. Jayasinghe, "Improvement of Transformer Saturation Modeling for Electromagnetic Transient Programs," *IPST, Vancouver,* 2013.

[81] (2013, December 28). *Design of Transformers* . Available: http://elearning.vtu.ac.in/16/ENotes/Elec%20Mac%20Des/Unit3-Era.pdf.

[82] J. Martinez, R. Walling, B. Mork, J. Martin-Arnedo and D. Durbak, "Parameter determination for modeling system transients-Part III: Transformers," *Power Delivery, IEEE Transactions on,* vol. 20, pp. 2051-2062, 2005.

[83] Siemens, "Siemens energy sector power engineering guide" Tech. Rep. Edition 7.

[84] (2013, December 28). *Lecture 3- Power Transformers*. Available: http://services.eng.uts.edu.au/pmcl/pct/Downloads/Lecture03.pdf.

[85] D. Boteler, "Characteristics of time-varying inductance," *Magnetics, IEEE Transactions on,* vol. 30, pp. 172-176, 1994.

[86] B. Hembroff, M. Ohlen and P. Werelius, "A Guide to Transformer Winding Resistance," *Application Notes, April,* 2010.

[87] B. Hembroff, "A Guide To Transformer DC Resistance Measurements, Part 2," *Electricity Today, April,* 1996.

[88] F. Prabhakara, J. Ponder and J. Towle, "Computing GIC in large power systems," *Computer Applications in Power, IEEE,* vol. 5, pp. 46-50, 1992.

[89] P. R. Price, "Geomagnetically induced current effects on transformers," *Power Delivery, IEEE Transactions on,* vol. 17, pp. 1002-1008, 2002.

[90] J. Bird, *Electrical and Electronic Principles and Technology.* Routledge, 2013.

[91] J. Bird and A. May, *Electrical Principles 3 Checkbook: The Checkbook Series.* Elsevier, 2013.

[92] T. Chai and R. R. Draxler, "Root mean square error (RMSE) or mean absolute error (MAE)?–Arguments against avoiding RMSE in the literature," *Geoscientific Model Development,* vol. 7, pp. 1247-1250, 2014.

[93] C. J. Willmott and K. Matsuura, "Advantages of the mean absolute error (MAE) over the root mean square error (RMSE) in assessing average model performance," *Climate Research,* vol. 30, pp. 79, 2005.

[94] F. A. Graybill, *Theory and Application of the Linear Model.* Cengage Learning, 2000.

[95] L. Trichtchenko and D. H. Boteler, "Response of power systems to the temporal characteristics of geomagnetic storms," in *Electrical and Computer Engineering, 2006. CCECE'06. Canadian Conference on,* 2006, pp. 390-393.

[96] L. Bolduc, A. Gaudreau and A. Dutil, "Saturation time of transformers under dc excitation," *Electr. Power Syst. Res.,* vol. 56, pp. 95-102, 11/1, 2000.

[97] C. Gaunt and G. Coetzee, "Transformer failures in regions incorrectly considered to have low GIC-risk," in *Power Tech, 2007 IEEE Lausanne,* 2007, pp. 807-812.

[98] W. Barlow, "On the spontaneous electrical currents observed in the wires of the electric telegraph," *Philosophical Transactions of the Royal Society of London,* vol. 139, pp. 61-72, 1849.

[99] C. W. T. McLyman, *Transformer and Inductor Design Handbook.* CRC press, 2004.

[100] N. Tleis, *Power Systems Modelling and Fault Analysis : Theory and Practice.* Oxford, 2008.

APPENDIX A: PLC specifications

Transmission method: IEEE 802.3, IEEE 802.3u

Transmission interface: RJ-45 MDI/MDIX, no jumper cable required

Baudrate: 10/100 Mbps, auto-detection

Network protocols: ICMP, IP, TCP, UDP, DHCP, SMTP, NTP, Modbus TCP

Power supply voltage: 24 V DC

Power consumption: 1.5 W

Insulation voltage: 500 V

APPENDIX B: Electric and magnetic field data used in chapter 7.1 to 7.3

Table B. Electric and magnetic field data sampled at time minute intervals

Sample	B_x [nT]	E_y [V/km]	B_y [nT]	E_x [V/km]
0	9846		-4325	
1	9854	-0.009	-4332	**0.033**
2	9856	0.024	-4337	**0.019**
3	9865	-0.051	-4339	**0.033**
4	9877	-0.059	-4345	**0.034**
5	9892	-0.069	-4350	**0.032**
6	9880	-0.013	-4342	**-0.006**
7	9866	0.024	-4339	**-0.012**
8	9854	0.046	-4329	**-0.03**
9	9851	0.03	-4325	**-0.028**
10	9852	0.025	-4317	**-0.048**
11	9854	0.029	-4308	**-0.052**
12	9842	0.042	-4284	**-0.101**
13	9842	0.004	-4258	**-0.116**
14	9843	0.015	-4249	**-0.089**
15	9852	-0.034	-4239	**-0.085**
16	9866	-0.047	-4242	**-0.05**
17	9867	-0.018	-4243	**-0.024**
18	9872	-0.042	-4245	**-0.007**
19	9880	-0.044	-4245	**-0.014**
20	9847	0.074	-4226	**-0.049**
21	9843	0.025	-4218	**-0.031**
22	9852	-0.001	-4227	**0.004**
23	9866	-0.034	-4271	**0.145**
24	9901	-0.103	-4329	**0.206**
25	9936	-0.137	-4384	**0.279**
26	9956	-0.165	-4427	**0.28**
27	9952	-0.063	-4448	**0.235**
28	9984	-0.167	-4453	**0.143**
29	10003	-0.139	-4442	**0.035**
30	9971	0.035	-4390	**-0.117**
31	10065	-0.307	-4374	**-0.08**
32	10041	-0.033	-4373	**-0.081**
33	9958	0.209	-4354	**-0.112**
34	9931	0.108	-4338	**-0.115**
35	9957	-0.027	-4343	**-0.025**
36	10081	-0.312	-4358	**0**

37	10001	0.158	-4337	**-0.08**
38	9979	0.031	-4278	**-0.202**
39	9954	0.075	-4202	**-0.313**
40	9916	0.152	-4176	**-0.192**
41	9921	0.11	-4172	**-0.163**
42	9897	0.127	-4140	**-0.213**
43	9872	0.185	-4113	**-0.181**
44	9789	0.271	-4013	**-0.372**
45	9777	0.16	-4001	**-0.156**
46	9773	0.166	-4039	**-0.008**
47	9843	-0.163	-4108	**0.142**
48	9871	-0.067	-4126	**0.081**
49	9850	-0.026	-4143	**0.15**
50	9860	-0.078	-4119	**0.05**
51	9824	0.052	-4091	**-0.036**
52	9800	0.106	-4091	**-0.018**
53	9784	0.105	-4104	**0.016**
54	9781	0.073	-4123	**0.06**
55	9751	0.133	-4153	**0.096**
56	9735	0.111	-4169	**0.116**
57	9733	0.067	-4173	**0.086**
58	9725	0.057	-4192	**0.11**
59	9720	0.059	-4199	**0.067**
60	9717	0.035	-4201	**0.048**
61	9707	0.049	-4209	**0.049**
62	9695	0.065	-4219	**0.065**
63	9683	0.059	-4231	**0.064**
64	9673	0.061	-4249	**0.094**
65	9678	0.022	-4270	**0.108**
66	9671	0.046	-4301	**0.155**
67	9676	-0.005	-4334	**0.172**
68	9702	-0.074	-4339	**0.108**
69	9710	-0.048	-4327	**0.038**
70	9699	0.002	-4320	**0.02**
71	9683	0.029	-4314	**0.002**
72	9691	-0.028	-4332	**0.041**
73	9793	-0.301	-4356	**0.092**
74	9803	-0.097	-4362	**0.054**
75	9824	-0.181	-4368	**0.056**
76	9863	-0.239	-4371	**0.048**
77	9872	-0.131	-4344	**-0.071**
78	9820	0.063	-4317	**-0.095**
79	9821	0.004	-4300	**-0.092**

80	9829	-0.009	-4306	**-0.039**
81	9838	-0.008	-4313	**-0.035**
82	9854	-0.021	-4310	**-0.036**
83	9859	-0.055	-4283	**-0.082**
84	9872	-0.085	-4257	**-0.097**
85	9875	-0.045	-4247	**-0.085**
86	9850	0.044	-4250	**-0.05**
87	9841	0.053	-4242	**-0.063**
88	9828	0.05	-4241	**-0.029**
89	9824	0.059	-4247	**0.009**
90	9821	0.046	-4245	**-0.007**

APPENDIX C: GIC profiles from section 7.1

Comparison between GIC values obtained with the Lehtinen and Pirjola method and the NAM method

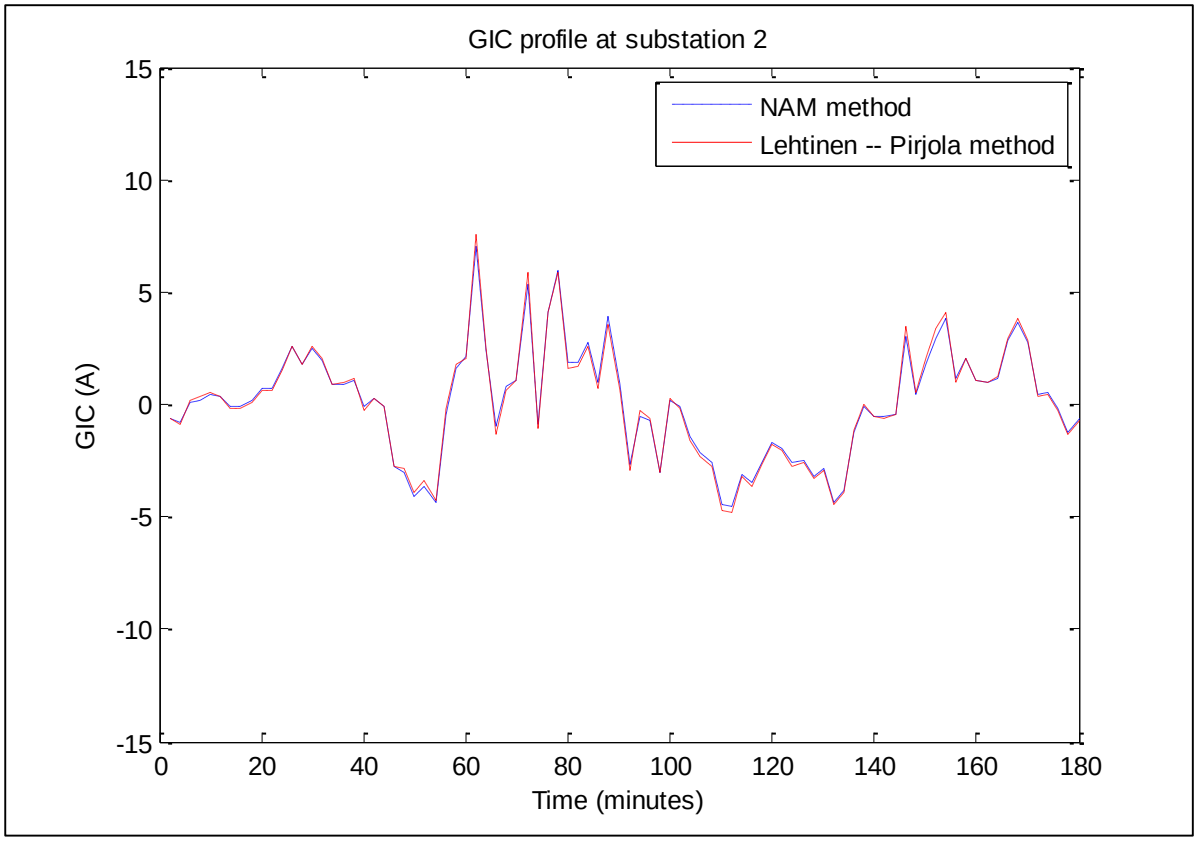

Figure C. 1 Substation 2: Comparison of GIC values obtained using Lehtinen-Pirjola and NAM methods

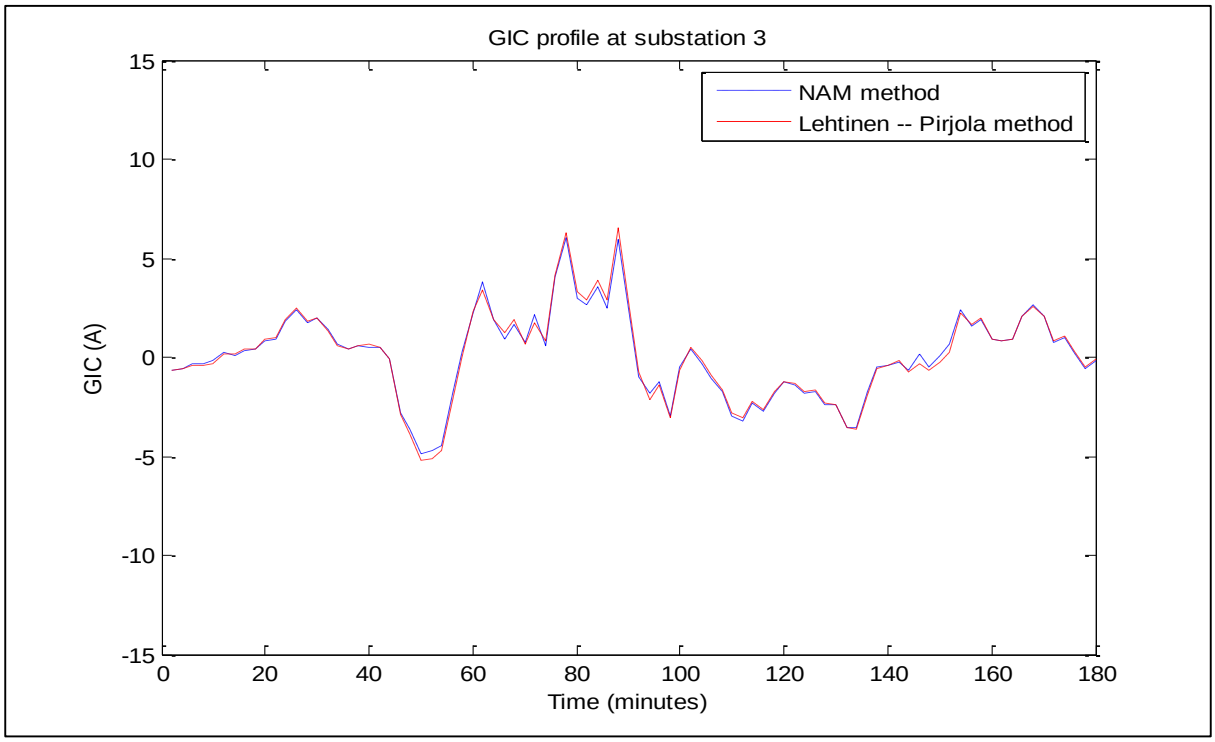

Figure C.2 Substation 3: Comparison of GIC values obtained using Lehtinen-Pirjola and NAM methods

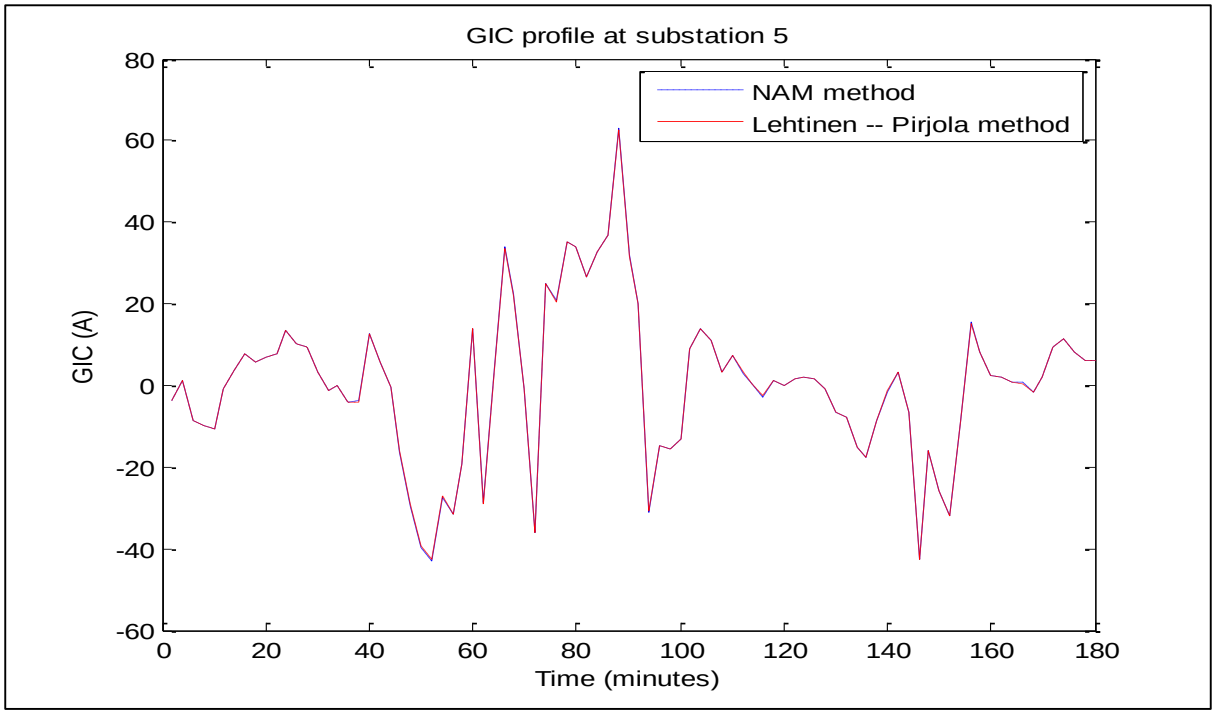

Figure C.3 Substation 5: Comparison of GIC values obtained using Lehtinen-Pirjola and NAM methods

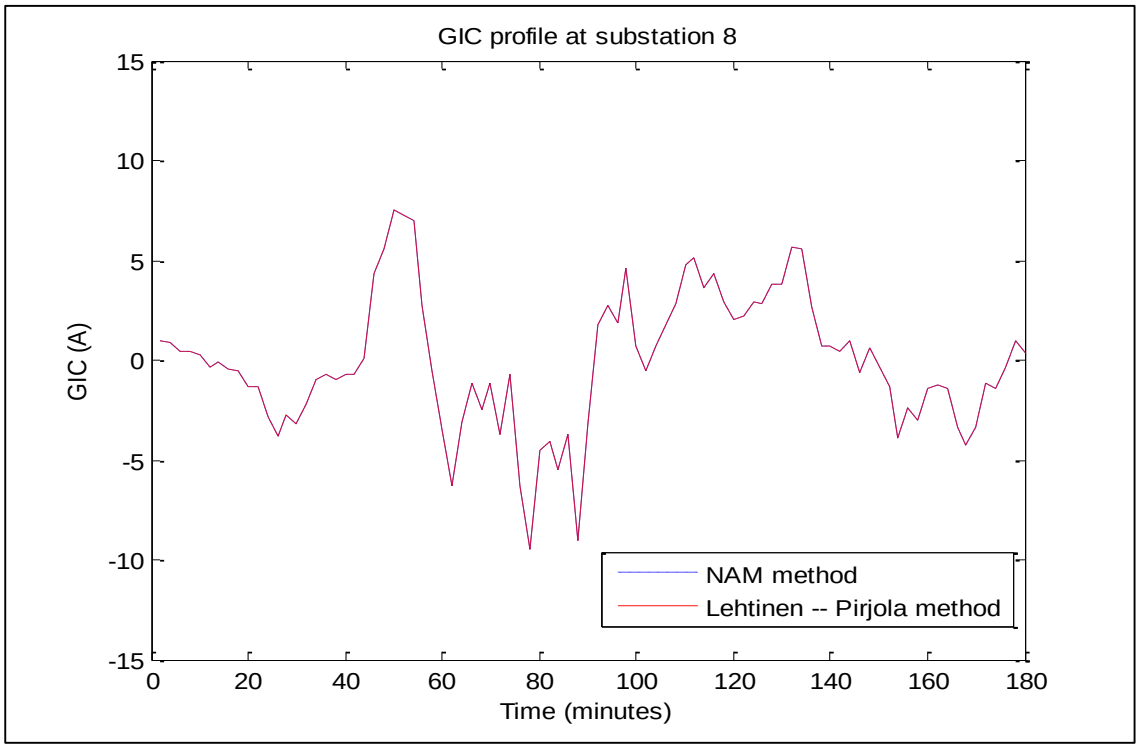

Figure C. 4 Substation 8: Comparison of GIC values obtained using Lehtinen-Pirjola and NAM methods

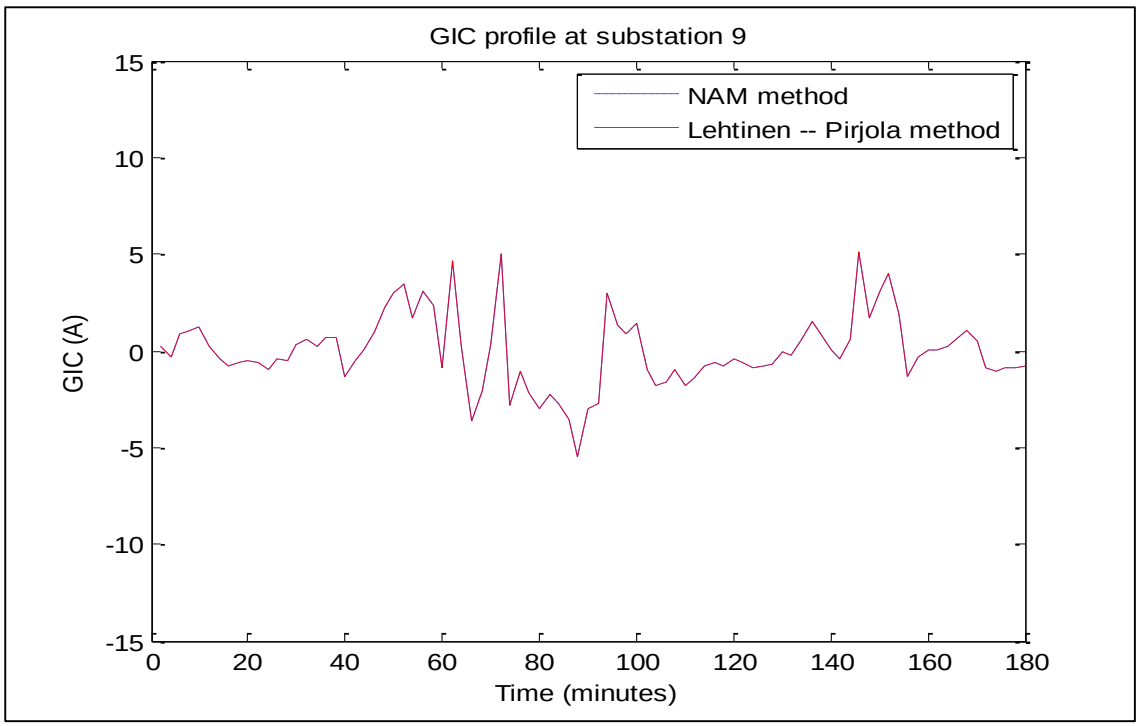

Figure C.5 Substation 9: Comparison of GIC values obtained using Lehtinen-Pirjola and NAM methods

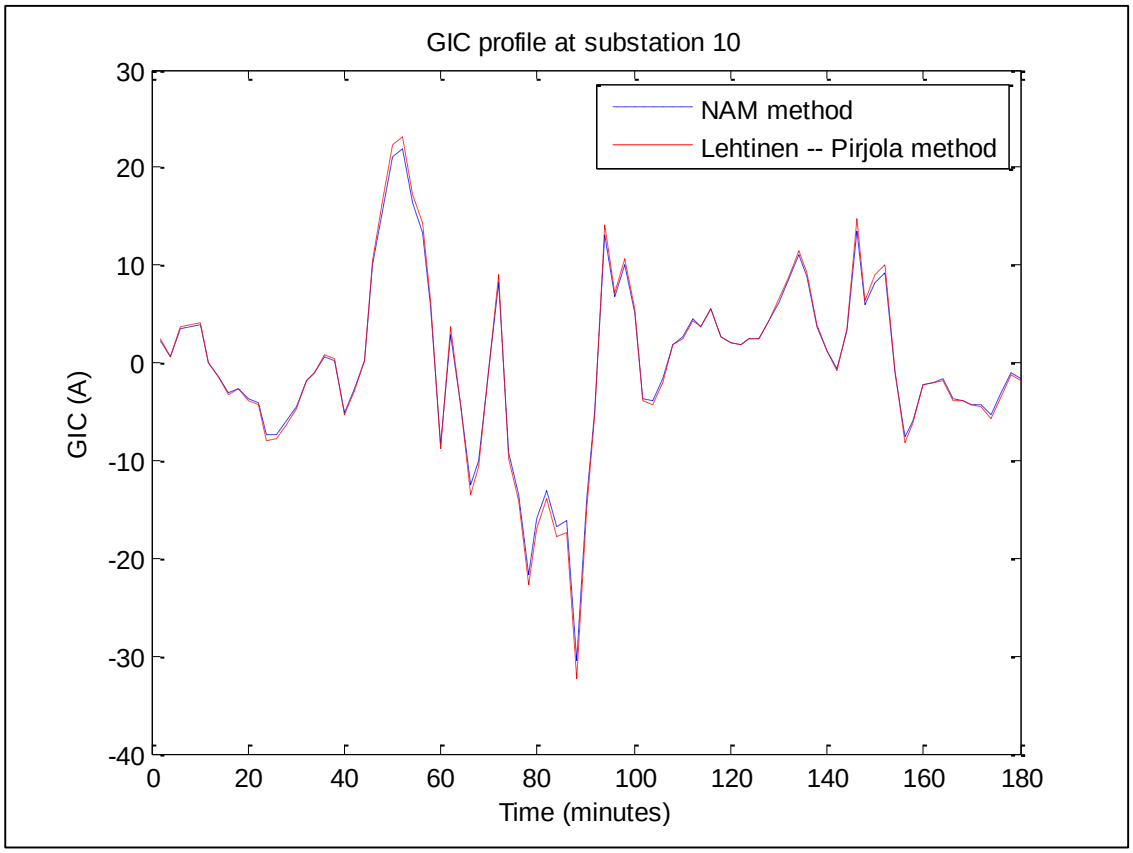

Figure C.6 Substation 10: Comparison of GIC values obtained using Lehtinen-Pirjola and NAM methods

APPENDIX D: Substation GIC profiles in case 1

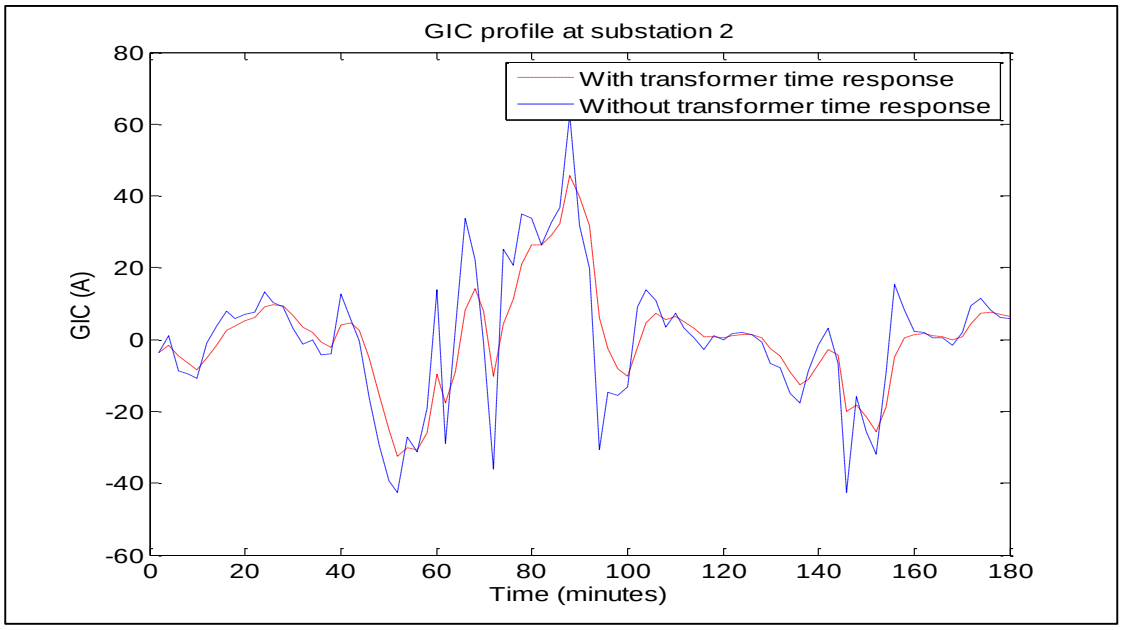

Figure D.1 Substation 2: Comparison between prospective GIC values with and without transformer time response

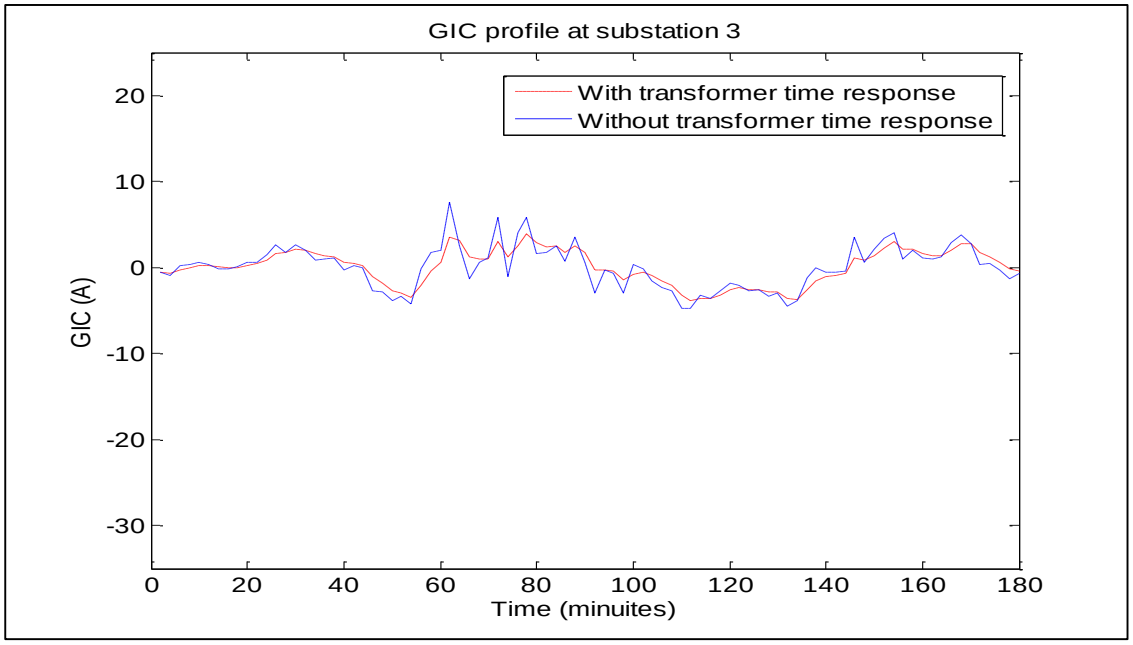

Figure D.2 Substation 3: Comparison between prospective GIC values with and without transformer time response

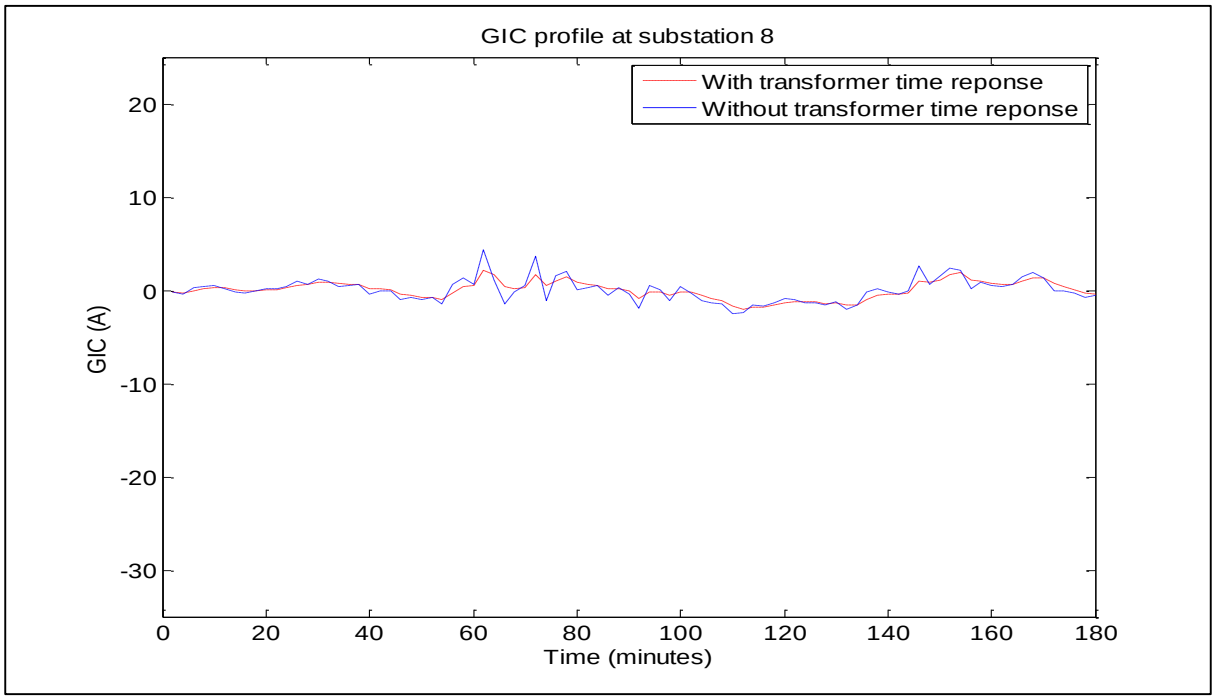

Figure D.4 Substation 8: Comparison between prospective GIC values with and without transformer time response

Figure D.5 Substation 9 Comparison between prospective GIC values with and without transformer time response

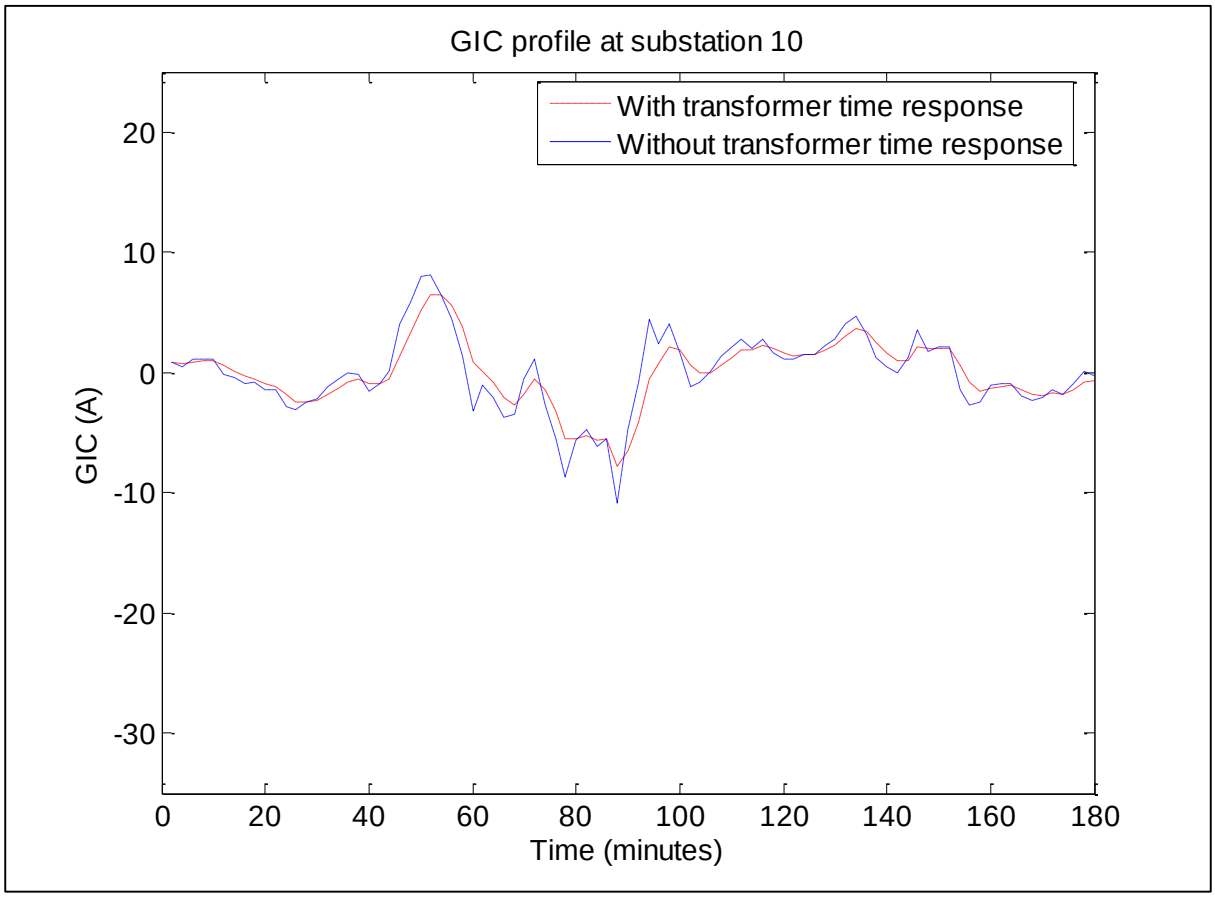

Figure D.6 Substation 10: Comparison between prospective GIC values with and without transformer time response

APPENDIX E: Substation GIC profiles in case 2

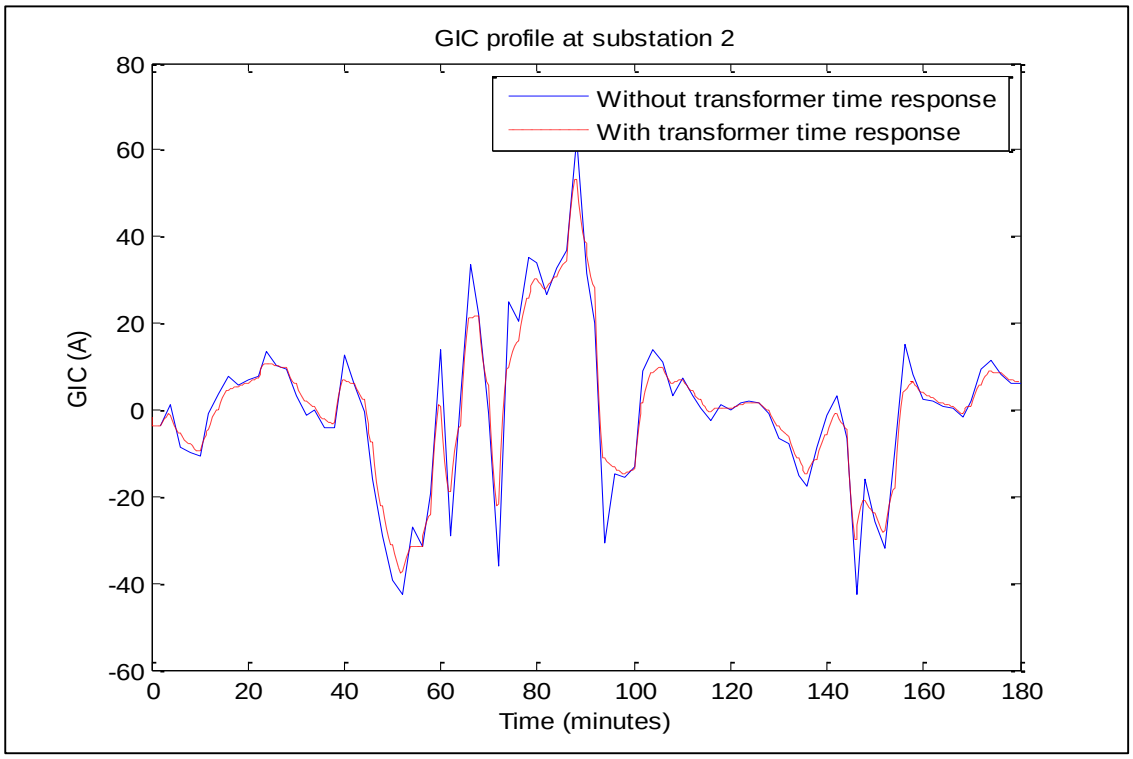

Figure E.1 Substation 2: Comparison between prospective GIC values with and without transformer time response

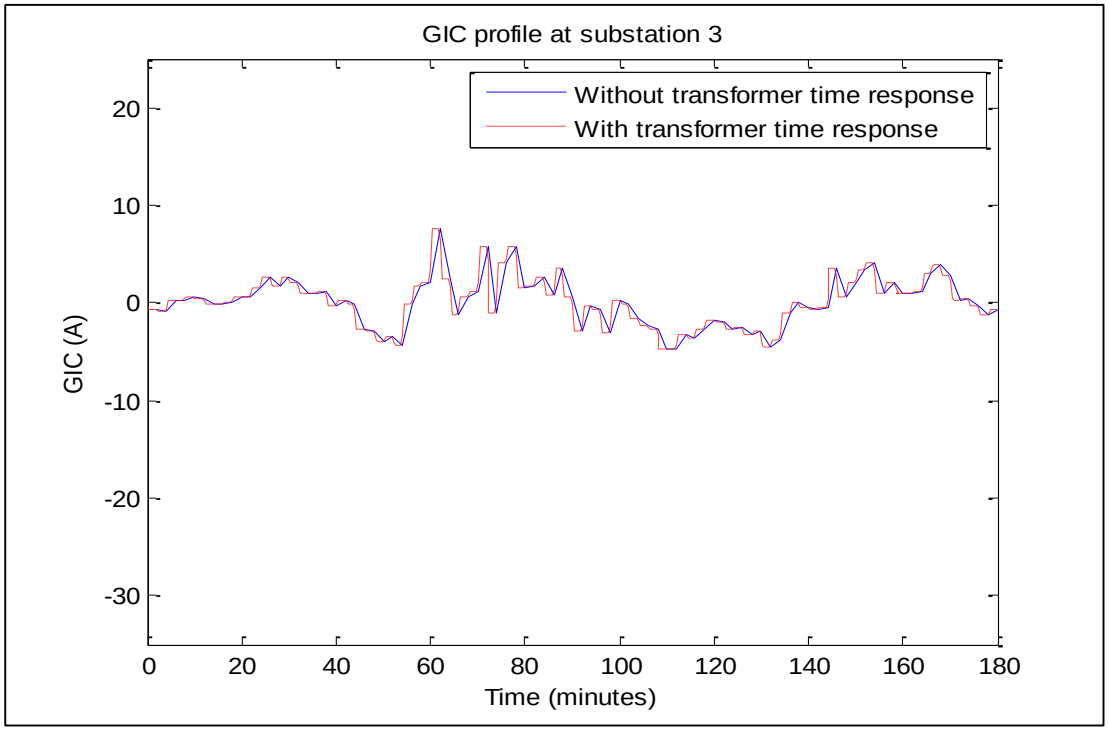

Figure E.2 Substation 3: Comparison between prospective GIC values with and without transformer time response

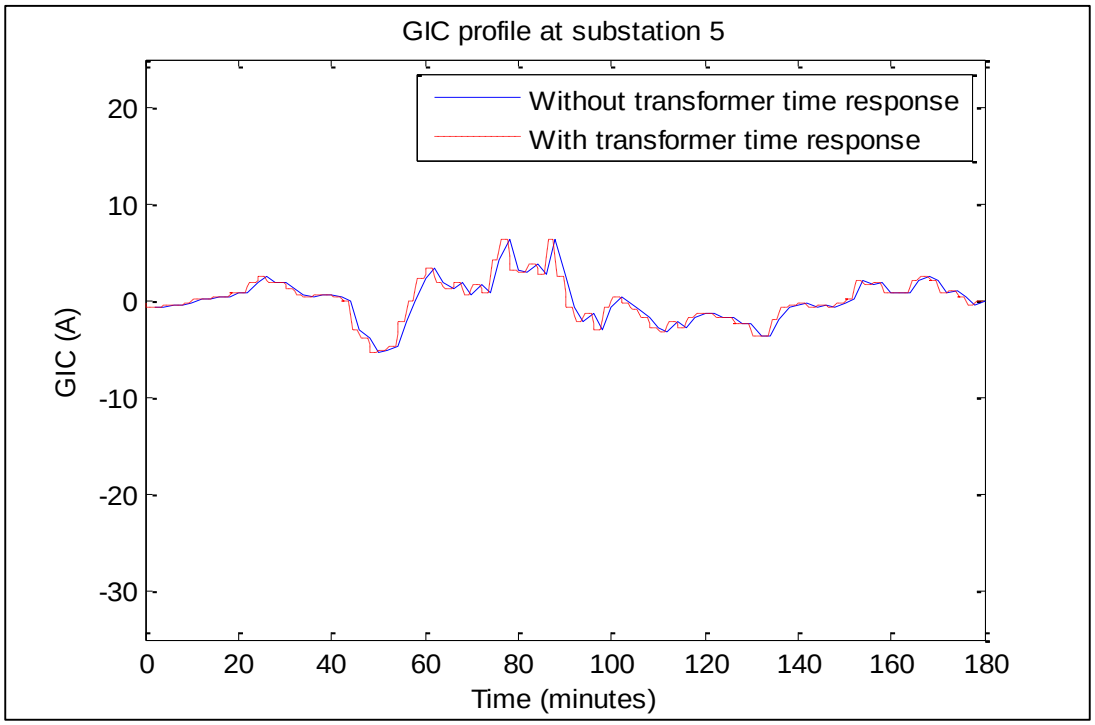

Figure E.3 Substation 5 Comparison between prospective GIC values with and without transformer time response

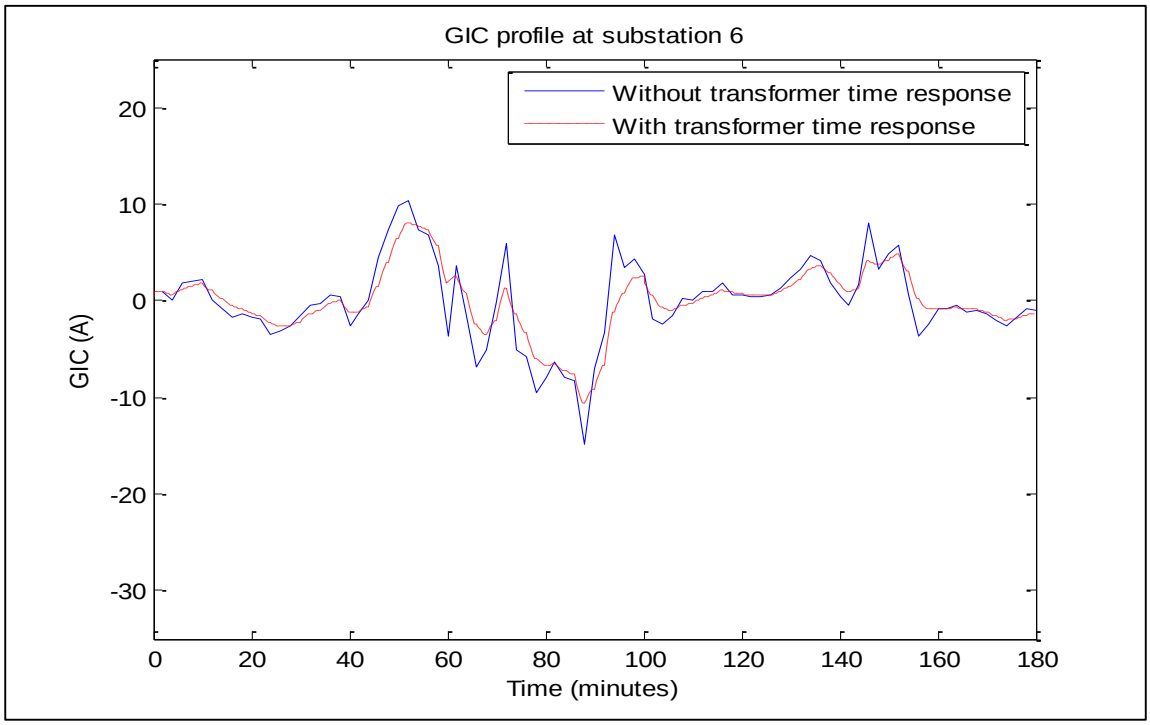

Figure E.4 Substation 6: Comparison between prospective GIC values with and without transformer time response

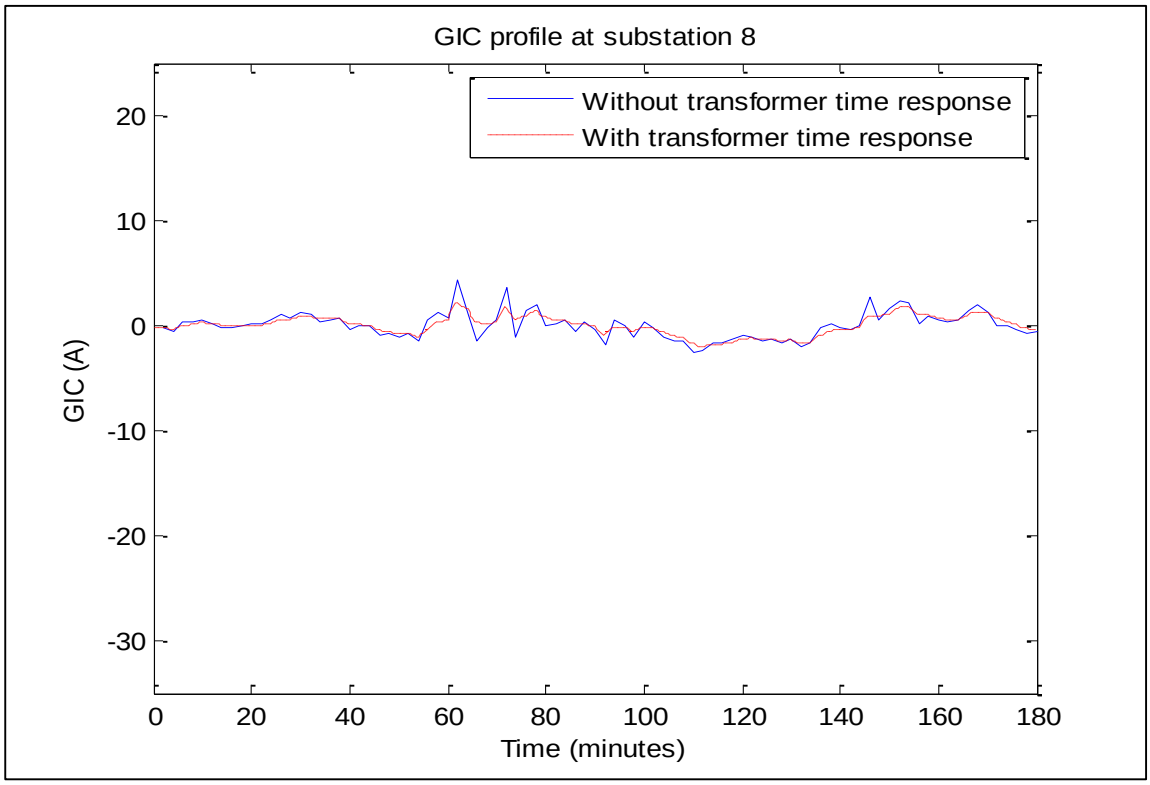

Figure E.5 Substation 8: Comparison between prospective GIC values with and without transformer time response

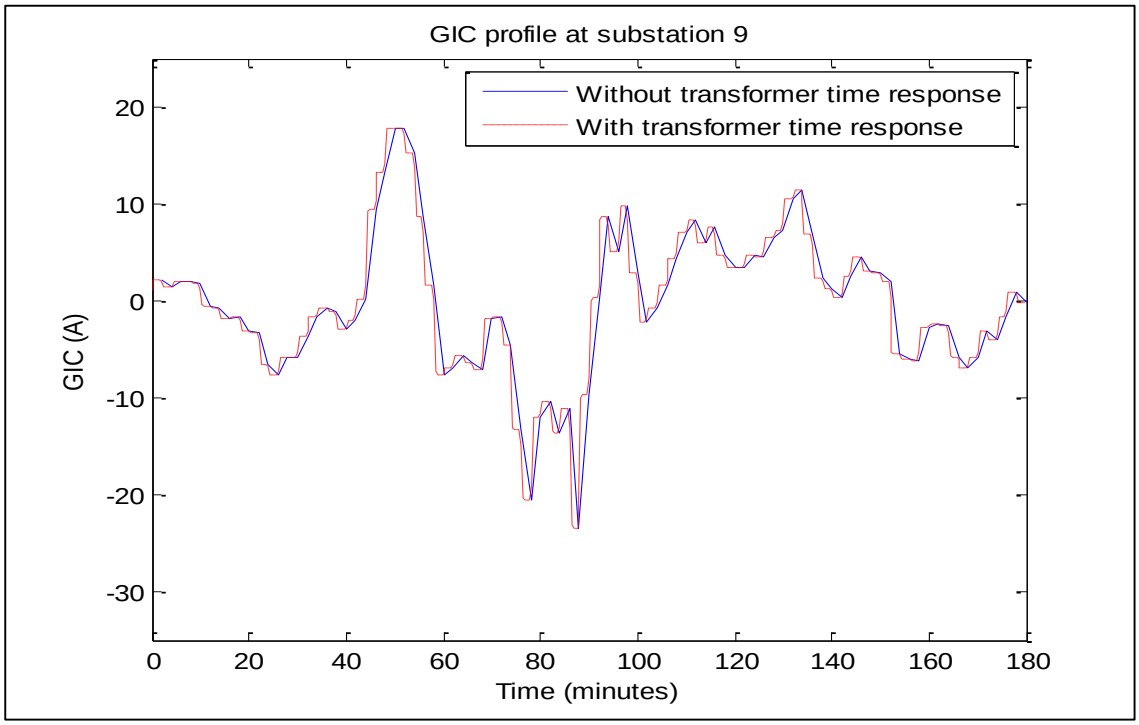

Figure E.6 Substation 9 Comparison between prospective GIC values with and without transformer time response

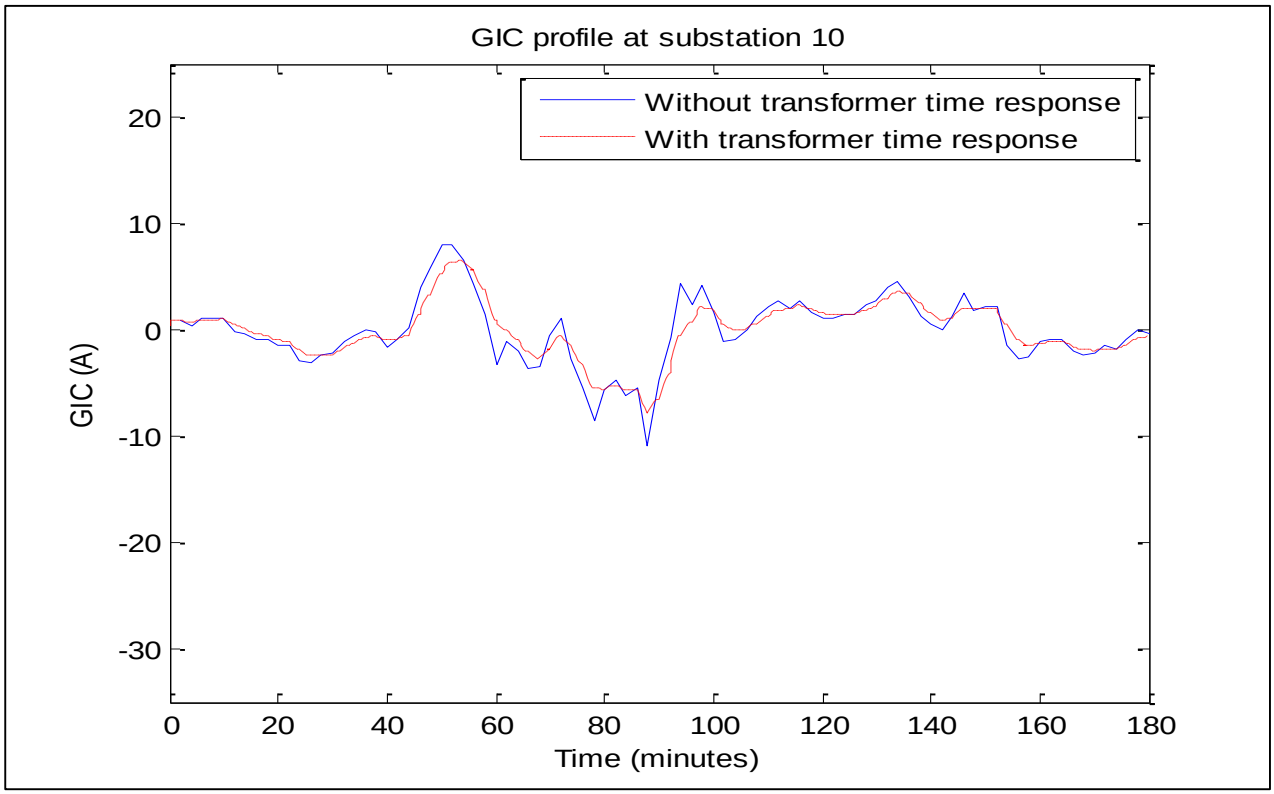

Figure E.7 Substation 10: Comparison between prospective GIC values with and without transformer time response

APPENDIX F: substation GIC profiles in case 3

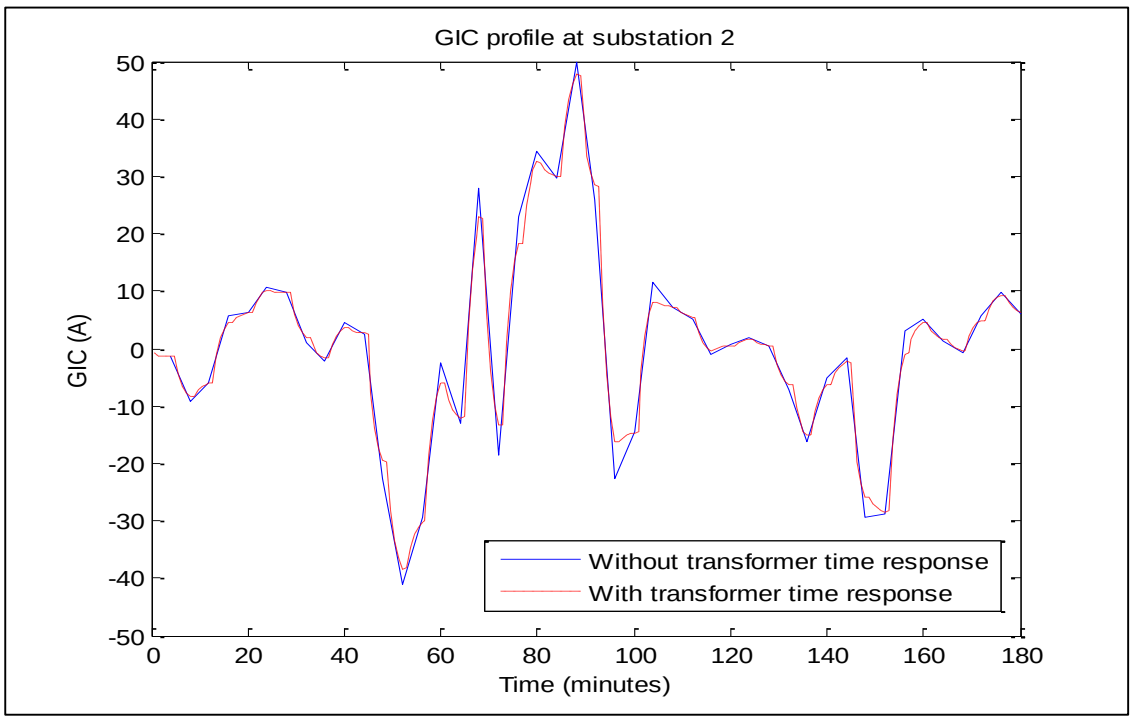

Figure F.1 Substation 2: Comparison between prospective GIC values with and without transformer time response

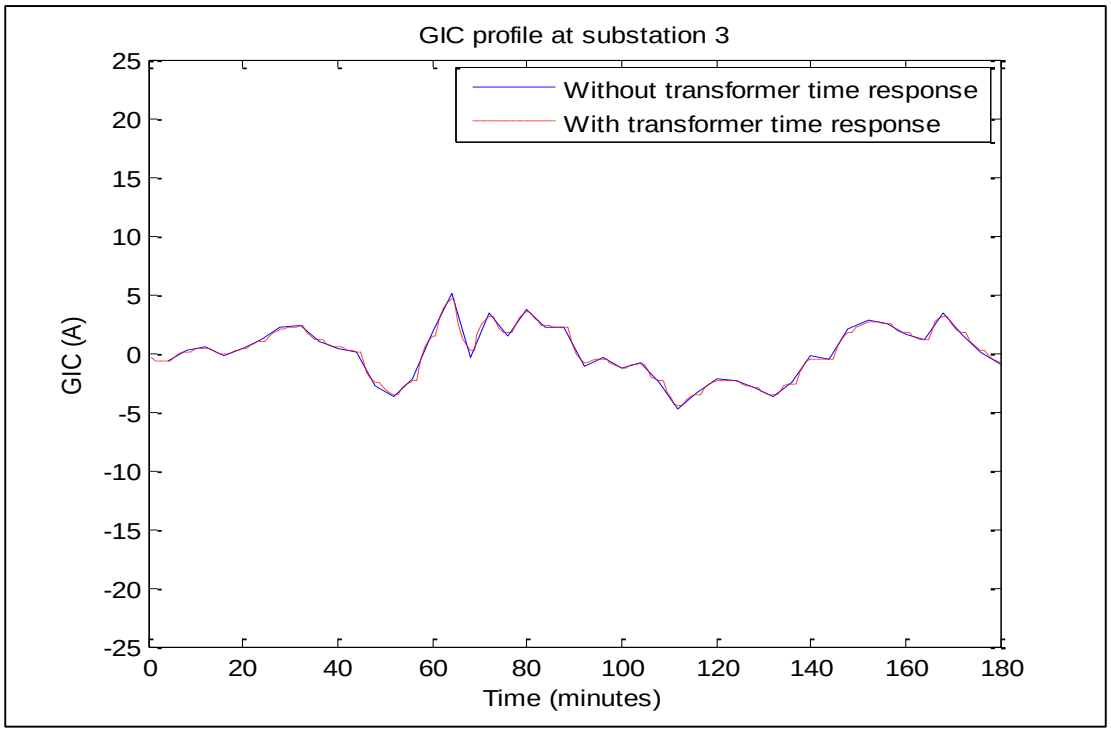

Figure F.2 Substation 3: Comparison between prospective GIC values with and without transformer time response

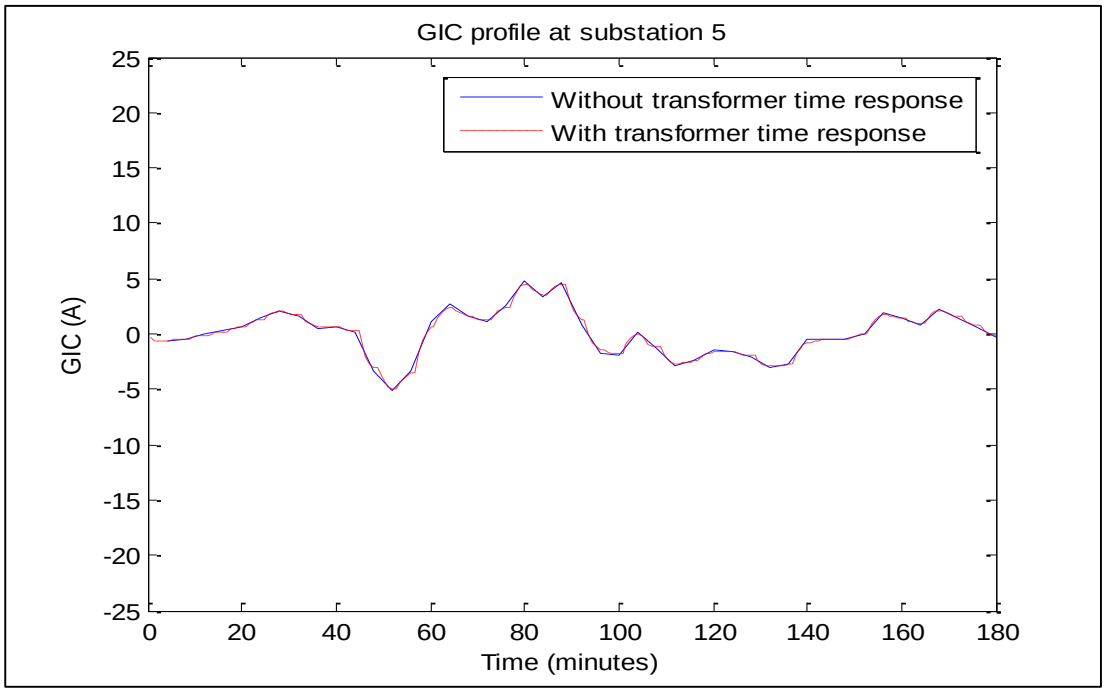

Figure F.3 Substation 5 Comparison between prospective GIC values with and without transformer time response

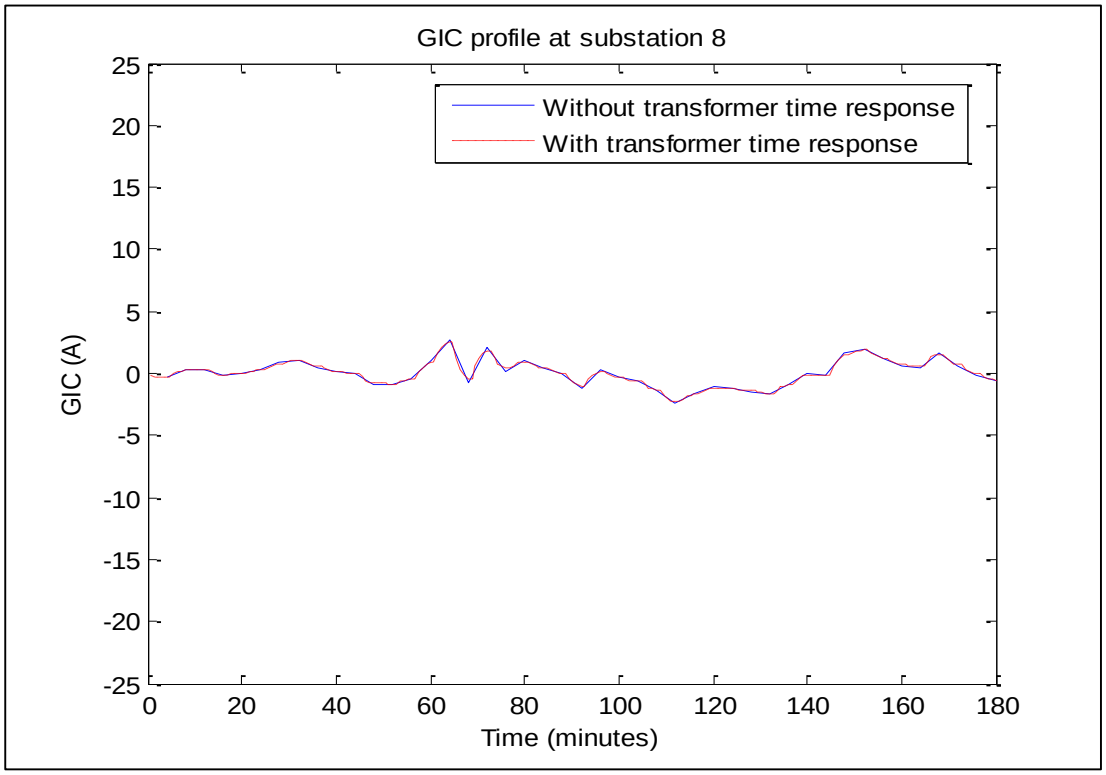

Figure F.4 Substation 8: Comparison between prospective GIC values with and without transformer time response

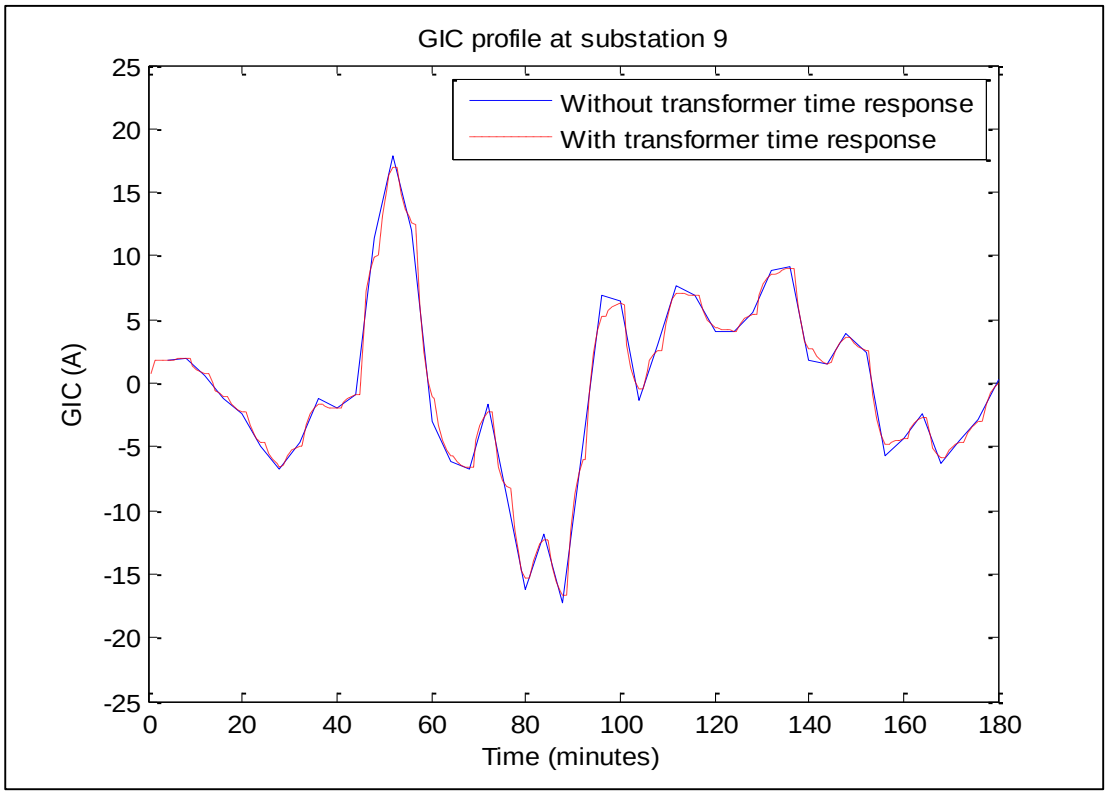

Figure F.5 Substation 9: Comparison between prospective GIC values with and without transformer time response

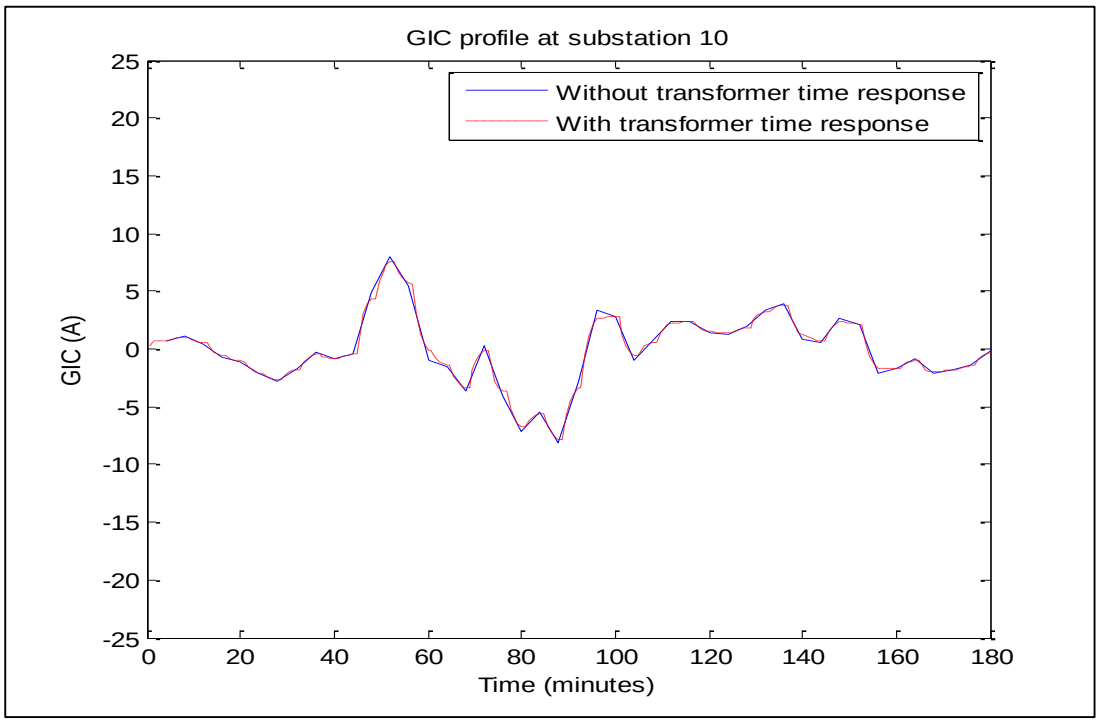

Figure F.6 Substation 10: Comparison between prospective GIC values with and without transformer time response

APPENDIX G: substation GIC profiles in case 4

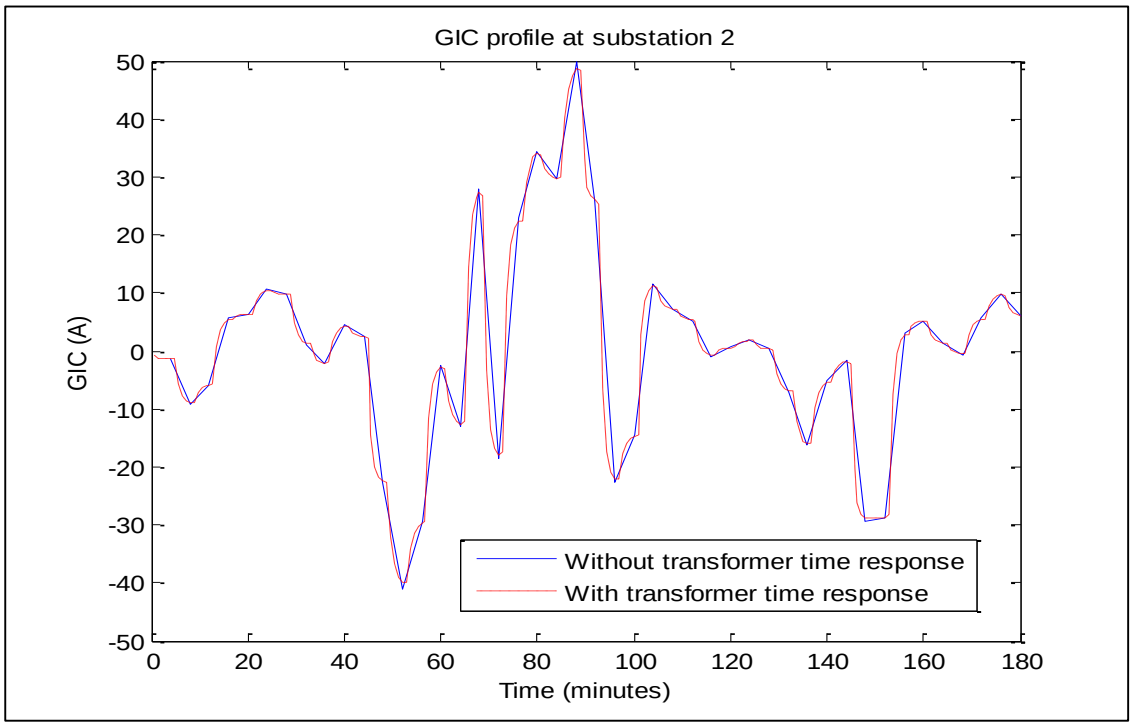

Figure G.1 Substation 2: Comparison between prospective GIC values with and without transformer time response

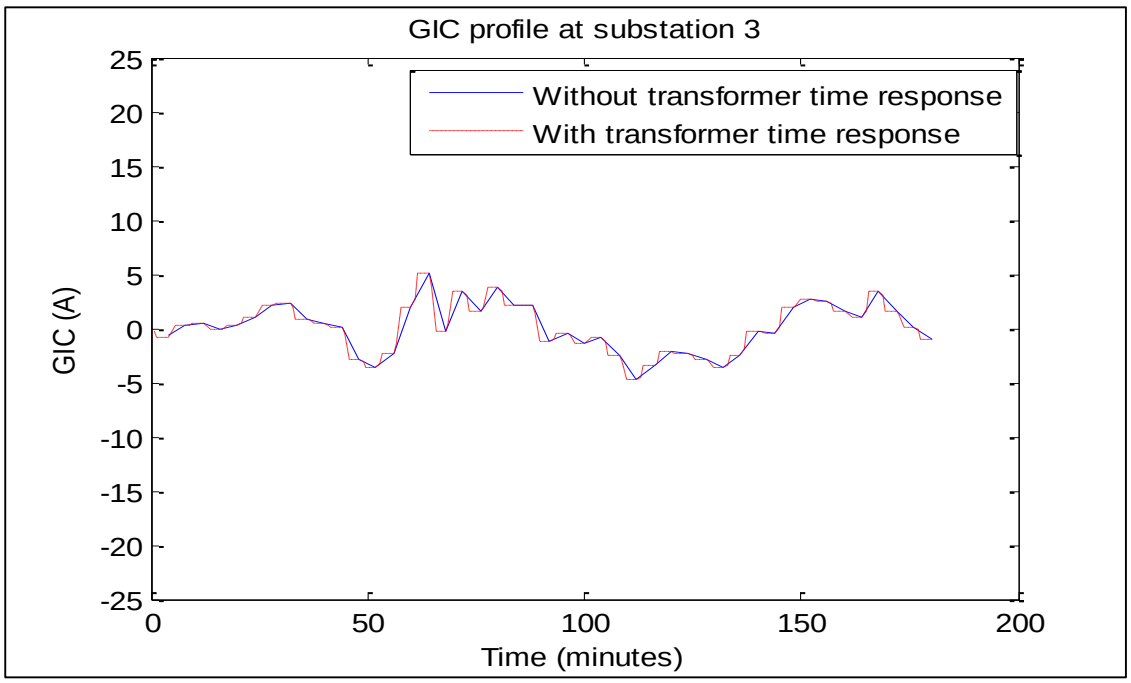

Figure G.2 Substation 3: Comparison between prospective GIC values with and without transformer time response

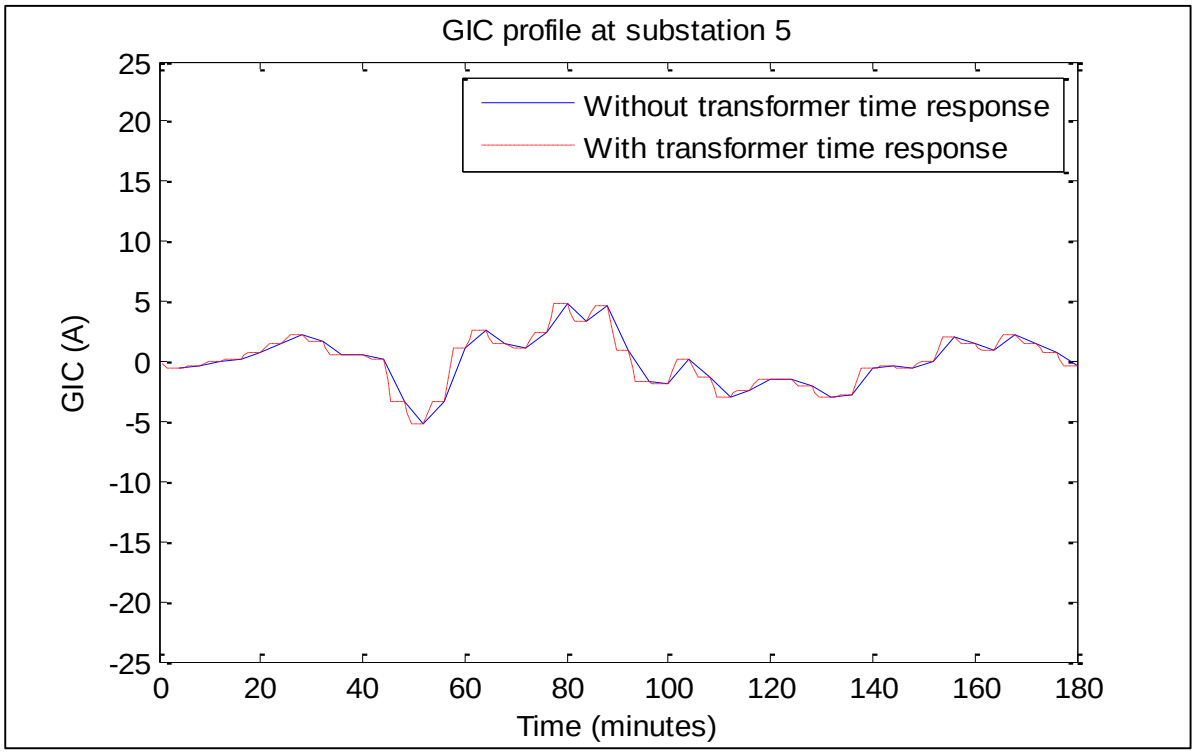

Figure G.3 Substation 5: Comparison between prospective GIC values with and without transformer time response

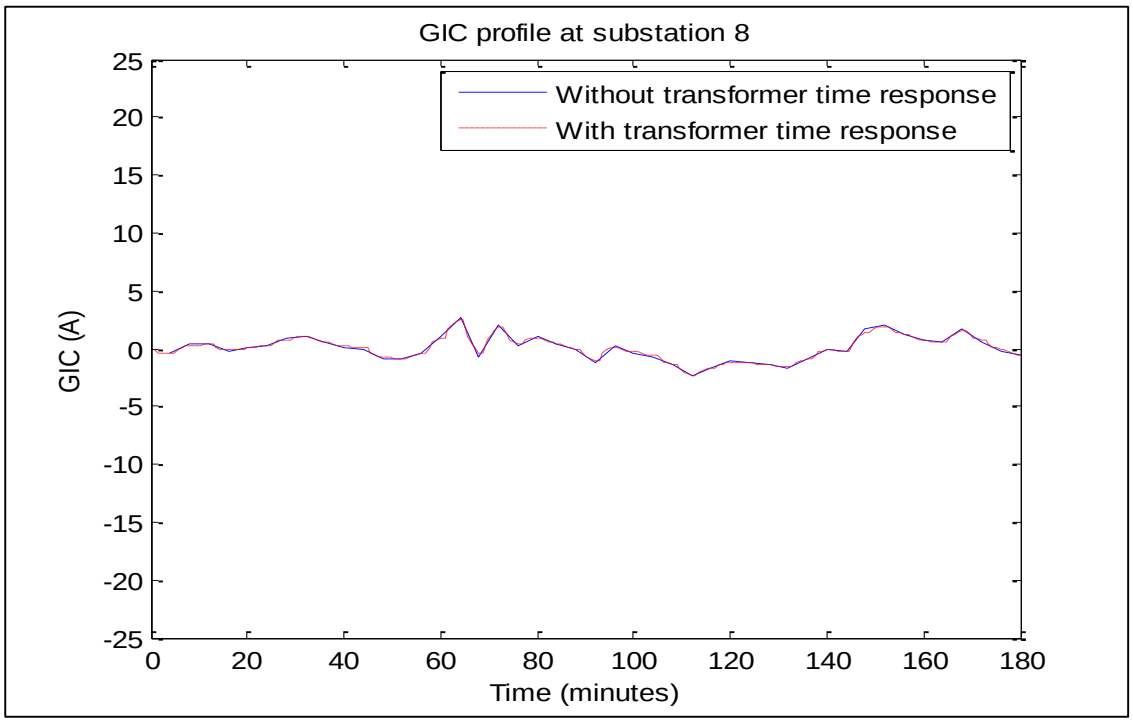

Figure G.4 Substation 8: Comparison between prospective GIC values with and without transformer time response

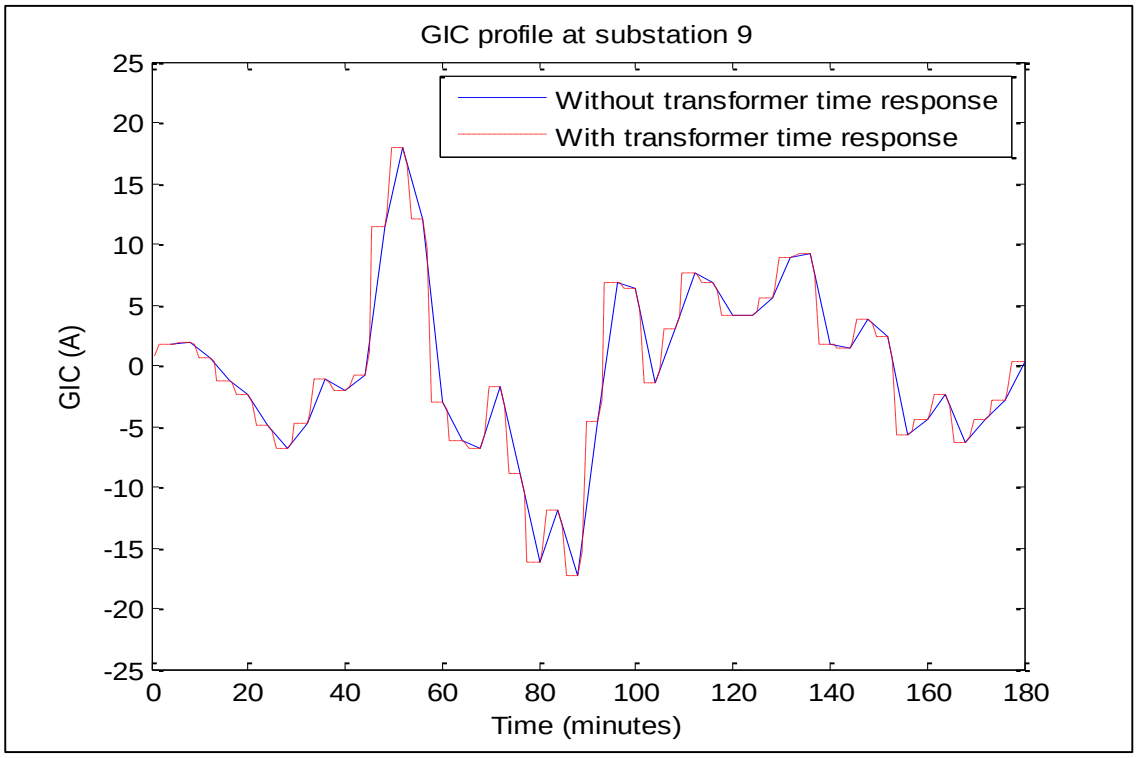

Figure G.5 Substation 9: Comparison between prospective GIC values with and without transformer time response

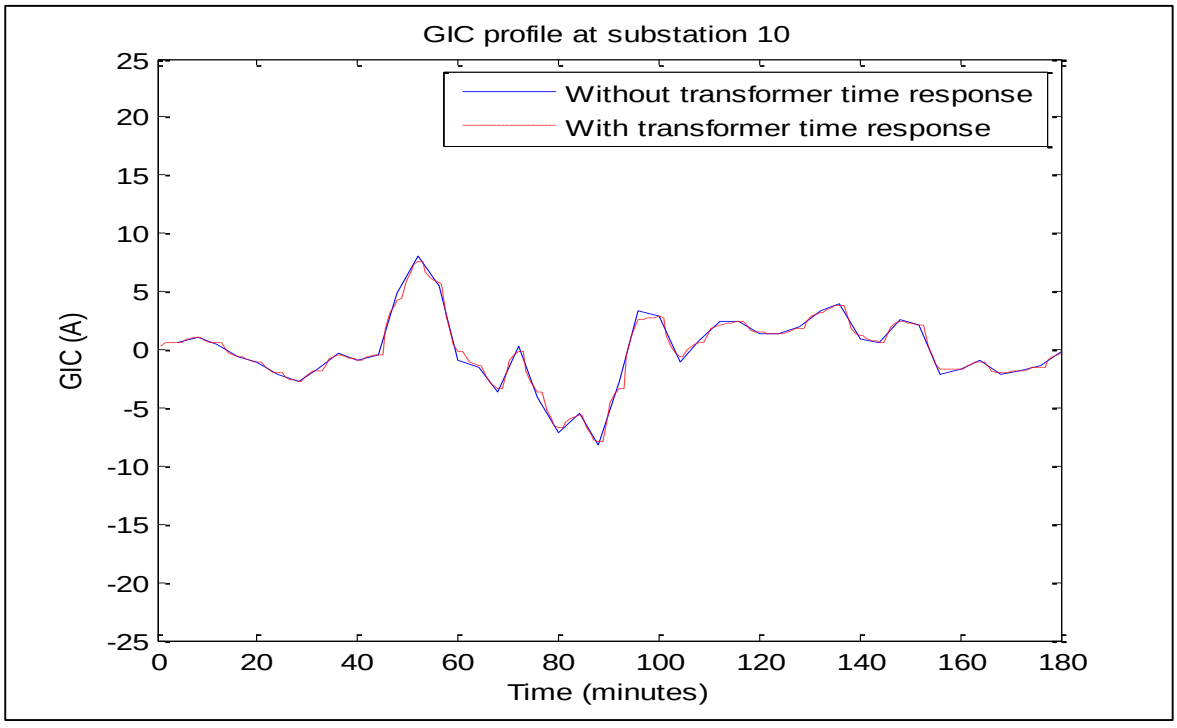

Figure G.6 Substation 10: Comparison between prospective GIC values with and without transformer time response

APPENDIX H: GIC values in chapter 7.2

Table H. 1 Prospective GIC with transformer time response values in the substations across the network in section 7.2

	Substation number									
Sample points	**1**	**2**	**3**	**4**	**5**	**6**	**7**	**8**	**9**	**10**
1	-0.76	-3.82	-0.60	-0.49	-0.66	1.03	2.43	-0.21	2.15	0.91
2	-0.78	-1.71	-0.72	-0.67	-0.61	0.62	1.64	-0.31	1.83	0.71
3	-0.55	-4.65	-0.34	-0.22	-0.53	1.12	2.49	-0.06	1.88	0.86
4	-0.39	-6.78	-0.06	0.11	-0.48	1.49	3.11	0.12	1.92	0.97
5	-0.22	-8.43	0.20	0.40	-0.41	1.76	3.53	0.29	1.86	1.02
6	0.01	-5.30	0.27	0.40	-0.15	1.06	2.04	0.25	0.88	0.54
7	0.01	-1.47	0.09	0.12	-0.03	0.29	0.55	0.08	0.22	0.14
8	0.10	2.46	-0.02	-0.08	0.14	-0.53	-1.08	-0.06	-0.62	-0.32
9	0.21	3.88	0.03	-0.07	0.27	-0.85	-1.77	-0.07	-1.08	-0.55
10	0.53	5.17	0.29	0.15	0.53	-1.22	-2.66	0.02	-1.92	-0.89
11	0.73	6.25	0.44	0.28	0.71	-1.51	-3.34	0.08	-2.51	-1.15
12	1.33	9.25	0.91	0.67	1.23	-2.32	-5.24	0.24	-4.20	-1.86
13	2.04	9.66	1.63	1.37	1.75	-2.65	-6.30	0.58	-5.68	-2.39
14	2.09	9.48	1.69	1.44	1.78	-2.63	-6.30	0.61	-5.75	-2.41
15	2.33	6.83	2.08	1.89	1.87	-2.19	-5.58	0.86	-5.79	-2.30
16	2.15	3.43	2.06	1.95	1.64	-1.44	-4.04	0.93	-4.85	-1.83
17	1.60	1.95	1.57	1.50	1.21	-0.96	-2.78	0.72	-3.52	-1.30
18	1.23	-0.68	1.31	1.31	0.86	-0.30	-1.29	0.65	-2.32	-0.77
19	1.09	-2.05	1.24	1.28	0.72	0.02	-0.59	0.65	-1.83	-0.54
20	0.79	4.17	0.61	0.50	0.69	-1.11	-2.61	0.21	-2.28	-0.97
21	0.67	4.73	0.46	0.34	0.62	-1.18	-2.68	0.12	-2.14	-0.95
22	0.35	2.55	0.23	0.17	0.33	-0.63	-1.43	0.06	-1.13	-0.50
23	-1.23	-5.18	-1.01	-0.87	-1.04	1.50	3.61	-0.37	3.35	1.39
24	-2.46	-15.14	-1.78	-1.38	-2.22	3.95	8.96	-0.52	7.50	3.28
25	-3.81	-25.15	-2.67	-2.01	-3.49	6.44	14.49	-0.73	11.89	5.24
26	-4.46	-32.55	-2.98	-2.13	-4.17	8.12	18.17	-0.72	14.39	6.43
27	-4.86	-30.24	-3.52	-2.73	-4.39	7.78	17.80	-1.04	14.79	6.46
28	-3.53	-30.74	-2.12	-1.33	-3.44	7.40	16.31	-0.34	12.22	5.60
29	-1.71	-25.83	-0.47	0.18	-1.99	5.77	12.11	0.35	7.76	3.84
30	0.13	-9.62	0.59	0.82	-0.18	1.77	3.62	0.49	1.40	0.85
31	2.56	-17.59	3.55	3.94	1.32	2.58	3.64	2.12	-2.08	0.04
32	2.56	-9.09	3.10	3.29	1.57	0.86	0.27	1.71	-3.55	-0.84
33	1.63	8.36	1.24	1.00	1.44	-2.39	-5.40	0.40	-4.76	-2.06
34	1.66	14.19	0.99	0.61	1.62	-3.50	-7.64	0.15	-5.75	-2.64
35	1.38	7.78	1.03	0.82	1.23	-2.09	-4.78	0.32	-4.09	-1.77

36	2.43	-10.17	3.06	3.29	1.42	1.26	0.95	1.73	-3.03	-0.57
37	1.47	4.21	1.30	1.18	1.18	-1.40	-3.61	0.54	-3.66	-1.46
38	2.93	11.11	2.48	2.18	2.44	-3.28	-8.06	0.96	-7.73	-3.17
39	4.78	21.00	3.90	3.33	4.06	-5.94	-14.14	1.43	-13.00	-5.47
40	4.11	26.39	2.93	2.24	3.73	-6.75	-15.37	0.83	-12.59	-5.55
41	3.62	26.43	2.42	1.73	3.38	-6.57	-14.76	0.59	-11.63	-5.21
42	3.80	29.05	2.48	1.73	3.58	-7.15	-16.00	0.56	-12.44	-5.60
43	3.24	32.27	1.74	0.92	3.28	-7.60	-16.54	0.12	-11.89	-5.56
44	4.60	45.69	2.50	1.35	4.63	-10.64	-23.08	0.21	-16.75	-7.81
45	3.56	39.79	1.71	0.71	3.72	-9.14	-19.64	-0.05	-13.74	-6.51
46	1.28	31.59	-0.24	-1.02	1.85	-6.69	-13.74	-0.82	-7.94	-4.10
47	0.01	6.11	-0.24	-0.36	0.16	-1.02	-2.39	-0.23	-1.08	-0.53
48	-0.54	-2.44	-0.40	-0.32	-0.48	0.83	1.68	-0.12	1.51	0.70
49	-1.84	-8.00	-1.49	-1.27	-1.57	2.34	5.45	-0.54	5.03	2.13
50	-1.22	-10.22	-0.74	-0.47	-1.18	2.52	5.50	-0.12	4.15	1.91
51	-0.58	-2.25	-0.48	-0.42	-0.48	0.65	1.55	-0.19	1.50	0.63
52	-0.69	4.52	-0.94	-1.04	-0.36	-0.66	-0.90	-0.56	0.59	0.00
53	-1.12	7.18	-1.53	-1.69	-0.59	-1.04	-1.37	-0.91	1.01	0.03
54	-1.70	5.60	-2.05	-2.16	-1.05	-0.52	-0.02	-1.12	2.42	0.58
55	-2.74	6.35	-3.17	-3.30	-1.78	-0.30	1.02	-1.69	4.38	1.22
56	-3.45	4.99	-3.84	-3.93	-2.33	0.23	2.44	-1.99	6.03	1.85
57	-3.30	3.12	-3.59	-3.63	-2.28	0.55	2.97	-1.82	6.04	1.94
58	-3.43	0.69	-3.60	-3.58	-2.44	1.08	4.07	-1.77	6.71	2.28
59	-3.04	0.91	-3.20	-3.19	-2.15	0.89	3.49	-1.58	5.89	1.99
60	-2.47	0.54	-2.60	-2.59	-1.76	0.77	2.92	-1.28	4.83	1.64
61	-2.23	0.97	-2.37	-2.37	-1.57	0.60	2.45	-1.18	4.27	1.43
62	-2.35	1.44	-2.52	-2.53	-1.64	0.55	2.42	-1.26	4.44	1.46
63	-2.38	1.45	-2.55	-2.56	-1.66	0.55	2.45	-1.28	4.49	1.48
64	-2.74	0.49	-2.87	-2.86	-1.95	0.87	3.28	-1.41	5.37	1.83
65	-2.90	-2.47	-2.89	-2.80	-2.15	1.52	4.62	-1.35	6.18	2.24
66	-3.64	-4.67	-3.55	-3.40	-2.75	2.22	6.40	-1.63	8.03	2.98
67	-3.99	-9.04	-3.69	-3.43	-3.13	3.22	8.53	-1.60	9.46	3.67
68	-3.12	-12.68	-2.61	-2.26	-2.62	3.64	8.84	-0.99	8.35	3.45
69	-1.98	-11.03	-1.50	-1.21	-1.75	2.90	6.76	-0.48	5.80	2.49
70	-1.38	-6.99	-1.08	-0.89	-1.20	1.88	4.44	-0.37	3.92	1.67
71	-0.97	-2.70	-0.87	-0.80	-0.78	0.88	2.27	-0.37	2.39	0.94
72	-0.87	-4.38	-0.68	-0.57	-0.75	1.18	2.79	-0.24	2.47	1.05
73	0.04	-20.01	1.08	1.58	-0.58	4.08	7.86	0.99	3.38	2.09
74	-0.07	-18.23	0.86	1.32	-0.60	3.72	7.23	0.84	3.27	1.96
75	0.28	-21.39	1.38	1.90	-0.44	4.21	7.96	1.16	3.08	2.03
76	0.88	-25.77	2.22	2.84	-0.14	4.85	8.87	1.66	2.62	2.07
77	1.98	-18.80	3.01	3.45	0.86	3.07	4.77	1.89	-0.75	0.59
78	1.87	-4.89	2.17	2.26	1.21	0.23	-0.54	1.16	-2.97	-0.82

79	2.08	0.62	2.12	2.08	1.52	-0.91	-2.91	1.02	-4.29	-1.52
80	1.69	1.30	1.68	1.63	1.25	-0.89	-2.66	0.79	-3.60	-1.30
81	1.41	1.60	1.38	1.32	1.06	-0.83	-2.41	0.63	-3.08	-1.14
82	1.32	1.18	1.31	1.27	0.99	-0.71	-2.13	0.61	-2.84	-1.03
83	1.96	0.90	1.99	1.95	1.44	-0.88	-2.83	0.95	-4.06	-1.44
84	2.66	-0.20	2.77	2.75	1.90	-0.90	-3.29	1.36	-5.25	-1.80
85	2.72	0.69	2.79	2.74	1.97	-1.10	-3.71	1.34	-5.52	-1.93
86	1.90	4.33	1.75	1.63	1.49	-1.54	-4.07	0.76	-4.51	-1.75
87	1.52	7.33	1.21	1.02	1.31	-2.00	-4.75	0.43	-4.26	-1.80
88	0.94	7.71	0.59	0.39	0.90	-1.87	-4.17	0.11	-3.18	-1.44
89	0.14	7.03	-0.21	-0.38	0.31	-1.45	-2.89	-0.26	-1.46	-0.82
90	-0.08	6.57	-0.42	-0.58	0.14	-1.28	-2.43	-0.35	-0.94	-0.62

APPENDIX I: Matlab code for calculating the prospective GIC with transformer time response

Matlab code for calculating GIC incorporating transformer response equations

```
%% GIC Calculation with transformer time response
 % Written by David Oyedokun, University of Cape Town. South Africa
 % email: davoyedokun@ieee.org
 %PhD Thesis
 %Version date: 30th December, 2013
%%


clc
clear

close all

load node_admit_Bank.txt

load store.txt

%% calcs the Emag and the component of Emag on the line

load Major1.txt
load E_d.txt

Major1;
E_d;

f=size(E_d);
fx=f(1);
fy=f(2);

g=size(Major1);
gx=g(1);
gy=g(2);

 E_store =[];
 E_ang_store =[];
 th3_store=[];

 EL_all=zeros(gx,fx);
 EL_all_test=zeros(gx,fx);  % TEST LINE
for j=1:fx;

    Emag= sqrt((E_d(j,1))^2+(E_d(j,2))^2);

    Eang= atan2( E_d(j,2), E_d(j,1))* 180/pi;
    th1=Eang ; % angle of the resultant e field
    th1=Eang + 180;  % angle of the resultant e field
```

```
    E_store= [E_store Emag];
    E_ang_store= [E_ang_store th1];

P1=[];
th3_store=[];
th2_store=[];

% getting the angle the line
for i=1:gx;

     th2=azimuth('rh',[Major1(i,5),Major1(i,6)],[Major1(i,7),Major1(i,8)]);

    th2_store= [th2_store th2];

    th3=abs(th2-th1);
%
     EL1_test= (Emag*cosd(th3)* Major1(i,9));
     EL_all_test(i,j)= EL1_test;

     th3_store= [th3_store th3];


end

j;
end
EL_all;

w=size(EL_all_test);
wy=w(2);

for p=1:wy;
    EL_I(:,p)= store(:,3).*EL_all_test(:,p);
end
 EL_I;


v=size(EL_I);
vy=v(2);

for j=1:3;

    admit_Bank (:,j) = store(:,j);

end
    for i=4:(vy+3)
         admit_Bank (:,i)= EL_I(:,(i-3));

    end
     admit_Bank;


%% creating the dto matix
```

```
disp(['In the matrix below:'] )
disp([' '] )
disp(['Col 1 is the  line "From Bus"'] )
disp(['Col 2 is line "To" Bus'] )
disp(['Col 3 is the line Admitance'] )
disp(['Col 4 is the line  Equivalent curr source'] )

admit_Bank;  % displays the admittance bank
 mad=size(admit_Bank);
 rowAdmit=mad(1);  % row size

nodes = input('Enter number of substations: ');

dto=zeros (nodes,nodes+1);
dto;


for i=1:rowAdmit

  if dto(admit_Bank(i,1),admit_Bank(i,2)+1)~=0



dto(admit_Bank(i,1),admit_Bank(i,2)+1)=dto(admit_Bank(i,1),admit_Bank(i,2)+
1)+ admit_Bank(i,3);
      dto(admit_Bank(i,2)+1-1,admit_Bank(i,1)+1)=  dto(admit_Bank(i,2)+1-
1,admit_Bank(i,1)+1) +admit_Bank(i,3);



  else

      dto(admit_Bank(i,1),admit_Bank(i,2)+1)= admit_Bank(i,3);
      dto(admit_Bank(i,2)+1-1,admit_Bank(i,1)+1)= admit_Bank(i,3);




  end

end
  dto(:,1)=node_admit_Bank(:,1);
  dto;

%% Calculating the Y bus

 m=size(dto);
 r=m(1);  % row size
 c= m(2);  % column size
 disp([' The Network has: ',num2str(r), ' nodes'] )

 newC= c-1;
```

```
 Yb=[]; % initialise the Y Bus matix
 for i=1:r;
     for j=1:newC  % use variable r for newC
         if i==j    % for the diagonal elements
             Yb(i,j)= sum(dto(i,:));

         else
             Yb(i,j)=-1. *dto(i,j+1);


         end

     end

 end
     %Yb(j,i)= Yb(i,j);
% end
 disp(' The Y bus matrix is: ')
  Yb ; %printing the Y bus

 ds=size(Yb);
 ds_r=ds(1);  % row size
 ds_c= ds(2);  % column size
 disp([' The Network has: ',num2str(ds_r), ' nodes'] );


  %% Creating the tope matrix

 m1=size(admit_Bank);
 r1=m1(1);  % row size
 c2= m1(2);  % column size
 %c3=c2-3;


 Vt=[];
 Ncurr=[];
 D_sum=[];

for runds=4:c2 %


tope=zeros (nodes,nodes);

for i=1:rowAdmit

  if tope(admit_Bank(i,1),admit_Bank(i,2))~=0


tope(admit_Bank(i,1),admit_Bank(i,2))=tope(admit_Bank(i,1),admit_Bank(i,2))
+ admit_Bank(i,runds);
      tope(admit_Bank(i,2),admit_Bank(i,1))=-1.*
tope(admit_Bank(i,1),admit_Bank(i,2));
  else
```

```
      tope(admit_Bank(i,1),admit_Bank(i,2))= admit_Bank(i,runds);
      tope(admit_Bank(i,2),admit_Bank(i,1))= -1.* admit_Bank(i,runds);
  end

end

tope;



D=[];
 for z = 1:r
     D(z,1)=sum(tope(z,:));


 end
D ; %

D_sum= [D_sum D];


disp(' The Nodal Voltages are:');

V=Yb\D;




Vt1=V.';

Ncurr1=dto(:,1).* Vt1(1,:)';


Ncurr= [Ncurr Ncurr1];


Vt=[Vt; Vt1];


end



 tc=size(EL_I);
 tcy=tc(2);% to determie the number of colmns
 Ncurr_tc=[];
 Ncurr_tc_p=[];
 shifft=0; % this creates the block of intervals ..


 intaval = input('Enter number of readings u want per interval.i.e., per
value of GIC: ');      %  nodes is the number of substations
```

```
 tm_in =  input('Enter the time interval at which the current will be
calculated e.g. every  5 seconds: ');


 jk=0;
 jl=0;
 jj=0;
 jjj=0;
 jp=0;

 for rx=1:nodes
       shifft=0;   % reset the block to zero
       tx=0.75;
       jj=jj+1;

 for le=1:tcy % loop for the number of sets
        jjj=jjj+1;
         tx=0.75;  % initialize the starting point
         tm=tm_in;  % the time interval at which

         if le > 1;


              DeltaI= Ncurr(rx,le)- interim1;


              GIC_pu= DeltaI/node_admit_Bank(rx,2);
              Core_type = node_admit_Bank(rx,3);
              z=GIC_pu;

              if Core_type==1

                 t_tau = -(0.0424*(z^4)) + (0.8971*(z^3)) - (6.2874*(z^2))
+ (16.455*(z)) + 5.2466;

                 t_tau2=(t_tau)/5;
              end

              if Core_type==2
                 t_tau = (0.0116*(z^4)) - (0.2189*(z^3)) + (1.2749*(z^2)) -
(2.4127*(z)) + 28.85;

                 t_tau2=(t_tau)/5   ;
              end


              if Core_type==3
                 t_tau =(0.116*z) + (0.0887);

                 t_tau2=(t_tau)/5;
              end


              if Core_type==4
```

```
                t_tau = -(0.0408*(z^4)) + (0.8626*(z^3)) - (6.0399*(z^2))
+ (15.778*(z)) + 5.9075;

                t_tau2=(t_tau)/5;
            end

            if Core_type==5
                t_tau = (0.0364*(z^3)) - (0.7728*(z^2)) + (5.2331*(z)) +
13.896;

                t_tau2=(t_tau)/5;
            end


            if Core_type==6
                z;
                t_tau= (0.1537*(z)) - 0.0402;


                t_tau2=(t_tau)/5;
            end


            if Core_type==7
                t_tau = (-0.0424*(z^4)) + (0.8971*(z^3)) - (6.2874*(z^2))
+ (16.455*(z)) + 5.2466;

                t_tau2=(t_tau)/5;
            end

            if Core_type==8
                t_tau = (0.0463*(z^3)) - (0.9218*(z^2)) + (5.738*(z)) +
16.561;

                t_tau2=(t_tau)/5;
            end


            if Core_type==9
                t_tau = (0.1547*(z)) + 0.0306;

                t_tau2=(t_tau)/5;

            end

           %t_tau2=(t_tau)/5;

          for px=1:intaval

              intrm2 = interim1  +  (DeltaI *(1-exp(-(tx/(t_tau2)))  ));
                jl=jl+1;
               Ncurr_tc(rx,(px+shifft)) = intrm2;
              % pause
             tx = tx+tm;
          end
```

```
            interim1=intrm2;

         else


            jp=jp+1;

            for px=1:intaval
                interim1 = (Ncurr(rx,le)*(1-exp(-(tx/1.2))  ))
                jk=jk+1;
                Ncurr_tc(rx,(px+shifft)) =  interim1

                tx = tx+tm;
            end

         end



    Ncurr_tc_p1(rx,le)= Ncurr_tc(rx,(px+shifft));


     shifft=shifft+intaval;
 end

 end
  Ncurr_tc;
 %%

disp(' The Nodal currents are:');
Ncurr;

dav=Ncurr';
disp(' The Nodal Voltages are:');
Vt;
```

APPENDIX J: Eskom 400 kV substations

APPENDIX K: Eskom 400 kV transmission line data

APPENDIX L: Eskom 400 kV substation admittance data

APPENDIX M: Sample calculations in case 2

Sample calculations for substation 7 and substation 4 in case 2.

Sample calculation for prospective GIC with transformer time response at substation 7:

For substation 7 at the fringes of the network which has 2 units of 500 MVA 3(1P-3L) GSUs, the response time profile for each transformer was obtained from Table 6.2. The relevant equation in Table 6.2 is equation M.1 and given below:

$$t_r = \begin{cases} 16.34 \quad if \quad 0 < z < 2 \\ 18.49 \quad if \quad 2 \leq z < 6 \\ 14.75 \quad if \quad 6 \leq z < 8 \\ 20.79 \quad if \; 8 \leq z \leq 10 \\ 13.66 \quad if \; 10 \leq z \leq 14 \end{cases} \tag{M.1}$$

where z is the GIC in per unit of the transformer magnetization current and t_r is the transformer response time in seconds. The magnetization current for the transformer from simulation in PSCAD is 1.65 A (from Table 6.1). The prospective GIC through each transformer in substation 7, from the *i* matrix in section 7.1 is:

$$\frac{\text{substation prospective GIC}}{No\ of\ transformers} = \frac{2.43\ \text{A}}{2} = 1.22\ A$$

Therefore,

$$z = \frac{i}{i_{mag}} = \frac{1.22\ A}{1.65\ A} = 0.74$$

Taking *z* as 0.74 in equation 7.6, t_r is 16.84 seconds.

To initialize the calculation in equation 7.6, we set $I_{gic\_a(t-1)}$ = 0.

The prospective GIC with transformer time response flowing through substation 7 is calculated using equation M.2.

$$I_{gic\_a(t)} = I_{gic\_a(t-1)} + \left[I_{gic\_p(t)} - I_{gic\_a(t-1)} \right] (1 - e^{\frac{-t_x}{T}}) \tag{M.2}$$

$T = \frac{t_r}{5}$ = 3.37 seconds

From Table 7.3 in section 7.1, the first prospective GIC in substation 7 is $I_{gp(1)}$ = 2.43 A. Hence,

$I_{gic\_a(1)} = 0 + [2.43 - 0](1 - e^{-\frac{1}{3.37}}) = 0.63$ A. This value is 55.98 % higher than the value in case 1 where substation 7 has a 3P-5L transmission transformer. Nevertheless, $I_{gic\_a(1)}$ < is $I_{gp(1)}$ because $I_{gic\_a(1)}$ is calculated at one second.

At t_x = two seconds,

From Table 7.3 in section 7.1, the second prospective GIC in substation 7 is $I_{gp(2)}$ = 0.55 A. Hence,

$$I_{gic\_a(2)} = I_{gic\_a(1)} + \left[I_{gp(2)} - I_{gic\_a(1)} \right] * (1 - e^{\frac{-2}{3.37}})$$

$= 0.40 + [0.55 - 0.63] * (0.47) \quad = 0.36\ A$. This value is 17.23 % lower than the value in case 1 where substation 7 has a 3P-5L transmission transformer. This reason for this is based the difference factor between $I_{gp(2)}$ and $I_{gic\_a(1)}$.

This calculation continues until the nth prospective GIC value is reached. From the calculation of the prospective GIC with and without transformer time response in substation 7 at 2 seconds, it can be seen that the transformer response time to GIC suppresses the prospective GIC, such that the difference between the prospective GIC with and without transformer time response is 34.54 %.

Sample calculation for bus 4:

For substation 4 within the network with a high number of interconnections has two units of 500 MVA 3P-3L transmission transformers, the response time profile for each transformer is obtained from Table 6.2. The relevant equation in Table 6.2 is equation M.3 as shown below:

$$t_r = \begin{cases} 0.23 & if \;\; 0 < z < 4 \\ 0.58 & if \;\; 4 \leq z < 6 \\ 0.92 & if \;\; 6 \leq z < 10 \\ 1.25 & if \;\; 10 \leq z \leq 14 \end{cases} \qquad \text{(M.3)}$$

The magnetization current for the transformer from simulation in PSCAD is 2.50 A. The prospective GIC through each transformer in substation 4 from Table 7.3 in section 7.1 is:

$$\frac{\text{substation prospective GIC}}{No\ of\ transformers} = \frac{-0.49\ \text{A}}{2} = -0.25\ A$$

Therefore,

$$z = \frac{i}{i_{mag}} = \frac{-0.25\ A}{2.50\ A} = -0.10.$$

The absolute value z is 0.10 which is 16.67 % lower than the absolute value of z in the corresponding calculation in case 1. This reflects the difference in time responses to GIC between different transformer types.

Taking the absolute value of z as 0.10 in equation 7.7, t_r is 0.23 seconds. This value was 27.77 seconds in the corresponding calculation in case 1.

To initialize the calculation in equation 7.6, we set $I_{gic\_a(t-1)}$ = 0.

The prospective GIC with transformer time response flowing through substation 4 is calculated using equation M.4.

$$I_{gic\_a(t)} = I_{gic\_a(t-1)} + \left[I_{gic\_p(t)} - I_{gic\_a(t-1)} \right] (1 - e^{\frac{-t_x}{T}}) \qquad \text{(M.4)}$$

$T = \frac{t_r}{5}$ = 0.05 seconds

From Table 7.3 in section 7.1, the first prospective GIC $I_{gp(1)}$ in substation 4 is - 0.49 A. Hence,

$I_{gic\_a(1)} = 0 + [(-0.49) - 0](1 - e^{-\frac{1}{0.05}})$ = - 0.49 A.

At t_x = two seconds,

From Table 7.3 in section 7.1, the second prospective GIC $I_{gp(2)}$ in substation 4 is -0.91 A. Hence,

$$I_{gic\_a(2)} = I_{gic\_a(1)} + \left[I_{gp(2)} - I_{gic\_a(1)} \right] * \left(1 - e^{\frac{-2}{0.05}}\right)$$

$$= -0.49 + [-0.91 - (-0.49)] * (0.99) \quad = -0.91\ A.$$

The results show that the prospective GIC values with and without transformer time response are the same. This is primarily because of the relatively shorter response time of the 3P-3L transformer.

Similar to the calculation for bus 7, this calculation continues till the n^{th} prospective GIC value is reached.

APPENDIX N: Sample calculations in case 3

Sample calculations for substation 7 and substation 4 in case 3.

Sample calculation for the prospective GIC with transformer time response at substation 7:

For substation 7 at the fringes of the network which has 2 units of 500 MVA 3P-5L transmission transformers, the response time profile for each transformer was obtained from Table 6.2. The relevant equation in Table 6.2 is equation N.1 given below as:

$$t_r = \begin{cases} 27.77 & if \;\; 0 < z < 6 \\ 28.48 & if \;\; 6 \leq z < 8 \\ 26.18 & if \;\; 8 \leq z < 10 \\ 28.98 & if \; 10 \leq z \leq 14 \end{cases} \qquad \text{(N.1)}$$

where z is the GIC in per unit of the transformer magnetization current and t_r is the transformer response time in seconds. The magnetization current for the transformer from simulation in PSCAD is 2.1 A. The first prospective GIC through each transformer in substation 7 from Table 7.6 in section 7.1 is:

$$\frac{\text{substation prospective GIC}}{No\ of\ transformers} = \frac{1.49\ \text{A}}{2} = 0.75\ A$$

Therefore,

$$z = \frac{i}{i_{mag}} = \frac{0.75\ A}{2.1\ A} = 0.36$$

Using the value of z as 0.36 in equation 7.9, t_r is 27.77 seconds.

The prospective GIC with transformer time response flowing through substation 7 is calculated using equation N.2.

$$I_{gic\_a(t)} = I_{gic\_a(t-1)} + \left[I_{gic\_p(t)} - I_{gic\_a(t-1)} \right] (1 - e^{\frac{-t_x}{T}}) \qquad \text{(N.2)}$$

To initialize the calculation in equation N.2, we set $I_{gic\_a(t-1)}$ = 0.

$T = \frac{t_r}{5}$ = 5.55 seconds

From Table 7.6 in section 7.1, the first prospective GIC in substation 7 is $I_{gp(1)}$ = 1.49 A. Hence,

$I_{gic\_a(1)} = 0 + [1.49 - 0](1 - e^{-\frac{1}{5.55}}) = 0.77$ A. This value is 48.64 % lower than the prospective value because it is calculated at one second.

At *t* = 2 seconds, the second prospective GIC in substation 7 is $I_{gp(2)}$ = 3.80 A. Hence,

$$I_{gic\_a(2)} = I_{gic\_a(1)} + \left[I_{gp(2)} - I_{gic\_a(1)} \right] * (1 - e^{\frac{-2}{5.55}})$$

$$= 0.40 + [3.80 - 0.77] * (0.30) \quad = 1.31\ A.$$

This calculation continues till the n[th] prospective GIC value is reached. From these results, it can be seen that the transformer response time to GIC suppresses the prospective GIC, such that the difference between the prospective GIC with and without transformer time response is 65.55 %.

<u>Sample calculation at substation 4:</u>

For substation 4 which has two units of 500 MVA 3P-5L transmission transformers, the response time profile for each transformer is obtained from Table 6.2. The relevant equation in Table 6.2 is equation N.1. The magnetization current for the transformer from simulation in PSCAD is 2.1 A. The prospective GIC through each transformer in substation 4 from Table 7.6 in section 7.1 is:

$$\frac{\text{substation prospective GIC}}{No\ of\ transformers} = \frac{-0.70\ \text{A}}{2} = -0.35\ A$$

Therefore,

$$z = \frac{i}{i_{mag}} = \frac{-0.35\ A}{2.1\ A} = -0.17.$$

Using the value of z as 0.17 in equation 7.9, t_r is 27.77 seconds.

The prospective GIC with transformer time response flowing through substation 4 is calculated using equation N.3.

$$I_{gic\_a(t)} = I_{gic\_a(t-1)} + \left[I_{gic\_p(t)} - I_{gic\_a(t-1)} \right] (1 - e^{\frac{-t_x}{T}}) \quad \text{(N.3)}$$

To initialize the calculation in equation N.3, we set $I_{gic\_a(t-1)}$ = 0.

$T = \frac{t_r}{5}$ = 5.55 seconds

From Table 7.6 in section 7.3, the first prospective GIC $I_{gp(1)}$ in substation 4 is - 0.70 A. Hence,

$I_{gic\_a(1)} = 0 + [(-0.70) - 0](1 - e^{-\frac{1}{5.55}}) =$ - 0.12 A.

At t_x = two seconds, the second prospective GIC $I_{gp(2)}$ in substation 4 is 0.48 A. Hence,

$$I_{gic\_a(2)} = I_{gic\_a(1)} + \left[I_{gp(2)} - I_{gic\_a(1)} \right] * (1 - e^{\frac{-2}{5.55}})$$

$$= -0.08 + [0.48 - (-0.12)] * (0.30) \quad = 0.10\ A.$$

From the calculation of the prospective GIC with transformer time response at two seconds, it can be seen that the transformer response time to GIC suppresses the prospective GIC, such that the difference between the prospective GIC with and without transformer time response is 79.17 %. In substation 7, this value was 65.55 %. It is expected that the values will vary due to the dynamic characteristics of the transformer time response to GIC.

The profiles for substation 1 and 4 at the middle of the network and substation 6 and 7 at the edge of the network are show in Figure 7.15 to Figure 7.18. The profiles for the other 6 substation are in Appendix F.

APPENDIX O: Sample calculations in case 4

Sample calculations for substation 7 and substation 4 in case 4.

Sample calculation at substation 7:

Substation 7 has 2 units of 500 MVA 3(1P-3L) GSUs. The response time profile for each transformer was obtained from Table 6.2. The relevant equation in Table 6.2 is equation O.1 given below as:

$$t_r = \begin{cases} 16.34 \quad if \quad 0 < z < 2 \\ 18.49 \quad if \quad 2 \leq z < 6 \\ 14.75 \quad if \quad 6 \leq z < 8 \\ 20.79 \quad if \; 8 \leq z \leq 10 \\ 13.66 \quad if \; 10 \leq z \leq 14 \end{cases} \qquad \text{(O.1)}$$

where z is the GIC in per unit of the transformer magnetization current and t_r is the transformer response time in seconds. The magnetization current for the transformer from simulation in PSCAD is 1.65 A. The first prospective GIC through each transformer in substation 7 from table 7.6 in section 7.1 is:

$$\frac{\text{substation prospective GIC}}{No\ of\ transformers} = \frac{1.49\ \text{A}}{2} = 0.75\ A$$

Therefore,

$$z = \frac{i}{i_{mag}} = \frac{0.75\ A}{1.65\ A} = 0.45$$

Using the value of z as 0.45 in equation 7.12, t_r is 16.34 seconds.

The prospective GIC with transformer time response flowing through substation 7 is calculated using equation O.2.

$$I_{gic\_a(t)} = I_{gic\_a(t-1)} + \left[I_{gic\_p(t)} - I_{gic\_a(t-1)} \right] (1 - e^{\frac{-t_x}{T}}) \qquad \text{(O.2)}$$

To initialize the calculation in equation 7.13, we set $I_{gic\_a(t-1)}$ = 0.

$T = \frac{t_r}{5}$ = 3.27 seconds

From Table 7.6 in this section, the first prospective GIC in substation 7 is $I_{gp(1)}$ = 1.49 A. Hence,

$I_{gic\_a(1)} = 0 + [1.49 - 0](1 - e^{-\frac{1}{3.27}}) = 0.39$ A.

This value is 73.65 % lower than the prospective value because it is calculated at one second.

At t_x = two seconds, the second prospective GIC in substation 7 is $I_{gp(2)}$ = 3.80 A. Hence,

$$I_{gic\_a(2)} = I_{gic\_a(1)} + \left[I_{gp(2)} - I_{gic\_a(1)} \right] * (1 - e^{\frac{-2}{3.27}})$$

$$= 0.25 + [3.8 - 0.39] * (0.46) \quad = 1.82\ A.$$

This value is 52.14 % lower than the prospective value because it is calculated at one second which is a measure of the percentage by which the prospective GIC is suppressed by the transformer time response at two seconds. Similar to case 1 and 2, this calculation continues till the nth prospective GIC value is reached.

Sample calculation at substation 4:

Substation 4 has 2 units of 500 MVA 3P-3L transmission transformers, the response time profile for each transformer is obtained from Table 6.2. The relevant equation in Table 6.2 is equation O.3.

$$t_r = \begin{cases} 0.23 & if \ \ 0 < z < 4 \\ 0.58 & if \ \ 4 \leq z < 6 \\ 0.92 & if \ \ 6 \leq z < 10 \\ 1.25 & if \ 10 \leq z \leq 14 \end{cases} \qquad \text{(O.3)}$$

The magnetization current for the transformer from simulation in PSCAD is 2.50 A. The first prospective GIC through each transformer in substation 4 from Table 7.6 in section 7.1 is:

$$\frac{\text{substation prospective GIC}}{No\ of\ transformers} = \frac{-0.70\ \text{A}}{2} = -0.35\ A$$

Therefore,

$$z = \frac{i}{i_{mag}} = \frac{-0.35\ A}{2.5\ A} = -0.14.$$

Taking the absolute value of z as 0.14 in equation 7.5, t_r is 0.23 seconds for substation 4.

The prospective GIC with transformer time response flowing through substation 4 is calculated using equation O.4.

$$I_{gic\_a(t)} = I_{gic\_a(t-1)} + \left[I_{gic\_p(t)} - I_{gic\_a(t-1)} \right] (1 - e^{\frac{-t_x}{T}}) \qquad \text{(O.4)}$$

To initialize the calculation in equation 7.15, we set $I_{gic\_a(t-1)}$ = 0.

$T = \frac{t_r}{5}$ = 0.05 seconds

From Table 7.3 in section 7.1, the first prospective GIC $I_{gp(1)}$ in substation 4 is - 0.70 A. Hence,

$I_{gic\_a(1)} = 0 + [(-0.70) - 0](1 - e^{-\frac{1}{0.05}})$ = - 0.69 A.

At t_x = two seconds, the second prospective GIC $I_{gp(2)}$ in substation 4 is 0.48 A. Hence,

$$I_{gic\_a(2)} = I_{gic\_a(1)} + \left[I_{gp(2)} - I_{gic\_a(1)} \right] * (1 - e^{\frac{-2}{0.05}})$$

$$= -0.12 + [0.48 - (-0.12)] * (1) \quad = 0.48\ A.$$

The results for substation 4 shows that the prospective GIC with and without transformer time response are the same. This is because of the relatively shorter response time of the 3P-3L transformer.

The profiles for substation 1 and 4 at the middle of the network and substation 6 and 7 at the edge of the network are show in Figure 7.19 to Figure 7.22. The profiles for the other 6 substation are in Appendix F.

APPENDIX P: DC Current rise time

Figure P.1 shows the rise time of the DC current in the neutral of the 3(1P-3L) transformer under 40 % load and 2.0 pu DC current.

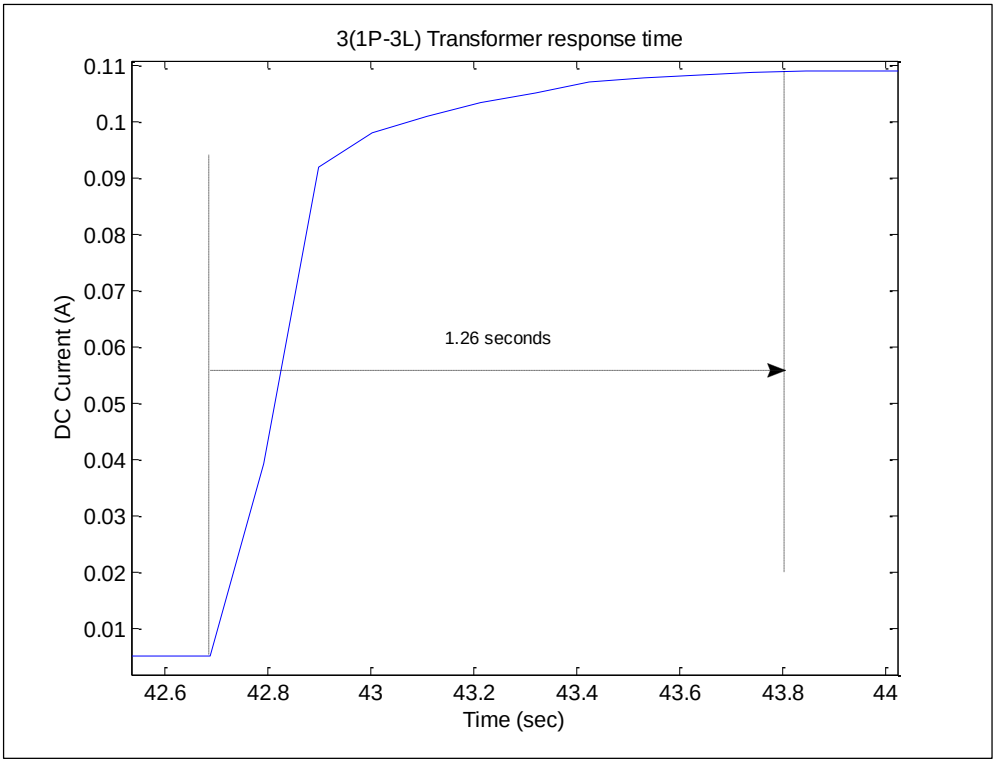

Figure P.1 Response time profile of the 3(1P-3L) transformer core time